EDITORS
SABRI KOCER
OZGUR DUNDAR

ARTIFICIAL INTELLIGENCE APPLICATIONS IN INTELLIGENT SYSTEMS

ISRES Publishing

Artificial Intelligence Applications in Intelligent System

Edited by

Sabri KOCER

Professor, Necmettin Erbakan University
Faculty of Engineering
Department of Computer Engineering, Konya, Türkiye

Ozgur DUNDAR

Asistant Professor, Necmettin Erbakan University
Faculty of Aeronautics and Astronautics
Department of Astronautical Engineering, Konya, Türkiye

ISRES Publishing

Artificial Intelligence Applications in Intelligent System

Editor

Sabri KOCER
Ozgur DUNDAR

This book was typeset in 10/12 pt. Times New Roman, Italic, Bold and Bold Italic.

Artificial Intelligence Applications in Intelligent System

Published by ISRES Publishing, International Society for Research in Education and Science (ISRES).

Includes bibliographical references and index.

ISBN

978-625-6959-22-4

Date of Issue

December, 2023

E-mail

isrespublishing@gmail.com

Address

Istanbul C. Cengaver S. No 2 Karatay/Konya/TÜRKİYE

www.isres.org

PREFACE

Artificial Intelligence Applications in Intelligent Systems 2023 is published annually from selected articles invited by editors. This edition contains 12 articles in Technology, Engineering, Basic Sciences, Artificial Intelligence, Intelligent and Smart Systems.

All submissions are reviewed by at least two international referees. The aim of the book is to provide readers with a scientific peer-reviewed publication in the field of basic sciences, engineering and technology. Artificial Intelligence Applications in Intelligent Systems 2023, Published by ISRES Publishing This book contains new ideas in Electronics, Communications, Mechatronics, Software, Artificial Intelligence, Aviation and Biomedical Engineering and Technology.

In this book, besides modeling real system behaviors with artificial intelligence based learning algorithms in computer environment, development and implementation of intelligent systems for health, manufacturing and service sectors using embedded systems have been carried out. At the same time, scientific studies including the contributions that can be made with artificial intelligence techniques to the problems that can be encountered in different disciplines are presented.

We hope that the book will arouse curiosity about science and technology, be useful to new scientists, science readers and anyone who wants to learn the mystery of science, and contribute to the literature.

December 2023

Sabri KOCER
Professor, Necmettin Erbakan University
Faculty of Engineering
Department of Computer Engineering, Konya, Türkiye
Email: skocer@erbakan.edu.tr

Ozgur DUNDAR
Asistant Professor, Necmettin Erbakan University
Faculty of Aeronautics and Astronautics
Department of Astronautical Engineering, Konya, Türkiye
Email: ozdundar@erbakan.edu.tr

IN THIS BOOK

In Chapter 1, Plant diseases are one of the main causes of damage to world agricultural development. Early detection of plant diseases can prevent this damage. Today, the use of artificial intelligence technologies for the early diagnosis of plant diseases is increasing. It is stated that the deep learning models presented in the studies brought to the literature can work successfully in real life problems. In this study, deep learning models are trained with the open source Plant Village dataset for the detection of plant diseases and their performance in real life problems is presented. In addition, explain ability maps are presented that show where in the image the trained deep learning models give the prediction of plant disease.

In Chapter 2, It presents a practical method to be used in the SIMULINK environment to determine the PID gain parameters of a DC motor. The study explains mathematically how to obtain the equivalent electrical circuit of a DC motor. Furthermore, the importance of PID parameters and the importance and effects of KP, KI and KD values on the performance of the PID controller are explained separately. In addition, the study mentions how to control a DC motor with transfer function using PID in SIMULINK environment. As a result, it is mentioned how to adjust the KP, KI and KD values with the auto-tuning feature of the SIMULINK PID block and how to obtain the most suitable gain values in the simulation environment. It is shown how to easily find the most suitable gain parameters with SIMULINK instead of complex mathematical analysis.

In Chapter 3 There has been a significant surge in the adoption of artificial intelligence solutions across various digital applications, including the management of digital data. However, this rapid digital transformation has resulted in a massive influx of data, posing challenges for existing data analysis tools in effectively extracting valuable insights from this huge amount of information. Topological data analysis is a mathematical approach grounded in algebraic topology which has recently been presented as a promising solution to such problems. Topological data analysis focuses on understanding data “shape” and offers unique advantages. This chapter aims to demystify topological data analysis by providing a comprehensive overview of its applications across diverse fields. Topological data analysis stands out for its robustness and efficiency, particularly in handling complex, high-dimensional datasets. It enhances artificial intelligence approaches. Topological data analysis can help understand complex data by transforming it into visual representations. The chapter explores topological data analysis’s applications, highlighting its contributions and addressing its strengths and limitations with extensive references. Topological data analysis shows promise in empowering intelligent applications, despite potential conceptual challenges in specific domains.

In Chapter 4 The artificial Bee Colony Algorithm, one of the Artificial Intelligence algorithms, is used in many engineering applications today. One of these areas is the optimization of controller parameters. In the study, a PID and LQR controller design was made for a mass-spring-damper system. Controller parameters were fine-tuning with the ABC algorithm and the results were interpreted in detail by comparing them with traditional approaches.

In Chapter 5 Due to the high use rate of microstrip antennas in telecommunication systems, those who design the microstrip antenna structures try easy and unique design methods for obtaining different antenna geometries. Artificial Intelligence algorithms are so popular to determine the physical and electrical parameters of the microstrip antenna

structures. These algorithms are used to examine the antenna dimensions, desired radiation pattern, operating frequency, etc. Machine Learning and Deep Learning are very useful algorithms for applications due to important components of the growing field of data science. In this section, Machine and Deep Learning methods used in microstrip antennas are examined with examples.

In Chapter 6 The development of smart prostheses is of vital importance, especially in order to improve the living conditions of disabled individuals who have to live an amputated life as a result of war and various injuries, which are the fate of the geographies we live in. Different prosthesis designs are available for individuals who lose their limbs for various reasons. Where possible, it has become technologically possible to move smart prototypes electronically as a result of the analysis of EMG signals taken from the individuals arm. In this book chapter, how to control a robotic arm produced with the help of a 3D printer and a system that learns human arm movements based on EMG signals are discussed. EMG signals were obtained from healthy subjects by Myo Armband in order to distinguish seven hand movements applicable in daily life. The pattern recognition system was used to analyze signals matched with movements in three stages (segmentation, feature extraction and classification). EMG signals are divided into sections using the interference technique. Six features were extracted using the TD-PSD method in the time domain. SVM classifier was preferred to find the optimum accuracy of the system. The required acceptable classification success was achieved by selecting the best parameters and features to control a prototype robotic arm so that it could operate in real time.

In Chapter 7 The study focused on the use of K-Means, DBSCAN and Hierarchical algorithms from clustering algorithms in business intelligence for customer segmentation. In the pre-processing stage, a negative correlation was found between age and spending score, indicating an inverse relationship. Graphical results support this, showing that women have higher expenditure scores than men. Different clustering algorithms were applied and all three were found to be suitable with minimal performance difference. K Means suggested six clusters, while the other two algorithms suggested five clusters with consistent cluster formations across the graphs. In summary, the study emphasized the efficiency of clustering algorithms in addressing customer segmentation in a business intelligence framework.

In Chapter 8 To relieve painful situations, it makes sense to stimulate the skin using either external (such as ultrasound, iontophoresis, heat, moist heat, cold, laser, acupuncture) or local (such as paralysing, massaging, or rubbing) methods. It is well known that electric current stimulates nerve tissues. Transcutaneous Electrical Nerve Stimulation (TENS) is one method of nerve stimulation. By applying electrical currents to the skin's intact surface, this method (transcutaneous) stimulates nerves located close to the body's surface. Conductive pads are used to deliver the electric current via the skin. TENS use appears to be safe and has fewer negative effects, according to research. Patients occasionally experience pain that radiates from its origins. In these situations. Identifying the initial source of pain and precisely positioning electrodes are essential to the patient's pain relief. The system's development around microcontrollers makes it affordable and portable. When compared to long-term medication therapy, TENS treatment is comparatively less expensive.

In Chapter 9 Artificial intelligence in medicine is the utilization of deep learning models to improve the diagnosis of diseases more precisely. The developments, happening in deep learning algorithms, allow us to use deep learning algorithms in various fields. A convolutional neural network is known as one of the most popular deep learning algorithms that are used widely to diagnose and classify diseases in the field of medicine. The convolutional neural networks performance depends on the networks; architecture and dataset. Unfortunately, most of the medical datasets are imbalanced, and this situation effects the classification performance of the classification algorithms negatively. Thus, many oversampling and under sampling techniques have been proposed for imbalanced datasets. In this study, an edge detection-based oversampling technique is proposed for imbalanced image datasets. The proposed edge detection-based oversampling technique generates more consistent and meaningful synthetic image samples by detecting the distinctive features of the original image samples for the minority class using the edge detection process.

In Chapter 10 This chapter describes the features of the Jetson TX2 platform and its applications in the field of robotics. Jetson TX2 is among the artificial intelligence development and application cards, as a card used to obtain and analyze data through digital platforms. In this section, you can learn about the physical structure, features and applications of Jetson TX2 in the field of robotics. An example robot design for use of the Jetson TX2 is also presented. This design will help you better understand the applications of the Jetson TX2 in robotics. This section is prepared for engineers, students and enthusiasts working in the field of robotics. It is designed as a resource that anyone who wants to learn about the features and application areas of Jetson TX2 can benefit from.

In Chapter 11 Sleep-related disorders negatively affect the flow of daily life and quality of life. Patients apply to the sleep laboratories for the detection of this disorder. Here, the sleep process is monitored clinically and the data obtained from various electrode are evaluated by specialist doctors over a long period of time. The evaluated data consists of important physiological parameters recorded by an electronic device, especially breathing, brain and muscular activities during sleep. Under normal conditions, physicians make this assessment based on the images reflected on the screen. For this reason, the scoring process turns into a long term and laborious work. Recently, expert systems that can perform sleep scoring have been studied in order to overcome these difficulties. These systems, which were able to offer low classification accuracy at first, have continued to develop day by day. Thanks to different mathematical approaches and deep learning algorithms, significant improvements have been achieved in classification accuracy. As a result of these developments, it will be possible to perform sleep scoring process entirely by expert systems in the near future.

In Chapter 12 The application of deep learning techniques to categorize scenes in satellite images has recently been one of the methods of choice. They provide important insights to researchers in the field and have been used effectively in remote sensing. Using MF-CNN technique has significantly impacted the accuracy and reliability of cloud recognition in remote sensing images. For cloud detection, especially in snow-covered areas, the cloud mask algorithm based on a neural network classifier augmented with radiative transfer simulations provides a threshold-free solution that outperforms traditional techniques. Another potential method for classifying clouds that accurately and efficiently classifies multispectral satellite data is the CS-CNN approach

Managing Editors

Sabri KOCER, PhD, He graduated from the Electrical Engineering Department of Selcuk University. He completed his graduate and his doctorate in Gazi University. Currently, Necmettin Erbakan University, Faculty of Engineering, Computer Engineering is working. Electronics, Computer, Artificial Intelligence, Image Processing, Telecommunication, Signal Processing and Biomedical studies in the area.

Email: skocer@erbakan.edu.tr, **ORCID:** 0000-0002-4849-747X

Ozgur DUNDAR, PhD, works at Necmettin Erbakan University, Department of Astronautical Engineering. He graduated from the Electrical and Electronics Engineering Department of Selcuk University. He worked as an Automation Engineer for a while. His master's and doctorate degrees are from Selçuk University, Institute of Science and Technology, Department of Electrical and Electronics Engineering. Special fields of study are Automation, Artificial Intelligence, Robotic, Communication, Electromagnetic and Micro Strip Patch Antenna designs.

Email: ozdundar@erbakan.edu.tr , **ORCID:** 0000-0002-4142-4446

CONTENTS

CONTRIBUTORS

CHAPTER 1	Ahmet Enes KILIC	Necmettin Erbakan University, Faculty of Engineering (Graduate), Department of Computer Engineering, Konya, Türkiye
	Murat KARAKOYUN	Necmettin Erbakan University, Faculty of Engineering, Department of Computer Engineering, Konya, Türkiye
CHAPTER 2	Tarik Unler	Necmettin Erbakan University, Department of Aviation Electrics and Electronics, Konya, Türkiye
	Mehmet DURSUN	Necmettin Erbakan University, Department of Aviation Electrics and Electronics, Konya, Türkiye
CHAPTER 3	Alperen EROGLU	Necmettin Erbakan University, Faculty of Engineering, Department of Computer Engineering, Konya, Türkiye
	Hatice UNLU EROĞLU	Necmettin Erbakan University, Faculty of Science, Department of Mathematics and Computer Science, Konya, Türkiye
CHAPTER 4	Hasan Huseyin BILGIC	Necmettin Erbakan University, Department of Aeronautical Engineering, Konya, Türkiye
	Hasan Engin COPUR	Necmettin Erbakan University, Department of Astronautical Engineering, Konya, Türkiye
CHAPTER 5	Rabia TOPRAK	Karamanoglu Mehmetbey University, Department of Electrical - Electronics Engineering, Karaman, Türkiye
CHAPTER 6	Ucman ERGUN	Afyon Kocatepe University, Faculty of Engineering, Department of Biomedical Engineering, Afyon, Türkiye
	Fazilet CANATAN ERGUN	Necmettin Erbakan University, Faculty of Engineering (PhD), Department of Biomedical Engineering, Konya, Türkiye

CHAPTER 7	Beyza DUNDAR	Necmettin Erbakan University, Faculty of Engineering (Graduate), Department of Computer Engineering, Konya, Türkiye
	HADIYE BÜYÜKTOLLUOĞLU	Konya Technical University, Faculty of Engineering (Graduate), Department of Computer Engineering, Konya, Türkiye
	Ozgur DUNDAR	Necmettin Erbakan University, Department of Astronautical Engineering, Konya, Türkiye
CHAPTER 8	Sabri KOCER	Necmettin Erbakan University, Faculty of Engineering, Department of Computer Engineering, Konya, Türkiye
	Ozgur DUNDAR	Necmettin Erbakan University, Department of Astronautical Engineering, Konya, Türkiye
CHAPTER 9	Muhammet KARAALTUN	KTO Karatay University, Department of Computer Engineering, Konya, Türkiye
	Omer OZCAN	Selcuk University, Department of Computer Technologies, Konya, Türkiye
CHAPTER 10	Mehmet Tuğrul KAYA,	Konya Technical University, Faculty of Engineering (Graduate), Department of Software Engineering, Konya, Türkiye
	Burak YILMAZ	Konya Technical University, Faculty of Engineering, Department of Software Engineering, Konya, Türkiye
CHAPTER 11	Mehmet DURSUN	Necmettin Erbakan University, Department of Aviation Electrics and Electronics, Konya, Türkiye
	Tarik UNLER	Necmettin Erbakan University, Department of Aviation Electrics and Electronics, Konya, Türkiye
CHAPTER 12	Yasin ER	System Administrator, Department of Meteorological Data Processing, Turkish State Meteorological Service, Ankara, Türkiye
	Sabri KOCER	Necmettin Erbakan University, Faculty of Engineering, Department of Computer Engineering, Konya, Türkiye

CHAPTER 1

Plant Diseases Detection Using Explainable Deep Learning Methods and Its Applicability in Real Life

Ahmet Enes KILIC
Necmettin Erbakan University, Türkiye

Murat KARAKOYUN
Necmettin Erbakan University, Türkiye

To Cite This Chapter:
Kilic A.E., Karakoyun M., (2023). Plant Diseases Detection Using Explainable Deep Learning Methods and Its Applicability in Real Life. In S. Kocer. & O. Dundar (Eds.), *Artificial Intelligence Applications in Intelligent Systems* (pp. 1–15). ISRES Publishing.

Introduction

Early diagnosis of plant diseases in agriculture is very important in terms of plant health and yield. In the event that plant disease is not taken into account, both the farmer is affected economically and the world changes in terms of climate. Recently, with the development of the internet, methods such as decision support systems and machine learning algorithms have been used in studies such as automatic detection of plant disease. However, due to insufficient data and inappropriate data situations, successful results cannot be obtained on real data. Automatic extraction of features has been provided by deep learning, which has developed recently, and it has been frequently used in real-world problems in fields such as industry, medicine, and industry. This situation has also spread to the field of agriculture and the use of deep learning in agriculture has gradually increased. With the increase in use cases, the data pool has expanded, and interdisciplinary studies have been focused on to gain value from this field. In this way, open-source datasets became widespread and shared for plant disease classification. Plant diseases are one of the main causes of damage to world agricultural development. Early diagnosis of plant diseases is very important for plant health and yield. Innovative technologies such as artificial intelligence instead of manpower in the detection of plant diseases facilitate early diagnosis. With the development of smart agriculture, large volumes of datasets have been brought to the literature in order to develop artificial intelligence models in the field of agriculture.

In this study, it is aimed to classify diseases by using deep learning methods from plant images using a large volume of open source PlantVillage dataset (Hughes & Salathé, 2015) obtained from the laboratory environment. In addition, the deep learning methods used with the large-volume open source PlantVillage dataset were directly tested on the Plant Pathology 2020 dataset (Competition, 2020) obtained from real life, and its performance in real-world problems was measured. Some studies in the literature with the PlantVillage dataset used in this study can be summarized as follows.

(Mohameth, Bingcai, & Sada, 2020) used three CNN-based deep learning models, ResNet50, VGG16, GoogLeNet, to extract the features of the images in the dataset. The features extracted by deep learning models are presented as input to SVM and KNN machine learning methods to classify plant leaf diseases. Thus, a hybrid approach is presented using both deep learning and machine learning methods.

(Atila et al., 2021) preferred CNN-based models that can perform automatic feature extraction for disease classification from plant leaf images, instead of machine learning methods where feature extraction must be flawless to obtain successful results. The performances of 12 deep learning methods, namely AlexNet, ResNet50, VGG16, InceptionvV3, and EfficientNet model variants (B0, B1, B2, B3, B4, B5, B6, B7) were compared.

(Chohan et al., 2020) made disease classification from plant leaves using a simple CNN model with 5 convolutional layers. They tested the model they developed on 100 real-world data obtained from a drone or phone. Since the data obtained were not included in the classes produced by the model, healthy and unhealthy classification was made only on real data. 96 out of 100 images were correctly classified as healthy/unhealthy.

(Saleem, Potgieter, & Arif, 2020) presents a comparative evaluation of deep learning methods for disease classification from plant images in two stages. In the first phase, LeafNet, VGG16, OverFeat, Improved Cifar10, Inception ResNetv2, Reduced MobileNet, Modified MobileNet, ResNet50, MLCNN, Inceptionv4, Improved GoogLeNet, AlexNet, DenseNet121, MobileNet, Hybrid AlexNet with VGG, ZFNet, Cascaded AlexNet and GoogLeNet and Xception 18 deep learning methods were trained and comparatively analysed on the test set. In the second stage, the 3 most successful models (Cascaded AlexNet with GoogLeNet, Improved GoogLeNet, Xception) are selected and the models are compared by changing the optimization function. A comparison is presented on 6 optimizers: SGD, RMSProp, Adagrad, Adamax, Adam and Adadelta.

(Wang, Sun, & Wang, 2017) used only apple images in the PlantVillage dataset to classify the diseases in apple images with VGG16, VGG19, InceptionV3 and ResNet50 models, which are CNN-based deep learning methods, and the model performances were compared.

(Too et al., 2019), in order to choose the architecture that can classify diseases in plant images in the fastest way, VGG16, InceptionV4, ResNet50, ResNet101, ResNet152 and DenseNet121 deep learning methods were used by transfer learning from pre-trained models on the ImageNet dataset containing 1.2 million natural images with 1000 classes. performance and time comparison.

(Ahila Priyadharshini et al., 2019) uses only corn images in the PlantVillage dataset to classify 4 diseases in corn images with the LeNet deep learning method developed with 97.89% accuracy.

(Russel & Selvaraj, 2022) studied two datasets, the PlantVillage dataset and the MepcoTrophicLeaf dataset. Using a CNN-based deep learning method that can learn in parallel with six channels in both datasets, firstly, plant leaf type classification and secondly plant disease classification were made. They were also compared with similar studies in the literature.

(Borhani, Khoramdel, & Najafi, 2022), Wheat Rust Classification, a small dataset, Rice Leaf Disease, a medium-level dataset, and PlantVillage datasets with a large dataset volume were studied. By combining the convolution layers, which form the basis of CNN models, and the attention layers, which form the basis of Transformer models, a new model is used to classify plant diseases. The performance of the VIT model developed with the traditional CNN-based model was compared in three datasets.

(Vallabhajosyula, Sistla, & Kolli, 2022), using 5 different optimizers: SGD, RMSPROP, NADAM, ADAMAX and ADAGRAD, ResNet50, ResNet101, InceptionV3, DenseNet121, DenseNet201, MobileNetV3 and NasNet CNN-based deep learning methods have made disease classification from plant images. In addition, in order to observe the results of all CNN models, a new deep ensemble neural network model has been developed, which realizes the learning situation by combining the results from the fully connected layers by removing the classification layer of the models.

(Saeed et al., 2021) presents a 4-step development process for disease classification from tomato, corn, and potato images in the PlantVillage dataset. In the first stage, deep features were extracted with VGG19, a CNN-based deep learning method. In the second stage, the extracted features are combined with the developed parallel fusion method. In the third stage, the best features were selected with the developed PLS method (partial least squares). At the last stage, the classification of plant diseases was made by training the ensemble baggage tree classifier with the selected features.

(Ahmed & Reddy, 2021) developed a CNN model with 3 convolutional layers with data collected from 3 different data sources: Kaggle, PlantVillage and Google Web Scraper. They deployed the deep learning model developed for plant disease classification to run on an Android-based mobile application.

(Hassan et al., 2021), 4 different CNN-based deep learning methods, namely InceptionV3, InceptionResNetV2, MobileNetV2 and EfficientNet-B0 for disease classification from plant images, were compared and it was emphasized which one could be effective temporally in real life.

(Geetharamani & Pandian, 2019) developed a 9-layer CNN deep learning model with augmented data using image filling, gamma correction, noise injection, principal component analysis (PCA) color augmentation, rotation, and scaling data augmentation methods.

(Chen et al., 2020), PlantVillage dataset was used for the classification of diseases in plant images, and 1000 corn and rice image datasets from the Fujian Institute of Subtropical Botany in China were used to reflect real life. A cascade model approach is presented with the VGG19 and Inception model, in which transfer learning is made from pre-trained models in the ImageNet dataset. Model results were compared in both datasets.

In the literature, it is suggested that deep learning methods used on the classification of plant diseases by using the large-volume open source PlantVillage dataset can be directly used in real-world problems. Based on this problem, in this study.

- Comparable analysis of deep learning methods developed on the open-source dataset and presenting them to the literature.
- Presenting the state of explainability that shows where deep learning methods developed on the open-source dataset make decisions by looking at the image.
- Test performance of deep learning methods developed on open source and a large dataset is presented on a real-life dataset.

Materials and Methods

In this study, PlantVillage, which consists of plant images obtained from the laboratory environment, and Plant Pathology 2020 (Competition, 2020) open-source datasets, which consists of apple plant images obtained from real life, were used.

PlantVillage Dataset

The dataset consists of a total of 61486 images, including a total of 39 classes, including 26 diseased plant classes for 14 plants, 12 healthy plant classes, and 1 background class that does not consist of plant images. Statistical information about the dataset is given in Table 1. The images in the dataset were created by augmenting with image filling, gamma correction, noise injection, principal component analysis (PCA) color augmentation, rotation, and scaling data augmentation methods. In Figure 1, an example of the images of each class is given.

Table 1.

PlantVillage Dataset Class Distribution

Class Name	Image Number
Apple with scab	1000
Apple with black rot	1000
Apple with cedar apple rust	1000
Healthy apple	1645
Blueberry with healthy	1502
Cherry with powdery mildew	1052
Cherry with healthy	1000
Corn with grey leaf spot	1000
Corn with common rust	1192
Corn with northern leaf blight	1000
Healthy corn	1162
Grape with black rot	1180
Grape with black measles	1383
Grape with leaf blight	1076
Healthy grape	1000
Orange with Huanglongbing	5507
Peach with bacterial spot	2297
Healthy peach	1000
Pepper with bacterial spot	1000
Healthy pepper	1478
Potato with early blight	1000
Healthy potato	1000
Potato with late blight	1000
Healthy raspberry	1000
Healthy soybean	5090
Squash with powdery mildew	1835
Healthy strawberry	1000
Strawberry with leaf scorch	1109
Tomato with bacterial spot	2127
Tomato with early blight	1000
Healthy tomato	1591
Tomato with late blight	1909
Tomato with leaf mold	1000
Tomato with septoria leaf spot	1771
Tomato with two spotted spider mite	1676
Tomato with target spot	1404
Tomato with mosaic virus	1000
Tomato with yellow leaf curl virus	5357
Background without leaf	1143
TOTAL	61486

Figure 1.

Sample images from each class in the PlantVillage dataset

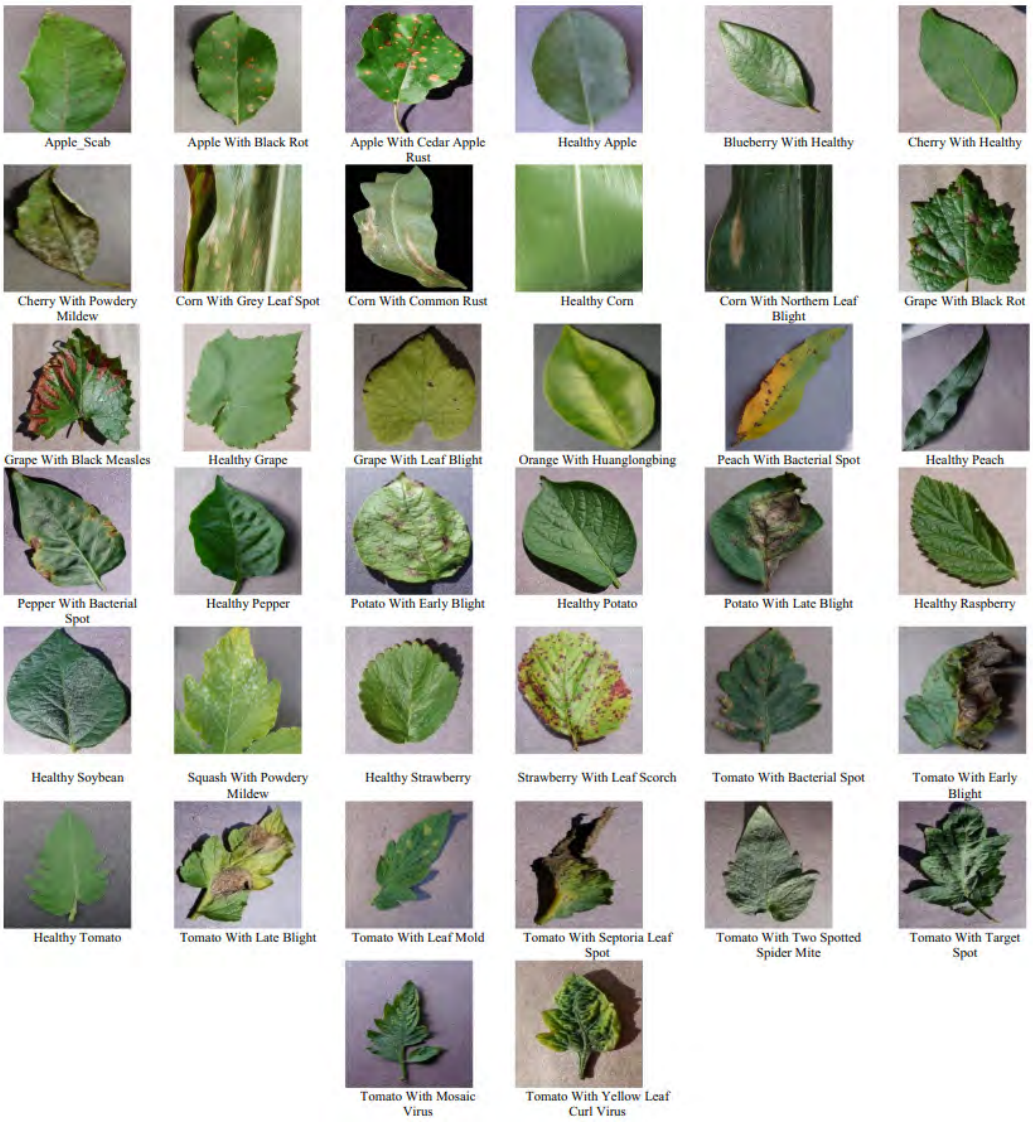

Plant Pathology 2020 Dataset

Plant Pathology 2020 and Plant Pathology 2021 competitions were held on the Kaggle platform in 2020 and 2021 for the classification of diseases from real-life apple leaf images. The Plant Pathology 2020 dataset, consisting of a total of 3642 apple images, 1821 in the training and 1821 test set, was used.

Data Pre-Processing

The images in the PlantVillage dataset consist of RGB images with random dimensions, that is, 3-channel images. Initially, images were resized to 256x256 for ResNet152, VGG16, EfficientNet-B0, EfficientNet-B1, DenseNe201 and GoogLeNet models, and to 224x224 for Vision Transformers Large 32. The reason why a separate resize process is done for the Vision Transformers Large 32 model is because the model receives the

image given in the learning process with 32x32 patch as input, the images are given as a multiple of 32. Afterwards, since the PyTorch framework was used, the pixel values of the data were normalized to the 0-1 range and converted to Tensor and provided as input to the model. Stratified 5-fold cross validation method was used for dataset separation.

State-of-The-Art Deep Learning Architectures

In this study, 7 deep learning methods, ResNet152 (He et al., 2016), VGG16 (Simonyan & Zisserman, 2014), EfficientNet-B0 (Tan & Le, 2019), EfficientNet-B1 (Tan & Le, 2019), DenseNet201 (Huang et al., 2017), GoogLeNet (Szegedy et al., 2015) and Vision Transformers Large 32 (Dosovitskiy et al., 2020), which are frequently used in the literature for disease classification from plant leaf images, were selected. It is based on deep learning methods ResNet152, VGG16, EfficientNet-B0, EfficientNet-B1, DenseNe201 and GoogLeNet convolutional neural network. Vision Transformers Large 32, on the other hand, is a Transformers-based deep learning method that has been used recently in the field of image processing. The deep learning methods used were model trainings by applying transfer learning from pre-trained models on the ImageNet dataset (Deng et al., 2009) containing 1.2 million natural images with 1000 classes. Hyperparameters are standardized in all deep learning methods. Stochastic Gradient Descent (SGD), batch size 32, learning rate 0.001 and cross entropy as loss function were used as optimization function in all model trainings.

Convolutional neural networks (CNN) were introduced by Yen LeCun in the 1980s (LeCun et al., 1989). However, it could not maintain its popularity. CNNs became more popular when AlexNet won the ImageNet competition with its deep learning method in 2012 (Borhani, Khoramdel, & Najafi, 2022). Nowadays, the solution of problems such as Image Classification, Object Detection, Object Tracking, Natural Language Processing, Style Transfer is based on convolutional neural network. Unlike traditional machine learning approaches, CNNs can learn directly from the original image with extracted features by sliding filters over the input image, rather than manually extracting certain features.

The basic architecture of deep learning methods or a typical CNN model used in this study consists of convolution layers, pooling layers, and fully connected layers, as can be seen in Figure 2. An image given as input to the CNN model for classification from plant leaf images.

- In the Convolution layer, by passing it, important features are extracted.
- In the Pooling layer, Size reduction is performed in order to reduce the computational complexity and prevent the risk of overfitting.
- In the fully connected layer, Class prediction is made using extracted features. Sigmoid, softmax are the most commonly used functions.

Figure 2.

A typical convolutional neural network structure (Too et al., 2019)

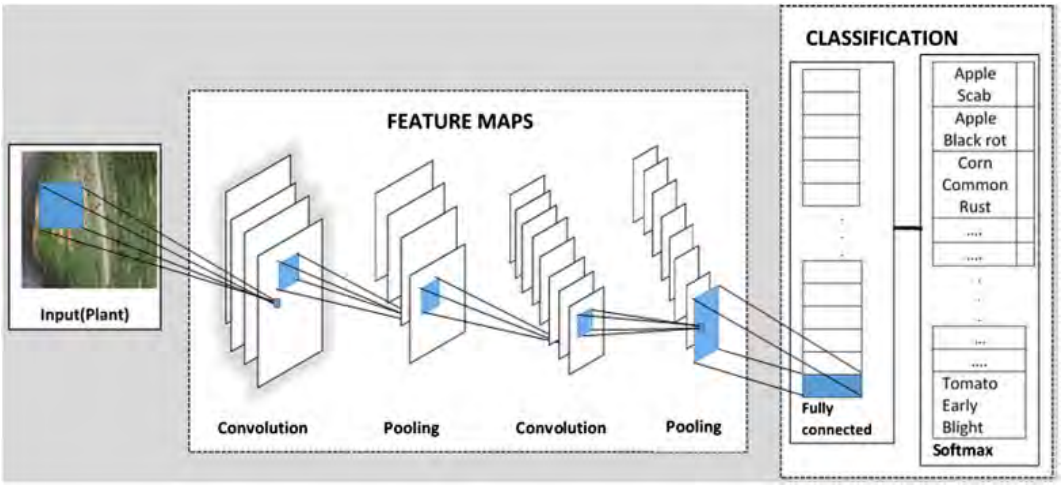

The concept of Transformer, which emerged with the article "Attention Is All You Need" (Vaswani et al., 2017), was primarily put forward for technologies carried out in the field of natural language processing. In the field of natural language processing, there is a development process that is successful enough to create the architecture behind even ChatGPT today. For this reason, it has been developed as Visual Transformers on the image processing side other than natural language processing. It was released as a competitor to CNN models. The most obvious difference from the CNN model is that while CNN models process the whole image, Transformer-based models process the image by separating it piece by piece. As can be seen in Figure 3, a basic visual transformers model consists of 4 architectures.

- Patch + Position Embedding architecture; it converts the input image into a series of image segments and adds a position number to know in what order the segments come.
- Linear projection of flattened patches architecture; image parts are converted to embeddings, the benefit of using embeddings instead of using images directly is that embeddings are an educationally learnable representation of the image.
- Transformer Encoder interprets the incoming embedding and location information by passing it through the attention layers.
- MLP head architecture; It is the output layer of the transformers structure; it transforms the learned properties of an input into a class output.

Figure 3.

Visual transformer structure (Dosovitskiy et al., 2020)

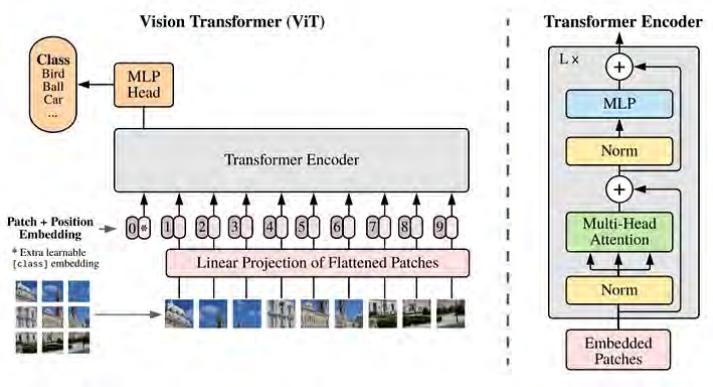

Explainability

When deep learning models make predictions from the image, they only return the predicted class. This causes these models to be accepted as black box. "Can we open the black box of AI?" published in 2016. With this study, a new explanatory perspective was gained to artificial intelligence models (Castelvecchi, 2016). Explainable artificial intelligence systems (XAI) show that developed deep learning models make predictions by focusing on where in the image. In this study, it is shown that the trained deep learning methods use the features in the latest convolution layers to classify the models by looking at the disease part or the wrong places in the image.

Evaluation Metrics

Since the open source PlantVillage dataset includes unstable classes, only the accuracy metric was not used to evaluate deep learning methods. In this study, accuracy, precision, recall and f1 score calculated in equations 1, 2, 3 and 4, respectively, using TP, TN, FP, FN values extracted from the confusion matrix in Table 2, were used as evaluation metrics. Since the dataset includes unbalanced classes, the f1-score metric is taken as the basis for choosing the best model.

Table 2.

Confusion Matrix

		Ground Truth	
		0	1
Prediction	0	TP	FN
	1	FP	TN

Accuracy = (TP + TN) / (TP + FP + TN + FN)	(1)
Precision = TP / (TP + FP)	(2)

Recall = TP / (TP + FN)	(3)
f1-Score = (2 x Precision x Recall) / (Precision + Recall)	(4)

Experimental Setup

In this study, 7 deep learning methods were trained with 5-fold cross validation method for the classification of plant diseases using the prepared PlantVillage dataset. The performance of deep learning methods trained on the PlantVillage dataset on real-life problems was tested and measured on the Plant Pathology 2020 dataset. In this study, only the training set of the Plant Pathology 2020 dataset was used for testing. Because while there is ground truth information for the training set, there is no ground truth information for the test set. Figure 4 shows the artificial intelligence workflow of the study.

Figure 4.

AI workflow

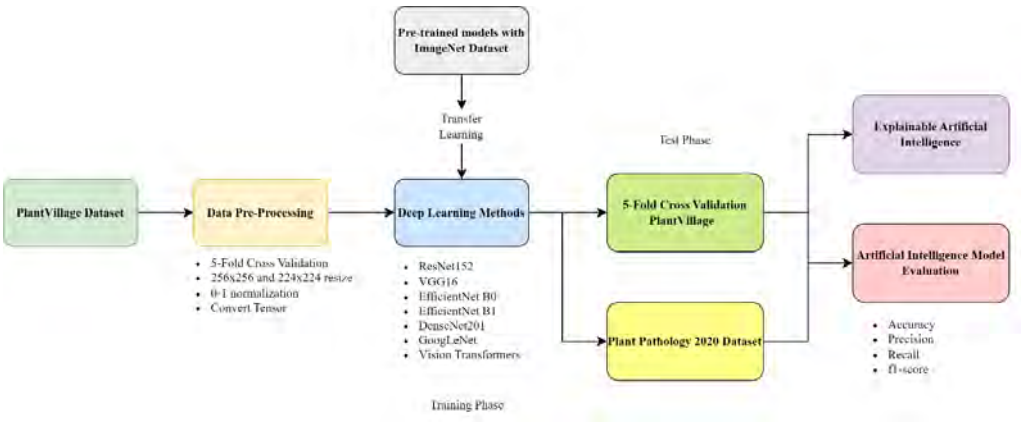

Deep learning methods are trained on AMD Ryzen 5 5600 processor, 16GB RAM and ASUS GeForce DUAL RTX 3060 V2 OC 12GB graphics card. Model implementations were carried out with Python programming language and PyTorch framework.

Results

Comparable Result

The model results of 7 deep learning methods trained using the PlantVillage dataset with the 5-Fold cross validation method for the classification of plant diseases and the results obtained by testing these models directly in the Plant Pathology 2020 dataset, which includes real-life data, are given in Table 2. According to Table 2; On the open source PlantVillage dataset, the most successful deep learning model is DenseNet201 with 99.74 f1-score, and the most unsuccessful deep learning model is ViT large 32 with 99.11 f1-score. When trained on the open source PlantVillage dataset and tested

directly on the Plant Pathology 2020 dataset containing real-life data, VGG16 according to accuracy, ResNet152 according to precision, EfficientNet-B1 are the best models according to recall and f1-score.

Tablo 3.

Deep Learning Models Results

	PlantVillage				Plant Pathology 2020			
CNN Models	Acc.	Precision	Recall	f1- score	Acc.	Precision	Recall	f1-score
ResNet152	99.79	99.72	99.72	99.72	22.11	68.07	19.06	26.55
VGG16	99.69	99.61	99.58	99.60	30.10	63.25	25.87	29.13
DenseNet201	99.81	99.74	99.74	99.74	25.97	63.09	21.36	30.00
Efficient-Net-B0	99.77	99.71	99.71	99.71	18.55	64.23	17.42	23.77
Efficient-Net-B1	99.74	99.67	99.64	99.65	28.61	59.18	26.38	31.33
GoogLeNet	99.54	99.43	99.39	99.41	19.36	58.15	17.34	24.48
ViT Large 32	99.27	99.13	99.10	99.11	14.19	53.05	11.52	13.56

Explainable Result

Comparative results of explainability maps of deep learning models trained with PlantVillage dataset are given in Figure 5. According to Table 4, ResNet152 and GoogLeNet models give the correct disease class decision by looking at a larger area. DenseNet201, EfficientNet-B0 and EfficientNet-B1 models converge more closely to the disease site. In this way, the focal point in the explainability maps of these models can be used as labels for segmentation problems. Although the VGG16 model has high performance (even if the plant disease decision is correct), the model makes the right decision by looking in the wrong place. This means that the deep learning model learns from the error.

Figure 5.

Examples of Explainability of Deep Learning Models

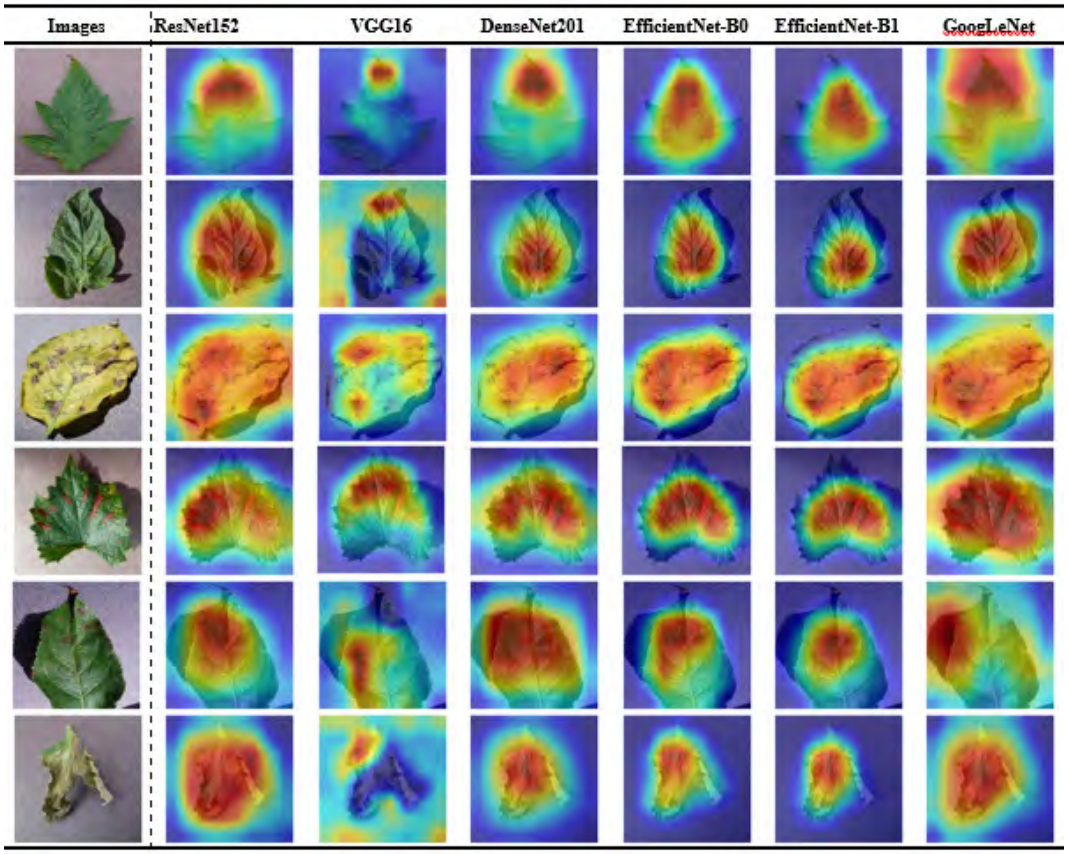

Conclusion

In this study, 7 deep learning methods, namely ResNet152, VGG16, EfficientNet-B0, EfficientNet-B1, DenseNe201, GoogLeNet and VisionTransformers, were developed for disease classification from plant images using the open source PlantVillage dataset, and the model results were compared. As a result of the comparison, DenseNet201 deep learning method gave the most successful result by looking at the accuracy, precision, recall and f1-socre metrics in the open source PlantVillage dataset. Many studies developed for plant disease classification have been brought to the literature. Most of the studies declare to work in modern agriculture or in real life. Based on this hypothesis, in this study, deep learning methods developed with open source PlantVillage were tested on a real-life dataset and their performance was measured. The open-source dataset was analysed, because it contains clean images, it could not perform on the real, complex data contained in the real-life dataset. Therefore, even if the data in the literature are in the same field as in this study, artificial intelligence models developed due to the environment and data difference produce incorrect results. To solve this problem, a model developed with open-source dataset is not expected to work directly on real-life data. Instead, the model can be generalized by feeding real-life data to the model. In this way, more successful results will be obtained.

References

Ahila Priyadharshini, R., Arivazhagan, S., Arun, M., & Mirnalini, A. (2019). Maize leaf disease classification using deep convolutional neural networks. *Neural Computing and Applications, 31*, 8887-8895.

Ahmed, A. A., & Reddy, G. H. (2021). A mobile-based system for detecting plant leaf diseases using deep learning. *AgriEngineering, 3*(3), 478-493.

Atila, Ü., Uçar, M., Akyol, K., & Uçar, E. (2021). Plant leaf disease classification using EfficientNet deep learning model. *Ecological Informatics, 61*, 101182.

Borhani, Y., Khoramdel, J., & Najafi, E. (2022). A deep learning based approach for automated plant disease classification using vision transformer. *Scientific Reports, 12*(1), 11554.

Castelvecchi, D. (2016). Can we open the black box of AI? *Nature News, 538*(7623), 20.

Chen, J., Chen, J., Zhang, D., Sun, Y., & Nanehkaran, Y. A. (2020). Using deep transfer learning for image-based plant disease identification. *Computers and Electronics in Agriculture, 173*, 105393.

Chohan, M., Khan, A., Chohan, R., Katpar, S. H., & Mahar, M. S. (2020). Plant disease detection using deep learning. *International Journal of Recent Technology and Engineering, 9*(1), 909-914.

Competition, K.-R. P. (2020). Plant Pathology 2020 - FGVC7. https://www.kaggle.com/c/plant-pathology-2020-fgvc7

Deng, J., Dong, W., Socher, R., Li, L.-J., Li, K., & Fei-Fei, L. (2009). Imagenet: A large-scale hierarchical image database. 2009 IEEE conference on computer vision and pattern recognition,

Dosovitskiy, A., Beyer, L., Kolesnikov, A., Weissenborn, D., Zhai, X., Unterthiner, T., Dehghani, M., Minderer, M., Heigold, G., & Gelly, S. (2020). An image is worth 16x16 words: Transformers for image recognition at scale. *arXiv preprint arXiv:2010.11929*.

Geetharamani, G., & Pandian, A. (2019). Identification of plant leaf diseases using a nine-layer deep convolutional neural network. *Computers & Electrical Engineering, 76*, 323-338.

Hassan, S. M., Maji, A. K., Jasiński, M., Leonowicz, Z., & Jasińska, E. (2021). Identification of plant-leaf diseases using CNN and transfer-learning approach. *Electronics, 10*(12), 1388.

He, K., Zhang, X., Ren, S., & Sun, J. (2016). Deep residual learning for image recognition. Proceedings of the IEEE conference on computer vision and pattern recognition,

Huang, G., Liu, Z., Van Der Maaten, L., & Weinberger, K. Q. (2017). Densely connected convolutional networks. Proceedings of the IEEE conference on computer vision

and pattern recognition,

Hughes, D., & Salathé, M. (2015). An open access repository of images on plant health to enable the development of mobile disease diagnostics. *arXiv preprint arXiv:1511.08060*.

LeCun, Y., Boser, B., Denker, J. S., Henderson, D., Howard, R. E., Hubbard, W., & Jackel, L. D. (1989). Backpropagation applied to handwritten zip code recognition. *Neural computation*, *1*(4), 541-551.

Mohameth, F., Bingcai, C., & Sada, K. A. (2020). Plant disease detection with deep learning and feature extraction using plant village. *Journal of Computer and Communications*, *8*(6), 10-22.

Russel, N. S., & Selvaraj, A. (2022). Leaf species and disease classification using multiscale parallel deep CNN architecture. *Neural Computing and Applications, 34*(21), 19217-19237.

Saeed, F., Khan, M. A., Sharif, M., Mittal, M., Goyal, L. M., & Roy, S. (2021). Deep neural network features fusion and selection based on PLS regression with an application for crops diseases classification. *Applied Soft Computing*, *103*, 107164.

Saleem, M. H., Potgieter, J., & Arif, K. M. (2020). Plant disease classification: A comparative evaluation of convolutional neural networks and deep learning optimizers. *Plants*, *9*(10), 1319.

Simonyan, K., & Zisserman, A. (2014). Very deep convolutional networks for large-scale image recognition. *arXiv preprint arXiv:1409.1556*.

Szegedy, C., Liu, W., Jia, Y., Sermanet, P., Reed, S., Anguelov, D., Erhan, D., Vanhoucke, V., & Rabinovich, A. (2015). Going deeper with convolutions. Proceedings of the IEEE conference on computer vision and pattern recognition,

Tan, M., & Le, Q. (2019). Efficientnet: Rethinking model scaling for convolutional neural networks. International conference on machine learning,

Too, E. C., Yujian, L., Njuki, S., & Yingchun, L. (2019). A comparative study of fine-tuning deep learning models for plant disease identification. *Computers and Electronics in Agriculture, 161*, 272-279.

Vallabhajosyula, S., Sistla, V., & Kolli, V. K. K. (2022). Transfer learning-based deep ensemble neural network for plant leaf disease detection. *Journal of Plant Diseases and Protection, 129*(3), 545-558.

Vaswani, A., Shazeer, N., Parmar, N., Uszkoreit, J., Jones, L., Gomez, A. N., Kaiser, Ł., & Polosukhin, I. (2017). Attention is all you need. *Advances in neural information processing systems, 30*.

Wang, G., Sun, Y., & Wang, J. (2017). Automatic image-based plant disease severity estimation using deep learning. *Computational intelligence and neuroscience, 2017*.

About the Authors

Ahmet Enes KILIC works as a Specialist Engineer in the Artificial Intelligence Unit of the Presidency of the Republic of Turkey Digital Transformation Office. He has a bachelor's degree in electrical and Electronics Engineering from Gazi University. He is doing his master's degree in computer engineering at Necmettin Erbakan University. Areas of interest; It can be defined as artificial intelligence, computer vision, deep learning, machine learning, production, and use of synthetic data. It has the second place in TEKNOFEST Artificial Intelligence in Health competition and provides technical consultancy for TEKNOFEST competitions.

E-mail: aekilica@gmail.com, ORCID: 0009-0004-9358-8743

Murat KARAKOYUN received the master and Ph.D. degrees from the Department of Computer Engineering of Selçuk University and Konya Technical University, respectively. He is working as an Assistant Professor at Computer Engineering Department of Necmettin Erbakan University. Areas of interest: artificial intelligence, image processing, data mining, machine learning.

Email: mkarakoyun@erbakan.edu.tr, ORCID: 0000-0002-0677-9313

Similarity Index

The similarity index obtained from the plagiarism software for this book chapter is 20%.

CHAPTER 2

Estimation of PID Gain Parameters of DC Motor with MATLAB SIMULINK

Tarik UNLER

Necmettin Erbakan University, Türkiye

Mehmet DURSUN

Necmettin Erbakan University, Türkiye

To Cite This Chapter:
Unler, T. & Dursun, M. (2023). Estimation of PID Gain Parameters of DC Motor with MATLAB SIMULINK. In S. Kocer. & O. Dundar (Eds.), *Artificial Intelligence Applications in Intelligent Systems* (pp. 16–26). ISRES Publishing.

Introduction

Nowadays control applications are more and more involved in industrial applications. Especially in motor control applications, many studies are carried out on both speed control and position control. In this section, the mathematical model of a DC motor that will be controlled with a PID (Proportional, Integrative and Derivative) will be created and it will be controlled with PID on Matlab. The most optimum PID KP, KI and KD gain values will be determined in the simulation environment by using the PID Tune feature of the SIMULINK plug-in of the Matlab program. Thus, the most appropriate PID parameters of the DC motor, whose mathematical model has been created, will be estimated through the mathematical model. A DC motor is a device that converts electrical energy into mechanical energy. One of the types of DC motors is brushed DC motors (Chotai & Narwekar,2018). In general, control systems are divided into two. One is classical control methods and the other is modern control systems. Classical control systems depend on feedback and transfer function. Modern control systems use artificial neural networks, Fuzzy and state space modeling (Ogata, 2010).

Although the PID controller is called classical control methods, it takes an advanced form of control with the addition of modern systems using high-speed microcontrollers and microcomputers (Fadali, 2009). PID controllers allow the DC motor to be controlled at the desired torque and speed. However, in order to perform the control operations in the desired way, it is necessary to optimize the P I and D parameters for the PID controller to control the desired speed and torque (Sen, 1996). This control is much more

important especially under varying load conditions. With the optimum determination of the parameters of the PID controller, a precise speed and torque control is possible (Saad et al., 2019).

Today, PID controllers are frequently used in industry. There are many applications in the literature where PID parameters are automatically controlled. (Vallejoa et al., 2010).

There are many PID applications that can self-tune using genetic algorithms (Habera et al., 2004). In control applications, data from sensors are received with sensors and sensor fusion is applied to control many parameters such as speed, motor torque control (Cinar et al., 2021). Artificial intelligence methods are also used in control applications. (Unler,2022). By combining PID and artificial intelligence applications, much more effective applications are made. Successful control applications have been developed using PID and AI (Artificial intelligence) in the studies (Kusuma, et al., 2021).

Mathematical Model of DC Motor

In order to simulate the DC motor on SIMULINK, a mathematical model must be created. Then a transfer function of the DC motor needs to be created according to this model. Figure 1. The electrical model of a DC motor is shown (Balamurugan & Umarani, 2020).

Figure 1.

Equivalent circuit of DC motor (Balamurugan,, & Umarani,2020)

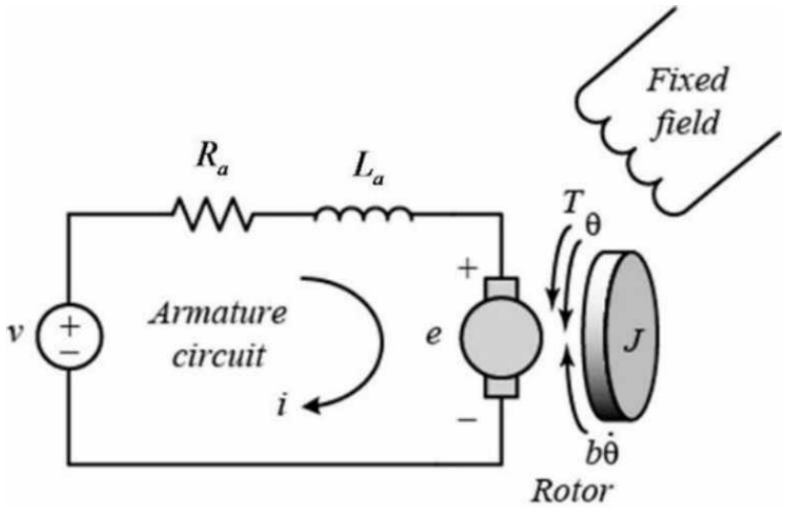

The DC motor voltage V(t) can be described by the following equation using the Kirchhoff law (Balamuruga, & Umarani,2020)

$$V_t = E_b + R_a.I_a + L_a.\frac{dI_a}{dt} \quad (1)$$

The voltage V(t) of the DC motor can be expressed as shown in equation 1. In the steady state, the current is zero. Consequently, as there would be zero change in current, equation 1 gets simplified to equation 2. utilizing Kirchoff.

$$V_t = E_b + R_a.I_a \tag{2}$$

Air gap power is represented as the product of electromagnetic speed and torque equation shown below;

$$P_a = \omega_m T = E_b.I_a \tag{3}$$

If we aim to obtain the electromagnetic torque, we can express it as a function of the motor speed (), the armature current (), and the torque (T) as shown in equation below;

$$T = \frac{E_b.I_a}{\omega_m} \tag{4}$$

The Back emf () is given by;

$$E_b = K_b \omega_m \tag{5}$$

$$T = K_b I_a \tag{6}$$

The moment of inertia J, viscous friction coefficient B, and acceleration torque are presented for the DC motor.

$$T_a = T - TI = J\frac{d\omega_m}{dt} + B\omega_m \tag{7}$$

Where represents the load torque, equations (1) and (6) explain the dynamics of a DC motor under load conditions. Applying Laplace transform to equations (1) and (6) yields:

$$I_a(s) = \frac{V(s) - K_b\omega_m(s)}{R_a + sL_a} \tag{8}$$

$$\omega_m(s) = \frac{K_b I_a(s) - T_l(s)}{B + sJ} \tag{9}$$

The open-loop transfer function of the DC motor speed is expressed as follows:

$$\frac{\theta}{V} = \frac{K}{(Js+b)+(Ls+R)+K^2} \tag{10}$$

Table 1 shows the parameters of a Pololu brand 240rpm DC motor;

Table 1.

DC Motor Parameters

Resistance (	2.9 ohm
Inductance (La)	0.47H
Electromotive force constant (Ke=Kt)	0.013 Nm/Amp
Moment of inertia of rotor (J)	0.012 kg.
Damping ratio of system (B)	0.1 Nms
Input (V)	Input Voltage

PID Controller Mathematics

A PID controller continually computes an error value between the desired set-point and a measured process variable, and implements corrective measures (Velagic et al., 2010).There are three parameters in PID controller, these are proportional P, integral I, derivative D. If these parameters shown in the PID controller are expressed as gain, they are expressed as KP, KI and KD. Figure 2 shows a standard PID closed loop.

Figure 2.

PID closed loop (Mehta et al., 2017)

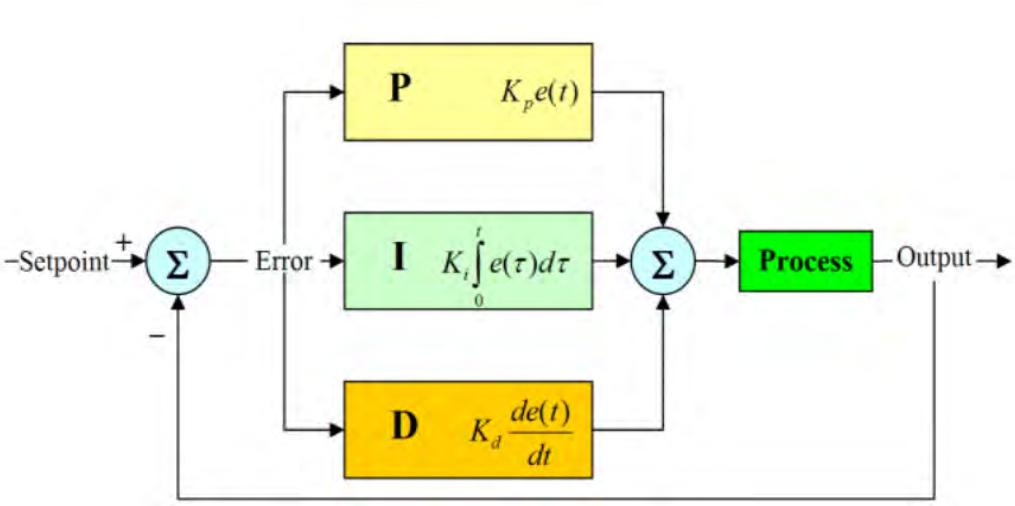

If the general form of the PID controller is formed by considering the gains, equation below is obtained;

$$u_{(t)} = K_p e(t) + K_i \int_0^t e(t)\,dt + K_d \frac{de}{dt} \tag{11}$$

In the equation u is the control signal and e is the error generated in the system. The control signal is equal to the product of the error times the proportional gain, the continuous sum of the error times the integral gain and the error times the KD gain.

KP KD and KI gains directly affect the rise time, settling time and over shot values. These parameters are shown in Figure 3.

Figure 3.

Rise time, settling time, and other typical step-response characteristics of PID controller (Leva et al.*, 2018)*

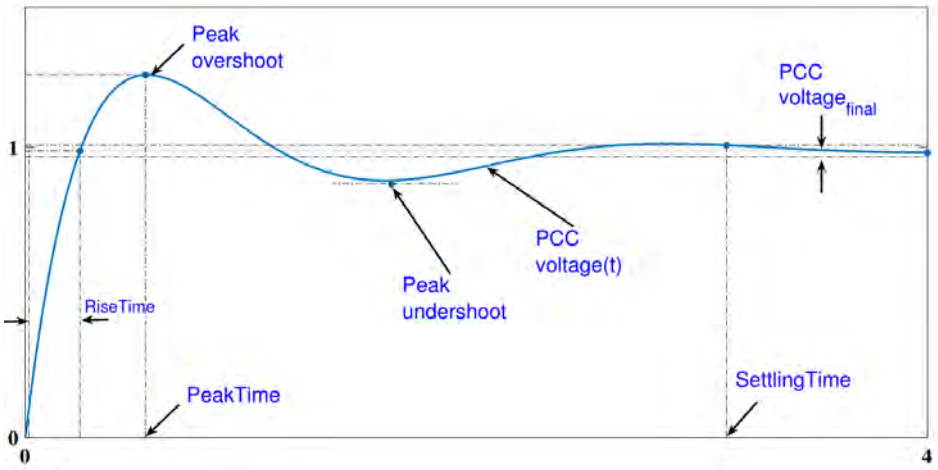

The effects of KP, KI and KD gains on the control signal are shown in Table 2

Table 2.

PID Characteristic

Closed Loop Response	Rise Time(	Over Shoot	Settling Time(	Steady State Error(e)
	Decrease	Increase	Small Change	Decrease
	Decrease	Increase	Increase	Eliminate
	Small Change	Decrease	Decrease	No Change

Figure 4, Figure 5, and Figure 6 show the effects of the controller on the system response according to the changes of KP, KI and KD values separately.

Figure 4.

effect of PID controller on system response (Farag, 2020)

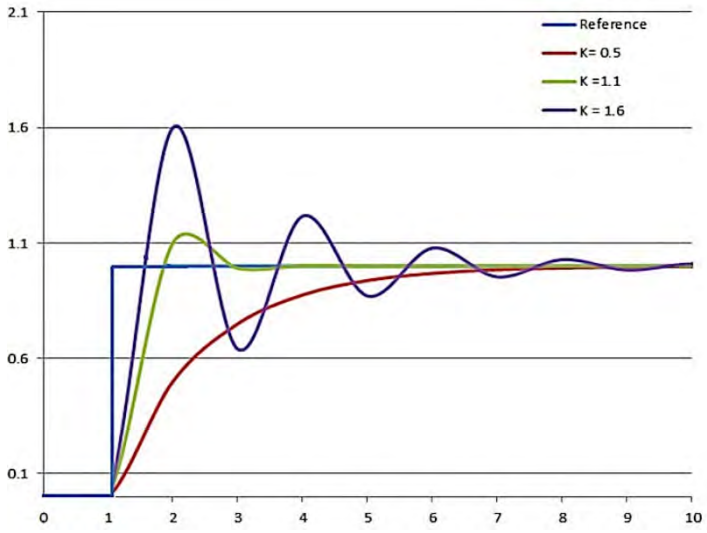

As seen in Figure 4, rise time and steady state error decrease with increasing KP value, but over shoot increases.

Figure 5.

Effect of PID controller on system response (Farag, 2020)

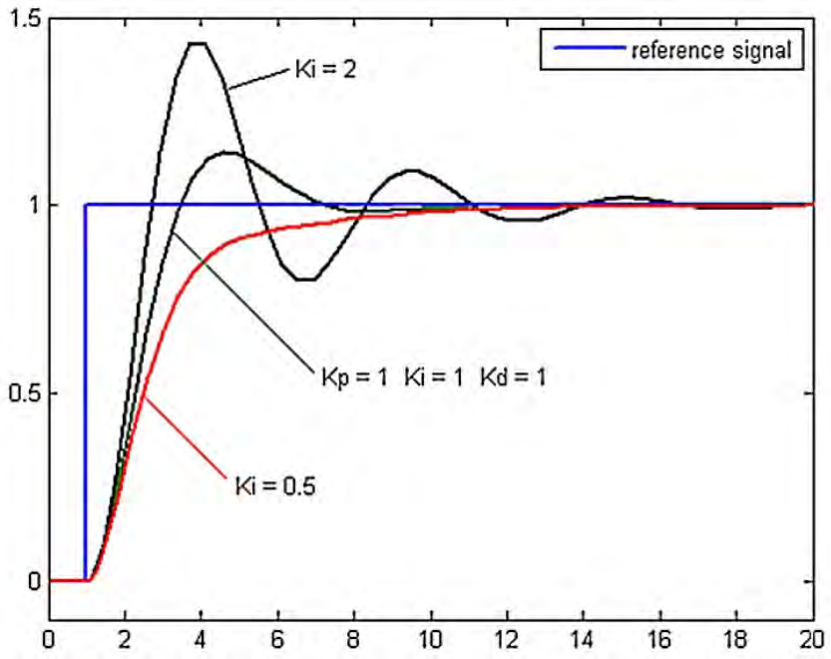

As can be seen in Figure 5, increasing KI value decreases rise time, while increasing overshoot and settling time.

Figure 6.

Effect of PID controller on system response (Farag, 2020)

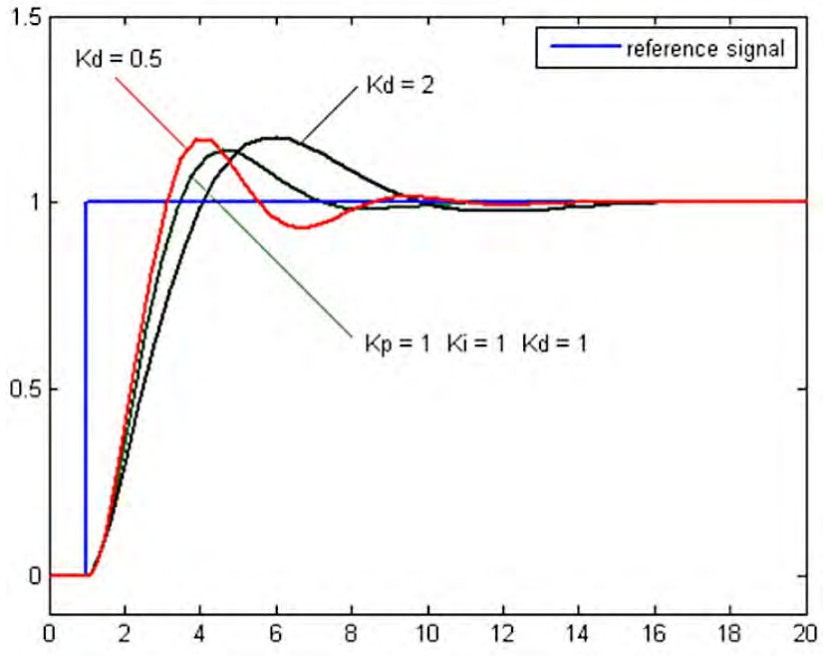

In Figure 6, a slight increase in rise time occurs as the KD value increases, whereas both

over-shoot and settling time decrease.

To create control applications with the PID controller yielding optimal system response, the KP, KI and KD gain values may be adjusted.

Transfer Function for PID controller

In order to simulate a DC motor in SIMULINK, the transfer function must be created according to the mathematical model. Equation below shows the transfer function for a DC motor;

$$\frac{\theta(s)}{V(s)} = \frac{0.0089s + 0.0052}{s^2 - 1.063s - 0.2578} \tag{12}$$

Where θ(s) =Motor Angle, V(s) Motor input voltage

Here, the representation of the motor PID control block on SIMULINK is as shown in Figure 7.

Figure 7.

SIMULINK model PID control of DC motor

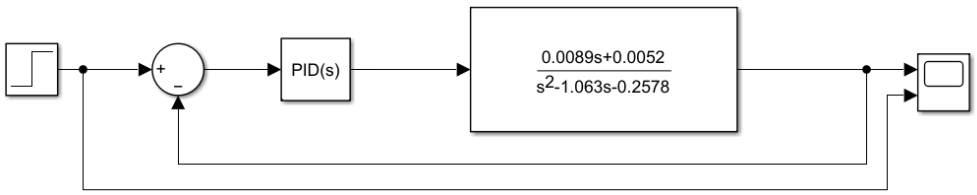

As seen in Figure 7, the PID closed loop is created by adding the transfer function. Here, the controller can be configured as P, PI or PID if desired within PID(s).

One of the most difficult operations in controller design is to determine the KP KD and KI values for the controller. For this process, gain values can be calculated using methods such as Ziegler-Nichols step response method. However, if a mathematical model of the system can be created in the SIMULINK program, these parameters can be determined much more easily using the Tune function. Here, PID parameters are determined with the transfer function of the system using SIMULINK. KP, KD and KI values can be determined in the most optimum way by using the tune feature in the PID blog. When the PID block is opened, if desired, KP, KI and KD values can be determined manually. In order to determine these features using the Tune feature, click on the Tune option shown in Figure 8 in the SIMULINK PID block.

Figure 8.

SIMULINK PID block configuration window

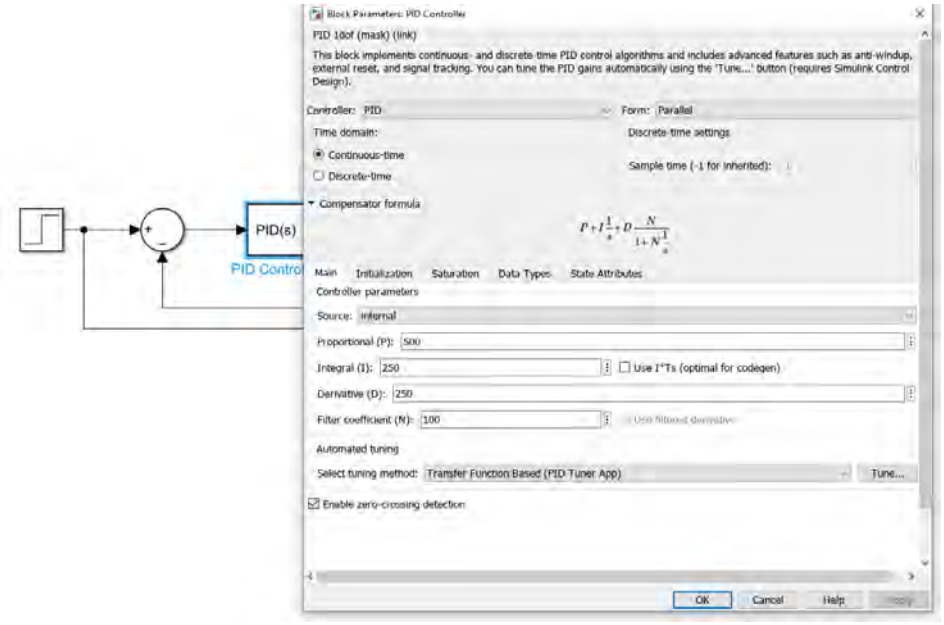

After this stage, the window where the PID related selections will be adjusted by sliding with a slider will open as shown below in Figure 9.

Figure 9.

SIMULINK model PID tune window (Before Tuning)

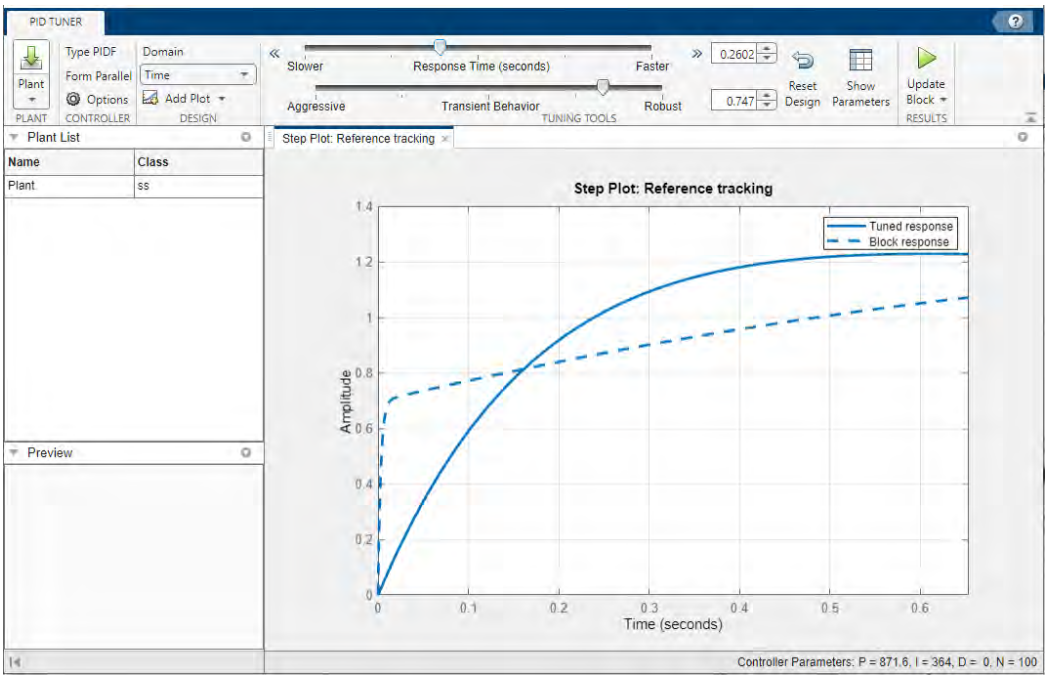

Within this interface, one can adjust the “Response Time” (in seconds) and “Transient Behaviour” sliders to ascertain the most suitable KP, KD, and KI values for the system. Therefore, instead of relying on intricate formulas, SIMULINK will enable the identification of the optimal system gain smoothly.

Figure 10 shows the KP, KI and KD values of the system by shifting the sliders.

Figure 10.

System response after PID tuning

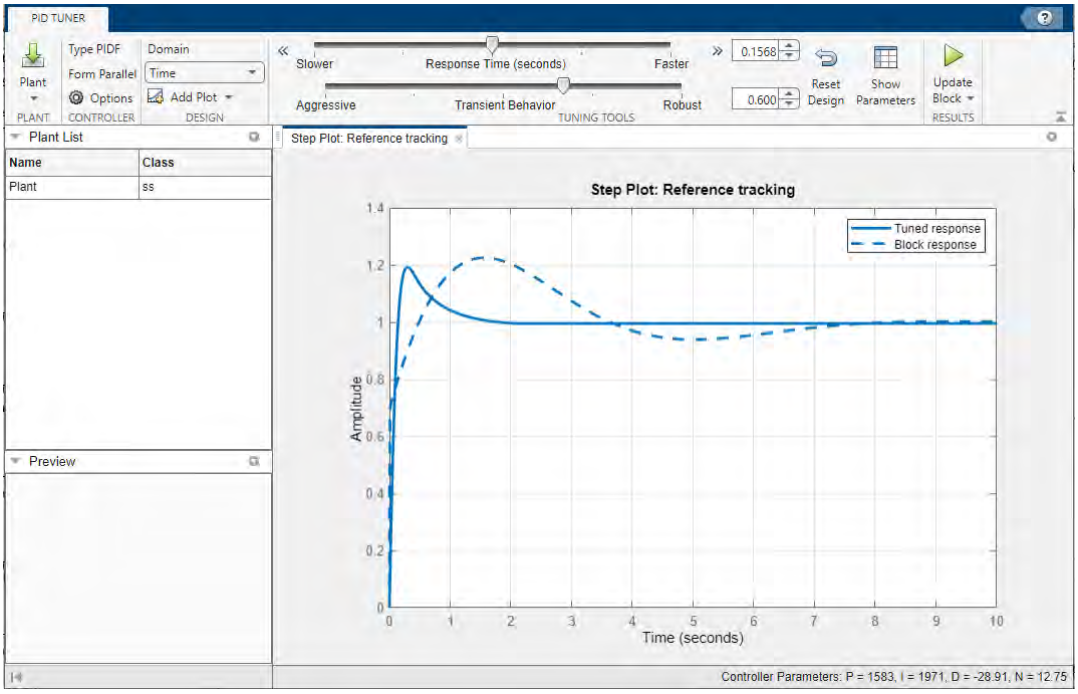

As illustrated in Figure 10, the PID parameters were established through the utilization of the SIMULINK tune feature, resulting in an appropriate system response. While the system response depicted in Figure 9 was characterized by a high level of error and was very slow, tuning effectively eliminated the aforementioned issues.

Thus, it is evident that the SIMULINK Tuning tool proves to be highly beneficial for the identification of PID parameters. As a result, the PID gain parameters of a mathematically modelled system can be easily determined with the help of SIMULINK and the system response can be observed. Gain determination is valid not only for PID controllers but also for PI and PD controllers.

Therefore, it is highly advantageous to employ SIMULINK PID-Tuner for determining the parameters of all PID control applications prior to implementation in real-world scenarios.

Reference

Balamurugan, S., & Umarani, A. (2020, September). Study of discrete PID controller for DC motor speed control using MATLAB. In 2020 International Conference on Computing and Information Technology (ICCIT-1441) (pp. 1-6). IEEE, W. (2020). *Complex trajectory tracking using PID control for autonomous driving. International Journal of Intelligent Transportation Systems Research*, 18(2), 356-366.

Cinar, I., Taspinar, Y.S., & Koklu, M. (2021). Artificial intelligence applications in engineering. In M. Ozaslan & Y. Junejo (Eds.), *Current Studies in Basic Sciences, Engineering and Technology* 2021(pp. 107–125). ISRES Publishing

Habera R, Schmitza U, Barsb R. Optimal choice of horizons for predictive

Farag, W. (2020). Complex trajectory tracking using PID control for autonomous driving. *International Journal of Intelligent Transportation Systems Research*, 18(2), 356-366.

J. Chotai and K. Narwekar, "Modelling and position control of brushed DC motor," in International Conference on Advances in Computing, Communication and Control 2017, ICAC3 2017, 2018,vol. 2018-January, pp. 1–5.Sin, A.K. & Zaman, H.B. (2010). Live Solar System (LSS): Evaluation of an Augmented Reality book-based educational tool. *In Information Technology* (ITSim), IEEE International Symposium,1, 1-6.

Jasmin Velagic(2010), Nedim Osmic(2010), Kemal Lutvica(2010) "Incubator System Identification and Temperature Control with PLC & HMI", *52nd International Symposium* ELMAR-2010, 15-17 September 2010

Katsuhiko Ogata, " Modern Control Engineering", *5th Edition, PrenticeHall,* ISBN 13: 978-0-13-615673-4, 2010

Kusuma, D. H., Ali, M., & Sutantra, N. (2016, August). The comparison of optimization for active steering control on vehicle using PID controller based on artificial intelligence techniques. In 2016 *International Seminar on Application for Technology of Information and Communication* (ISemantic) (pp. 18-22). IEEE.

Leva, S. & Mussetta, Marco & Le, Kim. (2018). A Comparative Study on Controllers for Improving Transient Stability of DFIG Wind Turbines During Large Disturbances. Energies. 11. 480. 10.3390/en11030480.

Mehta, Nikunj & Dharmendra, Chauhan & Patel, Sagarkumar & Mistry, Siddharth. (2017). Design of HMI Based on PID Control of Temperature. *International Journal of Engineering Research and*. V6. 10.17577/IJERTV6IS050074.

Mufti, A. (2013). The Effects of P, I and D Parameters in Automatic Liquid Level Control Using UniTrain Module. *Jurnal Rekayasa Elektrika*, 10(3), 120-130.

P.C. Sen, "Principles of Electrical Machines & Power Electronics", USA: John Wiley & Sons, 1996.

Saad MS, Jamaluddin M, Darus IZM. Implementation of PID controller tuning using differential evolution and genetic algorithms. *Int J Innovative Comput, Inform Control* 2012;9:7761–79.

Sami Fadali, "Digital Control Engineering Analysis and Design", Elsevier Inc., ISBN 13: 978-0-12-374498-2, 2009.

Unler T. , (2022). Vehicles of the Near Future: Driverless Autonomous Car, In S. Kocer, O. Dundar (Eds .). *Current Studies in Basic Sciences Engineering and Technology* (pp. 70–81). ISRES Publishing.

Vallejoa AJ, Morales-Menendezb R. Cost-effective supervisory control system in peripheral milling using HSM. *Annual Reviews in Control* 2010;34:155–62.

About the Authors

Tarik UNLER, PhD, is an Assistant Professor of Aviation Electrical and Electronic at Necmettin Erbakan University in Konya, Türkiye. He holds a PhD in Electric-Electronic Engineering from Konya Technical University. His main areas of interest are embedded systems, autonomous systems, RADAR and aviation applications.

E-mail: tunler@erbakan.edu.tr, ORCID: 0000-0002-2658-1902

Mehmet DURSUN, PhD, is an Assistant Professor of Aviation Electrical and Electronic at Necmettin Erbakan University in Konya, Türkiye. He holds a PhD in Electric-Electronic Engineering from Selçuk University. His main areas of interest are signal processing, image processing, electronics and fiber optics communication systems.

E-mail: mehmet.dursun@erbakan.edu.tr, ORCID: 0000-0002-0558-6309

Similarity Index

The similarity index obtained from the plagiarism software for this book chapter is 20%.

CHAPTER 3

Topological Data Analysis for Intelligent Systems and Applications

Alperen EROGLU
Necmettin Erbakan University, Türkiye

Hatice UNLU EROGLU
Necmettin Erbakan University, Türkiye

To Cite This Chapter:
Eroglu, A. & Unlu Eroglu, H. (2023). Topological Data Analysis for Intelligent Systems and Applications. In S. Kocer. & O. Dundar (Eds.), *Artificial Intelligence Applications in Intelligent Systems* (pp. 27–60). ISRES Publishing.

Introduction

With the advent of technology and the digital transformation era, the paradigm of the pervasive and ubiquitous fully connected world brings along with enormous data (Eroglu, A. 2022). We need to analyze such data to create intelligent applications and autonomous systems. Today, these data appear in many fields as high-dimensional and complex data. Topology, as a mathematical field, is concerned with the study of shapes (Edelsbrunner and Harer, 2022). Topological data analysis (TDA) extends this discipline to the examination of exceedingly complex data. It operates on the premise that all data possesses an inherent shape, and this shape carries significant meaning (Rabadan and Blumberg, 2019). Topological data analysis combines a variety of techniques from category theory, combinatorics, algebraic and geometric topology to examine the shape of these data (Ali et al., 2023). As an approach that brings together fields such as applied mathematics and data science, it has grown significantly because of the rapid increase in research conducted in the last few years (Chazal and Michel, 2021). It has become a reliable and easily applicable approach that can be used in practical applications in fields such as genomics, manufacturing, medicine, cybersecurity, forecasting and climate change. One of the most important benefits of TDA is that it can be used to improve the performance of artificial intelligence (AI), machine learning (ML) and deep learning (DL) techniques (Baas et al., 2020; Hensel et al., 2021).

In the literature there are different intelligent applications in different fields so that TDA can be used as an automated design paradigm. When data science research and

data-driven approaches in recent years are examined, it is observed that topological and geometric techniques are used as an important element in machine learning, deep learning, and other artificial intelligence applications. At this point, the research includes studies in which computer scientists, statisticians and mathematicians come to the fore and propose various TDA solutions (Azizi, 2022).

TDA is used as an effective solution approach for different domains and applications such as text analysis, materials science, physics, chemistry, image processing, natural processing, medicine, neuroscience, price predictions, anomaly detection, agriculture, computational biology, biomedicine, business, financial applications, critical infrastructures, disaster management, avionics systems, intelligent transportation, digital pathology, AI-based oncology, climate, and time-dependent applications (Carlsson and Vejdemo-Johansson, 2021). While this interest continues to increase, topology and geometry have proven themselves to be very useful tools in solving many problems in different fields. For example, while geometry is used in nonlinear dimensionality reduction problems, the geometric deep learning approach demonstrates successful performance, especially in structure data analysis. On the other hand, when we look at topological data analysis, it shows serious success in complex data problems, especially thanks to the persistent homology approach. This situation highlights the fact that topological and geometric solutions are very critical tools. When looking at the literature, there is a need for a comprehensive study that combines studies using topological data analysis to solve problems in various autonomous and artificial intelligence applications in many different digital sectors. In this chapter, this gap in the literature will be filled and the importance of the topological data analysis paradigm will be adequately revealed. With open research questions, this approach will be the subject of ongoing research and will contribute to the solution of many artificial intelligence applications.

The remaining structure of this chapter is as follows. In the successive section we explain the topological data analysis components: mapper and persistent homology. Section titled as “Topological Data Analysis and Artificial Intelligence” answers some of critical questions to clearly understand the relation between artificial intelligence, learning paradigms and TDA. Moreover, the implementation of TDA, its advantages and its restrictions are discussed in detail. In the section titled “Topological Data Analysis Applications for Intelligent Systems”, we analyze different smart systems and applications utilizing TDA. In the conclusion section we summarize the chapter.

Topological Data Analysis

Topological data analysis, which brings together the disciplines of mathematics and computer science, is defined in this section. It is revealed how it analyzes data by considering qualitative geometric features and which algorithms it must achieve it.

Topological data analysis focuses on the overall structure of data and is resilient to the presence of noise. It is assumed that data has a shape, and we want to extract the topological features of this shape. TDA has two well-known methods which are persistent homology and the Mapper algorithm. Persistent homology is a main tool in TDA. Persistent Homology tracks the changes of topological features across multiple scales and finds more persistent topological patterns of the underlying data space (Wasserman, 2018). Before giving the definition of persistent homology, we will give a background starting with the definition of a simplex.

Figure 1.

An illustration of simplicies which are 0-,1-,2- and 3-simplex, respectively

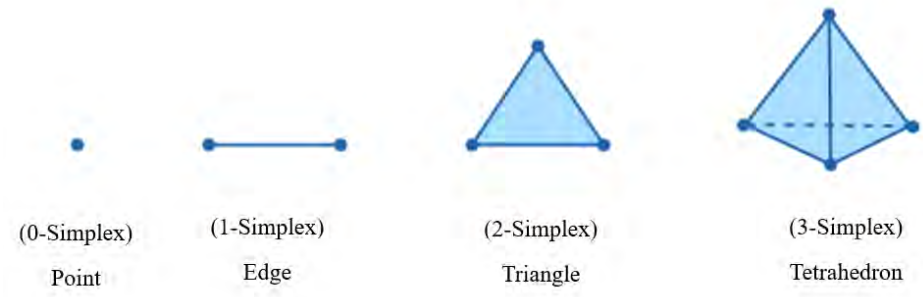

A simplex can be thought of as a generalization of a triangle as illustrated in Figure 1. Let's assume that there is a finite set $V = \{v_0, v_1, \ldots, v_k\}$ of affinely independent points in $\mathbb{R}^d$. The smallest convex set containing the points of V (convex hull of V) is called a k-simplex. Let us denote it by $\sigma^k = [v_0, v_1, \ldots, v_k]$. The points of V are called the vertices of σ^k. A 0-simplex represents a vertex, a 1-simplex represents an edge, a 2-simplex is a triangle and a 3-simplex is a tetrahedron. The simplicies spanned by non-empty subsets of V are called faces of the simplex σ^k. A simplicial complex K is a collection of simplices satisfying the following two properties: First, any face of a simplex from K belongs to K. Second, the intersection of any two simplices in K is either empty or a face of both. An abstract simplicial complex is a finite collection of sets $\tilde{K}$ such that $\tau \in \tilde{K}$ and $\sigma \subseteq \tau$ implies $\sigma \in \tilde{K}$. Although there are many types of simplicial complexes, the Vietoris-Rips complex is the most preferred because it can be calculated faster (Shiraj et al., 2023). Suppose that we are given a set of points V in a metric space (X, d) and $\epsilon > 0$. The Vietoris-Rips complex VR_ϵ contains simplicies $[v_0, v_1, \ldots, v_n]$ in which $d(v_i, v_j) < \epsilon$ for all $i, j \in \{0, 1, \ldots, n\}$. Another commonly used simplicial complex is the Cech complex. The Cech complex is the set of simplicies $[v_0, v_1, \ldots, v_n]$ such that intersection of the closed balls around each v_i is non-empty, i.e., $\bigcap_{i=0}^{n} B(v_i, \epsilon) \neq \emptyset$. There is a close relation between these two complexes (Paik and Koert, 2023).

Persistent homology examines how the homology of a parameterized space changes on a changing parameter. Homology is an algebraic topology tool which associates algebraic objects with topological spaces (Hatcher, 2002). If the homology groups of two

topological spaces are different, it is inferred that these two spaces are not topologically equivalent. Therefore, homology groups help us classify topological spaces. The rank of the homology groups is called the Betti numbers. The zeroth Betti number, β_0,the first Betti number, β_1, the second Betti number, β_2, of a topological space are the numbers of connected components, holes, and voids of the topological space, respectively. For example, the Betti numbers β_0, β_1, β_2 of a torus, which is the surface of a donut, are $1, 2, 1$. The higher Betti numbers β_i, $i \geq 3$, of a torus are 0.

Persistent homology computes the topological features of an increasing nested sequence of simplicial complexes $\emptyset = K^0 \subseteq K^1 \subseteq \ldots \subseteq K^m = K$, which is called a filtration of the simplicial complex K. As ϵ increases in the Vietoris-Rips complex, we get a filtration of Vietoris-Rips complex: For an increasing sequence of parameters $\epsilon_1 \leq \epsilon_2 \leq \cdots \leq \epsilon_n$ we get a filtration $VR_{\epsilon_1} \subseteq VR_{\epsilon_2} \subseteq \cdots \subseteq VR_{\epsilon_n}$. By passing to the homology, we obtain a sequence of homology groups connected by induced homomorphisms $\mathrm{H}_p(VR_{\epsilon_1}) \to \mathrm{H}_p(VR_{\epsilon_2}) \to \cdots \to \mathrm{H}_p(VR_{\epsilon_n})$ $\mathrm{H}_p(VR_{\epsilon_1}) \to \mathrm{H}_p(VR_{\epsilon_2}) \to \cdots \to \mathrm{H}_p(VR_{\epsilon_n})$ for each dimension p. For each dimension p and $0 \leq i \leq j \leq n$, the images of the homomorphisms $f_p^{i,j}: \mathrm{H}_p(VR_{\epsilon_i}) \to \mathrm{H}_p(VR_{\epsilon_j})$ are called the p-th persistent homology groups. And it is denoted by $\mathrm{H}_p^{i,j}$. The rank of $\mathrm{H}_p^{i,j}$ is called p-th persistent Betti number.

Given a filtration of a simplicial complex, the homology of the filtration changes as parameters increase. For instance, new connected components or loops can appear (are born) or existing components can merge an existing one (die). The persistence barcode allows us to visualize this information as shown in Figure 2. In the persistence barcode, each bar begins at some feature's birth and ends its death (Chazal and Michel, 2021). Each interval represents the lifespan of a homological feature. The short barcodes are considered as noise within data. If b is the birth time of a feature and d is the death time of the same feature, then we can represent each interval as a point (b, d) in $\mathbb{R}^2$. This gives us the persistence diagram which is a multiset of all such points. An example of a point cloud's persistence diagram is demonstrated in Figure 2. Since $0 < b < d$, the points under the line $y = x$ will not be considered. To understand how long a homological feature persists from the persistence diagram, we look at the distance to the line $y = x$. The further a point is from $y = x$ line, the more persistent it is.

Figure 2.

An example of a point cloud (A), its persistence barcode (B), and its persistence diagram (C)

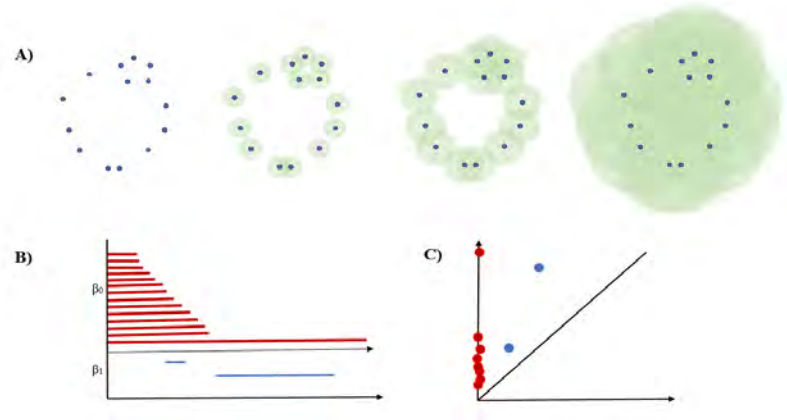

There are various representations of persistence diagrams such as persistence landscapes (Bubenik, 2015) and persistence images (Adams et al., 2017). With the help of these representations, we can use persistent homology and machine learning techniques together.

To benefit from the topological information obtained from persistent homology, it is necessary to be able to compare persistence diagrams. In fact, the space of persistence diagrams forms a metric space. The most common metrics used to compare two persistence diagrams are bottleneck distance and Wasserstein distance.

Persistent homology is the method that examines the homological characteristics of point clouds to comprehend their geometry, while the other approach called ***Mapper*** involves visualizing the data or finding associated images for point cloud data to gain a qualitative understanding via direct visualization, often using a graph representation (Munch, 2017). The fundamental concept behind Mapper is to identify local clusters within the point cloud and examine how these partial clusters interact with one another. Mapper algorithm is described in (Singh et al., 2007). Mapper algorithm takes the following inputs: a point cloud, a filter function, a metric space, clustering algorithm and other parameters (Sekuloski and Dimitrievska, 2019). It produces an output which is presented as a graph containing the main topological features.

Figure 3.

An illustration of the Mapper algorithm

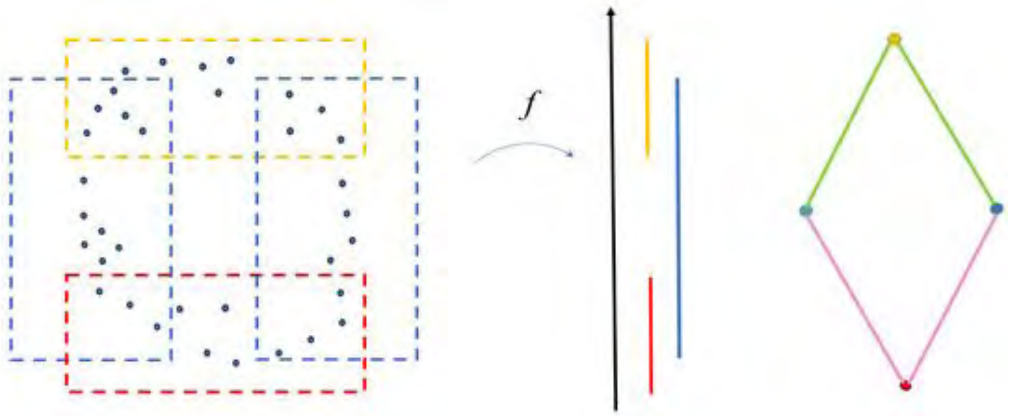

The **Mapper algorithm** can be outlined and put into practice through the following five steps:

Define a filter (or lens) function $f: X \to Z$ from a point cloud X with a metric to a lensed space Z, where Z is often chosen to be $\mathbb{R}$.

Choose a covering $\mathfrak{A} = \{U_\alpha\}_{\alpha \in A}$ of $f(X)$.

Take the preimage of each U_α in the covering $\mathfrak{A}$. The union of $X_\alpha := f^{-1}(U_\alpha)$ gives us a cover of X.

Perform a clustering algorithm on the sets X_α. Single-linkage clustering is a standard choice. This clustering process will yield a collection of clusters. Consequently, you will have a covering of the dataset X, which can be described by pairs (α, c), where α belongs to the set A, and c represents one of the clusters within X_α.

Create a simplicial complex by using a set of vertices formed by all conceivable pairs (α, c). Include (α_0, c_0), ..., (α_k, c_k) as the vertices of a k-simplex only if the clusters c_0, ..., c_k have a mutual point in common.

A simpler version of Mapper, as applied to the data, is designed to generate a graph as its primary objective. As depicted in Figure 3, the Mapper algorithm visualizes its input data as a graph comprising four vertices connected by four edges.

Topological Data Analysis and Artificial Intelligence

Topological data analysis has a very strong relationship between AI, Machine Learning, Deep Learning, Big Data, Natural Language Processing, and many other most prominent computer science paradigms like data science. In this section, we remark the following questions to reveal how this strong relationship can be built: 1) How does TDA burst Artificial Intelligence 2) How does TDA augment Machine and Deep Learning Techniques? 2) How TDA can be used in conjunction with NLP and Big Data Techniques? 3) What are the possible tools to implement TDA? 4) What are the limitations of TDA? How can we overcome such limitations?

Persistent homology can be seen as a supplementary approach to traditional feature representation techniques employed in artificial intelligence (Srinivasan, R., & Chander,

2019). Persistent homology can be used to improve the accuracy of deep learning and deep neural networks algorithms with providing topological features and inner representation of data, respectively (Deng and Duzhin, 2022; Watanabe and Yamana, 2020).

TDA presents a less biased and more rigorous method for analyzing complex datasets, as it doesn't rely on preexisting hypotheses or concentrate solely on pairwise data relationships, distinguishing it from established methods like clustering and traditional association analyses. Since interpreting the higher dimensional datasets is highly challenging due to their size and complexity, TDA comes to light to investigate such datasets as a Big Data tool (Nguyen et al., 2019; Sing and Wilsey, 2022; Tsaneva-Atanasova and Scotton, 2023). Topological data analysis plays a significant role in enhancing machine learning algorithms, spanning from unsupervised to supervised approaches. Its importance lies in its capacity to extract valuable insights from vast and intricate datasets, a pressing need for global enterprises dealing with massive and diverse data sources, including sensors, social, health, logs, and financial data. The exponential growth in data volume, combined with limited data science resources, has led to a search for innovative approaches like TDA to enhance the quality and speed of data analytics. TDA, combined with high-performance machines and algorithms, offers the potential for exponential improvements in data analysis, addressing the escalating demand for processing ever-increasing volumes of data.

Topological data analysis utilizes clustering to create a network representation of data, focusing on smaller data subsets rather than trying to identify distinct groups. It combines these "partial clusters" to provide an overview of data point similarities, making it suitable for connected representations of continuous datasets or data with varying densities. Unlike most clustering algorithms, which rely on global optimization and are sensitive to noise, TDA divides data into independent segments using lens functions. Clustering is then applied separately to each segment, resulting in multiple local optimizations that mitigate the impact of noise on the results.

Topological data analysis facilitates the automated implementation and synthesis of dimensionality reduction algorithms. TDA resolves the projection loss issue common in dimensionality reduction by clustering data in the original high-dimensional space, preserving the separation of data points in lower-dimensional representations. This allows for easier identification of distinct segments and sub-segments within the data that might be obscured by other dimensionality reduction methods. TDA automatically merges the outcomes of multiple dimensionality reduction algorithms into a single result, negating the necessity to specify the correct assumptions for any method.

TDA helps eliminate systematic errors by utilizing the output of global optimization-based supervised learning algorithms as input to identify specific areas within the data where systematic errors occur. TDA is tailored for local datasets, creating an ensemble of models that focus on different data segments instead of making global assumptions about the entire dataset, thereby avoiding the challenge of building a single model that

fits all the data, resulting in more accurate and flexible outcomes that can integrate various supervised algorithms. Using TDA on the feature space (transposed data) can significantly enhance the convergence abilities of advanced machine learning methods like artificial neural networks (ANNs). TDA minimizes the risk of overlooking crucial insights by diminishing the reliance on machine learning experts to select the correct algorithms, employing existing machine learning methods as input to uncover subtle patterns and insights within localized data. Nicolau et al., 2011 reveals the success of the Mapper algorithm in comparison to the other clustering methods to identify a subset of breast cancer by applying TDA on the dataset consisting of microarray gene expression data related to breast cancer.

In many Natural Language Processing (NLP) tasks, the initial step involves converting text into numerical representations, typically real-valued vectors, for computational purposes. These vectors aim to capture the meaning and relevance of words, with similar words being mapped close together in this vector space. Once text data is transformed into such a metric space, using Topological Data Analysis is a logical choice. TDA can uncover topological features based on the inherent geometry of points in this space. However, interpreting what these topological features, like holes and connected components, signify in the original text can often be unclear (Garcia, 2022).

To clearly understand how TDA can be applied to a dataset as an example, let's assume we have time series dataset which is investigated in (Fujitsu's TDA Technologies, 2021). When looking at the complex time series data, determining whether anomalies or noise are present by just seeing the original signal is a difficult problem. The first step is that the time series data to be analyzed is taken as an argument. The second step is called Embedding. Using time-delay embedding, the input signal is converted into a point cloud in Euclidean space. The trajectory drawn in this step represents the generation process of the input signal as a geometric shape. As the third step, feature extraction is used. In this step, TDA is applied to the point cloud from the previous step, and features are extracted by analyzing the geometric shape. Training and analysis come as the last step. Now the output of feature selection can be used by TDA in the classification process as well as for time-dependent applications like anomaly detection and other machine learning tasks.

Implementations of Topological Data Analysis

Mapper is predominantly employed as a data visualization tool for the purpose of investigating data substructures. *KepplerMapper* is currently known as the only open-source Mapper implementation based on Python that supports general-purpose functionality (Tauzin et al., 2021). There are different potential tools and software platforms implementing TDA to realize mapper and persistent homology. Table 1 presents the majority of the possible software frameworks and tools by utilizing the Python, MATLAB, R, Go, Haskell, Java, Julia, and C++ programming languages. There are various developed and implanted tools, algorithms, and frameworks to realize the topological data analysis applications in different programming languages.

Table 1.

A List Of TDA Tools, Frameworks, Libraries

Framework/ Tool/ Library/Algorithm	Base Programming Languages	Relevant Reference
giotto-tda	Python, C++	(Tauzin et al., 2021)
GUDHI	C++	(The GUDHI Project, 2020)
Scikit-tda	Python	(Saul and Tralie, 2019)
Dionysus 2	C++	(Morozov, 2018)
TopoEmbedding	Python, js	(Bao et al., 2022)
Javaplex	Java	(Tausz et al., 2011)
DIPHA	C++	(Bauer et al., 2017)
Perseus	C++	(Mischaikow and Nanda, 2013)
Persistent	Haskell	(Persistence Filtration, 2023)
Ripser	C++	(Day et al., 2019)
HomCloud	Python	(Obayashi et al., 2022)
Diamorse	Python, C++	(Delgado-Friedrichs, 2015)
Teaspoon	Python	(Teaspoon toolkit, 2023)
RedHom	C++	(Juda and Mrozek, 2014)
CubicleRipser	Python	(Wagner, 2023)
HomcCube	C++	(Kaji et al., 2020)
CliqueTop	MATLAB	(Giusti et al., 2015)
Eirene, TDA	Julia	(Hylton et al., 2019)
Ripser-Live	C++	(Joshi et al., 2019)
CHomP	C++	(Harer et al., 2015)
Hera	C++	(Alipourjeddi and Miri, 2023)
PHAT	C++	(Bauer et al., 2014)
tda (TDA in Go Lang)	Go	(Tda, 2019)
Spark Mapper, Spart TDA	Spark	(Ognis1205/spark-tda, 2023)
Ctl	C++	(Rahul-38-26-0111-0003/awesome-tda, 2023)
Knotter	Python	(Singh et al., 2007)
RIVET	C++	(RivetTDA/rivet, 2023)
TdaToolbox	Python	(Tutorials, 2023).
TTk	C++	(The Topology ToolKit, 2023)
TDAStats	Python	(CRAN - Package TDAstats, 2019)
Python Mapper	Python	(Lizliz – Overview, 2023).
Qsv	Python	(RottenFruits/qsv, 2023)
OpenTDA	Python	(Outlace/OpenTDA, 2023)
TMAP	Python	(Tmap 1.0, 2023)
Kohonen	Python	(Lmjohns3/kohonen, 2023).
GDA Public/geomdata	Python	(GDA toolbox, 2023).
Mapper implementation	Python	(Ksanjeevan/mapper-tda, 2023).
MoguTDA	Python	(Stephenhky/MoguTDA, 2023)
TDA, TDAmapper, TDAstats	R	(Lizliz – Overview, 2023).
Topology Toolkit	C++	(Merylldindin/TdaToolbox, 2023).
Simba, Simpler	C++	(Lizliz – Overview, 2023).
TDAview	R	(Walsh et al., (2020)

Opportunities and Limitations of TDA

TDA has many strong features to overcome the traditional approaches such as ML, DL, and ANNs. There are several restrictions of the traditional machine learning algorithms which are mostly addressed by TDA: identification of multivariate features based on shape, global and local variations, interpretability, sample sizes and bias, dimensionality, and noise. Persistent homology provides a way to reach easily analyzable visual conclusions through mathematical methods exclusively. This becomes valuable when dealing with data that is excessively intricate to analyze visually. Mapper is another tool within the realm of topological data analysis that provides significant benefit in data visualization and exploration. This algorithm condenses information from high-dimensional data into a straightforward topological framework known as a simplicial complex. This approach is especially beneficial for handling large and intricate datasets that would otherwise be challenging to assess visually or through traditional statistical methods. A new feature selection method, multiple scale structures, the representation in lower-dimensions, stability, robustness, high-dimension, and complex data analysis are some of the advantages of TDA (Skaf and Laubenbacher, 2022).

TDA has many powerful characteristics, however, it has also some restrictions. These limitations can be presented in a categorized manner such as *validation, availability, configurations of parameters, computational complexity, and geometric data loss (*Skaf and Laubenbacher, 2022). Even though it has recently begun to be used in many studies by mathematicians, computer scientists and statisticians, it has not yet shown its widespread impact in other scientific fields, especially in applied mathematics, as desired. Due to the lack of sufficient number of research studies within different domains in the literature, obtaining a limited number of resources containing reliable and adequate domain knowledge about TDA brings with it problems such as *availability* problems. Many published studies rely on closed-source software that most researchers cannot access, while open-source tools require more technical expertise. Researchers also need to interpret unfamiliar topological results and often lack of validation against standard tools in their fields, making it challenging to predict TDA's success in new research problems.

One of the challenging issues is related to *parameter configuration* or which inputs including measurements of similarities points or distance should be given to the Mapper or Persistent Homology algorithms. The parameter configuration and input selection have significant impact on the application of performance. The data types also pose some problems in different domains. The challenge of establishing inputs for non-traditional data types is a problem but not unique to TDA and is being explored in various fields. However, there is still room for further research in this area.

Robustness and *stability* are two important characteristics of topological data analysis. It is relatively resilient to noise, but it's not entirely immune to it. Stability properties ensure that output changes are limited compared to input perturbations, but in high-

dimensional data, even small perturbations in each coordinate can result in significant movement in the overall space. Dimensionality reduction, like Principal Component Analysis (PCA), is often used to reduce noise, but it can't eliminate it entirely and may lead to information loss. Mapper may only produce meaningful results within certain parameter ranges, making optimal parameter selection challenging, especially for non-technical users who may not fully understand the algorithm's intricacies.

TDA may have a higher *computational complexity*, particularly when calculating persistent homology across various parameter values, with complexity increasing as data size and feature dimension grow. Efforts to simplify computations have been made, but this remains an ongoing research area. Mapper, a TDA tool, is generally efficient, but it can face computational limitations, particularly in calculating covers and pairwise distances during clustering, especially for higher-dimensional data. While less demanding components can be substituted, dealing with big data inherently involves computational challenges that cannot be eliminated.

The insensitivity of TDA to variations in many geometric features has its advantages, offering features like coordinate invariance and noise resistance. However, it can also be a drawback as TDA may not detect these properties when they are relevant. In practice, this limitation can be mitigated by using TDA alongside other techniques, such as employing a geometrically-sensitive Mapper lens when specific geometric information is needed.

Topological Data Analysis Applications for Intelligent Systems

This section discusses different approaches, various implementations, and several paradigms to demonstrate and realize the strong relationship between topological data analysis, intelligent systems, and applications. Table 2 presents the state of the art for different digital areas and in different applications such as smart health, computational biology, security, intelligent transportation, time-dependent or time series data analysis, now-casting, smart agriculture, intelligent climate, forensic dentistry, critical infrastructures, music composition real time prediction, image analysis, business intelligence, consumer IoT, disaster management, dynamic systems, digital finance, smart materials and structures, sensor networks, triboinformatics, smart factory, smart manufacturing.

In Table 2, we demonstrate how different digital sectors and intelligent applications can apply TDA as a new, robust, and efficient data-driven tool. We present the relevant literature discussing which nontrivial and trendy paradigms can be conducted with TDA. It's crucial to recognize that TDA has a significant impact on various matters and is a easily applicable and efficient tool. Hence, we also discuss in detail these intelligent applications by mentioning each of them.

Table 2.

A Comprehensive Literature Review For TDA In Different Intelligent Applications

Intelligent Systems and Applications	Relevant and Prominent Paradigms	How/Why TDA is used?	References
AI Oncology	AI, Smart Health Single cell analysis, Tumor heterogeneity, Time-series data for cancer Biomedicine, Image analysis	• To select feature by considering noisy, incomplete, high-dimensional nature of biomedical data, • Taking advantage of TDA for the applications such as forecasting treatment prognosis and responses, disease classification, computer-aided diagnosis, tumor segmentation, cellular architecture identification, • To examine the time-series cancer data.	(Bukkuri et al., 2021) (Heilbroner and Mueller, 2021)
AI-powered Cardiology	AI, Smart Health, DL, ML, Cardiovascular image analysis, Data for Heart disease	• To analyze the shape of the intricate data, • To develop a similarity network for peer patients, • To improve machine learning and deep algorithms, • To investigate datasets to forecast the heart disease,	(Kagiyama et al., 2019) (Seetharam et al., 2021) (Seetharam et al., 2020) (Alijanobi and Lee, 2021)
Digital Pathology	AI, Smart Health DL, Classification, Neuroblastoma, Image analysis Big data	• To boost deep learning and machine learning results, • As a dimensionality reduction method, • Topological descriptor.	(Bussola et al., 2021), (Du et al., 2019)
Medical Imaging	AI, Smart Health Textural analysis DL, ML	• To generate filtrations for image texture.	(Bussola et al., 2021), (Singh et al., 2023)

Intelligent Systems and Applications	Relevant and Prominent Paradigms	How/Why TDA is used?	References
Intelligent Biomedicine	AI, Smart Health ML, Dig Data Analytics, Personalized Medicine, Biomedical informatics	• A tool for analysis, data visualization, exploration, • For deriving observations from complex data, • To design intelligent precision medicine and clinical care, • To enhance accuracy of a diagnosis process, • To analyze medical images, • To research on biology, • For investigating the structure of biomolecules, • To obtain optimized healthcare.	(Skaf and Laubenbacher, 2022) (Onyango et al., 2023) (Li et al., 2015) (Saeki et al., 2021) (Rabadan and Blumberg, 2019)
Ageing	AI, Smart Health, Big Data, ML	• A novel Big Data Tool, • To detect some fundamental factors which can be responsible for illnesses and ageing, • To ease the analysis of the complex systems.	(Fülöp et al., 2020)
Forensic Dentistry	AI, ML, Neural Network, DL, Age estimation, Decision-making	• To enhance DL algorithms, • As an alternative method to be used in analysis of X-ray images.	(Bui et al., 2023)
Intelligent Neuroscience	Brain Functions, AI, ML, smart health, Neuroimage, Hypergraph, Big Data	• To simplify intricate brain dynamics with the easily traceable presentations, • To efficiently investigate fMRI datasets without losing useful information, • To examine EEG signals, • To estimate traumatic brain injury.	(Saggar et al., 2018), (Rawson, 2022), (Nielson et al., 2015) (Xu et al., 2021) (Yin et al., 2022) (Phinyomark et al., 2017)

Intelligent Systems and Applications	Relevant and Prominent Paradigms	How/Why TDA is used?	References
Computational Biology and Bioinformatics	Protein Engineering, DL, AL, ML, NLP, image analysis, Deep generative modelling	• To forecasting s protein structure, • To provide a protein modelling by using point clouds, simplicial complexes, filtrations, • To boost protein engineering, • To present molecular generative models with a natural fit scheme, • Topological feature extractor, • To predict secondary structure of a protein, • To forecast the protein function, • To evaluate an abstract version of the large and complex data via topological signatures, • To inspect pattern variability.	(Qiu and Wei, 2023), (Schiff et al., 2023), (Hassanpour et al., 2021), (Martino et al., 2017), (Amézquita et al., 2020), (Topaz et al., 2015), (McGuirl et al., 2020) (Rabadan and Blumberg, 2019)
Blockchain	ML, fraud detection, reinforcement learning	• As the feature selector, • To produce topological features, • Ransomware prediction with a higher accuracy, • Smart contract scam identification.	(Chen et al., 2021) (Fan et al., 2020) (Abay et al., 2019) (Akcora et al., 2019) (Akcora et al., 2018)
Cyber Security	IoT, CPS, CTI	• To find out patterns in big data, • To produce predictors, • To intercept anomalies, • To detect outliers, • Activity prediction, • Device fingerprinting in IoT networks, • Ransomware prediction, • Traffic detection, • Ransomware payments, • Network telescopes, • Attack graphs.	(Akcora et al., 2019) (Cascavilla et al., 2023) (Davies, 2022a) (Davies, 2022b) (Bello et al., 2022)
Avionic Systems	Intelligent Transportation, Avionic data, Big data Avionic network Topologically-driven.	• To produce topological features for the study analyzing the connectivity on airport surface.	(Li et al., 2020) (Chung et al., 2020)

Intelligent Systems and Applications	Relevant and Prominent Paradigms	How/Why TDA is used?	References
Autonomous Vehicles	Intelligent Transportation Object detection, Point cloud data	• To investigate mobile LİDAR point cloud data via focusing on the shapes.	(Syzdykbayev and Karimi, 2020) (Kerboua-Benlarbi et al., 2022) (Liu et al., 2023)
Smart Driving	Intelligent Transportation, ML, Time-series	• To generate topological features, • To enhance ML algorithms, • To analyze time-series data collecting from sensors, • To predict drivers' behavior.	(Frahi et al., 2021) (Li et al., 2020)
Time-dependent/ or Time Series data analysis	Stochastic Process	• Extracting features from high-dimensional and large datasets, • To obtain a feature vector.	(Singh et al., 2023) (Umeda et al., 2019) (Rivera-Castro et al., 2019)
Price Prediction	Ethereum, Blockchain, Time series analysis, Smart contract, Intelligent forecasting, Neural networks, Ensemble Learning	• For graph analysis, • To pursue topological feature belonging to the blockchain network.	(Hafez et. al., 2022) (Abay et al, 2019) (Akcora et al., 2018)
Now-casting	Intelligent forecasting, ML, AI, ANN, DL Time series-data	• As a pipeline approach, Dimensionality reduction, • Visualization, • Improve performance, • UMAP Framework.	(Senekane et al., 2021)
Smart Agriculture	AI, NLP, genetic algorithms	• For simplification of large datasets including more noisy and missing data.	(Jiang et al., 2022) (De la Peña and Granados, 2023)
Intelligent Climate	ML, DL, pattern recognition	• To identify atmospheric rivers, • To obtain the characteristic of shapes and atmospheric river' statistics, • A topological descriptor for feature extraction in a threshold-free way, • To analyze large-scale dataset, • For data skeletonization.	(Muszynski et al., 2019) (Ver Hoef et al., 2023)

Intelligent Systems and Applications	Relevant and Prominent Paradigms	How/Why TDA is used?	References
Critical Infrastructures	Structural health monitoring, Sensor data, dynamics of structures	• To examine large data, • To predict the structural changes and damages in critical infrastructures like bridges, • To offer comparative analysis of different factors that will change the structures such as damage and temperature variations.	(Gowdridge et al., 2022) (Pereira et al., 2021)
Music Composition	AI, ANN, Machine composition	• To analyze a generated graph using raw music data, • To use Overlap matrix to generate an algorithm-based music composition.	(Tran et al., 2023) (Bergomi and Baratè, 2020)
Real Time Prediction	ML, data-driven approach, nonlinear regression, real-time learning	• To help a realization of a decision system in real-time, • To ease the investigation of complex microstructures' shapes and features, • Topological descriptor.	(Yun et al., 2020) (Frahi et al., 2021b)
Image Analysis	AI, ML, Satellite observations, Model interpretation Support vector machines, DNN, DL, Evaluation of Image quality, medical image analysis	• To obtain interpretable insights of a physical system, • To investigate satellite images, • To study on the images of eye fundus as a robust scheme to noisy and missing data.	(Singh et al., 2023), (Ver et al., 2023), (Avilés-Rodríguez et al., 2021)
Consumer IoT	Assemblage theory, IoT, predictive modelling	• To present the shape of the data without a coordinate system, • To make a compressed representation, • To produce hypothesis effectively.	(Novak and Hoffman, 2016)
Disaster Management	ML, Hazards prediction	• To forecast floods, • For flood control, monitoring and prediction, • To classify the hydrological regions based on flood risk levels, • To make a hybrid solution with the usage of unsupervised learning methods, • Its unique features such as deformative-invariance, coordinate-invariance, and compressed-representative.	(Ohanuba et al., 2023) (Flatken et al., 2023)

Intelligent Systems and Applications	Relevant and Prominent Paradigms	How/Why TDA is used?	References
Dynamic Systems	Bifurcation analysis, Chaotic systems	• To make analysis including bifurcation.	(Chukanov, 2023) (Güzel et al., 2022)
Digital Finance	Critical transactions, dynamic systems	• To identify critical transactions, • To analyze a financial time series data, • To detect speculative processes, • It offers early warning signs which encompasses both negative and positive financial bubbles, • To detect rapid increase and decrease transactions.	(Akingbade et al., 2023)
Smart Materials and Structures	structural health monitoring, large data cloud, Big Data	• It analyzes acoustic emission for reliable and early detection, • To extract corrosion-related information.	(Dubuc et. al., 2019) (Anand et al., 2022).
Sensor Networks	Computational Topology, Wireless Sensor Networks	• Cost-efficient computation, • Highest stability and robustness to noisy data, • Analytics for multimodal sensor data, • Feature engineering, • Target recognition capability.	(De Silva and Ghrist, (2007) Barsocchini et al., 2018) (Schrader, 2023)
Triboinformatics	ML, AI, Big Data Data Topology, Data-driven	• big-data framework, • the analysis of surface roughness, • to analyze multi-dimensional datasets, • To analyze visual images, • It focuses on topological features instead of principal components, • Used for friction modelling, • Used for examination of surface roughness, • Be employed for studying the contact between rough surfaces.	(Hasan and Nosonovski, 2022)
Smart Factory	Digital Revolution, IIoT, Big Data, Smart Manufacturing, Digital Twins, Li-Fi, Data Lake	• information processing and analysis tool, • A layer of Data Lake Framework.	(Cha et al., 2020)

Intelligent Systems and Applications	Relevant and Prominent Paradigms	How/Why TDA is used?	References
Smart Manufacturing	AI, Big Data, Industry 4.0, IIoT, DL	• Analyzing multi-dimensional data such as data obtained, • Identifies the shape, the underlying structure of shapes, or the pertinent low-dimensional attributes, • Simplified data, • Predictive analysis.	(Nguyen et al., 2022) (Gua and Banerjee, 2017) (Gua and Banerjee, 2016)

The ***smart healthcare*** paradigm has been developing and growing significantly in recent years (Kocer et al., 2022). There are several intelligent applications and fields including smart health studies such as *AI Oncology, Digital pathology, AI-supported Cardiology, intelligent and personalized biomedicine* applications. Topological data analysis, an innovative Big Data tool, has the potential to aid in the investigation of intricate systems by deriving insights from data through a comprehensive approach relying on topological concepts. TDA has demonstrated its potency as a tool, providing crucial insights into the prognosis of treatment, tumor segmentation and diagnosis, classification of diseases, and the characterization of cellular architecture in cancer research.

We observe that TDA can find applications in numerous fields, extending beyond the study of ***aging*** in ***biology***. While TDA is not inherently exclusive to aging research, it is well-suited for this purpose due to the increasing complexity of the aging process. Given the challenges posed by this complexity, it is worthwhile to explore a new method tailored for intricate data. In contrast to existing Artificial Intelligence (AI) methods and Big Data tools which primarily generate numerical summaries and patterns without considering causality, TDA stands out by extracting knowledge from data in the form of shapes, specifically topological invariants, and revealing non-trivial relationships between these shapes. It achieves this by extracting the intrinsic global structural shape, a holistic descriptor, from noisy multiscale high-dimensional data within a complex system. Because TDA is based on a robust theoretical framework, it is exceptionally well-suited for uncovering complex causal interactions across spatio-temporal scales. Consequently, it has the potential to establish meaningful connections between microscale and macroscopic emergent processes. Therefore, TDA holds promise in expanding our understanding of living systems and contributes to dissecting, to some extent, the underlying processes associated with aging and related diseases. TDA extracts universal topological patterns that remain consistent and invariant across different data sets. It has the potential to facilitate collaboration between scientists and clinicians, particularly in the field of systems biology. TDA can make a substantial contribution to the global effort focused on understanding the intricate and dynamic nature of aging,

which is characterized by complexity, hierarchy, diversity, and emergent properties. TDA provides solutions for the studies of biology. TDA can prove to be a valuable instrument for exploring the structural aspects of biomolecules.

Intelligent Biomedicine is an important application area of TDA. TDA encompasses a collection of techniques rooted in the mathematical domain of algebraic topology. Its primary objective is to characterize and utilize attributes associated with the "shape" of data. (Skaf and Laubenbacher, 2022) provides a comprehensive study with certain applications regarding biomedicine domain. Very important and widespread applications are carried out in this field using TDA. For instance, as precision medicine and clinical care, the patient subtyping, diabetes, aortic stenosis, Asthma, Traumatic brain injury, Oncology are some of them. TDA is utilized for analyzing medical images such as CT (computed tomography) and MRI (magnetic resonance imaging), and histology. The accuracy of diagnosing medical conditions may be difficult, especially when dealing with complex patients who have multiple comorbidities and illnesses characterized by ambiguous or varying symptoms. Computational models have the capacity to integrate a wealth of information that would be impractical to analyze manually. Therefore, these tools have the potential to function as valuable decision-support systems for challenging diagnoses. At this point, TDA can be used to augment the performance of diagnostic systems in case of pulmonary embolism to determine Arrhythmia.

In ***artificial intelligence-based cardiology*** applications, topological data analysis is used as a complex data analysis tool standalone or as a helper technology for machine learning algorithms. It leverages mathematical principles and enhances unsupervised machine learning and is used to construct a network composing of patient-patient similarities in this area. Topological data analysis allows for the integration of complex multidimensional data and the visualization of concealed patterns within that data. Topological data analysis serves as a framework for machine learning, drawing from and combining various machine learning algorithms to comprehend the inherent characteristics and structure of complex data. For instance, (Kagiyama et al., 2021) applies this technique to gain insights into the phenotypic representation which belongs to the left ventricular response patterns during the aortic stenosis progression. (Alijanobi and Lee, 2020) utilize the mapper tool of TDA to estimate heart disease.

In ***digital pathology***, the critical information of pathology is processed by using digital tools. Artificial intelligence schemes, neural networks, and deep learning methods are used for the process and manipulation of pathological data to boost the interpretability and reproducibility of the ML and DL models. In Bussola et al., TDA is employed to create activation maps from various layers of the neural network during various stages of the training process. These activation maps are described using Betti curves and persistence diagrams (PD). TDA is then combined with dimensionality reduction using the uniform manifold approximation and projection (UMAP) technique, as well as clustering using the hierarchical density-based spatial clustering of applications with noise (HDBSCAN)

algorithm. This integration is used to cluster deep features, identify relevant subgroups and structures, and explore different levels of the neural network.

Machine learning algorithms have been widely used in the analysis of ***medical images***. However, there are several issues including the traditional paradigms such as black-box nature, high dimensional data. In recent years, topological data analysis provides innovation with explainable outputs, and efficient image analysis. Different types of image data such as computed tomography images, fMRI (functional MRI) scans, and ultrasound images can be analyzed with the utilization of TDA tools as stated in (Singh et al., 2023).

The analysis of brain activities is one of the important topics in ***intelligent neuroscience***. Topological Data Analysis can be utilized to unveil the comprehensive arrangement of whole-brain activity maps at an individual participant level. This approach provides an interactive representation that avoids the arbitrary aggregation of data in either spatial or temporal dimensions. Brain activities can be presented in a hyper graph including edges with a group of vertices. This hyper graph can be converted to simplicial complexes. The utilization of topological data analysis for data-driven exploration and discovery in preclinical research related to spinal cord injury (SCI) and traumatic brain injury (TBI). Electroencephalography (EEG) serves as a crucial neurophysiological tool for discovering disorders and brain functions. TDA can uncover patterns within EEG signals that go beyond what conventional spectral and temporal features can capture.

Dental age assessment is an important implementation for ***forensic dentistry***. Topological data analysis can be used as a performance tuning tool for deep learning algorithms in such applications. It is considered as a standalone solution or as an underlying powered technology for DL to estimate age by analyzing tooth X-ray images.

Topological data analysis can be applied on ***cyber-security and blockchain*** based research. One of the mostly used tools, Mapper, has primarily been employed for visualization, offering an efficient means for analysts to gain a deeper understanding of extensive datasets, and identifying data points that warrant further examination. There is a huge potential to identify anomalies in the unlabeled classification within network data. Persistent homology can also be used as an analysis method on cybersecurity data. Both mapper and persistent homology are used as anomaly detection approach. The Mapper tool also can be implemented for network telescopes, ransomware payments and attack graphs. On the other hand, the persistent diagram can predict activity, the type of IoT device. In the field of ***cryptocurrency***, TDA is also utilized for analysis, selector of topological features, and for prediction of Bitcoin prices and attacks like ransomware. The relevant studies exhibit that topological features have an important impact on cryptocurrency prices. The local topological features are utilized for prediction dynamics and prices. They figure out that in addition to examining how the features of the topological structure of the Bitcoin network influence Bitcoin price dynamics and formation, it's worth considering that the topological characteristics of

other cryptocurrencies can also impact the price of Bitcoin.

Smart Driving, Autonomous vehicle and intelligent avionic systems are some of the applications of ***intelligent transportation*** in which topological data analysis are utilized as a new and reliable data analysis approach (Dundar and Kaplan, 2022; Unler, 2022). In (Frahi et al., 2021a), smart driving study presents the prediction of driver state by using motion sensors. TDA is used for the selection of topological features. The analysis of time-series data from sensors is conducted. One of the important topics relevant to intelligent transportation is Autonomous driving. TDA is also used as an analysis tool for this purpose. As stated in (Syzdykbayev and Karimi, 2020), persistent homology (PH) stands as a fundamental method in TDA, offering the capacity to examine qualitative characteristics of intricate data across various scales. The application of the PH method to point cloud datasets derived from Laser Imaging Detection and Ranging (LiDAR) technology is growing in significance, driven by the widespread accessibility and adoption of this technology. (Li et al., 2020) informs that using the abstractions provided by algebraic topology for real aviation applications and investigating aviation data sets with approaches encountering topological features are among the recently proposed methods. Various research endeavors, spanning from investigating aircraft trajectories to utilizing geographical data for designing UAV geofences, demonstrate the adaptability of topological data analysis and persistent homology.

A common strategy for addressing the challenges posed by high-dimensional data and large datasets is to extract features, especially from ***time series data***, and utilize the resulting feature vector as a representation of the original time series. There are several intelligent systems which produce different types of time series data such as weather data, heart rate monitoring (EKG) data, rainfall measurements, brain monitoring or electrocardiogram (EEG) data, sensor network traffic data like temperature readings, and prices.

Topological Data Analysis helps in monitoring the topological information derived from the blockchain network for ***price prediction***. TDA, a discipline employed in graph analysis, allows for the tracking of topological characteristics via persistent homology tool. For instance, execution and deployment of smart contracts, token movements, moving volume and account transactions are considered as topological features. The presentation of the dynamic and interactions of cryptocurrencies provide features, these features constitute snapshots which are presented a s graph, and to investigate these snapshots, the persistent homology is utilized. Several researchers have utilized TDA, like in (Abay et al., 2019), (Akcora et al., 2018), and (Chazal and Michel, 2021), to demonstrate the impact of topological features on Bitcoin prices. Additionally, it has been investigated by (Li et al., 2020) to identify token prices' anomalies in the Ethereum network.

Short-term forecasting, commonly referred to as now-casting, entails predicting time-series data for a brief timeframe, typically spanning just a few hours. The examples for

the now-casting applications include predictions related to wind conditions, electricity pricing, electricity demand forecasting, rainfall forecasting, predictions for solar irradiance and predictions regarding solar power output. TDA involves the application of computational geometric and algebraic topological principles to examine data, primarily for tasks like reducing dimensionality and facilitating visualization. To augment the performances of machine learning algorithms such as extreme gradient boosting, linear regression (LR), k-nearest neighbor (k-NN), Random Forest (RF) and Decision Tree (DT). Deformation invariance, Co-ordinate freeness and compressed representation are considered three important topological features. TDA can be defined as a set of statistical techniques that employ topological and geometric principles to identify patterns within data. TDA allows for the examination of overarching characteristics within high-dimensional data, all without necessitating any assumptions or the need for feature selection. This makes it a potent tool for exploring complex datasets, particularly those with multiple dimensions and noise. Additionally, TDA finds utility in tasks such as data visualization and unsupervised learning, including clustering and dimensionality reduction.

The combination of TDA and an ML framework has the potential to be a powerful method for characterizing and detecting various ***climate*** and weather phenomena, including but not limited to jet streams and blocking events (Muszynski et al., 2019). TDA offers a distinctive approach to describing weather events in a dataset. An approach based on TDA has effectively been utilized for the process of data segmentation and skeletonization. The significant benefit of the topological feature descriptors employed in this study is their threshold-free nature, allowing them to efficiently capture the most crucial topological characteristics of atmospheric rivers (Ars). In this way, threshold criteria are not a necessity to be established for the TDA step. Unlike most other AR-detection methods that rely on heuristic approaches, when the spatial resolution of the climate model is altered, no parameter retuning is required in this case. TDA is defined as a method that is likely to be applied without any parameter tuning when different climate change scenarios are analyzed.

The use of topological data analysis has the potential to assist acoustic emission (AE) techniques in detecting early indications of corrosion in prestressed ***concrete structures***. The shape, specifically the topological aspects, of the acoustic emission data cloud, which may contain information related to corrosion, is subsequently examined in a quantitative manner using TDA. The extensive AE data set exhibited holes that appeared and disappeared at specific stages during the corrosion process. TDA is used to measure and analyze these voids, demonstrating their association with corrosion mechanisms and their potential for early detection. These findings underline the capability of TDA to assist in extracting corrosion-related insights from AE data. Moreover, by combining TDA with traditional AE monitoring, there is the potential to provide early and more

accurate indications of concrete cracking before visible external signs appear.

Topological data analysis is a technique within the big-data framework that has found application in the ***analysis of surface*** roughness. TDA involves the use of concepts from topology, a branch of geometry concerned with the properties of objects that remain unchanged under continuous deformations, to analyze multidimensional datasets. To analyze visual images
It focuses on topological features instead of principal components. Usef for friction modelling
TDA has been primarily utilized in the examination of surface roughness, particularly to investigate surface anisotropy across various scales. Additionally, it can also be employed for studying the contact between rough surfaces.

Topological data analysis is an analysis tool with powerful features that has emerged recently to obtain certain inferences by analyzing multi-dimensional different types of data such as data obtained from various networks, graphic data, 3D scanning data, image data, which may be noisy and incomplete. The fundamental concept of TDA revolves around identifying the shape, the underlying structure of shapes, or the pertinent low-dimensional attributes of data that exists in high-dimensional spaces. TDA facilitates the solution of a big problem which is solving and examining very large-scale and sophisticated data, by simplifying it. The Mapper algorithm, as one of the tools belonging to TDA, was applied for the predictive analysis of a semiconductor etching process data set for error detection and a chemical production process data set for yield prediction. (Gua and Banerjee, 2017) is the first successful implementation of TDA in the ***manufacturing*** systems.
Intelligent climate, smart agriculture, critical infrastructures, music composition, real time prediction, image analysis, business intelligence, consumer IoT, disaster management, dynamic systems, digital finance, smart materials and structures, sensor networks triboinformatics, smart factory, smart manufacturing domains exploit ***TDA*** as a cost-efficient computation tool providing highest stability and robustness to noisy data and boosting other AI techniques. TDA is preferred as a mechanism for information processing, an analysis tool, a visualization tool, a simplification approach of complex data in various scales, a layer of data lake framework for some of these applications.

Conclusion

The rapid advancement of digital technologies in recent decades has resulted in a significant increase in available data. To make sense of this vast amount of information, it needs to undergo processing and analysis to reveal hidden meaning that may be concealed in its raw form. By processing such amount of data to get valuable insights, it will be possible to make many processes autonomous today and soon. Due to the

rapid advancements in machine learning and deep learning techniques, researchers have transitioned their focus from conventional automated operations and maintenance to the integration of artificial intelligence. At this point, we give TDA more prominence, which is a rapidly evolving computational data-driven tool, with ongoing developments and advancements. The fundamental concept driving topological data analysis is that a set of data points, often referred to as a data cloud, possesses a distinctive shape, and this shape carries significant meaning and information. The important question is that what is needed, consequently, is an advanced approach to analyze the data cloud, allowing us to reveal its underlying topological structure. TDA is specifically developed to fulfill this objective by leveraging the positional relationships among data points to convert the data cloud into a topological entity, enabling the measurement of topological attributes. This topological entity takes the form of a collection of simplices, referred to as a simplicial complex, which is built by assessing the data cloud's connectivity at a specified scale. TDA provides two commonly and mostly used tools which are Mapper and Persistent Homology. TDA tools are designed to process extensive, high-dimensional, and intricate datasets as input and produce a more straightforward, lower-dimensional representation that preserves topological characteristics linked to shape and connectivity. The primary techniques include persistent homology, which proves valuable in creating a quantitative depiction of homological features across various scales, thus serving as a distinctive topological identifier for the input data. Another key method is Mapper, which is convenient for carrying out exploratory data analysis, constructs a concise visual summary with a graph representation.

This chapter explores various approaches, implementations, and paradigms to illustrate the close connection between topological data analysis, intelligent systems, and applications. It delves into the current state of affairs in different digital domains and their application areas, including smart health, computational biology, security, intelligent transportation, time-dependent data analysis, real-time prediction, smart agriculture, intelligent climate monitoring, forensic dentistry, critical infrastructures, music composition, image analysis, business intelligence, consumer IoT, disaster management, dynamic systems, digital finance, smart materials and structures, sensor networks, triboinformatics, smart factory, and smart manufacturing. Numerous studies have demonstrated the versatility and reliability of topological data analysis, showcasing its efficacy in various domains. This study has thoroughly examined how and why TDA is applied, highlighting its contributions to different research areas. They have provided in-depth insights into the strengths and weaknesses of this method, supported by extensive references from the literature.

References

Abay, N. C., Akcora, C. G., Gel, Y. R., Kantarcioglu, M., Islambekov, U. D., Tian, Y., & Thuraisingham, B. (2019, November). Chainnet: Learning on blockchain graphs with topological features. In 2019 IEEE international conference on data mining (ICDM) (pp. 946-951). IEEE.

Adams, H., Emerson, T., Kirby, M., Neville, R., Peterson, C., Shipman, P., ... & Ziegelmeier, L. (2017). Persistence images: A stable vector representation of persistent homology. Journal of Machine Learning Research, 18.

Akcora, C. G., Dey, A. K., Gel, Y. R., & Kantarcioglu, M. (2018). Forecasting bitcoin price with graph chainlets. In Advances in Knowledge Discovery and Data Mining: 22nd Pacific-Asia Conference, PAKDD 2018, Melbourne, VIC, Australia, June 3-6, 2018, Proceedings, Part III 22 (pp. 765-776). Springer International Publishing.

Akcora, C. G., Li, Y., Gel, Y. R., & Kantarcioglu, M. (2020). BitcoinHeist: Topological data analysis for ransomware prediction on the Bitcoin blockchain. Twenty-Ninth International Joint Conference on Artificial Intelligence Special Track on AI in FinTech, 4439–4445.

Akingbade, Samuel W. and Gidea, Marian and Manzi, Matteo and Nateghi, Vahid, Why Topological Data Analysis Detects Financial Bubbles? (April 14, 2023). Available at http://dx.doi.org/10.2139/ssrn.4418395

Ali, D., Asaad, A., Jimenez, M. J., Nanda, V., Paluzo-Hidalgo, E., & Soriano-Trigueros, M. (2023). A survey of vectorization methods in topological data analysis. IEEE Transactions on Pattern Analysis and Machine Intelligence.

Alipourjeddi, N., & Miri, A. (2023, February). Evaluating Generative Adversarial Networks: A Topological Approach. In 2023 International Conference on Computing, Networking and Communications (ICNC) (pp. 202-206). IEEE.

Aljanobi, F. A., & Lee, J. (2021, January). Topological data analysis for classification of heart disease data. In 2021 IEEE International Conference on Big Data and Smart Computing (BigComp) (pp. 210-213). IEEE.

Amézquita, E. J., Quigley, M. Y., Ophelders, T., Munch, E., & Chitwood, D. H. (2020). The shape of things to come: Topological data analysis and biology, from molecules to organisms. Developmental Dynamics, 249(7), 816-833.

Anand, D. V., Xu, Q., Wee, J., Xia, K., & Sum, T. C. (2022). Topological feature engineering for machine learning based halide perovskite materials design. npj Computational Materials, 8(1), 203.

Avilés-Rodríguez, G. J., Nieto-Hipólito, J. I., Cosío-León, M. D. L. Á., Romo-Cárdenas, G. S., Sánchez-López, J. D. D., Radilla-Chávez, P., & Vázquez-Briseño, M. (2021). Topological data analysis for eye fundus image quality assessment. Diagnostics, 11(8), 1322.

Azizi, T. (2022). Topological Properties of Periodic and Chaotic Attractors. Novel Research Aspects in Mathematical and Computer Science Vol. 8, 90-105.

Baas, N. A., Carlsson, G. E., Quick, G., Szymik, M., & Thaule, M. (2020). Topological Data Analysis. Springer International Publishing.

Bao, X., Liu, G., & Iuricich, F. (2022). TopoEmbedding, a web tool for the interactive analysis of persistent homology. arXiv preprint arXiv:2204.09783.

Barsocchi, P., Cassará, P., Giorgi, D., Moroni, D., & Pascali, M. A. (2018, January). Computational topology to monitor human occupancy. In Proceedings (Vol. 2, No. 2, p. 99). MDPI.

Bauer, U., Kerber, M., & Reininghaus, J. (2014, May). Distributed computation of persistent homology. In 2014 proceedings of the sixteenth workshop on algorithm engineering and experiments (ALENEX) (pp. 31-38). Society for

Industrial and Applied Mathematics.

Bauer, U., Kerber, M., Reininghaus, J., & Wagner, H. (2017). Phat–persistent homology algorithms toolbox. Journal of symbolic computation, 78, 76-90.

Bello, H. J., Palomar-Ciria, N., Baca-García, E., & Lozano, C. (2022). Suicide classification for news media using convolutional neural networks. Health communication, 1-10.

Bergomi, M. G., & Baratè, A. (2020). Homological persistence in time series: an application to music classification. Journal of Mathematics and Music, 14(2), 204-221.

Bubenik, P. (2015). Statistical topological data analysis using persistence landscapes. J. Mach. Learn. Res., 16(1), 77-102.

Bui, R., Iozzino, R., Richert, R., Roy, P., Boussel, L., Tafrount, C., & Ducret, M. (2023). Artificial Intelligence as a Decision-Making Tool in Forensic Dentistry: A Pilot Study with I3M. International Journal of Environmental Research and Public Health, 20(5), 4620.

Bukkuri, A., Andor, N., & Darcy, I. K. (2021). Applications of topological data analysis in oncology. Frontiers in artificial intelligence, 4, 659037.

Bussola, N., Papa, B., Melaiu, O., Castellano, A., Fruci, D., & Jurman, G. (2021). Quantification of the immune content in neuroblastoma: Deep learning and topological data analysis in digital pathology. International Journal of Molecular Sciences, 22(16), 8804.

Carlsson, G., & Vejdemo-Johansson, M. (2021). Topological Data Analysis with Applications. Cambridge: Cambridge University Press. doi:10.1017/9781108975704

Cascavilla, G., Tamburri, D. A., Leotta, F., Mecella, M., & Van Den Heuvel, W. (2023). Counter-terrorism in cyber-physical spaces: Best practices and technologies from the state of the art. Information and Software Technology, 107260.

Cha, B., Park, S., Shin, B. C., & Kim, J. (2020). Draft design of Li-fi based acquisition layer of DataLake framework for IIoT and smart factory. In Advances in Networked-based Information Systems: The 22nd International Conference on Network-Based Information Systems (NBiS-2019) (pp. 317-324). Springer International Publishing.

Chazal, F., & Michel, B. (2021). An introduction to topological data analysis: fundamental and practical aspects for data scientists. Frontiers in artificial intelligence, 4, 108.

Chen, F., Wan, H., Cai, H., & Cheng, G. (2021). Machine learning in/for blockchain: Future and challenges. Canadian Journal of Statistics, 49(4), 1364-1382.

Chukanov, S. N. (2023). Comparison of complex dynamical systems based on topological data analysis. Computer Research and Modeling, 15(3), 513-525.

Chung, S. H., Ma, H. L., Hansen, M., & Choi, T. M. (2020). Data science and analytics in aviation. Transportation research part E: logistics and transportation review, 134, 101837.

CRAN - Package TDAstats. (2019, December 12). The Comprehensive R Archive Network. https://cran.r-project.org/web/packages/TDAstats/index.html

Davies, T. (2022). A Review of Topological Data Analysis for Cybersecurity. arXiv

preprint arXiv:2202.08037.

Davies, T. (2022). Topological Data Analysis for Anomaly Detection in Host-Based Logs. arXiv preprint arXiv:2204.12919.

De la Peña, N., & Granados, O. M. (2023). Artificial intelligence solutions to reduce information asymmetry for Colombian cocoa small-scale farmers. Information Processing in Agriculture.

De Silva, V., & Ghrist, R. (2007). Homological sensor networks. Notices of the American mathematical society, 54(1).

Delgado-Friedrichs, O. (2015). Diamorse: digital image analysis using discrete Morse theory and persistent homology.

Deng, R., & Duzhin, F. (2022). Topological data analysis helps to improve accuracy of deep learning models for fake news detection trained on very small training sets. Big Data and Cognitive Computing, 6(3), 74.

Dey, T. K., Hou, T., & Mandal, S. (2019). Persistent 1-cycles: Definition, computation, and its application. In Computational Topology in Image Context: 7th International Workshop, CTIC 2019, Málaga, Spain, January 24-25, 2019, Proceedings 7 (pp. 123-136). Springer International Publishing.

Dmitriy Morozov. Dionysus 2. (2018). Library for computing persistent homology. URL

Du Nguyen, H., Tran, K. P., Castagliola, P., & Megahed, F. M. (2022). Enabling smart manufacturing with artificial intelligence and big data: a survey and perspective. In Advanced Manufacturing Methods (pp. 1-26). CRC Press.

Du, Y., Zhang, M., Stonis, G., & Juan, S. (2019, November). Topological Data Analysis on Magnetic Resonance Image Biomarkers. In 2019 IEEE International Conference on Bioinformatics and Biomedicine (BIBM) (pp. 1185-1187). IEEE.

Dubuc, B., Ebrahimkhanlou, A., & Salamone, S. (2019). Corrosion monitoring of prestressed concrete structures by using topological analysis of acoustic emission data. Smart Materials and Structures, 28(5), 055001.

Dundar, O., & Kaplan, S. (2022). Swarm Concept and Swarm UAV Systems. Current Studies in Basic Sciences, Engineering and Technology, 183. ISRES Publishing.

Edelsbrunner, H., & Harer, J. L. (2022). Computational topology: an introduction. American Mathematical Society.

Eroglu, A. (2022). 5G and Beyond Networks for Digital Transformation: Opportunities and Productivity. Current Studies in Digital Transformation and Productivity, 98.

Fan, S., Fu, S., Luo, Y., Xu, H., Zhang, X., & Xu, M. (2022, October). Smart Contract Scams Detection with Topological Data Analysis on Account Interaction. In Proceedings of the 31st ACM International Conference on Information & Knowledge Management (pp. 468-477).

Flatken, M., Podobas, A., Fellegara, R., Basermann, A., Holke, J., Knapp, D., ... & Gerndt, A. (2023). VESTEC: Visual Exploration and Sampling Toolkit for Extreme Computing Urgent decision-making meets HPC: Experiences and future challenges. IEEE Access.

Frahi, T., Chinesta, F., Falco, A., Badias, A., Cueto, E., Choi, H. Y., ... & Duval, J. L. (2021b). Empowering advanced driver-assistance systems from topological

data analysis. Mathematics, 9(6), 634.

Frahi, T., Sancarlos, A., Galle, M., Beaulieu, X., Chambard, A., Falco, A., ... & Chinesta, F. (2021a). Monitoring weeder robots and anticipating their functioning by using advanced topological data analysis. Frontiers in Artificial Intelligence, 4, 761123.

Fujitsu's TDA Technologies. (2021, March 31). http://tda.labs.fujitsu.com/en/

Fülöp, T., Desroches, M., Cohen, A. A., Santos, F. A. N., & Rodrigues, S. (2020). Why we should use topological data analysis in ageing: Towards defining the "topological shape of ageing". Mechanisms of Ageing and Development, 192, 111390.

Garcia, J. S. (2022). Applications of topological data analysis to natural language processing and computer vision (Doctoral dissertation, Colorado State University).

GDA toolbox. (2023). GDA toolbox v1.0 manual. Online. Available: GitHub Pages. https://geomdata.github.io/gda-public/

Giusti, C., Pastalkova, E., Curto, C., & Itskov, V. (2015). Clique topology reveals intrinsic geometric structure in neural correlations. Proceedings of the National Academy of Sciences, 112(44), 13455-13460.

Gowdridge, T., Dervilis, N., & Worden, K. (2022). On topological data analysis for structural dynamics: an introduction to persistent homology. ASME Open Journal of Engineering, 1.

Guo, W., & Banerjee, A. G. (2016, August). Toward automated prediction of manufacturing productivity based on feature selection using topological data analysis. In 2016 IEEE international symposium on assembly and manufacturing (ISAM) (pp. 31-36). IEEE.

Guo, W., & Banerjee, A. G. (2017). Identification of key features using topological data analysis for accurate prediction of manufacturing system outputs. Journal of Manufacturing Systems, 43, 225-234.

Güzel, I., Munch, E., & Khasawneh, F. (2022). A case study on identifying bifurcation and chaos with CROCKER plots. arXiv preprint arXiv:2204.06321.

Hafez, S. M., El Nainay, M., Abougabal, M., & Kosba, A. (2022, December). Ethereum Price Prediction using Topological Data Analysis. In 2022 IEEE Global Conference on Artificial Intelligence and Internet of Things (GCAIoT) (pp. 146-153). IEEE.

Harer, J., Mischaikow, K., Mukherjee, S., & Duke University Durham United States. (2015). Inferring network controls from topology using the chomp database (p. 0015). tech. report, Duke University Durham United States.

Hasan, M. S., & Nosonovsky, M. (2022). Triboinformatics: machine learning algorithms and data topology methods for tribology. Surface Innovations, 10(4–5), 229-242.

Hassanpour, A., Izadkhah, H., & Isazadeh, A. (2021, December). Protein Secondary Structure Prediction using Topological Data Analysis. In 2021 7th International Conference on Signal Processing and Intelligent Systems (ICSPIS) (pp. 1-6). IEEE.

Hatcher A. (2002). Algebraic topology. Cambridge University Press.

Heilbroner, S., & Mueller, J. (2021). AJS-1 Identifying subgroups at high-risk of ICI associated cardiac adverse events: An approach using topological data analysis. Annals of Oncology, 32, S232. https://github.com/mrzv/dionysus.

Hensel, F., Moor, M., & Rieck, B. (2021). A survey of topological machine learning methods. Frontiers in Artificial Intelligence, 4, 681108.

Hylton, A., Henselman-Petrusek, G., Sang, J., & Short, R. (2019). Tuning the performance of a computational persistent homology package. Software: Practice and Experience, 49(5), 885-905.

Jiang, T., Huang, M., Segovia-Dominguez, I., Newlands, N., & Gel, Y. R. (2022, June). Learning space-time crop yield patterns with zigzag persistence-based LSTM: Toward more reliable digital agriculture insurance. In Proceedings of the AAAI Conference on Artificial Intelligence (Vol. 36, No. 11, pp. 12538-12544).

Joshi, M., Joshi, D., & Sharma, V. (2019, September). Persistent homology techniques for big data and machine intelligence: A survey. In International Conference on Machine Intelligence and Signal Processing (pp. 97-111). Singapore: Springer Singapore.

Juda, M., & Mrozek, M. (2014). CAPD: RedHom v2-homology software based on reduction algorithms. In Mathematical Software–ICMS 2014: 4th International Congress, Seoul, South Korea, August 5-9, 2014. Proceedings 4 (pp. 160-166). Springer Berlin Heidelberg.

Kagiyama, N., Shrestha, S., Farjo, P. D., & Sengupta, P. P. (2019). Artificial intelligence: practical primer for clinical research in cardiovascular disease. Journal of the American Heart Association, 8(17), e012788.

Kaji, S., Sudo, T., & Ahara, K. (2020). Cubical Ripser: Software for computing persistent homology of image and volume data. arXiv preprint arXiv:2005.12692.

Kerboua-Benlarbi, S., Mziou-Sallami, M., & Doufene, A. (2022). A novel GAN-based system for time series generation: Application to autonomous vehicles scenarios generation. In AI and IoT for Sustainable Development in Emerging Countries: Challenges and Opportunities (pp. 325-352). Cham: Springer International Publishing.

Kocer, S., Ocal, H., Dundar, O., & Dundar, H. B. (2022). Use of IoT and Wearable Technology Design Fundamentals in Healthcare Industry. Current Studies in Basic Sciences, Engineering and Technology, 168. ISRES Publishing.

Ksanjeevan/mapper-tda. (2023). Mapper implementation (Topological data analysis) in Python. Online. Available: GitHub. https://github.com/ksanjeevan/mapper-tda

Li, L., Cheng, W. Y., Glicksberg, B. S., Gottesman, O., Tamler, R., Chen, R., ... & Dudley, J. T. (2015). Identification of type 2 diabetes subgroups through topological analysis of patient similarity. Science translational medicine, 7(311), 311ra174-311ra174.

Li, M. Z., Ryerson, M. S., & Balakrishnan, H. (2019). Topological data analysis for aviation applications. Transportation Research Part E: Logistics and Transportation Review, 128, 149-174.

Li, Y., Islambekov, U., Akcora, C., Smirnova, E., Gel, Y. R., & Kantarcioglu, M. (2020). Dissecting Ethereum blockchain analytics: What we learn from topology and geometry of the Ethereum graph? In Proceedings of the 2020 SIAM international conference on data mining (pp. 523-531). Society for Industrial and Applied Mathematics.

Li, Z., Xu, S., & Wang, T. (2020). A Method of Interest Degree Mining Based on Behavior Data Analysis. International Journal of Pattern Recognition and Artificial Intelligence, 34(09), 2059030.

Liu, W. K., Bessa, M. A., Chinesta, F., Li, S., & Trask, N. (2023). Special issue of computational mechanics on machine learning theories, modeling, and applications to computational materials science, additive manufacturing, mechanics of materials, design and optimization. Computational Mechanics, 1-2.

Lizliz - Overview. (2023). Online. Available: GitHub. https://github.com/lizliz

Lmjohns3/kohonen. (2023). Kohonen vector quantizers. Online. Available: GitHub. https://github.com/lmjohns3/kohonen

Martino, A., Rizzi, A., & Mascioli, F. M. F. (2018, July). Supervised approaches for protein function prediction by topological data analysis. In 2018 International joint conference on neural networks (IJCNN) (pp. 1-8). IEEE.

McGuirl, M. R., Volkening, A., & Sandstede, B. (2020). Topological data analysis of zebrafish patterns. Proceedings of the National Academy of Sciences, 117(10), 5113-5124.

Merylldindin/TdaToolbox. (2023). Topological data analysis toolkit, with examples. Online. Available: GitHub. https://github.com/merylldindin/TdaToolbox

Mischaikow, K., & Nanda, V. (2013). Morse theory for filtrations and efficient computation of persistent homology. Discrete & Computational Geometry, 50, 330-353.

Munch, E. (2017). A User's Guide to Topological Data Analysis. Journal of Learning Analytics, 4(2), 47–61. https://doi.org/10.18608/jla.2017.42.6

Muszynski, G., Kashinath, K., Kurlin, V., & Wehner, M. (2019). Topological data analysis and machine learning for recognizing atmospheric river patterns in large climate datasets. Geoscientific Model Development, 12(2), 613-628.

Nguyen, H. D., Tran, K. P., Zeng, X., Koehl, L., Castagliola, P., & Bruniaux, P. (2019, July). Industrial Internet of Things, big data, and artificial intelligence in the smart factory: A survey and perspective. In ISSAT International Conference on Data Science in Business, Finance and Industry (pp. 72-76).

Nicolau, M., Levine, A. J., & Carlsson, G. (2011). Topology based data analysis identifies a subgroup of breast cancers with a unique mutational profile and excellent survival. Proceedings of the National Academy of Sciences, 108(17), 7265-7270.

Nielson, J. L., Paquette, J., Liu, A. W., Guandique, C. F., Tovar, C. A., Inoue, T., ... & Ferguson, A. R. (2015). Topological data analysis for discovery in preclinical spinal cord injury and traumatic brain injury. Nature communications, 6(1), 8581.

Novak, T., & Hoffman, D. L. (2016). Visualizing emergent identity of assemblages in the consumer Internet of Things: a topological data analysis approach. Available at SSRN 2840962.

Obayashi, I., Nakamura, T., & Hiraoka, Y. (2022). Persistent homology analysis for materials research and persistent homology software: HomCloud. journal of the physical society of Japan, 91(9), 091013.

Ognis1205/spark-tda. (2023). SparkTDA is a package for Apache spark providing topological data analysis Functionalities. Online. Available: GitHub. https://

github.com/ognis1205/spark-tda

Ohanuba, F. O., Ismail, M. T., & Ali, M. K. M. (2023). Application of topological data analysis to flood disaster management in Nigeria. Environmental Engineering Research, 28(5).

Onyango, A., Okelo, B., & Omollo, R. (2023). Topological Data Analysis of COVID-19 Using Artificial Intelligence and Machine Learning Techniques in Big Datasets of Hausdorff Spaces. Journal of Data Science and Intelligent Systems.

Outlace/OpenTDA. (2023). Open source Python library for topological data analysis (TDA). Online. Available: GitHub. https://github.com/outlace/OpenTDA

Paik, T., & van Koert, O. (2023). Expected invariants of simplicial complexes obtained from random point samples. Archiv der Mathematic, 120(4), 417-429.

Pereira, L. M., Torres, L. C., & Amini, M. H. (2021, June). Topological data analysis for network resilience quantification. In Operations Research Forum (Vol. 2, pp. 1-17). Springer International Publishing.

Persistence Filtration. (2023). Introduction Hackage. Online. Available: https://hackage.haskell.org/package/Persistence-2.0.3/docs/Persistence-Filtration.html

Phinyomark, A., Ibanez-Marcelo, E., & Petri, G. (2017). Resting-state fMRI functional connectivity: Big data preprocessing pipelines and topological data analysis. IEEE Transactions on Big Data, 3(4), 415-428.

Qiu, Y., & Wei, G. W. (2023). Artificial intelligence-aided protein engineering: from topological data analysis to deep protein language models. Briefings in Bioinformatics, bbad289.

Rabadan, R., & Blumberg, A. (2019). Topological Data Analysis for Genomics and Evolution: Topology in Biology. Cambridge: Cambridge University Press. doi:10.1017/9781316671665

Rahul-38-26-0111-0003/awesome-tda. (2023). A curated list of topological data analysis (TDA) resources and links. Online. Available: GitHub. https://github.com/rahul-38-26-0111-0003/awesome-TDA

Rawson, M. G. (2022). Entropic Hyper-Connectomes Computation and Analysis. arXiv preprint arXiv:2203.00519.

Rivera-Castro, R., Pilyugina, P., Pletnev, A., Maksimov, I., Wyz, W., & Burnaev, E. (2019). Topological data analysis of time series data for B2B customer relationship management. arXiv preprint arXiv:1906.03956.

RivetTDA/rivet. (2023). RIVET is a tool for topological data analysis, in particular two-parameter persistent homology. Online. Available: GitHub. https://github.com/rivetTDA/rivet

RottenFruits/qsv. (2023). This application is data structure visualizer by topological data analysis method. Online. Available: GitHub. https://github.com/RottenFruits/qsv

Saeki, Y., Saito, A., Cousty, J., Kenmochi, Y., & Shimizu, A. (2021, September). Statistical modeling of pulmonary vasculatures with topological priors in CT volumes. In International Workshop on Interpretability of Machine Intelligence in Medical Image Computing (pp. 108-118). Cham: Springer International Publishing.

Saggar, M., Sporns, O., Gonzalez-Castillo, J., Bandettini, P. A., Carlsson, G., Glover, G., & Reiss, A. L. (2018). Towards a new approach to reveal dynamical organization of the brain using topological data analysis. Nature communications, 9(1), 1399.

Saul, N. and Tralie, C. (2019). Scikit-tda: Topological data analysis for python. URL https://doi.org/10.5281/zenodo.2533369.

Schiff, Y., Chenthamarakshan, V., Hoffman, S. C., Ramamurthy, K. N., & Das, P. (2022, May). Augmenting molecular deep generative models with topological data analysis representations. In ICASSP 2022-2022 IEEE International Conference on Acoustics, Speech and Signal Processing (ICASSP) (pp. 3783-3787). IEEE.

Schrader, P. T. (2023, June). Topological multimodal sensor data analytics for target recognition and information exploitation in contested environments. In Signal Processing, Sensor/Information Fusion, and Target Recognition XXXII (Vol. 12547, pp. 114-143). SPIE.

Seetharam, K., Raina, S., & Sengupta, P. P. (2020). The role of artificial intelligence in echocardiography. Current Cardiology Reports, 22, 1-8.

Seetharam, K., Shrestha, S., & Sengupta, P. P. (2021). Cardiovascular imaging and intervention through the lens of artificial intelligence. Interventional Cardiology: Reviews, Research, Resources, 16.

Sekuloski, P., & Dimitrievska Ristovska, V. (2019). MAPPER ALGORITHM AND IT'S APPLICATIONS. Mathematical Modeling.

Senekane, M., Matjelo, N. J., & Taele, B. M. (2021, December). Improving Short-term Output Power Forecasting Using Topological Data Analysis and Machine Learning. In 2021 International Conference on Electrical, Computer and Energy Technologies (ICECET) (pp. 1-6). IEEE.

Shiraj, M. M. B., Rahman, M. M., Hossain, M. M., Haque, M. D., Al-Imran, M., Liza, M. Z. A., ... & Akhter, N. (2023). An approximation to Čech complex using median of triangles for computing Betti numbers of some point cloud data. World Journal of Advanced Engineering Technology and Sciences, 9(2), 037-048.

Singh, G., Mémoli, F., & Carlsson, G. E. (2007). Topological methods for the analysis of high dimensional data sets and 3d object recognition. PBG@ Eurographics, 2, 091-100.

Singh, M. K., Chaube, S., Pant, S., Singh, S. K., & Kumar, A. (2023). An integrated image visibility graph and topological data analysis for extracting time series features. Decision Analytics Journal, 100253.

Singh, R. P., & Wilsey, P. A. (2022, December). Persistence Homology of Proximity Hyper-Graphs for Higher Dimensional Big Data. In 2022 IEEE International Conference on Big Data (Big Data) (pp. 65-74). IEEE.

Singh, Y., Farrelly, C. M., Hathaway, Q. A., Leiner, T., Jagtap, J., Carlsson, G. E., & Erickson, B. J. (2023). Topological data analysis in medical imaging: current state of the art. Insights into Imaging, 14(1), 1-10.

Skaf, Y., & Laubenbacher, R. (2022). Topological data analysis in biomedicine: A review. Journal of Biomedical Informatics, 130, 104082.

Srinivasan, R., & Chander, A. (2019). Understanding Bias in Datasets using Topological Data Analysis. In AISafety@ IJCAI.

Stephenhky/MoguTDA. (2023). Topological data analysis in Python: Simplicial complex. Online. Available: GitHub. https://github.com/stephenhky/MoguTDA

SymphonyAI Industrial. (2020). TDA and Machine Learning: Better Together https://symphonyindustrial.ai/wp-content/uploads/2020/08/TDA_and_ML-Better_Together2020-V2.pdf

Syzdykbayev, M., & Karimi, H. A. (2020). Persistent homology for detection of objects from mobile lidar point cloud data in autonomous vehicles. In Advances in Computer Vision: Proceedings of the 2019 Computer Vision Conference (CVC), Volume 2 1 (pp. 458-472). Springer International Publishing.

Tausz, A., Vejdemo-Johansson, M., & Adams, H. (2011). A research software package for persistent (co) homology. In International Congress on Mathematical Software (pp. 129-136).

Tauzin, G., Lupo, U., Tunstall, L., Pérez, J. B., Caorsi, M., Medina-Mardones, A. M., ... & Hess, K. (2021). giotto-tda: A topological data analysis toolkit for machine learning and data exploration. The Journal of Machine Learning Research, 22(1), 1834-1839.

Tda. (2019, 11). tda: Topological data analysis in Golang. Online. Available: https://pkg.go.dev/github.com/kshedden/tda

Teaspoon: Topological signal processing in Python — teaspoon 1.3.7 documentation. (n.d.). Site not found · GitHub Pages. https://teaspoontda.github.io/teaspoon/

The GUDHI Project. (2020). GUDHI User and Reference Manual. GUDHI Editorial Board, 3.1.1 edition. URL https://gudhi.inria.fr/doc/3.1.1/.

The Topology ToolKit. (2023). Topology ToolKit. Online. Available: https://topology-tool-kit.github.io/

tmap 1.0. (2023). Welcome to tmap's documentation! — tmap 1.0 documentation. Online. Available: https://tmap.readthedocs.io/en/latest

Topaz, C. M., Ziegelmeier, L., & Halverson, T. (2015). Topological data analysis of biological aggregation models. PloS one, 10(5), e0126383.

Tran, M. L., Lee, D., & Jung, J. H. (2023). Machine composition of Korean music via topological data analysis and artificial neural network. Journal of Mathematics and Music, 1-22.

Tsaneva-Atanasova, K., & Scotton, C. (2023). How to handle big data for disease stratification in respiratory medicine? Thorax, 78(7), 640-642.

Tutorials. (2023). GUDHI library. Online. Available: https://gudhi.inria.fr/tutorials/

Umeda, Y., Kaneko, J., & Kikuchi, H. (2019). Topological data analysis and its application to time-series data analysis. Fujitsu Scientific & Technical Journal, 55(2), 65-71.

Unler, T. (2022). Vehicles of the Near Future: Driverless Autonomous Cars. Current Studies in Basic Sciences, Engineering and Technology, 70. ISRES Publishing.

Ver Hoef, L., Adams, H., King, E. J., & Ebert-Uphoff, I. (2023). A primer on topological data analysis to support image analysis tasks in environmental science. Artificial Intelligence for the Earth Systems, 2(1), e220039.

Ver Hoef, L., Adams, H., King, E. J., & Ebert-Uphoff, I. (2023). A primer on topological data analysis to support image analysis tasks in environmental science. Artificial Intelligence for the Earth Systems, 2(1), e220039.

Wagner, H. (2023). Slice, Simplify and Stitch: Topology-Preserving Simplification

Scheme for Massive Voxel Data. In 39th International Symposium on Computational Geometry (SoCG 2023). Schloss Dagstuhl-Leibniz-Zentrum für Informatik.

Walsh, K., Voineagu, M. A., Vafaee, F., & Voineagu, I. (2020). TDAview: an online visualization tool for topological data analysis. Bioinformatics, 36(18), 4805-4809.

Wasserman, L. (2018). Topological Data Analysis. Annual Review of Statistics and Its Application. 5, 1, 501-532.

Watanabe, S., & Yamana, H. (2020, December). Deep neural network pruning using persistent homology. In 2020 IEEE Third International Conference on Artificial Intelligence and Knowledge Engineering (AIKE) (pp. 153-156). IEEE.

Xu, X., Drougard, N., & Roy, R. N. (2021). Topological Data Analysis as a New Tool for EEG Processing. Frontiers in Neuroscience, 15, 761703.

Yin, J., & Wang, Y. (2022, May). Topological correlation of brain signals. In ICASSP 2022-2022 IEEE International Conference on Acoustics, Speech and Signal Processing (ICASSP) (pp. 1411-1415). IEEE.

Yun, M., Argerich, C., Cueto, E., Duval, J. L., & Chinesta, F. (2020). Nonlinear regression operating on microstructures described from Topological Data Analysis for the real-time prediction of effective properties. Materials, 13(10), 2335.

About the Authors

Alperen EROGLU received his B.Sc. degree at the department of electronics and computer education as the valedictorian of the department from Fırat University, Elazığ, Turkey in 2009, the M.Sc. and Ph.D. degrees in computer engineering from METU, Ankara, Turkey in 2015 and 2020, respectively. During the M.Sc. and Ph.D., he researched and studied in the fields of robotics, artificial intelligence, software engineering, system architecture and modeling, embedded systems, wireless networks, computer networks. He accomplished his M.Sc. and Ph.D. studies in the field of wireless networks. He has a post-doctorate study at the department of computer engineering at METU. He is currently an assistant professor at the department of computer engineering at Necmettin Erbakan University. His research interests are in 5G mobile networks, the Internet of Things, wireless and computer networks. He is a member of the Wireless Systems, Networks and Cybersecurity Laboratory (WINSLab). He is a member of IEEE.

E-mail: aeroglu@erbakan.edu.tr, **ORCID:** 0000-0002-1780-7025

Hatice UNLU EROGLU received her B.Sc. degree at the department of mathematics from Ege University, İzmir, Turkey in 2011, her Ph. D. degree at the department of mathematics from METU, Ankara, Turkey in 2018. Her research area is geometric topology, mapping class group, Riesz spaces and topological data analysis. She has been a research assistant at Necmettin Erbakan University since 2018.

E-mail: hueroglu@erbakan.edu.tr, **ORCID:** 0000-0002-9106-459X

Similarity Index

The similarity index obtained from the plagiarism software for this book chapter is 14%.

CHAPTER 4

Optimization of Controller Coefficients by Using Metaheuristic Algorithms

Hasan Huseyin BILGIC
Necmettin Erbakan University, Türkiye

Engin Hasan COPUR
Necmettin Erbakan University, Türkiye

To Cite This Chapter:
Bilgic, H. H. & Copur, E. H. (2023). Optimization of Controller Coefficients by Using Metaheuristic Algorithms. In S. Kocer. & O. Dundar (Eds.), *Artificial Intelligence Applications in Intelligent Systems* (pp. 61–72). ISRES Publishing.

Introduction

In mathematics, optimization, which is as old as human history, refers to systematically examining or solving problems by selecting real or integer values and placing them in the function in order to maximize or minimize a real function. In engineering, it is defined as achieving certain goals (such as reducing costs, increasing profits, increasing capacity utilization, increasing efficiency) by using the resources available for any system (such as labor, time, finance, processes, raw materials, capacity, equipment) in the most efficient way.

The concept of metaheuristic, which was first proposed in 1986, is formed from the combination of the Greek words “meta” and “heuristic” and means more advanced or higher level heuristic (Glover, F. 1986). The algorithms expressed in this context are called artificial intelligence algorithms. In cases where classical optimization approaches fail to find the exact solution in solving a problem, metaheuristic algorithms are used to find an approximate solution. Metaheuristic algorithms are developed by observing events occurring in nature and describing these events with a series of mathematical expressions. Artificial Bee Colony Algorithm, which observes the resource search behavior of bees, the Particle Swarm Optimization algorithm, which examines the behavior of living swarms, and the Genetic Algorithm, which examines the biological processes in living things can be given as examples of metaheuristic search algorithms (Sevim et al. 2021, Bilgiç et al. 2016). Table 1 gives the chronology of Metaheuristic Search Algorithms that are frequently used in the optimization of engineering problems.

Table 1.

Time History of Metaheuristic Algorithms

No	Algorithm Name	Year	Reference
1	Genetic Algorithm (GA)	1975	Holland 1975
2	Tabu Search (TS)	1986	Glover 1986
3	Ant Colony Optimization (ACO)	1992	Colorni & Maniezzo 1991
4	Particle Swarm Optimization (PSO)	1995	Eberhart & Kennedy 1995
5	Differential Evolution (DE)	1997	Storn & Price 1997
6	Big bang-big Crunch (BBBC)	2006	Erol & Eksin 2006
7	Artificial Bee Colony Algorithm (ABC)	2007	Karaboğa 2007
8	Firefly Algorithm (FA)	2009	Yang 2009
9	Cuckoo Search (CS)	2009	Yang & Deb 2009
10	Teaching-learning based Optimization (TLBO)	2011	Rao et al. 2011
11	Ray Optimization (RO)	2012	Kaveh & Khayatazad 2012
12	Grey Wolf Optimizer (GWO)	2014	Mirjalili et al. 2014
13	Dragonfly Algorithm (DF)	2016	Mirjalili 2016
14	Whale Optimization Algorithm (WOA)	2016	Mirjalili & Lewis 2016
15	Vibrating Particles System (VPS)	2017	Kaveh & Ghazaan 2017

In this part of the book, the use of artificial intelligence techniques in optimizing controller parameters will be explained in detail. For clarity, the controller gains of PID and LQR controllers will be optimized for position control of a mass in a mass-spring-damper system. Artificial Bee Colony (ABC) Algorithm, proposed by Derviş Karaboğa (Karaboğa 2007) in 2007, was used as the metaheuristic optimization algorithm. ABC Algorithm is a population-based, intuitive search algorithm that mimics the collective intelligence features of bees, such as resource-seeking behavior for nectar and water, learning, remembering, and sharing information. ABC algorithm entirely consists of three different bee groups called employed bees, onlooker bees and scout bees. In the algorithm model, some colonies were selected as worker bees and the remaining half were designated as onlooker bees. There is only one worker bee for each nectar source, and the number of worker bees equals the nectar source. Food resources are the parameters of the system to be optimized. Figure 1 presents the flow diagram of the ABC Algorithm.

Figure 1.

Flow-chart of ABC Algorithm (Randazzo, A. 2012)

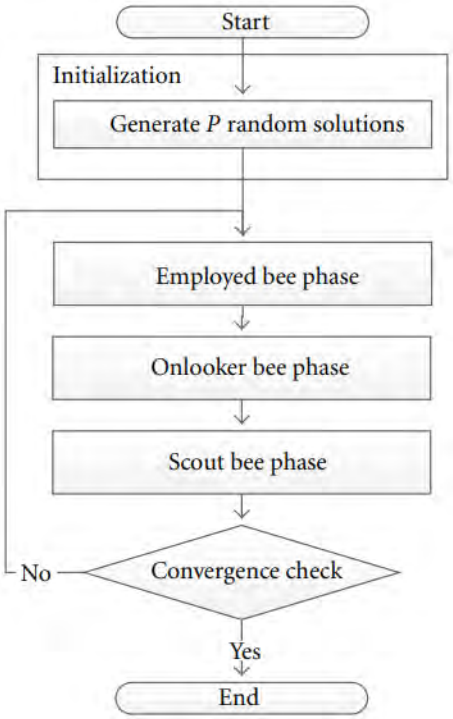

In recent years, many studies have been conducted on the applications of the ABC Algorithm to engineering problems with the purpose of the optimization of controller gains. Demirören et al., designed a FOPID controller to balance an unstable magnetic ball suspension system and optimized the controller gains by using different algorithms, including ABC algorithm. Demirören et al. demonstrated that the ABC algorithm can be successfully applied in controller design. (Demirören et al. 2021). Hadi et al. have designed hybrid Fuzzy–proportional–integral–derivative controller tuned by using the ABC algorithm to suppress vibration of experimental horizontal flexible platestructure. The results revealed that the vibrations were able to be suppressed more successfully with the proposed hybrid-PID controller than the traditional PID controller (Hadi et al. 2020). In another study, Bilgiç et al. designed an LQR controller for a flexible link and optimized the coefficients of the LQR controller according to a user-defined objective function with the Bees Algorithm. To show the effectiveness of their proposed approach, it was compared with the controllers designed in the previous studies in the literature. The experimental results showed that their proposed method was significantly successful at improving transient response behaviour (Bilgiç et al. 2021). Kesarkar and Selvaganesan have designed a fractional order PID controller for a high-dimensional multimode system to minimize the performance indices in the literature. They optimized the controller parameters with the ABC algorithm and compared the results with the 'deterministic' Nelder–Mead simplex algorithm (Kesarkar & Selvaganesan 2015).

Conventional Controllers

Proportional-Integral-Derivative PID Controller

The first use of PID controllers in feedback control technologies dates to the 1920s-1940s (Han, 2009). Today, it is still one of the most preferred controllers in many industrial automation applications. Indeed, the increasing demand for PID controllers is driven by its simple structure, easy implementation and its proven capability for active disturbance suppression and tracking control.

A general PID controller is a combination of three components connected together in parallel as shown in Figure 2. In this general PID configuration, the error signal $e(t)$ is the difference between the reference signal $r(t)$ and the measured output $y(t)$, i.e., $e(t) = r(t) - x(t)$. Then, the control input produced by PID controller can be determined by

$$u(t) = K_p e(t) + K_i \int_0^t e(t)dt + K_d \frac{de(t)}{dt} \quad (1)$$

The control input is the summation of three components on the right side of Equation 1. The first component is the proportional controller, and it is proportional to the error signal by a gain K_p. The second component is known as the integral controller, and it is proportional to the integral of the error signal by a gain K_d. Finally, the last term is known as the derivative controller, and it is proportional to the derivative of the error signal by a gain K_d.

In the PID control method, these gains must be tuned properly to satisfy the desired control performance since the gains have great effects on the transient and steady state response characteristics of a controlled plant. Therefore, different tuning methods have been developed and used in the real time applications.

Figure 2.

Mass-spring-damper system

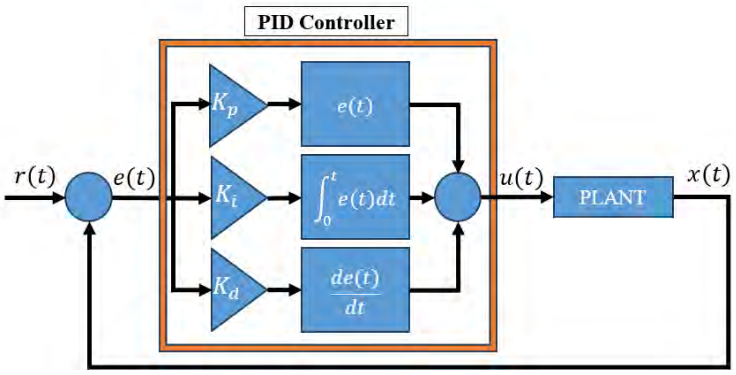

Linear Quadratic Regulator (LQR) Controller

Linear Quadratic Controller is an optimal control approach in the control community. Optimal control approaches are based on minimizing a cost function or performance index formed in terms of the integral performance measures such as the integral square

error (Bishop, 2017). These performance measures are usually determined by design criteria.

Now consider a state space model in a compact form as

$$\dot{x} = Ax + Bu$$

where $x \in R^n$ is the state vector, $A \in R^{n\times n}$ is the system matrix, $B \in R^{n\times m}$ is the control input matrix, and $u \in R^m$ is the control input. In LQR control theory, the following quadratic cost function

$$J = \int_0^\infty (x^\top Qx + u^\top Ru)dt$$

can be minimized by using the state feedback control law introduced as

$$u = -Kx$$

where $K \in R^{m\times n}$ is the feedback gain and when $K = R^{-1}B^\top P$, the minimum cost function value is obtained. Here, $P \in R^{n\times n}$ is a symmetric positive definite matrix and is found by solving the algebraic Riccati equation given by

$$A^\top P + PA - PBR^{-1}B^\top P + Q = 0$$

where $Q \in R^{n\times n}$ is the symmetric semi-positive definite state cost matrix and $R \in R^{n\times n}$ is the symmetric positive definite control cost matrix. They are also known as the weighting matrices of the cost function.

The selection of these weighting matrices is very important in the controller design since they have a strong influence on the system response. Therefore, the control engineers may need to put a lot of time and effort into the selection process. When a large Q matrix is selected, small changes in the state vector x is generally observed to keep the cost function value as minimum as possible. On the other hand, larger R matrix also results in less control effort to ensure a minimum cost function value but also larger changes in states. Therefore, there is a trade-off between the requirements for the states and the control inputs. This design issue can be solved by using artificial intelligence methods in predicting the weighting matrices so that they are able to meet the desired control performance.

Case Study: Mass-Spring-Damper System

Mass-spring-damper system is one of the widely used mechanical systems to develop control laws either for reference tracking or disturbance rejection. This useful mechanical structure consists of three basic mechanical components, i.e., mass, spring, and damper. In linear control theory, these components are usually selected to be time-invariant. However, in some cases, a mass-spring-damper system with time-varying coefficients (Li & Yin, 2017) or state dependent coefficients (Zhuo et al., 2019) can be also considered. In this case study, a linear mass-spring-damper architecture is only considered since the

main purpose of this study is to show how to use the artificial intelligence algorithms for fine-tuning of control parameters.

A general schematic representation of the mass-spring-damper system is illustrated in Figure 3. As seen clearly, the system includes the linear spring with the constant stiffness coefficient k and the linear damper with the constant damping coefficient b. When the external force $F(t)$ is applied to the mass of m, it starts moving on a horizontal frictionless surface. The mathematical model of this system can be derived from Newton's 2nd Law and given by

$$m\ddot{x} + b\dot{x} + kx = F \tag{2}$$

Figure 3.

Mass-spring-damper system

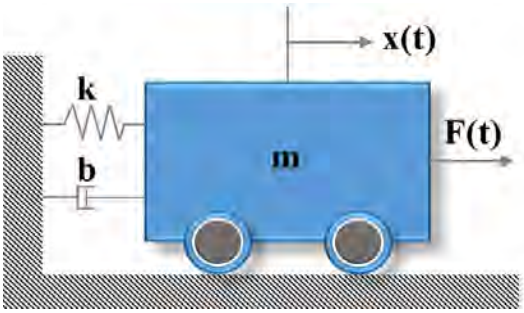

Now, the control problem can be stated as follows:

For the mass-spring-damper system whose dynamics is mathematically expressed by Equation 2, find the control input $u(t)$ such that the output of the system can follow a reference input. In the control architecture shown in Figure 4, the position of the mass $x(t)$ is the output of the system and the external force $F(t)$ is the control input $u(t)$. In addition, PID and LQR controllers are separately implemented in the control architecture to control the position of the mass.

Figure 4.

Control architecture for position control of mass-spring-damper system with a) PID controller b) LQR controller

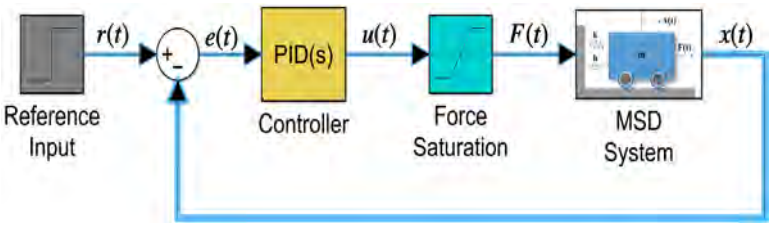

(a)

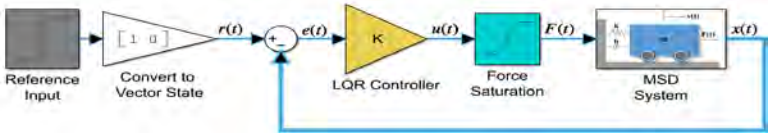

(b)

When optimizing controller parameters, fine-tuning is made by taking the transient system response into consideration. In controller design with metaheuristic research algorithms, the system response is evaluated with user-defined functions. Traditional fitness functions, whose effectiveness has been proven in the literature, are frequently used for this purpose (Ho et al. 1996, Mousakazemi 2021). In this study, the traditional fitness functions Integral Absolute Error (IAE), Integral Square Error (ISE) and Integral Time Absolute Error (ITAE) were used. These functions are presented by Equation 3-5. In the equations, e represents the error between the reference value and the system response.

$$IAE = \int_0^t |e(t)|dtIAE = \int_0^t |e(t)|dt \quad (3)$$

$$ISE = \int_0^t e^2(t)dtISE = \int_0^t e^2(t)dt \quad (4)$$

$$ITAE = \int_0^t t|e(t)|dtITAE = \int_0^t t|e(t)|dt \quad (5)$$

Traditional fitness functions often fail to improve the system's transient response as desired. In this case, the designer must update the fitness function in line with the requirements given for transient time behaviour. While a tolerable overshoot can be defined in some systems, some systems can be expected to respond very quickly.

Figure 5.

Step Response of 2nd order System and transient response characteristics

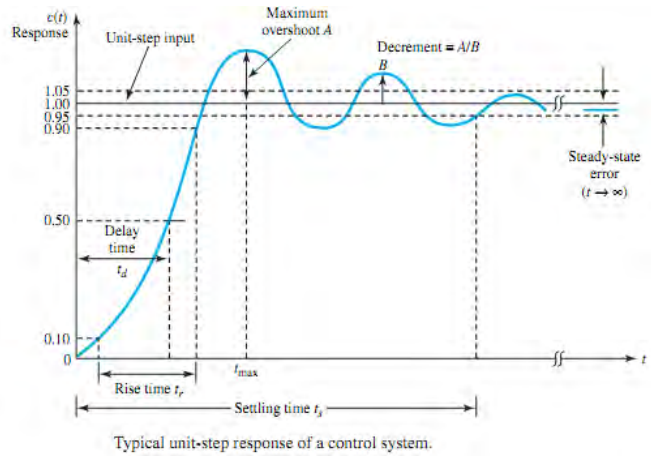

Typical unit-step response of a control system.

The fitness function can be defined as follows, based on the transient behavior of a system given in Figure 5.

$$J_{OBJ} = w_1 t_d + w_2 t_r + w_3 t_s + w_4 t_p + w_5 e_{ss} + w_6 A \quad (6)$$

Here; w_i is the weight factor, t_d is the delay time, t_r is the rise time, t_s is the settling time, t_p is the time to reach the maximum, e_{ss} is the steady state error A, the maximum overshoot. The objective function (OBJ) for the system under consideration is defined as in Equation 6.

$$OBJ = 3.417t_r + 2.072t_s + 1.851t_p + 0.991A \quad (7)$$

While determining the weights of the objective function, the objective function is designed so that the effects of rise time, settling time, peak time and maximum overshoot are equal to each other. While optimizing controller gains, it systematically searches for PID gains (k_p, k_i and k_d) and LQR weights(q_1, q_2 and r) in the search space with the ABC algorithm. The success of the results is determined by the convergence of the fitness functions and objective function values to zero. Algorithm was run for 50 worker bees, 0.4 modification rate and 100 iterations. PID coefficients (k_p, k_i and k_d) and LQR weights (q_1, q_2 and r) obtained as a result of optimization are presented in Table 1. In addition, PID coefficients and LQR gains obtained by traditional methods are also shared to demonstrate the success of the proposed approach.

Table 1.

Optimised Controller Parameters

	PID gains			LQR weights and gain			
	k_p	k_i	k_d	q_1	q_2	r	K
IAE	499.73	6.26	81.29	500	4.25	0.0001	[705.3091 96.0861]
ISE	500	6.2	76.69	500	2.7982	0.0001	[705.3091 88.25]
ITAE	438.82	6.26	71.72	500	4.3844	0.0001	[705.3091 96.7771]
OBJ	438.82	6.26	71.72	500	4.9198	0.0001	[705.3091 99.4914]
non-optimized	14.07	3.4	10.2822	200	200	0.02	[98.2162 102.9766]

The changes in IAE, ISE, ITAE and OBJ function values are given in Figure 6. When Figure 6 is examined, it can be seen that the local minimum value for all fitness functions and objective functions is provided for PID controllers. In Table 2, the minimum values for the fitness functions and the objective functions are given.

Figure 6.

Convergence graphs

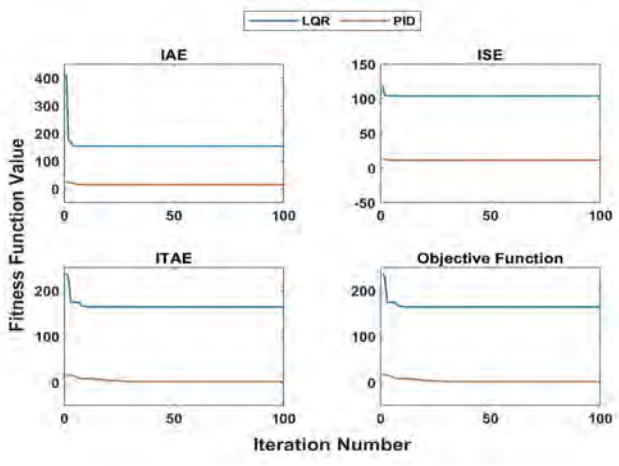

Table 2.

Minimum values of the fitness and objective functions

	PID	LQR
IAE	14.437	154.008
ISE	11.311	104.123
ITAE	2.243	164.245
OBJ	3.024	3.4345

The unit step responses of ABC Algorithm based PID and LQR controllers designed for the mass-spring-damper system are shown in Figure 7 for each function. To demonstrate the success of the proposed approaches, the responses of PID and LQR controllers designed with traditional approaches were compared. When the figures are examined, it can be seen that the transient time responses can be improved with the proposed methods.

Figure 7.

Time responses controlled by optimised PID, LQR and non-optimised controllers

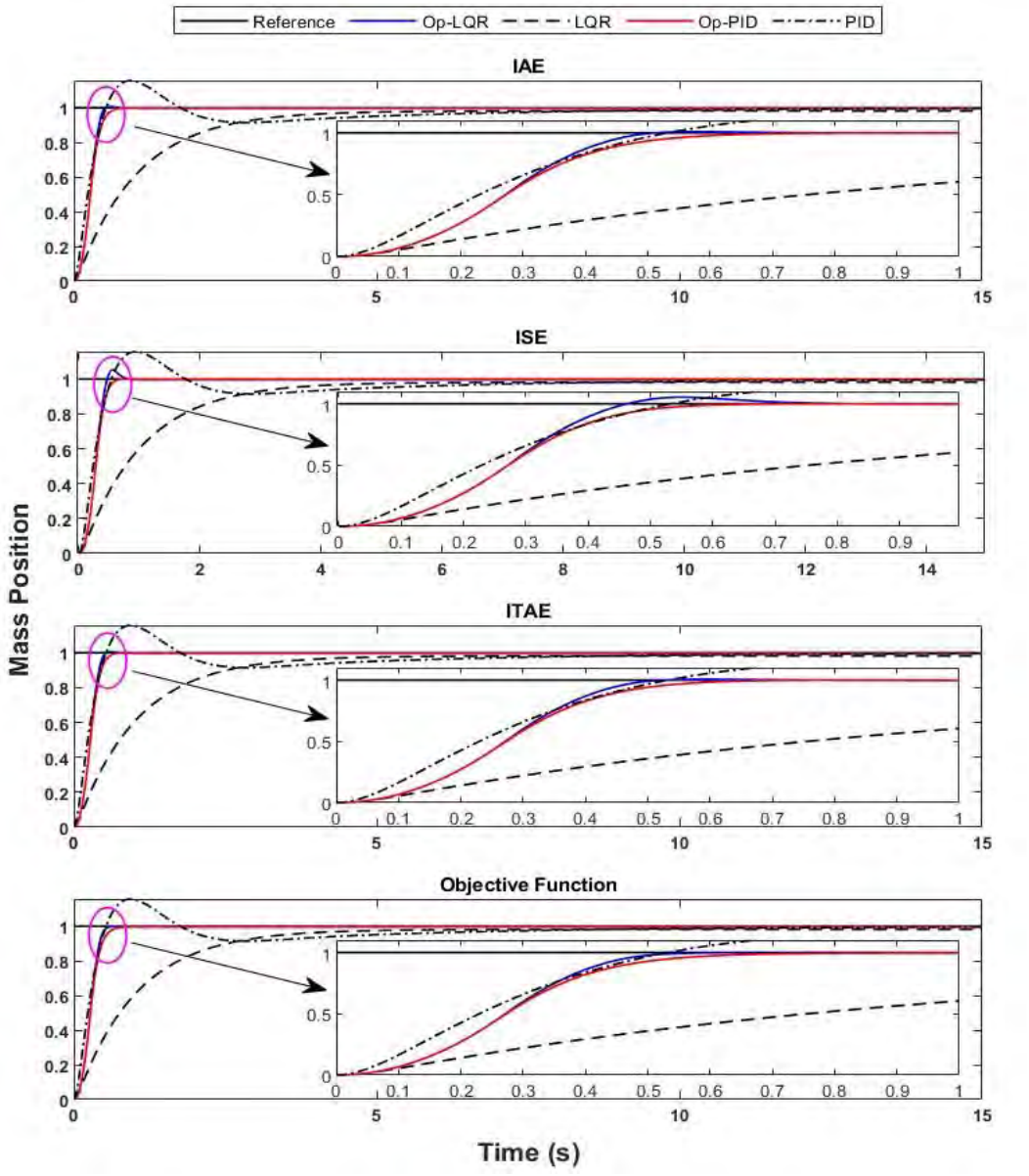

Conclusion

PID and LQR controllers are frequently used in industrial applications. The success of these controllers depends on fine-tuning of the gain coefficients while taking control performance into account. However, when the fine-tuning process is performed by using traditional methods, the desired performances cannot always be achieved. This study demonstrates how to use metaheuristic research algorithms in optimization controller parameters and specificaly focuses on optimizing the controller parameters of a physical system. Although the approach is explained through a case study, this approach can be easily applied in the controller designs of different complex systems.

References

Bilgic, H. H., Sen, M. A., & Kalyoncu, M. (2016). Tuning of LQR controller for an experimental inverted pendulum system based on The Bees Algorithm. *Journal of Vibroengineering*, *18*(6), 3684-3694.

Bilgic, H. H., Sen, M. A., Yapici, A., Yavuz, H., & Kalyoncu, M. (2021). Meta-heuristic tuning of the LQR weighting matrices using various objective functions on an experimental flexible arm under the effects of disturbance. *Arabian Journal for Science and Engineering*, *46*(8), 7323-7336.

Bishop, R. C. & Dorf, R. H. (2017) Modern control systems. 13th Edition,

Colorni, A., Dorigo, M., & Maniezzo, V. (1991, December). Distributed optimization by ant colonies. In *Proceedings of the first European conference on artificial life* (Vol. 142, pp. 134-142).

Demirören, A., Ekinci, S., Hekimoğlu, B., & Izci, D. (2021). Opposition-based artificial electric field algorithm and its application to FOPID controller design for unstable magnetic ball suspension system. *Engineering Science and Technology, an International Journal*, *24*(2), 469-479.

Eberhart, R., & Kennedy, J. (1995, October). A new optimizer using particle swarm theory. In *MHS'95. Proceedings of the sixth international symposium on micro machine and human science* (pp. 39-43). Ieee.

Erol, O. K., & Eksin, I. (2006). A new optimization method: big bang–big crunch. *Advances in engineering software*, *37*(2), 106-111.

Glover, F. (1986). Future paths for integer programming and links to artificial intelligence. *Computers & operations research*, *13*(5), 533-549.

Hadi, M. S., Darus, I. Z. M., Tokhi, M. O., & Jamid, M. F. (2020). Active vibration control of a horizontal flexible plate structure using intelligent proportional–integral–derivative controller tuned by fuzzy logic and artificial bee colony algorithm. *Journal of Low Frequency Noise, Vibration and Active Control*, *39*(4), 1159-1171.

Han, J. (2009). From PID to active disturbance rejection control. IEEE transactions on Industrial Electronics, 56(3), 900-906.

Ho, W. K., Gan, O. P., Tay, E. B., & Ang, E. L. (1996). Performance and gain and phase margins of well-known PID tuning formulas. *IEEE Transactions on Control Systems Technology*, *4*(4), 473-477.

Holland, J. (1975). Adaptation in natural and artificial systems, univ. of mich. press. *Ann*

Arbor, *7*, 390-401.

Karaboga, D., & Basturk, B. (2007). A powerful and efficient algorithm for numerical function optimization: artificial bee colony (ABC) algorithm. *Journal of global optimization*, *39*, 459-471.

Kaveh, A., & Ilchi Ghazaan, M. (2017). A new meta-heuristic algorithm: vibrating particles system. *Scientia Iranica*, *24*(2), 551-566.

Kaveh, A., & Khayatazad, M. (2012). A new meta-heuristic method: ray optimization. *Computers & structures*, *112*, 283-294.

Kesarkar, A. A., & Selvaganesan, N. (2015). Tuning of optimal fractional-order PID controller using an artificial bee colony algorithm. *Systems Science & Control Engineering*, *3*(1), 99-105.

Li, Z., & Yin, Z. (2017, May). Position tracking control of mass spring damper system with time-varying coefficients. In 2017 29th Chinese Control and Decision Conference (CCDC) (pp. 4994-4998). IEEE.

Mirjalili, S. (2016). Dragonfly algorithm: a new meta-heuristic optimization technique for solving single-objective, discrete, and multi-objective problems. *Neural computing and applications*, *27*, 1053-1073.

Mirjalili, S., & Lewis, A. (2016). The whale optimization algorithm. *Advances in engineering software*, *95*, 51-67.

Mirjalili, S., Mirjalili, S. M., & Lewis, A. (2014). Grey wolf optimizer. *Advances in engineering software*, *69*, 46-61.

Mousakazemi, S. M. H. (2021). Comparison of the error-integral performance indexes in a GA-tuned PID controlling system of a PWR-type nuclear reactor point-kinetics model. *Progress in Nuclear Energy*, *132*, 103604.

Randazzo, A. (2012). Swarm optimization methods in microwave imaging. *International Journal of Microwave Science and Technology*, *2012*.

Rao, R. V., Savsani, V. J., & Vakharia, D. P. (2011). Teaching–learning-based optimization: a novel method for constrained mechanical design optimization problems. *Computer-aided design*, *43*(3), 303-315.

Sevim, U. K., Bilgic, H. H., Cansiz, O. F., Ozturk, M., & Atis, C. D. (2021). Compressive strength prediction models for cementitious composites with fly ash using machine learning techniques. *Construction and Building Materials*, *271*, 121584.

Storn, R., & Price, K. (1997). Differential evolution–a simple and efficient heuristic for global optimization over continuous spaces. *Journal of global optimization*, *11*, 341-359.

Yang, X. S. (2009, October). Firefly algorithms for multimodal optimization. In *International symposium on stochastic algorithms* (pp. 169-178). Berlin, Heidelberg: Springer Berlin Heidelberg.

Yang, X. S., & Deb, S. (2009, December). Cuckoo search via Lévy flights. In *2009 World congress on nature & biologically inspired computing (NaBIC)* (pp. 210-214). Ieee.

Zhuo, M., Xia, M., & Sun, Q. (2019). Analytical solution of a mass-spring system containing shape memory alloys: Effects of nonlinearity and hysteresis. International Journal of Solids and Structures, 171, 189-200.

About the Authors

Hasan Huseyin BILGIC is received MSc. from Department of Mechanical Engineering, Mustafa Kemal University, Hatay, Turkey, in 2014 and then received PhD from Department of Mechanical Engineering, İskenderun Technical University, Hatay, Turkey, in 2018. Now he is Assistant Professor at Department of Aeronautical Engineering, Necmettin Erbakan University, Konya, Turkey. His current research interests include command/input shaping, sliding mode control, artificial intelligence, linear and nonlinear control systems, UAV system design and control.

E-mail: bilgichh@gmail.com, ORCID: 0000-0001-6006-8056

Engin Hasan COPUR received his B.Sc. and M.Sc. degrees in mechanical engineering from Gazi University, Ankara, Turkey, in 2007 and 2011, respectively. He also earned a Ph.D. degree in electronics and electrical engineering from the University of Southampton, Southampton, U.K., in 2017. Between 2009 and 2012, he served as a Research Assistant in the Department of Mechanical Engineering at Gazi University. Since 2017, he has held the position of Assistant Professor in the Department of Astronautical Engineering at Necmettin Erbakan University, Konya, Turkey. His current research interests include linear and nonlinear control methods including SMC, MRAC and SDRE, learning control, repetitive control, and their applications to biomechanical, aeronautical and astronautical research areas.

E-mail: ehcopur@erbakan.edu.tr, ORCID: 0000-0003-0837-1255

Similarity Index

The similarity index obtained from the plagiarism software for this book chapter is 20%.

CHAPTER 5

Artificial Intelligence Applications for Microstrip Antennas

Rabia TOPRAK

Karamanoglu Mehmetbey University, Türkiye

To Cite This Chapter:
Toprak, R. (2023). Artificial Intelligence Applications for Microstrip Antennas. In S. Kocer. & O. Dundar (Eds.), *Artificial Intelligence Applications in Intelligent Systems* (pp. 73–84). ISRES Publishing.

Introduction

Important equipments in communication applications are antennas. To transmite an information taking to a supply and receivie from another supply, antenna structures are utilized. Antennas that radiate electromagnetic energy are essential means for the telecommunication applications. There are several antena types such as microstrip, horn, log-periodic, monopol, Vivaldi, dipol, loop, Bow-Tie and etc. There are vital parameters used for antenna applications such as operating frequency, gain, and radiation pattern. The other parameters are Voltage Standing Wave Ratio (VSWR), impedance, bandwith, directivity and etc. They explain the characteristics of antennas. For example, the efficiency of the antenna structure is an another important parameter. The efficiency is very important because it defines a ratio of the power reached to the antenna related to the power beamed from the antenna. The change of the power radiated by an antenna as a assembly of the direction away from the antenna is defined as the radiation pattern. Therefore, far field graphics such as gain, electric field explain with pattern graphics (Balanis, 2013).

Microstrip antennas (MAs) have two conduction layer. There is a dielectric layer called as subtrate between the layers. Substrate is a material has different dielectric electrical parameters. The permittivity and thickness of substrate could be formed differently by each companies. The MAs design make easily. MAs are also known as microstrip patch antennas, too. Therefore, MAs are prefered in large research/development fields (Abbassi, Badra, Allam, & El-Rafei, 2019; B. J. Kwaha, O. N. Inyang, 2011; Bahrami, Moloudian, Miri-Rostami, & Bjorninen, 2021; Dey & Mittra, 1996; Kanj & Popovic, 2005; Khan, De, & Uddin, 2013; Nalam, Rani, & Mohan, 2014; Peixeiro, 2011; Rabbani & Ghafouri-Shiraz, 2017; Soontornpipit, Furse, & Chung, 2004; Top, Gültekin, & Uzer,

2017, 2020b, 2020a; Top, Ünlü, Gültekin, & Uzer, 2019; Uyanik, Uzer, Top, & Gultekin, 2020; Yang, Kishk, Wireless, & 2008, n.d.). MAs have many advantages. One of the advantages is that can directly be printed onto a PCB (Printed Circuit Board). The other advantage is low design cost. Easy design, lightness, huge design utility and etc. are possible to sort as other positives. The drawbacks of MAs are small gain value. By applying different methods, the gain values of MAs are able to increase. So, MAs are wanted for any different research/development applications all over the world (Singh & Tripathi, 2011).

The parameters of MAs develop day by day. Especially Artificial Intelligence (AI) Applications are very popular to make this. AI is the popular and developing technology of today and the future. AI Applications are investigating for antenna application systems (Dundar, Yelken, & Kocer, 2022; Güneşer, 2019; Q. Liu, Yang, Zhuang, Barnawi, & A Alzahrani, 2019; Prajapati, Sadanandam, & Nalla, 2020; Rentapalli & Roy, 2023; Wu & Feng, 2018). Intelligent Antennas/Systems are prefered in the literature due to implement several applications (Shi, Lian, Cui, Chen, & Liu, 2022). Also, 5G applications, biomedical researches, industiral solutions and etc. are some examples for AI Antenna Applications.

In this chapter, AI Applications of microstrip antennas are explained by expanding from samples in the literature. Machine Learning, Deep Learning and Artificial Neural Network (ANN) Applications are presented.

Machine Learning Applications

Machine learning (ML) is a subfield of artificial intelligence (AI) that focuses on building systems that improve or learn the performance based on the data they consume. AI is a huge term that refers to machines or systems that mimic human intelligence. Machine learning and artificial intelligence are often considered together. They are used interchangeably in some cases, but they are not the same. An important difference is that while all machine learning solutions are AI, not all AI solutions are ML.

Today, ML works everywhere. When we interact with use social media, banks or shop online, ML algorithms come into play to ensure we have an efficient, seamless and secure experience. Machine learning and the technology within this framework are developing rapidly.

ML is so popular and is frequently used to design and analyse MAs in the literature. For example, ML based on ANN algorithms is used to optimize the proposed design (Tak, Kantemur, Sharma, & Xin, 2018). Here, 3-D printed 75-110 GHz slotted waveguide array antenna (SWAA) is presented. Design parameters and the angle of slots are optimized with ML. Firstly, the SWAA is designed in HFSS and Multilayer perceptions (MLPs) are successfully applied. SWAA is printed by the 3-D printer. Then, metallization is applied to SWAA, and its performance is compared with each other. The figure of optimized SWAA is presented in Figure 1.

Figure 1.

(a) The photograph of fabricated SWAA, (b) (left and middle) SWAA after metalization, (right) ready SWAA for measurement (Tak et al., 2018)

(a)

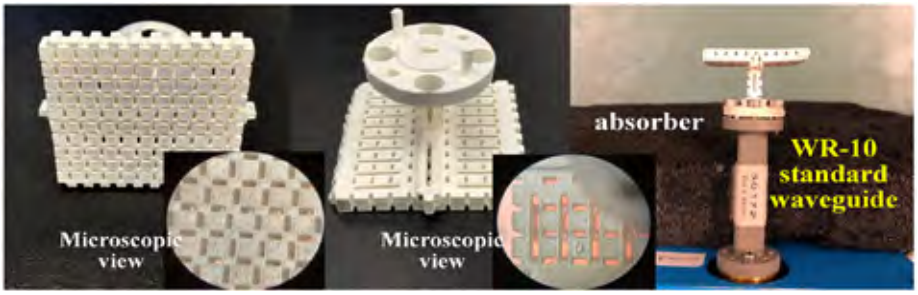

(b)

In another example, ML is used to obtain intelligent antenna synthesis systems (Shi et al., 2022). The system could select the suitable antenna type and geometric dimension of antenna. SVM (Support Vector Machine) is used to classify the antenna type. The performance values of different antenna types are analysed. Microstrip, horn and spiral antenna types are utilized to show the efficiency/accuracy of proposed model. Figure 2 shows the proposed antenna types from (Shi et al., 2022). Figure 3 shows the return loss graphs according to antenna types.

Figure 2.

Top wiev of (a) microstrip patch, (b) colonical horn, (c) spiral antenna (Shi et al., 2022)

(a) (b) (c)

Figure 3.

(a) The return loss of (a) microstrip patch, (b) colonical horn, (c) spiral antenna (Shi et al., 2022)

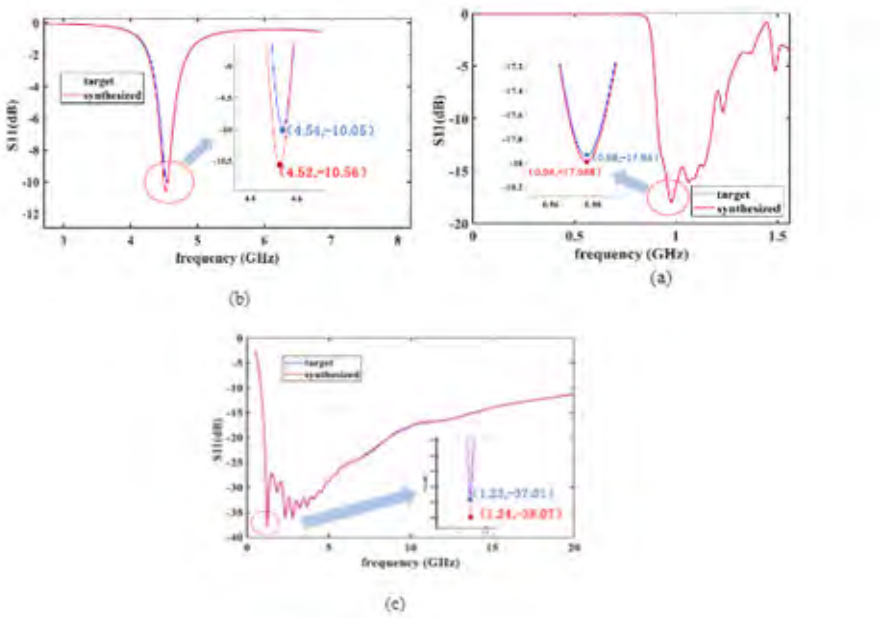

The intelligent antenna systhesis system is realized the smart antenna productions. When Figure 2 and 3 are examined, it is shown that ML algorithm is successfully worked. The return loss graphics of wanted and proposed/designed antennas are very compatible with each other. So, the geometric antenna parameters are obtained from the system.

ML is used to optimize an antenna array structure for 5G mobile communication applications (Zhang, Akinsolu, Liu, & Zhang, 2022). Antenna array operates from 36 to 40 GHz. The substrate has zero gap and integrated a waveguide. The localization and dimension of vias are optimized by ML algorithm. To do this, parallel surrogate model-assisted hybrid differential evolution for antenna synthesis (PSADEA) is utilized. In Figure 4, there is the configuration of proposed antenna array. There are three vias. Feeding method is coaxial probe. By using ML algorithm, the position and size of vias are examined. According to conventional method, PSADEA optimization method has more advantages both efficiency and solutions. Once the proposed antenna is compared other antennas, gain value is higher than others. Impedance matching is well. Therefore, the antenna is suitable candidate for 5G mobile applications.

Figure 4.

The design of antenna array (Zhang et al., 2022)

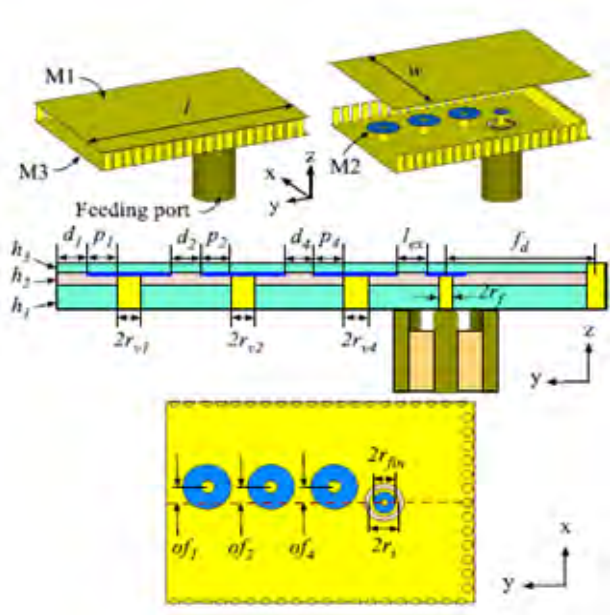

In another study, decoupling structure design is taken over by using ML algorithm (Huang, Yang, & Wang, 2023). K-means algorithm and Masked auto encoding (MAE) method are used to design decoupling structure. With this work, the efficiency of a proposed antenna obtained from intelligent algorithm is evidenced by achieving -18 dB return loss value between 3.5 and 9.7 GHz. Neutralization line is utilized for validating the aaccuracy of proposed optimization method. Figure 5 shows the proposed antenna configuration obtained from (Huang et al., 2023).

Figure 5.

Firstly proposed antenna desing (Huang et al., 2023)

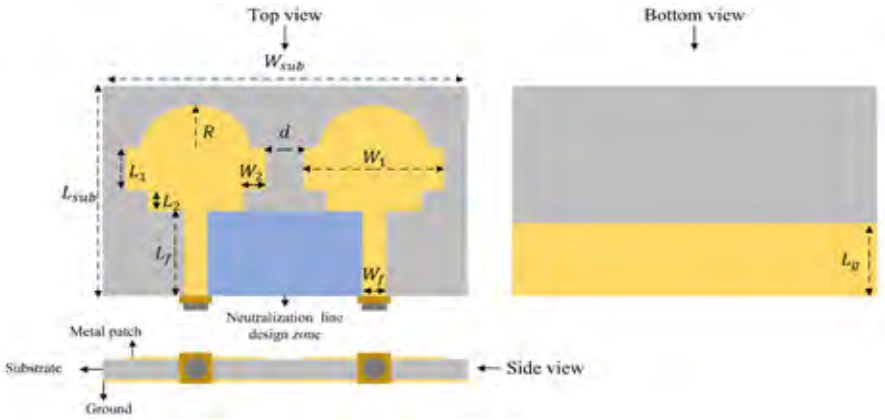

It is presented some examples used ML algorithms. They are antenna dimensions, decoupling structure, waveguide compatibility, via dimension and localization and etc. There are a lot of applications used ML in the literature. ML is selected for lots of advantages according to another artificial intelligence methods (Chhaya, Khanzode, & Sarode, 2020).

Deep Learning Applications

Deep Learning (DL) is powered by layers of neural networks, which are algorithms loosely modeled after the way the human brain works. Training with large amounts of data is about configuring neurons in a neural network. The result is a deep learning model that processes new data after being trained. DL models take information from multiple sources and analyse this data in real time without the need for human intervention. In DL, graphics processing units (GPUs) are optimized for training models because they can handle multiple calculations simultaneously (Shinde & Shah, 2018).

DL classifies information through layers of neural networks that have a series of inputs that take raw data. For example, if a neural network is trained with images of birds, it can be used to recognize images of birds. More layers provide more accurate results, such as distinguishing a crow from a raven compared to distinguishing a crow from a chicken. Deep neural networks, which underlie deep learning algorithms, have several hidden layers between input and output nodes, meaning they can perform more complex data classifications. The deep learning algorithm must be trained on large datasets, and the more data it receives, the more accurate it becomes. The algorithm will need to be fed thousands of bird images before it can classify new bird images correctly (Janiesch, Zschech, & Heinrich, 2021).

One of the biggest advantages of deep learning is the use of neural networks to uncover hidden insights and relationships from previously invisible data. One of the biggest disadvantages of deep learning is the necessity of huge database (Chhaya et al., 2020).

In the literature, for 5G applications, circularly polarized dual-band patch antenna that has the shape of bone is optimized by using the DL algorithm (Montaser & Mahmoud, 2021). 28-38 GHz frequency region is selected for antenna simulations. 150 antenna designs has different geometry and electrical properties are obtained and used to apply Deep Neural Network (DNN). As a result of DNN, an appropriate design of antenna is found in terms of suitable operating frequency. Figure 6 shows that the proposed antenna configuration. Return loss and gain graphics of the antenna is presented in Figure 7.

Figure 6.

Proposed antenna configuration (left) top view and (right) back view (Montaser & Mahmoud, 2021)

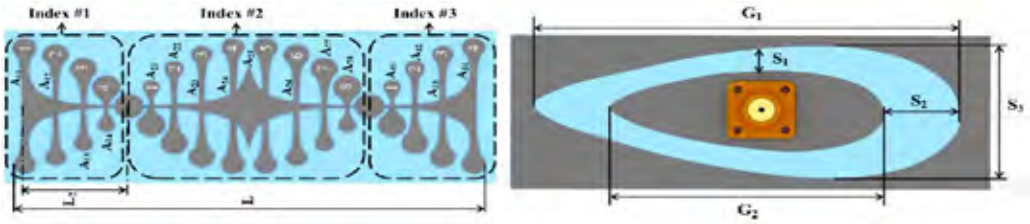

Figure 7.

Return loss of the antenna (left) and gain of antenna (right) (Montaser & Mahmoud, 2021)

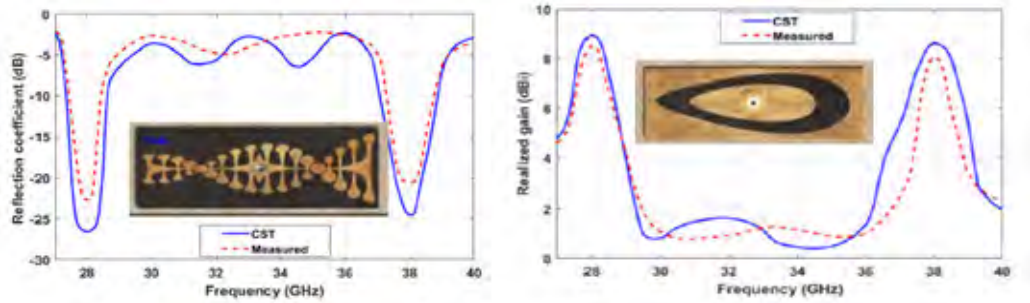

In another study, DNN is used to determine optimum radiation pattern synthesis (Kim & Choi, 2020). An array antenna is utilized to decide wanted radiation pattern as inputs; phase angle and amplitude. 6859 pattern shapes are optimized for 4 x 1 array antenna solutions. Finally, the radiation pattern obtained from DNN and input radiation pattern are congruous with each other. Figure 8 shows that proposed array antenna design.

Figure 8.

Array antenna configuration (Kim & Choi, 2020)

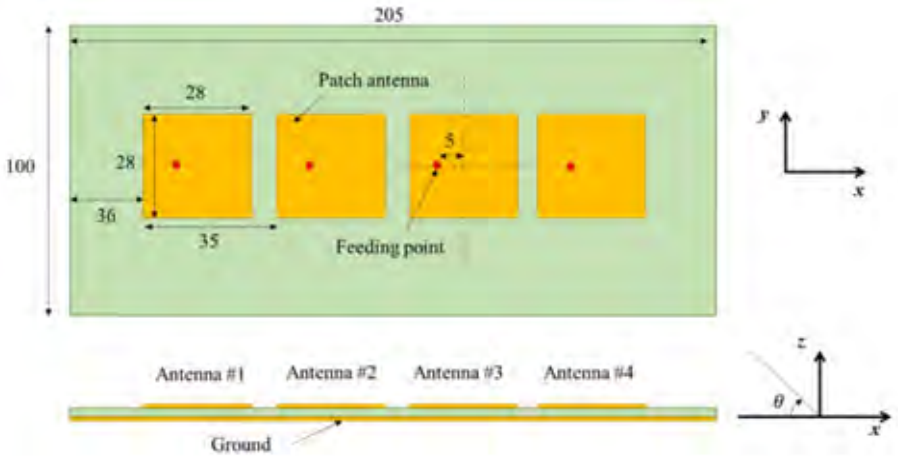

Both ML and DL are AI subfields. Also, there are other algorithms such as ANN, Genetic Algorithm and etc. AI is developing at that moment. So, the development of it is unremitting continuing.

In this chapter, ML and DL applications are presented some examples. There is a lot of

researches about AI applications of MAs in the literature. Some of them are (Aldalbahi et al., 2021; P. Liu & Chen, 2023; Y. Liu et al., 2022; Mojabi, Khoshdel, & Lovetri, 2020; Nouri et al., 2023; Phasukkit, 2022; Phasukkit & Wongketsada, 2021; Reimer & Pistorius, 2022; Ren et al., 2020; Rizwan et al., 2021; Wei et al., 2023).

Conclusion

The usability of microstrip antennas for research and development is expanding day by day. With the development of Artificial Intelligence applications, the algorithms of Artificial Intelligence are integrated with microstrip antennas structures.

In the literature, there are many Artificial Intelligence applications by optimising the dimensions of antennas, radiation pattern, gain values, the locations of via, modification of ground plane, operating frequency and etc. The relation between microstrip antennas and Artificial Intelligence applications will continue in the future. The easy design of microstrip antennas is an important advantage of that. Considering the usage areas of microstrip antennas, the development of it is a necessity.

All of the explanations shows that microstrip antenna examples are also very comely candidates for Artificial Intelligence applications. Machine Learning and Deep Learning applications are so popular subfield of Artificial Intelligence.

The output Machine Learning applications of microstrip antennas structure have good agreements of wanted/beginning optimization solutions.

Deep Learning requires many input databases but the output of Deep Learning gives very similar result according to input or desired database.

The results of examples demonstrate that both methods produce positive and stable results. The usage the artificial intelligent method in microstrip antenna designs will make it easier the researches and developments in the future. Therefore, the design of an antenna for any aims will readily find.

References

Abbassi, P. K., Badra, N. M., Allam, A. M. M. A., & El-Rafei, A. (2019). WiFi Antenna Design and Modeling using Artificial Neural Networks. *Proceedings of 2019 International Conference on Innovative Trends in Computer Engineering, ITCE 2019*, (February), 270–274. https://doi.org/10.1109/ITCE.2019.8646616

Aldalbahi, A., Jasim, M. A., Shahabi, F., Mazin, A., Siasi, N., & Oliveira, D. (2021). Deep Learning for Primary Sector Prediction in FR2 New Radio Systems. *IEEE Access*, *9*. Retrieved from https://ieeexplore.ieee.org/document/9615238/

B. J. Kwaha, O. N. Inyang, P. A. (2011). The circular microstrip patch antenna-design and implementation. *International Journal of Recent Research and Applied Studies (IJRRAS)*, *8*(1), 86–95.

Bahrami, S., Moloudian, G., Miri-Rostami, S. R., & Bjorninen, T. (2021). Compact Microstrip Antennas with Enhanced Bandwidth for the Implanted and External Subsystems of a Wireless Retinal Prosthesi. *IEEE Transactions on Antennas and Propagation*, *69*(5), 2969–2974. https://doi.org/10.1109/TAP.2020.3025245

Balanis, C. A. (2013). *Anten teorisi : Analiz ve Tasarım*. Nobel Akademik Yayıncılık.

Chhaya, K., Khanzode, A., & Sarode, R. D. (2020). Advantages and Disadvantages of

Artificial Intelligence and Machine Learning: A Literate Review. *International Journal of Library & Information Science (IJLIS)*, *9*(1), 3. Retrieved from http://iaeme.com

Dey, S., & Mittra, R. (1996). Compact microstrip patch antenna. *Microwave and Optical Technology Letters*, *13*(1), 12–14. https://doi.org/10.1002/(sici)1098-2760(199609)13:1<12::aid-mop4>3.0.co;2-q

Dundar, O., Yelken, E., & Kocer, S. (2022). *Artificial Intelligence Methods Used in Microstrip Antennas* (Y. Uzun & R. Butuner, eds.). ISRES Publishing.

Güneşer, M. T. (2019). Artificial intelligence solution to extract the dielectric properties of materials at sub-THz frequencies. *IET Science, Measurement & Technology*, *13*(4), 523–528. https://doi.org/10.1049/IET-SMT.2018.5356

Huang, H., Yang, X. S., & Wang, B. Z. (2023). Machine-Learning-Based Generative Optimization Method and Its Application to an Antenna Decoupling Design. *IEEE Transactions on Antennas and Propagation*, *71*(7), 6243–6248. https://doi.org/10.1109/TAP.2023.3270716

Janiesch, C., Zschech, P., & Heinrich, K. (2021). Machine learning and deep learning. *Electronic Markets*, *31*(3), 685–695.

Kanj, H., & Popovic, M. (2005). Miniaturized microstrip-fed "Dark Eyes" antenna for near-field microwave sensing. *IEEE Antennas and Wireless Propagation Letters*, *4*. Retrieved from https://ieeexplore.ieee.org/document/1532173/

Khan, T., De, A., & Uddin, M. (2013). Prediction of slot-size and inserted air-gap for improving the performance of rectangular microstrip antennas using artificial neural networks. *IEEE Antennas and Wireless Propagation Letters*, *12*, 1367–1371. https://doi.org/10.1109/LAWP.2013.2285381

Kim, J. H., & Choi, S. W. (2020). A Deep Learning-Based Approach for Radiation Pattern Synthesis of an Array Antenna. *IEEE Access*, *8*, 226059–226063. https://doi.org/10.1109/ACCESS.2020.3045464

Liu, P., & Chen, Z. N. (2023). Full-Range Amplitude-Phase Metacells for Sidelobe Suppression of Metalens Antenna Using Prior-Knowledge-Guided Deep- Learning -Enabled Synthesis. *IEEE Transactions on Antennas and Propagation*, *71*(6), 5036–5045. https://doi.org/10.1109/TAP.2023.3263929

Liu, Q., Yang, J., Zhuang, C., Barnawi, A., & A Alzahrani, B. (2019). Artificial Intelligence Based Mobile Tracking and Antenna Pointing in Satellite-Terrestrial Network. *IEEE Access*, *7*, 177497–177503. https://doi.org/10.1109/ACCESS.2019.2956544

Liu, Y., Shen, Y., Lyu, Z., Liang, Y., He, W., Gao, Y., … Yu, L. (2022). Real-Time 3-D MIMO Antenna Tuning With Deep Reinforcement Learning. *IEEE Transactions on Cognitive Communications and Networking*, *8*(2), 1202–1215. https://doi.org/10.1109/TCCN.2022.3167549

Mojabi, P., Khoshdel, V., & Lovetri, J. (2020). Tissue-Type Classification With Uncertainty Quantification of Microwave and Ultrasound Breast Imaging: A Deep Learning Approach. *IEEE Access*, *8*. Retrieved from https://ieeexplore.ieee.org/document/9210075/

Montaser, A. M., & Mahmoud, K. R. (2021). Deep Learning Based Antenna Design and Beam-Steering Capabilities for Millimeter-Wave Applications. *IEEE Access*, *9*, 145583–145591. https://doi.org/10.1109/ACCESS.2021.3123219

Nalam, M., Rani, N., & Mohan, A. (2014). Biomedical Application of Microstrip Patch Antenna. *International Journal of Innovative Science and Modern Engineering*

(IJISME), *2*(6), 6–8.

Nouri, M., Behroozi, H., Jafarieh, A., Aghdam, S. A., Piran, M. J., & Mallat, N. K. (2023). A Learning-Based Dipole Yagi-Uda Antenna and Phased Array Antenna for mmWave Precoding and V2V Communication in 5G Systems. *IEEE Transactions on Vehicular Technology*, *72*(3), 2789–2803. https://doi.org/10.1109/TVT.2022.3217372

Peixeiro, C. (2011). Microstrip patch antennas: An historical perspective of the development. *Undefined*, 684–688. https://doi.org/10.1109/IMOC.2011.6169224

Phasukkit, P. (2022). Non-Ionic Deep Learning-Driven IR-UWB Multiantenna Scheme for Breast Tumor Localization. *IEEE Access*, *10*. Retrieved from https://ieeexplore.ieee.org/document/9667505/

Phasukkit, P., & Wongketsada, T. (2021). Triple Coaxial-Half-Slot Antenna Scheme With Deep Learning-Based Temperature Prediction for Hepatic Microwave Ablation: Finite Element Analysis and In Vitro Experiment. *IEEE Access*, *9*. Retrieved from https://ieeexplore.ieee.org/document/9439448/

Prajapati, G. K., Sadanandam, K., & Nalla, S. (2020). Artificial Intelligence based Antenna Design for Future Millimeter Wave Wireless Communication in Fifth Generation. *2020 International Conference on Computer Science, Engineering and Applications, ICCSEA 2020*, 1–6. https://doi.org/10.1109/ICCSEA49143.2020.9132872

Rabbani, M. S., & Ghafouri-Shiraz, H. (2017). Liquid Crystalline Polymer Substrate-Based THz Microstrip Antenna Arrays for Medical Applications. *IEEE Antennas and Wireless Propagation Letters*, *16*. Retrieved from https://ieeexplore.ieee.org/document/7809072/

Reimer, T., & Pistorius, S. (2022). The Diagnostic Performance of Machine Learning in Breast Microwave Sensing on an Experimental Dataset. *IEEE Journal of Electromagnetics, RF and Microwaves in Medicine and Biology*, *6*(1). Retrieved from https://ieeexplore.ieee.org/document/9416743/

Ren, A., Zahid, A., Zoha, A., Shah, S. A., Imran, M. A., Alomainy, A., & Abbasi, Q. H. (2020). Machine Learning Driven Approach towards the Quality Assessment of Fresh Fruits Using Non-Invasive Sensing. *IEEE Sensors Journal*, *20*(4), 2075–2083. https://doi.org/10.1109/JSEN.2019.2949528

Rentapalli, V. R., & Roy, B. (2023). Artificial Intelligence Enhanced Signal Processing in Low-Profile Wearable Wideband Antenna for Future 5G Wireless communications. *2023 3rd International Conference on Artificial Intelligence and Signal Processing, AISP 2023*, 1–5. https://doi.org/10.1109/AISP57993.2023.10135066

Rizwan, A., Zoha, A., Mabrouk, I. Ben, Sabbour, H. M., Al-Sumaiti, A. S., Alomainy, A., … Abbasi, Q. H. (2021). A Review on the State of the Art in Atrial Fibrillation Detection Enabled by Machine Learning. *IEEE Reviews in Biomedical Engineering*, *14*, 219–239. https://doi.org/10.1109/RBME.2020.2976507

Shi, D., Lian, C., Cui, K., Chen, Y., & Liu, X. (2022). An Intelligent Antenna Synthesis Method Based on Machine Learning. *IEEE Transactions on Antennas and Propagation*, *70*(7), 4965–4976. https://doi.org/10.1109/TAP.2022.3182693

Shinde, P. P., & Shah, S. (2018). A review of machine learning and deep learning applications. *2018 Fourth International Conference on Computing Communication Control and Automation (ICCUBEA)*, 1–6.

Singh, I., & Tripathi, V. S. (2011). Micro strip Patch Antenna and its Applications: a Survey. In *Article in International Journal of Computer Applications in Technology*.

Retrieved from https://www.researchgate.net/publication/232318276

Soontornpipit, P., Furse, C. M., & Chung, Y. C. (2004). Design of implantable microstrip antenna for communication with medical implants. *IEEE Transactions on Microwave Theory and Techniques*, *52*(8 II), 1944–1951. https://doi.org/10.1109/TMTT.2004.831976

Tak, J., Kantemur, A., Sharma, Y., & Xin, H. (2018). A 3-D-printed W-band slotted waveguide array antenna optimized using machine learning. *IEEE Antennas and Wireless Propagation Letters*, *17*(11), 2008–2012. https://doi.org/10.1109/LAWP.2018.2857807

Top, R., Gültekin, S. S., & Uzer, D. (2017). A Microstrip Patch Antenna Design to Determine the Level of Occlusion in Heart Vein. *5th International Conference on Advanced Technology & Sciences (ICAT'17)*, 644–647.

Top, R., Gültekin, S. S., & Uzer, D. (2020a). Evaluation and Comparison of Electromagnetic and Scattering Parameters Data of Two Microstrip Patch Antennas Operating in ISM Band for Cancer Detection. *1st International Conference on Computer, Electrical and Electronic Sciences*. Konya.

Top, R., Gültekin, S. S., & Uzer, D. (2020b). Evaluation and Comparison of Electromagnetic and Scattering Parameters Data of Two Microstrip Patch Antennas Operating in ISM Band for Cancer Detection. *Avrupa Bilim ve Teknoloji Dergisi*, 237–244. https://doi.org/10.31590/EJOSAT.804330

Top, R., Ünlü, Y., Gültekin, S. S., & Uzer, D. (2019). Microstrip antenna design with circular patch for skin cancer detection. *Advanced Electromagnetics*, *8*(2), 71–76. https://doi.org/10.7716/aem.v8i2.996

Uyanik, H., Uzer, D., Top, R., & Gultekin, S. S. (2020). Determination of Cardiovascular Occlusion with Microstrip Antennas. *4th International Symposium on Multidisciplinary Studies and Innovative Technologies, ISMSIT 2020 - Proceedings*. https://doi.org/10.1109/ISMSIT50672.2020.9254528

Wei, Z., Zhou, Z., Wang, P., Ren, J., Yin, Y., Pedersen, G. F., & Shen, M. (2023). Automated Antenna Design via Domain Knowledge-Informed Reinforcement Learning and Imitation Learning. *IEEE Transactions on Antennas and Propagation*, *71*(7), 5549–5557. https://doi.org/10.1109/TAP.2023.3266051

Wu, Y. chen, & Feng, J. wen. (2018). Development and Application of Artificial Neural Network. *Wireless Personal Communications*, *102*(2), 1645–1656. https://doi.org/10.1007/S11277-017-5224-X/FIGURES/2

Yang, S., Kishk, A., Wireless, K. L.-I. A. and, & 2008, undefined. (n.d.). Frequency reconfigurable U-slot microstrip patch antenna. *Ieeexplore.Ieee.Org*. Retrieved from https://ieeexplore.ieee.org/abstract/document/4473039/?casa_token=M2HcpwXTq4AAAAAA:zVuv_8-0kazFzy7LT-wJyjyLd72kz1NPPZEJiEuvbpJbvOoqw0D5Ud3p883_6BPdlaO5c6f3Y4k

Zhang, J., Akinsolu, M. O., Liu, B., & Zhang, S. (2022). Design of Zero Clearance SIW Endfire Antenna Array Using Machine Learning-Assisted Optimization. *IEEE Transactions on Antennas and Propagation*, *70*(5), 3858–3863. https://doi.org/10.1109/TAP.2021.3137500

About the Author

Rabia TOPRAK, PhD, is a Research Assistant of Electrical and Electronics Engineering at Karamanoglu Mehmetbey University in Karaman, Türkiye. She holds a PhD in Electrical and Electronics Engineering from Konya Technical University and a MSc in Electrical and Electronics Engineering from Selcuk University. Her main areas of interest are antenna structures, microstrip antennas, biomedical applications of antenna structures and electromagnetic fields/waves.

E-mail: rabiatop@kmu.edu.tr, ORCID: 0000-0002-3306-1163

Similarity Index

The similarity index obtained from the plagiarism software for this book chapter is 18%.

CHAPTER 6

Robotic Fingers Controlled with EMG

Ucman ERGUN
Afyon Kocatepe University, Türkiye

Fazilet CANATAN ERGUN
Necmettin Erbakan University, Türkiye

To Cite This Chapter:
Ergun, U. & Canatan Ergun, F. (2023). Robotic Fingers Controlled with EMG. In S. Kocer. & O. Dundar (Eds.), *Artificial Intelligence Applications in Intelligent Systems* (pp. 85–102). ISRES Publishing.

Introduction

Amputation, not only physical restrictions are imposed on the person's lifestyle, but also negatively affects the person's psychological state. Some diseases and accidents can result in amputation. For example, limb loss may occur in diseases caused by circulatory disorders such as diabetes or gangrene, or in dangerous situations such as work accidents, traffic accidents, wars, use of explosive devices, weapons, and electric shock.

With the development of technology, researchers are working on robotic solutions that can perform the desired movements and using wearable technologies. The developed solutions aim to eliminate the deficiencies caused by missing limbs. So much so that sometimes such solutions can be implemented by attaching various prostheses to the body, and sometimes by remote control of robotic arms. Even solutions that will reduce the possible risks of personnel working in risky areas or offered to surgeons for sensitive operations can be evaluated from this perspective.

Nowadays, there are some applications in which robots are controlled using EMG (Electromyogram) signals. Studies on this subject are carried out in areas such as the control of prosthetic limbs, robotic devices and toys with EMG signals. Control with EMG signals can be achieved with motion recognition algorithms based on signal analysis and classification.

The orders coming from the brain are transferred to the arms via nerve cells. Various commercial solutions have been developed to detect EMG signals reaching the muscle from the brain. For example, we can give examples such as *Myo Armband, Leap Motion Controller, Nod Gesture Control Ring* and *Gesture Glove* for wirelessly transferring EMG signals taken from the muscle to the computer.

Biomechanical Examination of Hand Movement

The complexity of the hand challenges our ability to fully understand its biomechanics (Duncan et al. 2013). The wrist has an average of 65-80º flexion, an average of 55-75º extension, 35-45º ulnar and 15-20º radial deviation movement. However, for most daily living activities, 5º flexion, 30-40º extension, 10º radial and 15-30º deviation are sufficient.

Hand movements are divided into two parts: finger movements and joint movements (Eryiğit 2012). The movement of the thumb differs from the directional movements of the other fingers. As seen in Figure 1, it completes the task of grasping an object and pressing on it (Köklükaya 2008).

Figure 1.

Thumb Movements (Eryiğit 2012)

As for the movement of the other fingers on the hand, their function is flexion, extension and abduction as shown in Figure 2.

Figure 2.

Hand Finger Gestures

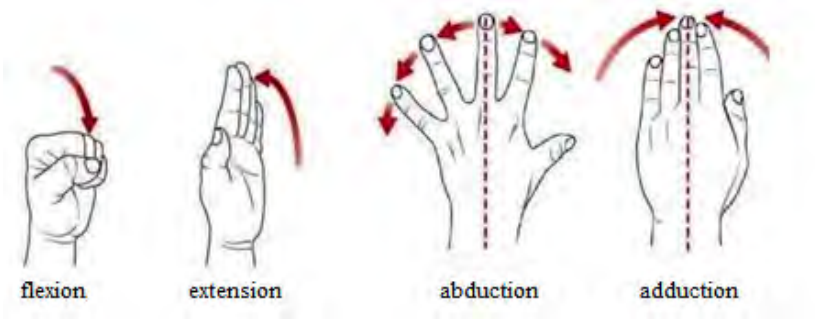

EMG

EMG is a technique used to evaluate and record the electrical activity produced by skeletal muscles. EMG measurement is made using a tool called electromyogram. A typical EMG signal is as shown in Figure 3.1. While EMG signals are measured, power

and frequency values are recorded. To talk about the characteristic features of the EMG signal, the amplitude range varies between 0-10mV or 0-1.5mV RMS values. Although the signal frequency is between 50 and 500 Hz, it frequently takes values in the range of 50-150 Hz (De Luca 2002).

Formation and Characteristics of EMG Signals

The basic unit in the body is the balance of ions inside and outside our cells. As a result of the change in ion balance, neurons create an electrical potential that stimulates the brain to cause action when we want to perform a voluntary movement. This potential is called action potential (AP). A nerve cell that produces AP changes the ion balance of the nerve cells connected to it, thus creating AP in these nerve cells. In this method, as the stimulus is transmitted to the target muscle area via the spinal cord, interconnected neurons are stimulated and motor nerves transmit the stimulus. Different numbers of motor units are involved in the operation of a muscle. The difference in muscle function depends on the number of motor units. If the electrical properties of EMG signals are examined, the amplitude is in the microvolt level and the value may vary depending on the age, gender and type of the muscle taken.

Since EMG is non-stationary, it does not have a specific frequency value. As seen in Figure 3, the frequency band is between 10-500 Hz and the dominant frequency value is around 30-150 Hz.

Figure 3.

EMG signal frequency range

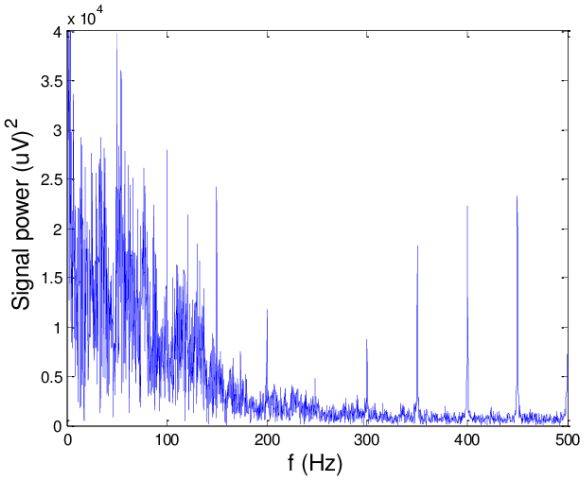

The EMG signal is a complex signal resulting from the contraction and relaxation of muscles controlled by the nervous system. EMG signals carry information about the muscular nervous system and are suitable for use as control signals for prosthetic systems. EMG signals are not static because they are analog signals that are not periodic or deterministic. EMG signals are not repeated at regular intervals and these signals obtained during the recording period cannot be represented by a single mathematical

expression. Ambient noise, magnetic effects and vibration sources affect the properties of EMG signals during the recording process (Christov 2018). Conclusions about the role of different muscle motor units in different motor tasks:

- Analysis of changes in muscle function caused by various neuromuscular diseases.
- Control of various technical devices such as orthoses, external structures, prostheses.

EMG is particularly important in making people's lives easier. Popular solutions can be produced thanks to more accurate and faster analysis of EMG signals and the development of control systems.

The sEMG signal is a complex interference pattern of electrical activity during muscle contraction. It is closely related to muscle activity and exercise status. Its amplitude is generally between 0.01 mV and 10 mV, and its main energy is concentrated between the frequency band 0-500 Hz. Detection of sEMG signals is a non-invasive method and is of great importance in clinical diagnosis, rehabilitation medicine and smart prosthesis control (Wu et al 2019). Figure 4 shows eight sEMG signal channels obtained from a Myo armband starting at low amplitude, varying with muscle contraction activity.

Figure 4.

Raw sEMG signal obtained by Myo Armband

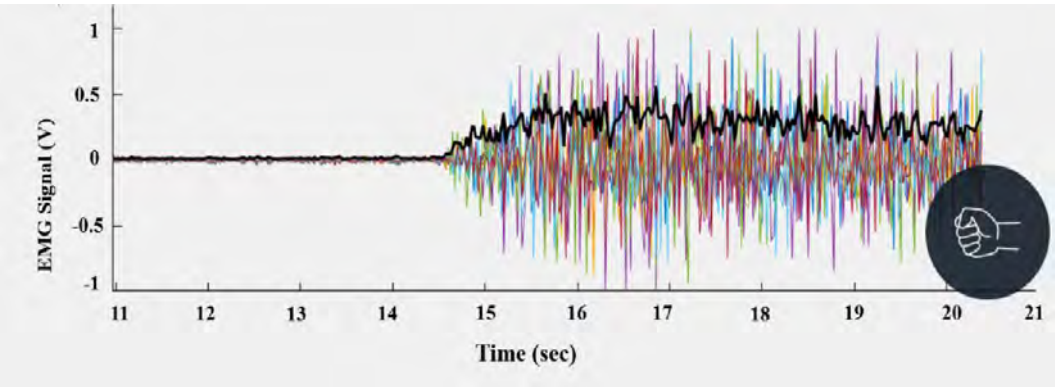

Myo Armband

With the continuous development of our lives, wearable technologies are emerging in many areas, including advanced devices that detect muscle movements in the human body. EMG signals can be obtained using the Myo Armband designed by Thalmic Labs. It is a wearable bracelet with eight channels. Myo Armband also includes a nine-axis IMU (Inertial Measurement Unit) that acquires gyroscope, accelerometer and magnetometer data. Sensors are used to detect movement along the x-axis and y-axis and rotation along the y-axis. A Myo Armband is shown in Figure 5 (Ahmed et al. 2021). Figure 6 shows the location of Myo Armband channels. (Table 1) shows which muscles Myo Armband receives data from according to the location of its channels.

Figure 5.

Myo Armband

Figure 6.

Location of Myo Armband channels, (a) lower part of the upper extremity. (b) upper part of the upper limb (Morales ve Pozo 2017)

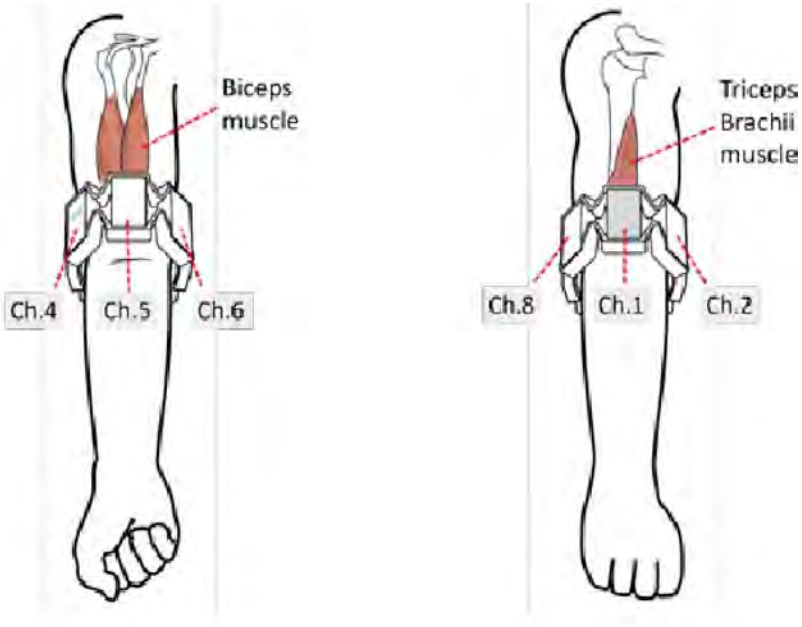

(a) bottom of upper limb (b) top of upper limb

Table 1.

Location of Myo Armband channels

Myo Armband	Muscle
Channel 1	Exstansör digitoium communis
Channel 2	Exstansör karpi radialis
Channel 3	Brakiyoradıalis
Channel 4	Pronator teres
Channel 5	Fleksör digitorum sublimis
Channel 6	Fleksör karpi ulnaris
Channel 7	Fleksör digitorum profundus
Channel 8	Exstansör karpi ulunaris

Figure 7 shows the components of Myo Armband:

- Blue color: BLE NRF51822 wireless data transfer chip.
- Red color: ARM Cortex M4 processor drives the arm strap.
- Gray color: Antenna.
- Brown: Vibration motor.
- Purple color: Micro-USB connector used to charge the battery and update the firmware on the device (Visconti et al. 2018).

Figure 7.

Internal parts of Myo Armband (Visconti vd. 2018)

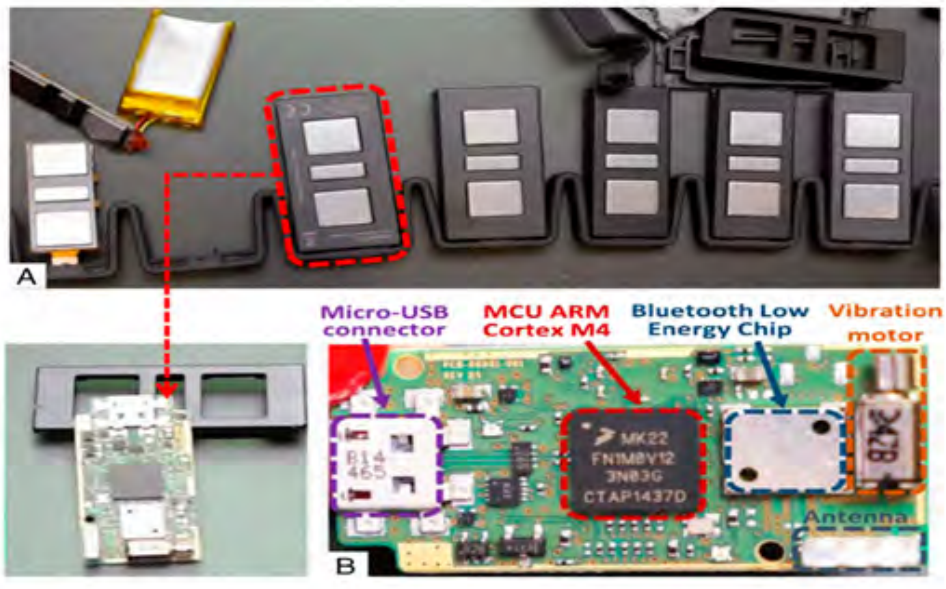

Processing Stages of EMG Signal

Raw data of sEMG signals can be processed by Matlab software by blocking and digitizing unwanted signals. The pattern recognition algorithm is an important part of sEMG signal analysis and processing as it identifies the patterns and regularity of the data in which the prosthesis is moved. The pattern recognition system consists of three main stages shown in Figure 8 (Hassan et al. 2018).

Figure 8.

A block diagram showing signal usage stages

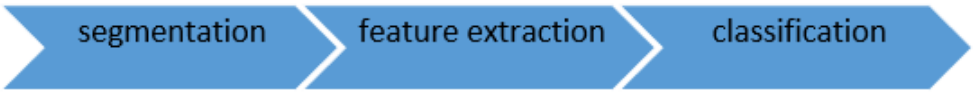

The EMG signal is complex and unstable, and signal processing is a complex task as muscles have a role in the outcome of electrical activity (Yavuz and Eyüpoğlu 2019). The signal is divided into windows or short periods of time to extract features. The feature extraction step occurs when appropriate features are selected to extract information from each window for sEMG signals, as shown in Figure 9. The characteristics of sEMG signals can be categorized by time domain, frequency domain, and time and frequency shift (Hassan et al. 2018). Time-dependent energy spectrum descriptors (TD-PSD) are a set of time domain features.

Figure 9.

Segmentation of analysis windows of EMG recording (Li 2011)

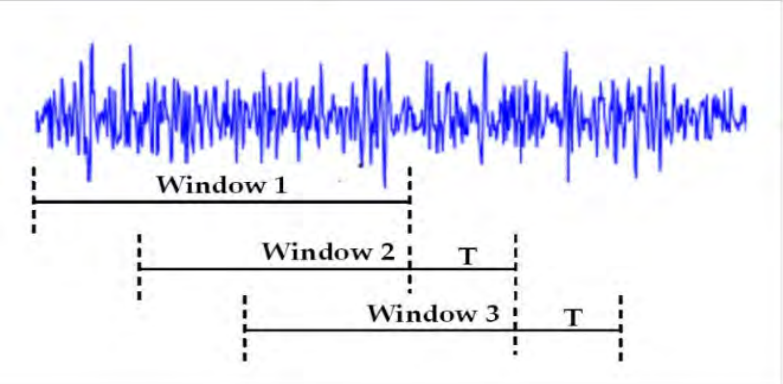

It contains six features: *log(m_0), log(m_0-m_2), log(m_0-m_4), log(S), log(IF)* and root square zero-order moment (m_0), where m_0, m_2, m_4 are respectively root square second moment (m_2), root square fourth moment (m_4), normalized by *log(S), log(IF)* and *log(WLR)*. It represents *Sparseness (S), Irregularity Factor (IF)* and *Width Length Ratio*

(WLR), respectively (Al-Timemy et al. 2015).

In the classification phase, a classifier algorithm suitable for the system is selected. The classifier will determine the intended movement based on predefined sets of feature classes. Classifiers are applied to distinguish different sets of features.

Receiving an EMG Signal Using Myo Armband

1. Pattern Recognition

Multiple electrodes, such as the Myo Armband, should be used to extract reproducible patterns of muscle activity from sEMG signals associated with an entire muscle group. To classify a dynamic range of different movements and allow users with varying degrees of freedom to control their electromuscular prostheses, a pattern recognition method is used to distinguish patterns from sEMG signals. The EMG input signal is divided and features are extracted to transform each part into a feature set. These features have useful data about each segment that is then used to categorize them.

2. Signal Preprocessing

An important step in sEMG signal processing is signal segmentation. The accuracy of the segmentation result is directly related to the accuracy of feature extraction and classification (Shi et al. 2013). The windowing method and the size of the windows are important in real-time processing of EMG signals. Since there will be fewer features of the signal in small window sizes, the accuracy of recognizing the motion class will decrease. Increasing the window size to obtain more features will cause the real time limit to be exceeded. The actual response time limitation in active hand and arm prostheses is approximately 300 ms. For this reason, the window length to be determined must be less than 300 ms. The window method relates to whether each window is contiguous or overlapping across the EMG signal cluster. If the data processing time is shorter than the window length, processor idle time will occur (Oskoei and Hu 2007). Using the nested window method, it separates sEMG signals into windows with regular overlapping time intervals.

In the interference technique, the classification decision (D) can be calculated as follows:

$$D = \frac{1}{2} T_a + \frac{1}{2} T_{new} + \tau \quad (1)$$

In equation (1), T_a represents the analysis window length, T_{new} represents the window increment, and τ represents the processing time. When $T_{new} = T_a$, the technique is called adjacent windowing. (Ali et al. 2016).

3. Features extraction

The split sEMG signal contains information that can be used to identify different patterns. The basis for distinguishing sEMG signal patterns are features related to frequency and amplitude information (Ali 2013). The TD-PSD method was developed to reduce real-time signal processing times by directly extracting the power spectrum of sEMG signals in the time axis. In this study, a set of features belonging to the time domain category were selected. The feature set consists of six features extracted from each window: *log*(m_0), *log*(m_0-m_2), *log*(m_0-m_4), *log*(S), *log*(IF) ve *log*(WLR).

Time-dependent energy spectrum descriptors

Time-dependent energy spectrum descriptors (TD-PSD) are time domain features. It is a feature extraction algorithm proposed by Khoshaba et al. First, based on Fourier transform relations and Parseval's theorem, a series of signal power spectral moments are directly extracted from the time domain. To extract the feature of spectral moments of the signal, this step is used to reduce the processing time taken in the time domain. The moments of the energy spectrum will be subtracted logarithmically from the sEMG signals, which will consequently change the form of the known cepstral feature extraction. In the first step, it is necessary to normalize to reduce the effect of noise resulting from the application of derivatives.

Second, cosine similarity is used to evaluate the direction between the features of the power spectrum extracted from the raw sEMG signals and the nonlinear cepstral emission. The TD-PSD algorithm is shown in Figure 10 (Khushaba 2014).

Figure 10.

Schematic diagram of TD-PSD feature extraction process (Al-Timemy vd. 2015)

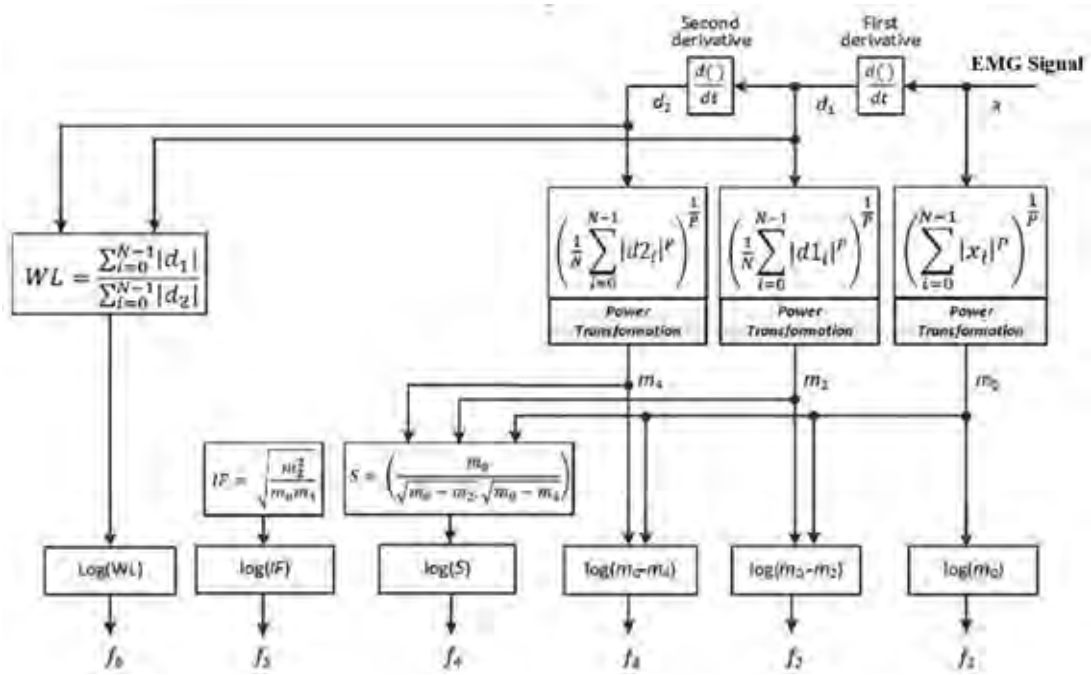

The sampled sEMG signal is denoted by *x[j]*. Using DFT, the sEMG trace over a given time can be expressed as a function of frequency *x[k]*. The feature extraction procedure starts with checking Parseval's theorem, which states that the sum of squares of the transformed function is equal to the sum of the squares of the transformed function.

$$\sum_{j=0}^{N-1} |x[j]|^2 = \frac{1}{N} \sum_{k=0}^{n-1} |x[k]x*[k]| = \sum_{k=0}^{N-1} P[K] \quad (2)$$

Multiplying the conjugate of equation (2) by *X*[k]* and then dividing by *N* produces the phase-excluded power spectrum *p[k]*, where k is the frequency index (Al-Timemy vd. 2015).

As a result of this symmetry consuming the entire spectrum, the spectral density of the power in the time domain cannot be directly estimated. As a result, all single moments will be equal to zero according to the frequency distribution form, which is consistent with the moment definition (M) of the n-order spectral density of the signal power in Equation (3).

$$M_n = \sum_{K=0}^{N-1} K^n P[K] \quad (3)$$

When *n* equals zero, Parseval's theorem applies (Equation 4). Otherwise, the temporal differentiation property of the Fourier transform is used. For discrete-time signals, the *n*th derivative of a time domain function, denoted Δ^n, is equivalent to multiplying the spectrum by *k* raised to the *n*th power:

$$F[\Delta^n x[j] = K^n X[K]] \quad (4)$$

The total power in the frequency domain is expressed by this feature. In other words, it indicates the strength of muscle contraction as shown in Equation (5-7):

$$M_0 = \sqrt{\sum_{j=0}^{N-1} X[j]^2} \quad (5)$$

$$M_2 = \sqrt{\sum_{j=0}^{N-1} K^2 P[K]} = \frac{1}{N} \sqrt{\sum_{K=0}^{N-1} (KX[K])^2} = \sqrt{\frac{1}{N} \sum_{j=0}^{N-1} (\Delta_x[j])^2} \quad (6)$$

$$M_4 = M_4 = \sqrt{\sum_{K=0}^{N-1} K^4 P[K]} = \sqrt{\frac{1}{N} \sum_{j=0}^{N-1} (\Delta^2 x[j])^2} \quad (7)$$

The signal strength is reduced for the presence of second and fourth derivatives of the signals. Therefore, to reduce the effect of noise on all torques, normal torque coverage (m_0, m_2 *and* m_4) per transducer is applied as in Equation (8-10):

$$m_0 = \frac{M_0^{\lambda}}{\lambda} \quad (8)$$

$$m_2 = \frac{M_2^{\lambda}}{\lambda} \tag{9}$$

$$m_4 = \frac{M_4^{\lambda}}{\lambda} \tag{10}$$

where $\boldsymbol{\lambda} = 0.1$. The first three feature extractions are defined by the variables in Equation (11-13):

$$f_1 = log(m_0) \tag{11}$$

$$f_2 = log\ log\ (m_0 - m_2) \tag{12}$$

$$f_3 = log\ log\ (m_0 - m_4) \tag{13}$$

Sparseness: The S property determines how much of the vector energy is packed into only a few components.

$$f_4 = log(\frac{m_0}{\sqrt{m_0 - m_2}\sqrt{m_0 - m_4}}) \tag{14}$$

This property defines a vector with all elements equal to zero scattering scale as in Equation (14), i.e. $m_2,\ m_4 = 0$.

Irregularity Factor: IF is the fifth feature that calculates the ratio of the number of upward zero crossings to the number of vertices. It represents the spectral moments of a signal. The property can be written as in Equation (15):

$$f_5 = log\ log\ \left(\frac{ZC}{NP}\right) = log\left(\frac{\sqrt{\frac{m_2}{mo}}}{\sqrt{\frac{m_4}{m_2}}}\right) = log\left(\frac{m_2}{\sqrt{m_0 m_4}}\right) \tag{15}$$

Waveform Length Ratio (WLR): This feature divides the waveform length of the fundamental derivative by the waveform length of the second derivative. Here WLR is the absolute sum of the derivative value of the signals. This property is written as in Equation (16):

$$f_6 = log\left(\frac{\sum_{j=0}^{N-1} |\Delta_x|}{\sum_{j=0}^{N-1} |\Delta^2 x|}\right) \tag{16}$$

The feature list of six features represents a cepstral version of the sEMG activity, where the energy spectrum features of raw sEMG signals can be extracted. Additionally, non-linear versions use the cepstral direction vector as a suggested feature set that can be used in a class method using cosines.

Classification

The function of the classifier is to determine the data type of the pattern. In previous literature, various classifiers have been applied to achieve the highest classification accuracy, including LDA, SVM, KNN, ANN, FL, NF, and others. SVM are data points that are close to the hyperplane and affect the location and orientation of the hyperplane. These carrier vectors are used to maximize the accuracy of the classifier. Removing the support vector changes the position of the hyperplane.

Multiple parent levels can be defined to separate two categories of data points. There is a level with a larger margin for the category, which is the maximum distance between two data points. To maximize the margin range, it improves future classification of data points more confidently.

SVM classifiers are implemented in existing detection frameworks due to their excellent generalizability and reputation ability on training datasets for high accuracy. This method is based on statistical theory and structural risk mitigation principles. The strategy of this classifier is to focus the samples at the edge of the class distribution to find the optimal hyperplane.Many applications have data states that cannot be separated from each other. Kernel functions play an important role in the process of developing a classification model using SVM. This is because it helps you map the dataset to a higher dimensional space and better interpret the classification model. But actually, there are many applicable types of kernel functions, such as linear and radial basis functions, sigmoid functions, and polynomials. In this study, the kernel of the linear and radial basis function was used as in Equations 17 and 18.

$$K(x_n,\ x_i) = exp\left(-y\|x_n - x_i\|^2 + C\right) \tag{17}$$

$$K(x_n, x_i) = (x_n, x_i) \tag{18}$$

Here C, γ, r and degree represent cost, gamma, coefficient and degree respectively. The mathematical expression for $K(x_n, x_i)$ represents the transformation of a data field into a new, higher-dimensional data field. Here x_i represents the data point vector. *C* stands for penalty cost; If *C* is large enough, error reduction occurs. Otherwise, if *C* is small, the margin increases. The parameter γ (gamma) is the inverse of the standard deviation of the kernel of the radial linear function (Gaussian function).

Production and testing of robot arm prototype

In this chapter, in addition to describing the electrical circuits applied to sEMG signals using the low-cost Myo Armband device, there is an applied part of this study that includes the steps of designing, manufacturing and testing the robotic arm.

The forearm base used for the prosthetic hand prototype seen in Figure 11 consists of the

forearm, hand and 5 servo motors. Four of the servo motors used are MG995 models. The fifth servo motor used for abduction and adduction movements of the thumb is MG90S type. The motors used are a micro servo motor type that has all the features of servo motors.

Figure 11.

All parts of a three-dimensional humanoid prosthetic hand

In Figure 12, which shows the fingers of the hand, each finger is collected separately and each finger consists of three parts, and during the movement of the fingers, the parts of the fingers are connected to each other with a strong and flexible rubber thread. By placing the wires properly, attention was paid to their circulation and rotation, and friction of the rotation axis was prevented. The finished hand performed most of the specific movement tasks investigated by the study, requiring control of 5 motors to return to a specific position.

Figure 12.

All parts of the prosthetic hand

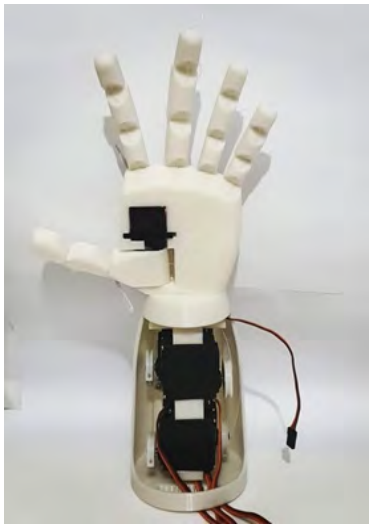

Servo Motors

MG995 type servo motors were selected from TowerPro motors. Servo motor features:

- Voltage (4.8V~6.0V),
- No-load current: (4.8V) 150mA,
- Operating range: -20°C to +60°C,
- Weight: 45g,
- Torque (4.8kg.cm) (4.8V)

The job of these actuators in the robotic hand is to translate the recorded sEMG signals and convert them into motion by which the fingers of the hand are moved.

Figure 13.

Block diagram of prosthetic hand control system with EMG

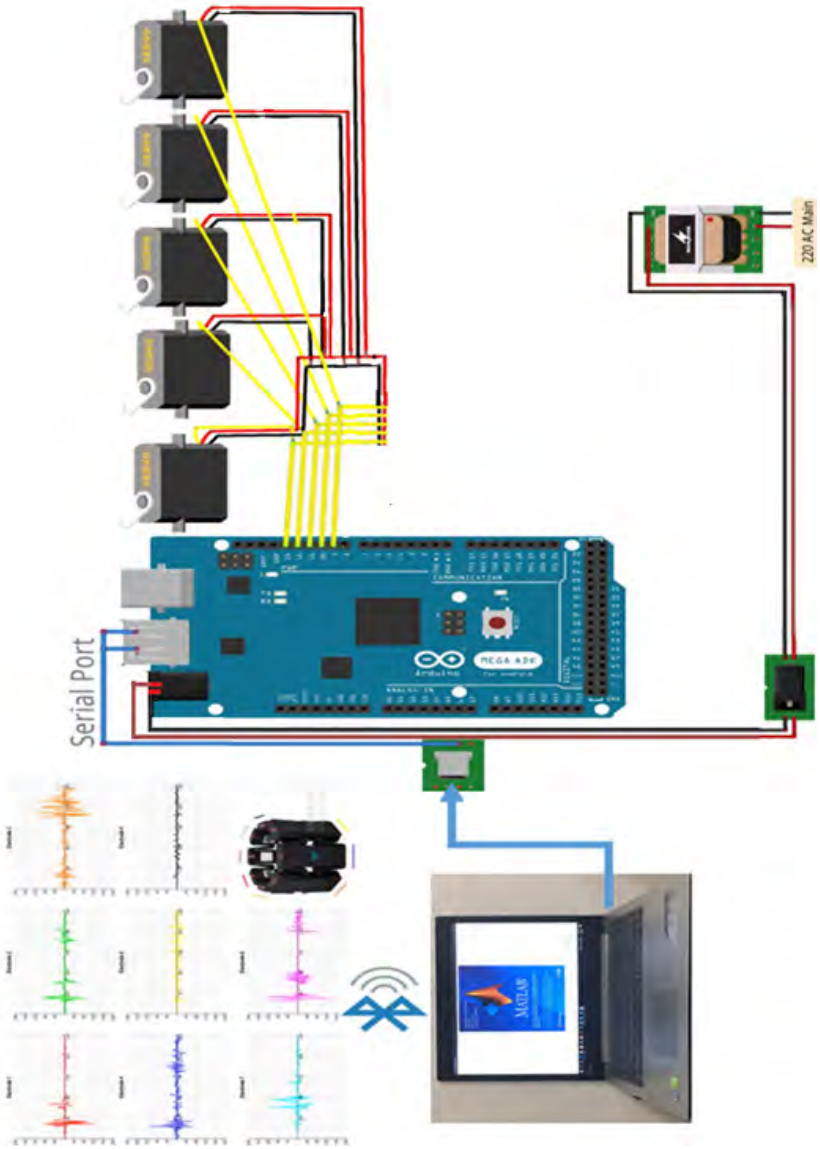

Prosthetic Hand Control Device with Myo Armband

The block diagram shown in Figure 13 represents the total diagram of the electrical

circuit controlling the 3D printed hand. It shows the Myo Armband connection via laptop bluetooth and shows the laptop connection to the Arduino microcontroller board via serial port. This part shows the first stage of the electrical circuit. The second stage is the servo shield connection. The third stage is the servo motors connected to the servo shield and fed from an external power source to control finger movements. Each pin connection from Arduino to servo motors is shown below:

- pin 5-Motor in the palm,
- pin 6-thumb,
- pin 7 index finger,
- pin 8-middle finger,
- pin 9-ring and little finger.

Using the Myo Armband device, after the previously mentioned data collection, pre-processing, data segmentation, extraction and classification. As mentioned, the sEMG signal is a complex signal and contains a lot of noise, but the Myo Armband device filters out all the noise in the signal.

Pattern recognition system consists of three main stages: segmentation, feature extraction and classification stage. Analyze and process sEMG signals to distinguish seven hand movements: right wrist, left wrist, open hand, close hand, pliers grip, key grip, and rest hand. The seven hand movements are shown in Figure 14.

Figure 14.

Seven hand gestures of the proposed system

It is very important to prepare in a comfortable sitting position and focus with the cooperation of the volunteer. The volunteer should be taught the necessary movements, duration of the movement, rest period and number of repetitions in advance by the researcher. The volunteer wears the Myo Armband device and connects to a laptop. Rest time, number of repetitions and number of movements are important.

The Process of Learning EMG Signals

Data collection in offline system mode aims to improve system accuracy and reduce the overall response time of the robotic arm. To achieve this goal, the sEMG signal is first recorded, then the offline mode searches for the best transmission position of the signal obtained from the Myo Armband, and evaluates the noise in the Myo Armband

signal and the effect of the channel number. Segmentation window size and features are examined in the extraction process. Finally, a comparison is made between two types of classification techniques.

In real-time mode, the movement of the robotic arm is linked to the movement of the human hand through a pattern recognition algorithm. The tested data recorded by Myo Armband offline on the laptop is carried out by its software. With Arduino, the laptop receives information about the hand movement each time to move the robotic arm.

Data Segmentation: The length of the sEMG signal segment affects classification accuracy and system idle time. When the window length is relatively small, the classification accuracy will be low, and the slowdown time will increase if the window length is gradually increased. Accuracy and latency must be balanced to ensure high accuracy and low latency.

Robotic Hand

Servo motor angles were calculated for the movement of the fingers of the robotic hand printed with a 3D printer. As a result of the classification of EMG signals on Matlab software, the hand movements made by the subject were detected. Angle values are coded in the microcontroller software to ensure that these fingers take appropriate positions. Studies were conducted on four movements that can be performed by the prototype hand (open hand, closed hand, pliers grip and rest). The fingers were moved by the prototype hand by sending EMG signals from the Myo Armband to the laptop via Bluetooth. As seen in Figure 15, the applied finger movements were carried out successfully.

Figure 15.
Robotic hand movements

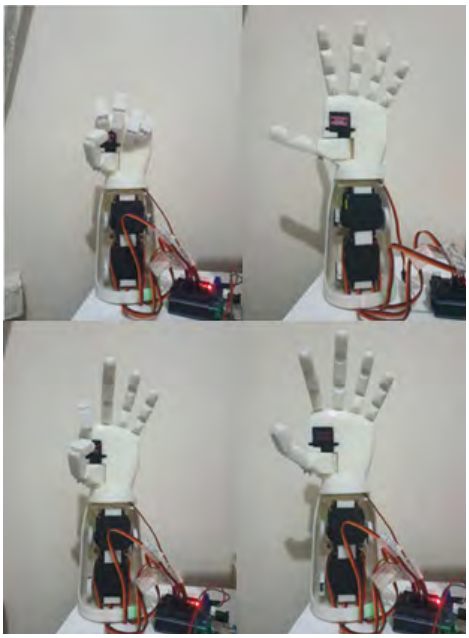

Conclusion

EMG signals can be analyzed to distinguish seven hand movements (right, left, open hand, closed hand, pliers grip, key grip, and rest) and classify patterns. Fingers controlled by 5 servo motors can be moved in real time as a result of the classification of EMG signals coming from Myo Armband.

There is a particular need to develop wearable robotic arm designs. Therefore, devices that obtain different types of EMG signals should be investigated. Myo Armband type devices are designed to obtain EMG signals in a specific region. New designs are needed to obtain EMG signals from larger regions.

It is important to continue studies in this field, especially in order to work on algorithms, methods and solutions that will make the lives of disabled individuals who have to live an amputated life as a result of injuries and the war environment, which is a fate in the geography we live in, and to produce smart prostheses that are more capable and more affordable each time.

References

Ahmed, S. S., Almusawi A. R., Yilmaz B. & Dogru N. (2021). Design and multichannel electromyography system-based neural network control of a low-cost myoelectric prosthesis hand. *Mechanical Sciences*, 12(1), 69-83.

Ali A. H. (2013). An investigation of Electromyographic (EMG) Control of Dextrous Hand Prostheses for Transradial Amputees, Doktora Theses, England.

Al-Timemy A. H., Khushaba R. N., Bugmann G. & Escudero J. (2015). Improving the performance against force variation of EMG controlled multifunctional upper-limb prostheses for transradial amputees. *IEEE Transactions on Neural Systems and Rehabilitation Engineering*, 24(6), 650-661.

Christov I., Raikova R. & Angelova S., (2018). Separation of electrocardiographic from electromyographic signals using dynamic filtration. *Medical Engineering & Physics*, 57, 1-10.

De Luca, C. J. (2002). Surface electromyography: Detection and recording. *DelSys Incorporated*, 10(2), 1-10.

Duncan S. F., Saracevic C. E. & Kakinoki R. (2013). Biomechanics of the hand. *Hand clinics*, 29(4), 483-492

Eryiğit S. (2012). Sağlıklı kişilerde farklı üst ekstremite pozisyonlarında elde kavrama kuvvetlerinin analizi, Master's thesis, İstanbul.

Hassan H. F., Abou-Loukh S. J. & Ibraheem I. K. (2018). Teleoperated Robotic Arm Movement Using EMG Signal With Wearable MYO Armband. arXiv preprint arXiv:1810.09929.

Khushaba R. N., Takruri M., Miro J. V. & Kodagoda S. (2014). Towards limb position invariant myoelectric pattern recognition using time-dependent spectral features. *Neural Networks*, 55, 42-58.

Köklükaya P. D. E. (2008). EMG işaretlerinin işlenmesi ve sınıflandırılması, Master's thesis, Sakarya Üniversitesi.

Li G. (2011). Electromyography pattern-recognition-based control of powered multifunctional upper-limb prostheses. *Advances in Applied Electromyography*, 6, 99-116.

Morales L. & Pozo D. (2017). An experimental comparative analysis among different classifiers applied to identify hand movements based on sEMG. In 2017 IEEE Second Ecuador Technical Chapters Meeting (ETCM) (pp. 1-6). IEEE.

Oskoei M. A. & Hu H. (2007). Myoelectric control systems-A survey, *Biomedical Signal Processing and Control*, 2, 275-294.

Shi L., Liu Z. & Wang Q. (2013). A Novel Method of sEMG Signal Segmentation. IEEE 9th International Conference on Mobile Ad-hoc and Sensor Networks (pp. 515-520).

Visconti P., Gaetani F., Zappatore G. A. & Primiceri P. (2018). Technical features and functionalities of Myo armband: An overview on related literature and advanced applications of myoelectric armbands mainly focused on arm prostheses. *Int. J. Smart Sens. Intell. Syst*, 11(1), 1-25.

Wu J., Li X., Liu W. & Wang Z. J. (2019). sEMG signal processing methods: A review. *In Journal of Physics: Conference Series,* 1237(3), p. 032008.

Yavuz E. & Eyupoglu C. (2019). A cepstrum analysis-based classification method for hand movement surface EMG signals. *Medical & biological engineering & computing*, 57(10), 2179-2201.

About The Authors

Uçman ERGUN is an associate professor and senior researcher in the Department of Biomedical Engineering at Afyon Kocatepe University. He completed his doctorate at the Department of Electronic Computer Education at Gazi University. His main research interests are biomedical signal processing, artificial intelligence, machine learning and microcontroller applications. In addition, he has many academic works such as articles, essays, posters published in many national and international journals.

Email: uergun@aku.edu.tr, ORCID: 0000-0002-9218-2192

Fazilet Canatan ERGUN received her B.Sc. degree at the department of Biomedical Engineering from Isparta University of Applied Science. She is a Ph. D. student at Necmettin Erbakan University, Department of Biomedical Engineering. She has worked in the fields of nanoparticle, nanofiber, also working biomedical materials.

Email: fzlt.cntn93@gmail.com, ORCID: 0000-0003-0379-9033

Similarity Index

The similarity index obtained from the plagiarism software for this book chapter is 8%.

CHAPTER 7

Detection of Shopping Frequency According to Customer Personal Analysis

Beyza DUNDAR
Necmettin Erbakan University, Türkiye

Hadiye BUYUKTOLLUOGLU
Konya Technical University, Türkiye

Ozgur DUNDAR
Necmettin Erbakan University, Türkiye

To Cite This Chapter:
Dundar B., Buyuktolluoglu H. & Dundar O. (2023). Detection of Shopping Frequency According to Customer Personal Analysis. In S. Kocer. & O. Dundar (Eds.), *Artificial Intelligence Applications in Intelligent Systems* (pp. 103–119). ISRES Publishing.

Introduction

The developments in the field of marketing has increased the importance of determining the needs, wishes and preferences of the audience addressed by the markets and taking action accordingly. In order to increase efficiency and take the right steps, the concept of business intelligence has emerged that supports decision processes with tasks such as recording and analyzing data. Markets and companies have found ways to move themselves forward, such as taking the right steps by using the data they have with business intelligence solutions. For example, the fact that markets struggle to retain customers in the long term, where they can make more profit, requires customer segmentation.

Customer segmentation, which emerged as one of the business intelligence solutions, is the process of grouping customers according to common characteristics. In determining

marketing campaigns for customer groups, identifying potentially profitable customers and not getting customers by competing markets, customer loyalty is very important and helps to identify customers (Erarslan, 2023). Efficiency is increased with the help of the techniques used. The most important step in applying customer segmentation is to collect data. The data in the segmentation, which may change depending on the purpose, may be the geographic location of the customer or more specific data such as age and gender. Artificial intelligence applications are used as a technological solution to the customer segmentation problem.

Artificial intelligence is a computer that mimics human intelligence to solve a problem (Samuel, 1959). Machine learning, one of the sub-branches of artificial intelligence, teaches computers to learn. In other words, it is the whole algorithm that enables it to predict the results with the help of software programs and to get more accurate results. As a result of introducing the input data to the machine, the outputs update themselves with the help of machine learning and predict other outputs. There are 4 types of machine learning (Ayodele, 2010). These are:

- Supervised Machine Learning
- Unsupervised Machine Learning
- Semi-Supervised Machine Learning
- Reinforced Machine Learning

Supervised Machine Learning

Provides information to the model created by the expert and trains the model. It isexpected that the trained model will predict the result with the data that is not given. Thedata we give to the model are labeled data. Labeled data indicates what information thedata has (Kocer et al.,2022).

Regression is a type of supervised learning problem. In these problems, the desired value to be estimated is the continuous value. These values take a value from the set of uncountable values and are in an infinite range of values. Value type is numeric data type.

Another supervised learning problem is Classification. In these problems, the desired value to be estimated is the discrete value. That is, it is in the limited value range. Value type is categorical data type.

Unsupervised Machine Learning

It is the type of learning in which the model is trained to find the structures of data without labels. The model is presented with a large number of examples but contains only input data. Its purpose is to reveal the structure of the data, to identify relationships and

patterns that may not be immediately noticeable. It is used to reduce the dimensionality of the data (Öztemel, 2003).

As an example of unsupervised learning algorithms; Clustering Algorithms it groups similar data points according to their properties, proximity and density(Singh et al., 2022;Deng 2020).

K-Means Clustering Algorithm: A center point is randomly determined for clusters. Elements outside the central element are clustered according to the nearest center point. For this, the distances of each element to the center point are calculated. Within the clustered element groups, the center point is calculated again. These processes continue until the center point becomes fixed.

Hierarchical Clustering Algorithm: There are two approaches in this algorithm as Agglomerative and Devisive. In *Agglomerative* each data is first clustered in its own way. It then merges with the nearest cluster to form a new cluster. Up until there is just one significant cluster, this process continues. In contrast to this approach, all data is contained in a single cluster in *Devisive*. Each data performs division until it becomes a cluster.

DBSCAN Clustering Algorithm: In this algorithm, it calculates the densities of objects while creating clusters. Clusters are defined by high-density data objects. Clusters with low-density objects show noisy or outliers.

Dimensionality Reduction Algorithm: This algorithm aims to reduce the number of features and variables in the data while preserving important information.

Anomaly Detection Algorithm: This algorithm identifies abnormal data that does not fit the patterns in the dataset. SVM, automatic encoders or isolation forest are used for anomaly detection.

Association Rule Learning Algorithm: These algorithms find relationships between variables in the dataset.

Generative Algorithm: This algorithm models the fundamental distribution of the data. They generate new samples similar to the training data.

Semi-Supervised Machine Learning

It is similar to both learning methods by including labeled data used by supervised learning and unlabeled data in unsupervised learning. These two types of data are used simultaneously.

Reinforced Machine Learning

Although the results of the information are certain, it does not need prior knowledge even

in cases where it is not sufficient. It is an algorithm that can start the process without any data.

Problem Definition

Without a customer segmentation perspective and business intelligence solutions, the records kept by the markets were not fully effective in revealing the customer profile. The effort to respond to the emerging needs has led to the emergence of these issues and solutions have been tried to be produced. Machine learning applications have emerged to solve such problems and continue to develop.

It has also produced different solutions according to the shape of the machine learning problem, which has sub-titles. These algorithms, which emerged with different approaches and theoretical studies, brought solutions to the problem of this study.

Accordingly, in the data set we used in the study, there are records kept about the customers of the markets. Among the algorithms known to be effective and widely used in the world of machine learning, k means was selected from the clustering algorithms suitable for this problem, and it was also desired to observe how some other clustering algorithms solved the problem and how the results were.

Our motivation and purpose is to try, observe, interpret and draw conclusions on the problem of machine learning algorithms and techniques that make it easier for people to work in general in the different areas that we have learned.

Methods

In the selected problem, the results of three clustering algorithms were evaluated. These are respectively; K Means, DBSCAN and Hierarchical algorithms.

K-Means Algorithm

In 1967 J.B. The k means algorithm developed by MacQueen is an unsupervised algorithm that solves problems with clustering. According to this algorithm, centroids are determined for clustering in the data set. The centroid number corresponds to the k expression in the name of the algorithm. The number of clusters is chosen in this way. The next step is to calculate the distance between each data point and the centroid using the Euclidian Distance formula (Ahmed et al., 2020;Hashim et al., 2022).

$$\sqrt{\sum_{i=1}^{n}\left(x_i - y_i\right)^2} \tag{1}$$

Data points are assigned to the point with the least distance value, that is, the closest point. Since centroids are randomly assigned at the beginning, the clustering process is completed after selecting and following the same steps until the correct centroids are found. However, the random selection process may cause the desired result not to be

achieved. K-Means ++ was introduced to solve this problem. While the algorithm is the same, only a change has been made to select the points in order to avoid the possible problem in centroid assignment (Ahmed et al., 2020; Hashim & Muhammed, 2022).

Taking a different route in centroid selection, K-Means++ randomly selects a point in the first step. The data point where the distance of all data points to this selected point is maximum is determined as the new centroid. These steps are performed cyclically until the specified number of clusters occurs. Accordingly, the centroids are at the most possible distance from each other and distribute the data points in the most appropriate way, thus solving the problem.

DBSCAN

Another clustering algorithm, DBSCAN, was proposed by Martin Ester, Hans-Peter Kriegel, Jörg Sander and Xiaowei Xu in 1996. It is a density based algorithm. It tries to cluster according to the points where the data points are high in terms of density. One of its most important features is that it performs well on datasets where the data points are not regular.

There are two parameters required for the DBSCAN algorithm; *Epsilon(*ε) and *minPoints(n)*. Epsilon parameter is required to make assignments to the cluster. In other words, it is a distance measure used to determine the density around any point and to select points. The minPoints parameter, on the other hand, refers to the minimum data point required to create a density somewhere in the dataset. The algorithm steps are as follows;

- A random point is chosen.
- Epsilon and minPoints values are set.
- It is decided whether the first selected point is the appropriate core point of the cluster. If appropriate, a cluster is created according to the parameters.
- If the selected point is the border point, the next point is checked.
- The algorithm continues until all points are processed (Sen, 2014).

Hierarchical Algorithm

The hierarchical clustering algorithm is used to group unlabeled data into a cluster. It is an unsupervised machine learning algorithm. The purpose of this algorithm is to generate a set of nested data in clusters. It works by grouping the data in a cluster tree. Clustering is started by considering each data point as a separate cluster. It determines the two clusters that are closest to each other and a new cluster is formed. This event continues until all clusters are a cluster.

In this algorithm, the question “How many clusters will we find the best result” is found with a dendrogram. So this hierarchy is represented by the dendrogram. A dendrogram is a graph of clusters that come together and the distance between those clusters. The optimum number of clusters is the number of lines connecting the vertical cluster and the point at which the distance between two horizontal lines drawn horizontally without intersecting a cluster is maximum. There are two approaches, agglomerative and divisive, based on the basic logic of the hierarchical clustering algorithm.

Agglomerative: Takes a bottom-up approach to grouping data points into clusters. At the initial stage, each data set is considered as a single set. Then it combines with the closest pair of clusters to form a new cluster. This situation lasts until all datasets are merged into a single dataset.

Divisive: It operates in opposition to the agglomerative strategy. It exhibits a top-bottom approach. In other words, it exhibits a discriminatory approach. In the initial phase, there is only one cluster. At each stage, the data are separated from the main cluster according to the distance and similarity matrices and form different subsets. In the final stage, each data forms a cluster (Alzubi et al., 2018;Ran et al., 2023).

The distance and similarity calculations between the data are updated for each stage. The calculated similarity and distance values matrix represents the use of the chosen connection method. Commonly used connection techniques are divided into 3 (Kimes et al., 2017;Shirole et al., 2021).

Connection based techniques;

It is divided into 3 groups as Single connection, Full connection and Average connection.

- Single Linkage: By using the distance matrix, the two closest data sets are combined. The procedure’s drawback is that it takes a while.
- Complete Linkage: Combining the clusters is performed by considering the distance at the farthest distance between the data sets. The disadvantage is that the dataset is sensitive to endpoints.
- Average Linkage: Combining the clusters is performed by considering the average values of the distance between the data in the two data sets. This connection is a more suitable choice among others.

Variance Based Techniques;

Ward’s Linkage: Ward(1963) proposed a method to measure the loss of each cluster in a way that minimizes information loss and can be easily interpreted. Information loss was interpreted as the sum of squares of error. The purpose of this method is to combine clusters so that the diversity of data within these clusters does not increase. Thus, clusters

in the form of homogeneous clusters are formed.

Centralization Based Techniques;

It is divided into 2 as Median Linkage and Centroid Linkage.

- Median Linkage: It was proposed by Gower in 1967. If the difference between the sizes of the two clusters to be merged is large, the center of gravity of the new cluster is close to the center of gravity of the larger cluster.
- Centroid Linkage: Euclidean distance is used as the distance measure between two clusters. Each cluster is represented by the centroid of the current cluster.

As a result of the merger of the two clusters, it is sufficient for the weight points to be at a minimum distance between each other. The most important advantage is that it is not affected much by observations of different nature.

Library

- NumPy: It was created in 2005 by Travis Oliphant, adding to the Numeric library by changing the Numarray's properties. It is a library for the Python programming language that adds high-level mathematical functions for multidimensional array and matrix data structures. NumPy is an open source library (McKinney, 2012).
- Pandas: In 2008, Wes McKinney developed this high-performance library to analyze financial data. It is an open-source, free library. It is used for data processing and data analysis. It is used to process numerical tables and time series (McKinney & Team, 2015; Gangwar, 2022).
- Matplotlib: Written by John Hunter in 2003. It is a data visualization and drawing library used for the numpy library. Provides object-oriented API for drawing, visualizing graphics to applications using general-purpose GUI toolsets. The matplotlib.pyplot.plot() method offers a standardized interface for making various chart kinds. The plot() function is used in the most basic example to plot values as x,y coordinates in a data graph (Bercowsky, 2022; Embarak, & Karkal. 2018).
- Seaborn: Python's Seaborn package allows you to create statistical visuals. It builds on top of matplotlib and integrates closely with pandas data structures. Plot functions work on data frames and arrays containing entire datasets and internally perform the semantic mapping and statistical aggregation necessary to produce informative graphs. Its dataset-driven, declarative API specifies what the different elements of charts mean (Bisong, 2019; Waskom, 2021).
- I/O: The Python io module allows us to manage the input and output operations

related to the file. The benefit of using the IO module is that we can expand the capability to enable writing to Unicode data by using the existing classes and procedures.

- Warning: Warnings are provided to alert the developer about situations that are not necessarily exceptions. Typically, the keyword, function, or class, etc. A warning is issued when some of the certain programming elements, such as A warning in a program is different from an error. If an error occurs, the Python program is terminated immediately. Conversely, a warning is not critical. It shows a message, but the program is running. The warn()" function is used to display warning messages. Warning module is actually a subclass of Exception, which is a built-in class in Python.
- Plotly Express: Plotly Express is a new high-level Python visualization library: a wrapper for Plotly.py that exposes a simple syntax for complex plots. It was developed with a focus on having a clear, consistent, and simple-to-learn API, and it was inspired by ggplot2 and seaborn. With just a single import, it can produce complex interactive images, including direction, maps, animations, in a single function call (Matthes, 2023).
- Sklearn: It is a Python-based library used to build machine learning models. It uses a variety of learning techniques for classification, clustering, and regression. Sklearn is compatible with NumPy and SciPy. So it can easily work with different Python libraries.
- SciPy: Scipy (Scientific Python) is an open source library that helps calculate complex mathematical or scientific problems. It has a built-in mathematical function and libraries that can be used in science and engineering to solve different types of problems. It also includes optimization, eigenvalue problems, differential equations, integration, interpolation, algebraic equations, statistics, etc. Scipy is a numerical Python extension that makes data manipulation incredibly quick and effective. High-level commands and classes provide an easy way to manipulate and visualize data. It includes a vast array of scientific subpackages and can interface with many different contexts (Arslan, 2019).

The dataset used in this project is Mall Customers, which is used in machine learning and is suitable for applying clustering algorithms. It is used for customer segmentation because it has data about store customers.

There are five variables, namely two hundred observation units of the column, in the data set. The variables are respectively Customer ID, Gender, Age, Annual Income(k$), Spending Score (1-100). While the personal data of the customers are in the first four

columns, the Spending Score variable represents the value assigned by the store according to the customer's spending status. While the Customer ID, Age, Annual Income and Spending Score variables are included in the data set as numerical discrete data types, the Gender variable appears as a categorical nominal data type.

Before applying the algorithm, the information obtained is as follows when it is examined in terms of an overview of the data set. There is no missing value in the data set. The number of women and men is distributed as 56% female and 44% male. In addition, mean, median and standard deviation values were also examined. According to the standard deviation, the age variable has a smaller value compared to the income and expenditure score. In summary, outliers are less than income and spending score. Graphics that support this situation appear when visualization techniques are used to prove this result. In addition, graphs were created to observe the relationship of the variables with the spending score. Algorithms were applied after the preprocessing step.

Experiments

When the algorithms described under the title of Methods are applied to the problem, their effects are observed as follows.

K-Means Algorithm

The first applied K Means algorithm was tested on the data set using the Elbow method. The performance of the K-means clustering algorithm depends on the high-yield clusters it creates. But choosing the optimum number of clusters is a big job. The ideal number of clusters can be discovered in a variety of ways. The elbow technique is one among them.

The Elbow method is a dating method used to determine cluster selection in a dataset. The method consists of plotting the comprehensive variant as a function of cluster weight and choosing the amount of bend of the curve as the usage cluster. The same method can be used to select parameter selection in other data-driven models, such as base values numbers for windows of a dataset. The WCSS value is used to find the optimal dataset. WCSS, Intra-cluster Sum of Squares, which describes the total variations within a set.

The following image shows the Elbow graph, which was designed to determine the number of clusters. According to this graph, it was seen that the most appropriate number of clusters for the problem was five and the K Means algorithm was created according to this number of clusters.

Figure 1.
Elbow graphic

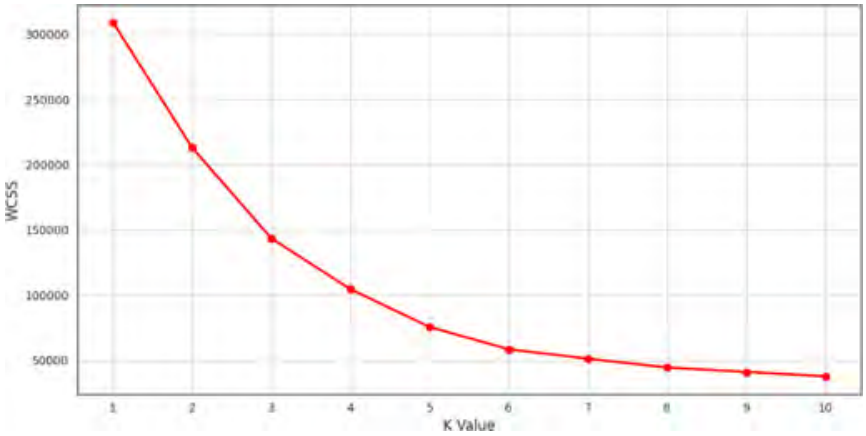

According to this graph, it was seen that the most appropriate number of clusters for the problem was five and the K-Means algorithm was created according to this number of clusters.

The image of the clusters formed when the algorithm is applied is as follows. A three-dimensional graphic is created in Figure 1.

Figure 2.
K-Means graphic

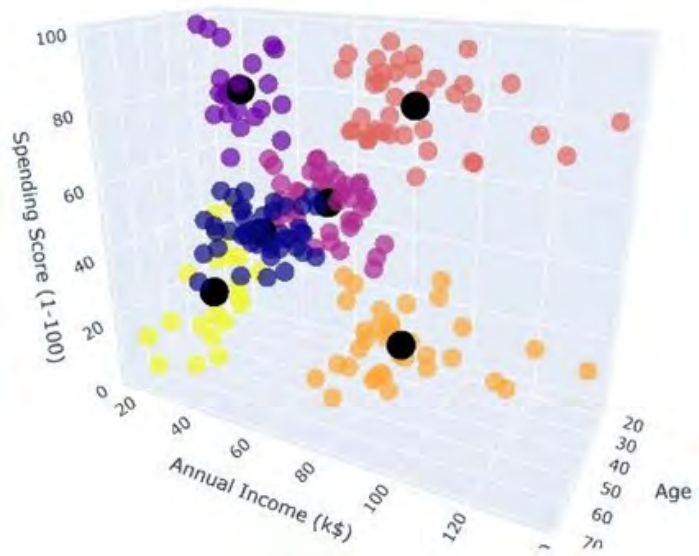

In addition, the effect of the variables on the expenditure score one by one was observed with two different graphs. The comments that can be made according to these graphs are as follows;

- According to the Age-Expenditure Score clustering graph, it can be said that

the age group with the highest score is between the ages of 18-40.

- Customers aged 40-70 have lower spending scores compared to customers aged 18-40.
- According to the Income-Expenditure Score graph, there are two groups with high expenditure scores. These two groups, whose income is in the range of 15-40 (k$) and between 65-140 (k$), have high spending scores. In this respect, it cannot be said that income literally affects the spending score. Because it is a result that can be deduced from the graph that the spending score of individuals with a lower income is too high

Silhouette score ,which is also used to evaluate score, is a value used to determine the optimum number of clusters in the k means algorithm like the elbow method. This score selects data points in all clusters one by one and calculates both their distance from points in the same cluster (a) and their distance from data points in other clusters (b). The calculation formula is as follows (Shi et al., 2021).

$$(b-a)/max(a,b) \tag{2}$$

According to this formula, the results vary in the range of [-1,1]. As the result gets closer to 1, it determines that the performance in the cluster is high and that there is a suitable number of clusters for this algorithm. As the value decreases and turns negative, this probability also decreases and the result is that the number of clusters is not suitable for the algorithm.

Figure 3.

Silhouette score

```
Cluster 2 silhouette score : 0.29
Cluster 3 silhouette score : 0.38
Cluster 4 silhouette score : 0.41
Cluster 5 silhouette score : 0.45
Cluster 6 silhouette score : 0.45
Cluster 7 silhouette score : 0.44
Cluster 8 silhouette score : 0.43
Cluster 9 silhouette score : 0.41
```

As can be seen in Figure 3 the most suitable number of clusters for this algorithm was determined as six.

DBSCAN

While applying the DBSCAN algorithm, two parameters that are important for this algorithm were tested by changing the epsilon and minimum points values. The graphics are shown below.

Figure 4.

Annual income- spending score graphic

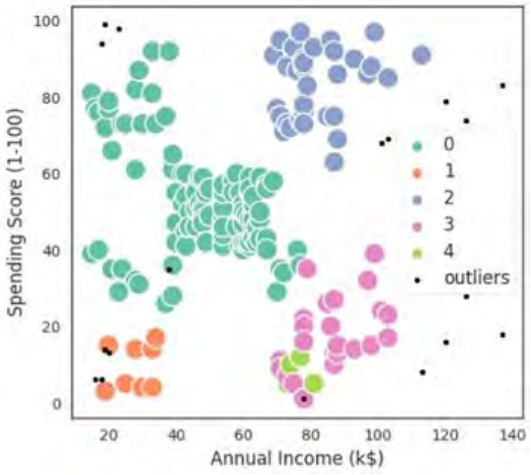

Figure 5.

Spending score- age graphic

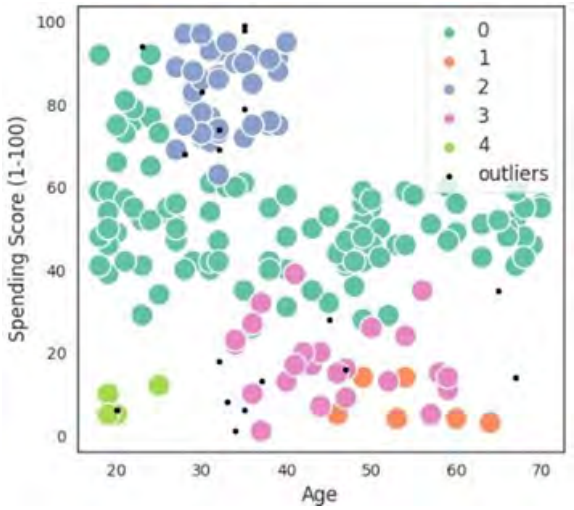

As a result of these trials, when the epsilon value was assigned as 12.5 and the minimum points value as 4, five clusters were formed as seen in the graphs in Figure 4 and Figure 5. Compared to other trials, there are fewer outliers in these parameters. When the parameter values are changed, the number of clusters decreases and the outlier increases.

As an example of the study in which different parameters were tested, the following graphs were obtained when the epsilon value was given as 12.5 and the minimum points 6.

Figure 6.

Annual income- spending score graphic

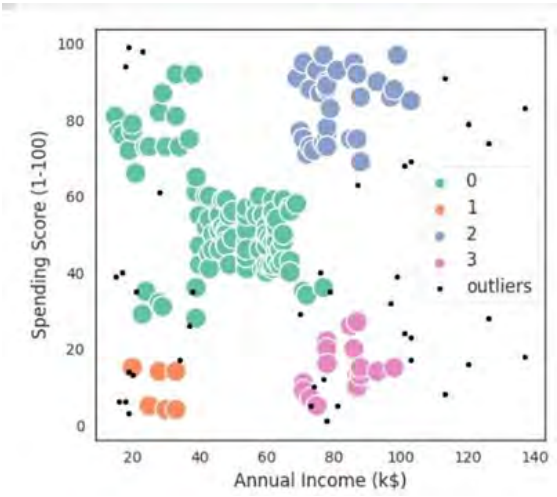

Figure 7.

Spending score- age graphic

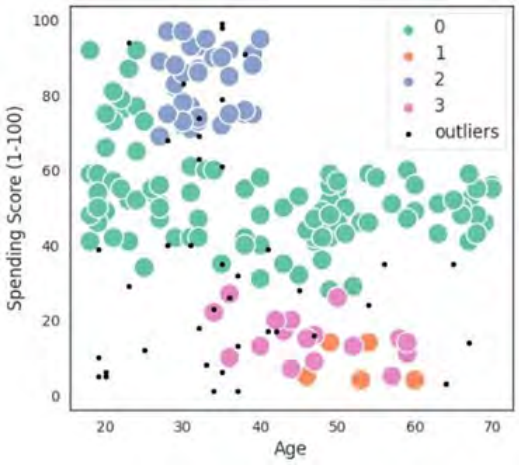

As an example of the study in which different parameters were tested, the following graphs were obtained when the epsilon value was given as 12.5 and the minimum points 6.

As seen in the results in Figure 6 and Figure 7, the number of clusters decreased compared to the previous experiment, and the outlier values increased.

Hiererchical Algorithm

The graphics results of the hierarchical algorithm are shown with the help of the dendrogram described in the methods section. Agglomerative method was used. The datasets were merged with the closest clusters until they became a single cluster. We found that five clusters are formed when a horizontal line is drawn that cuts the last vertical lines. In Figure 5, the dendrogram for the problem is shown.

Figure 8.

Dendrogram

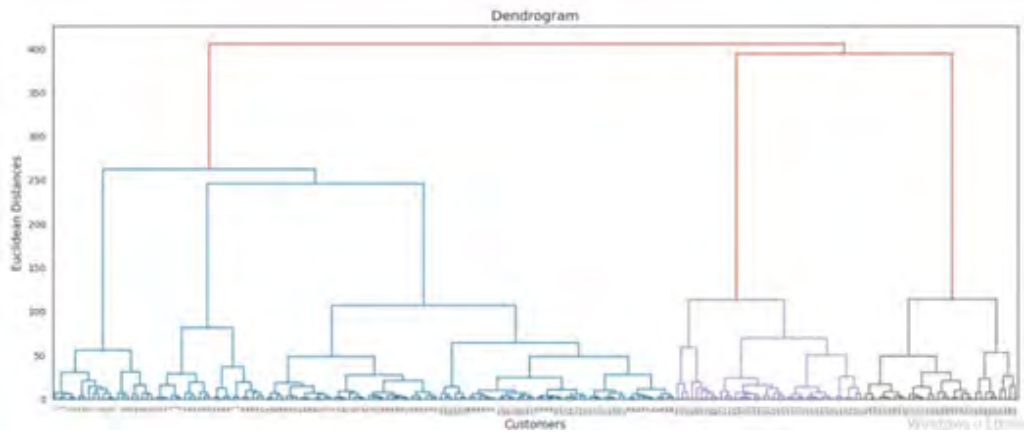

Figure 9.

Hierarchical algorithm clustering

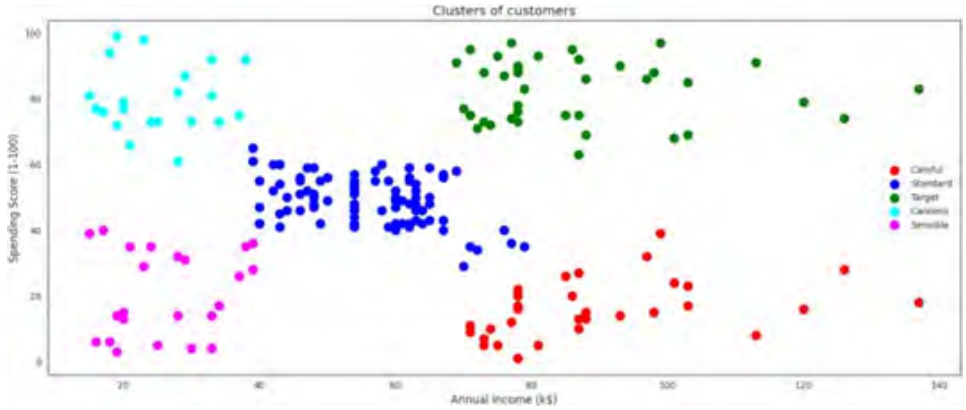

Results

In this study, the customer segmentation problem, which is solved by technological techniques within the scope of business intelligence, has been examined. Among these solutions, clustering algorithms suitable for the problem were examined in detail and the results were evaluated when applied to the problem.

Accordingly, the results obtained are as follows;

First of all, some information was obtained in the preprocessing stage for the data set. These were calculations of the correlation between the spending score and other variables. As a result of the calculations, a negative correlation was observed between age and expenditure score, while a large correlation was not observed in income and expenditure scores. In short, the relationship between age and spending score is inverse, and as one increases, the other decreases. In the income and expenditure scores, such an effect is not observed much.

The graphic results described under the title of experiment also support the correlation

situation. It has been revealed that a similar interpretation can be made in the clusters formed as a result of the algorithm.

Figure 10.

Gender – Spending score boxplot

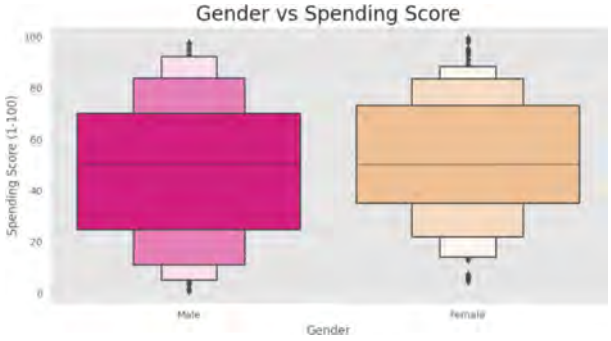

It can be said that the spending score of women is higher than that of men according to the graph above.

In the customer segmentation problem, which is the aim of the study, different clustering algorithms were applied to the data set we have. In addition to the results obtained from the graphics, the results were also obtained from the algorithms.

When the results were evaluated in this study, in which three different algorithms were used, it was observed that these algorithms were suitable for the problem.

One of the main results about the algorithms is that there is no big difference in terms of the solutions they produce to the data set in terms of performance. The reasons for reaching this conclusion are as follows.

- All three algorithms found close values as the optimum number of clusters. While the optimum number of clusters for K Means was six, the other two algorithms found the number of clusters to be five.
- It was seen that the clustering in the graphs that emerged at the end of the algorithms were similar to each other.

Finally, in this study, we have experienced and observed that the algorithms used for customer segmentation problems are efficient and perform well for such problems.

References

Ahmed, M., Seraj, R., & Islam, S. M. S. (2020). The k-means algorithm: A comprehensive survey and performance evaluation. Electronics, 9(8), 1295.

Alzubi, J., Nayyar, A., & Kumar, A. (2018, November). Machine learning from theory to algorithms: an overview. In Journal of physics: conference series (Vol. 1142, p. 012012). IOP Publishing.

Arslan, İ. (2019). Python ile veri bilimi. Pusula.

Ayodele, T. O. (2010). Types of machine learning algorithms. New advances in machine learning, 3, 19-48.

Bercowsky Rama, A. (2022). Python: Data handling, analysis and plotting. In Bioimage Data Analysis Workflows–Advanced Components and Methods (pp. 29-57). Cham: Springer International Publishing.

Bisong, E., & Bisong, E. (2019). Matplotlib and seaborn. Building Machine Learning and Deep Learning Models on Google Cloud Platform: A Comprehensive Guide for Beginners, 151-165.

Deng, D. (2020, September). DBSCAN clustering algorithm based on density. In 2020 7th international forum on electrical engineering and automation (IFEEA) (pp. 949-953). IEEE.

Erarslan, Havva Gülsüm. *Bir e-ticaret firması için rfm analizi ve kümeleme algoritmaları kullanılarak müşteri segmentasyonu ve analizi / Customer segmentation using rfm analysis and customer segmentation and analysis with using clustering algorithms.* Yüksek Lisans Tezi. İstanbul Medeniyet Üniversitesi, 2023.

Gangwar,M.(August3, 2022).Python Pandas Module Tutorial.

Hashim, D. K., & Muhammed, L. A. N. (2022). Performance of K-means algorithm based an ensemble learning. Bulletin of Electrical Engineering and Informatics, 11(1), 575-580.

Kimes, P. K., Liu, Y., Neil Hayes, D., & Marron, J. S. (2017). Statistical significance for hierarchical clustering. Biometrics, 73(3), 811-821

Koçer, S., Jama, B. S. A., Er, Y. & Dündar, Ö. (2022). A Comparative Study for Evaluating the Performance of Various Classification Techniques on Brain Tumour, Five Zero, 2(1), 1-12

Matthes, E. (2023). Python crash course: A hands-on, project-based introduction to programming. no starch press.

McKinney, W. (2012). Python for data analysis: Data wrangling with Pandas, NumPy, and IPython. " O'Reilly Media, Inc.".

McKinney, W., & Team, P. D. (2015). Pandas-Powerful python data analysis toolkit. Pandas—Powerful Python Data Analysis Toolkit, 1625

Öztemel, E. (2003). Yapay sinir ağları. Papatya Yayıncılık, Istanbul

Rai, P., & Singh, S. (2010). A survey of clustering techniques. International Journal of Computer Applications, 7(12), 1-5.

Ran, X., Xi, Y., Lu, Y., Wang, X., & Lu, Z. (2023). Comprehensive survey on hierarchical clustering algorithms and the recent developments. Artificial Intelligence Review, 56(8), 8219-8264.

Samuel, A. L. (1959). Some studies in machine learning using the game of checkers. IBM Journal of research and development, 3(3), 210-229.

Sen,Tolga. Kümeleme Ve Genetik Algoritma Destekli Yaklaşimlarla Kapasite Kisitli Araç Rotalama Probleminin Çözümü: Perakende Zincirinde Uygulanmasi. Yüksek Lisans Tezi , Sakarya Üniversitesi, 2014.

Shi, C., Wei, B., Wei, S., Wang, W., Liu, H., & Liu, J. (2021). A quantitative discriminant method of elbow point for the optimal number of clusters in clustering algorithm. Eurasip Journal on Wireless Communications and Networking, 2021(1), 1-16.

Shirole, R., Salokhe, L., & Jadhav, S. (2021). Customer segmentation using rfm model and k-means clustering. Int. J. Sci. Res. Sci. Technol, 8, 591-597.

Singh, H. V., Girdhar, A., & Dahiya, S. (2022, May). A Literature survey based on DBSCAN algorithms. In 2022 6th International Conference on Intelligent Computing and Control Systems (ICICCS) (pp. 751-758). IEEE.

Waskom, M. L. (2021). Seaborn: statistical data visualization. Journal of Open Source Software, 6(60), 3021.

About The Authors

Beyza DUNDAR, graduated from KTO Karatay University, Department of Computer Engineering. She is a master's student at Necmettin Erbakan University, Department of Computer Engineering. The system studied data science, artificial intelligence, image processing, machine learning and natural language processing.

Email: dundarbeyza777@gmail.com , ORCID: 0000-0002-2843-1043

Hadiye BUYUKTOLLUOGLU, is a graduated of KTO Karatay University Computer Engineering. She is a master student at Konya Technical University Computer Engineering, worked in the fields of data science and machine learning, also working on mobile application development with Flutter.

Email: hadiye756@gmail.com ,ORCID: 0009-0008-2586-9307

Ozgur DUNDAR, PhD, works at Necmettin Erbakan University, Department of Astronautical Engineering. He graduated from the Electrical and Electronics Engineering Department of Selcuk University. He worked as an Automation Engineer for a while. His master's and doctorate degrees are from Selçuk University, Institute of Science and Technology, Department of Electrical and Electronics Engineering. Special fields of study are Automation, Robotic, Communication, Electromagnetic and Micro Strip Patch Antenna designs.

Email: ozdundar@erbakan.edu.tr ,ORCID: 0000-0002-4142-4446

Similarity Index

The similarity index obtained from the plagiarism software for this book chapter is 7%.

CHAPTER 8

Microcontroller-Based Design Electrostimulation (TENS) for Therapeutic Purposes

Sabri KOCER
Necmettin Erbakan University, Türkiye

Ozgur DUNDAR
Necmettin Erbakan University, Türkiye

To Cite This Chapter:
Kocer, S. & Dundar O. (2023). Microcontroller-Based Design Electrostimulation (TENS) for Therapeutic Purposes.In S. Kocer. & O. Dundar (Eds.), *Artificial Intelligence Applications in Intelligent Systems* (pp. 120–144). ISRES Publishing.

Introduction

It is important to diagnose diseases correctly and treat them appropriately and in a timely manner. However, the primary goal of medicine is to prevent these diseases. Treatment and rehabilitation medicine are as indispensable as preventive medicine (Sonkaya, A. 2019).

Rehabilitation of diseases involving the musculoskeletal system with a good team will minimize disability and disability. As important as the rehabilitation team is, physical medicine practices to assist the team are equally important and necessary.

Electric current, which has been used in various diseases for centuries, still maintains its importance. Advances in computer and electronic device technology and the addition of new scientific data on neuromuscular physiology have enabled the appropriate adjustment of the intensity, duration, wavelength, frequency and direction of these two types of current and the development of more effective new electrotherapy methods. These methods applied through the skin stimulate the skin, nerve and muscle. These currents, which can be separated according to their frequencies, create a magnetic field around the application area and give a different form to the treatment. In addition to normal muscle and nerve stimulation, it is also possible to stimulate denervated muscles directly with these currents.

It seems possible to deliver various drugs and substances to deep tissues, joints and periarticular structures with these currents (Harrison, 2021).

From a dynamic point of view, it can be said that the human body, like all other living things, is made up of a myriad of chemical and physical events that come together to perform specific functions and are in constant interaction with each other. Chemical events occur as a result of the interaction of atoms or molecules. At the basis of this interaction, the positive and negative electric charges that make up the atom are of great importance. On the other hand, in cells, which are the building blocks of the organism, displacement can be observed in the form of ion transfer between intracellular and extracellular environments through the physical force defined as "membrane potential". Membrane potential is an electrical potential formed by negative charges inside the cell and positive charges outside the cell (Karacan I., 2003).

On a macro scale, displacement and movement are observed as walking, running, flying and swimming at the end of a very complex process in which the movement command from the brain is transmitted to the muscle via peripheral nerves and the muscle contracts. The generation, transmission and stimulation of this movement command to the target organ depends on the generation of a propagating electrical activity known as an "action potential". Electrotherapy should not be understood only as a treatment approach applied by applying electric current. Today, the aim of electrotherapy in a broad sense can be considered as the normalization of dysfunctions that occur due to pathological electrical activities in muscle and nerve tissue that function with electrical principles (Gidon, 2020).

Electrotherapy has two basic elements: the electric current used for treatment and the tissues to which this treatment is applied. In order to understand electrotherapy, it is useful to consider the electrophysiological properties of the electric current and the tissues to which it is applied (Rueda, 2023).

Properties Of Tissues

General Electrophysiologic Properties

The effects of electric current in tissues are related to the electrical properties of these tissues. The main electrical properties of the cell, the smallest functional unit of the body, are the membrane resting potential and the action potential, which expresses the state of excitation (Trayanova, 2021).

Membrane resting potential

The membrane resting potential is -90 mV in thick skeletal muscle and nerve fiber and -40 mV to -60 mV in thinner skeletal muscle and nerve fiber. These values of membrane potential are influenced by the distribution of intracellular and extracellular ions. The

intracellular environment contains more potassium (K^+) and less sodium (Na^+) than the extracellular environment. Among the negatively charged ions, protein and phosphates are more abundant in the intracellular fluid compartment and chlorine (Cl^-) in the extracellular medium.

The semipermeable and selective properties of the cell membrane play an important role in the formation of this ion distribution. While large molecules such as protein, sulfate and organic phosphate compounds cannot pass through this membrane, small molecule ions can easily pass through. Since the inner and outer surface of the cell membrane is covered with a lipid layer, only lipid-soluble molecules can directly pass through this membrane. However, the passage of membrane potential-forming and water-soluble ions such as Na^+, K^+, Cl^- is only possible through protein channels and carrier proteins (Benarroch, 2020).

Protein channels are of two types: leakage channels and gated channels. Ions pass freely through the leakage channels depending on the concentration and electrical gradient. Potassium leakage channels are about 100 times more permeable than sodium leakage channels. Gated channels have special gates that prevent the free passage of ions. There are two types of gated channels depending on the stimulus that opens and closes these gates. Voltage-gated channels are of two types: sodium and potassium channels. Sodium channels have two gates. One is the activation gate on the extracellular fluid compartment (extracellular) side of the channel and the other is the inactivation gate on the intracellular side of the channel. In the resting membrane, the Sodium activation gate is closed and the inactivation gate is open (Rueda, 2023; Trayanova, 2021; Benarroch, 2020).

The activation gate opens as the membrane potential increases from -90 mV to zero mV. Usually this gate opens between -70 and -50 mV. During this period the permeability to Na+ ion increases 500-5000 times. The inactivation gate closes approximately 0.1 ms after the activation gate opens during the decrease in membrane potential. It remains closed until the membrane potential returns to the resting potential (-90 mV). The activation gate opens fast and the inactivation gate closes slowly.

Membrane resting potential formation

In the depolarized membrane, there is an accumulation of K^+ inside the cell and Na+ outside the cell with the activation of the active transport mechanism. This process leads to the formation of a concentration and electrical gradient between the inside and outside of the cell. Due to the concentration gradient, there is an outflow of K^+ out of the cell and an inflow of Na^+ into the cell through the leakage channels by simple diffusion. K^+ transit is 100 times higher than Na+ transit. Since the membrane is impermeable to most of the intracellular anions, K^+ leakage out of the cell is not accompanied by an equal rate

of anion passage. The leakage of K^+ out of the cell due to the concentration gradient also causes an increase in intracellular negative charge. This prevents a continuous outflow of K^+ out of the cell and thus the concentration gradient is balanced by the electrical gradient. Similar balancing of Na^+ ion entry into the cell through leakage channels prevents excessive accumulation of positive charge inside the cell (Chrysafides, 2019).

Action potential formation and propagation

Electrical, chemical or mechanical stimuli can stimulate the nerve. The response to these stimuli may be limited to a local area or may spread. Examples of local responses include "synaptic potentials" (excitatory and inhibitory postsynaptic potentials) and "generator potentials" in receptors. Responses that are not limited to a local area and that propagate are called action potentials (Raghavan, 2019).

When the action potential starts, the sodium voltage channel is suddenly activated and Na^+ permeability increases 5000-fold. During this period, the permeability of Na^+ ions is thousands of times higher than that of K^+. Therefore, the intracellular positive ion increase is much greater than the positive ion depletion due to K+ ion leakage and the membrane potential increases rapidly from -90mV to zero. This process of the action potential is defined as the depolarization period. In thick nerve fibers, the membrane potential also exceeds zero and thus takes on a positive value. In thin nerve fibers and the vast majority of neurons in the central nervous system, this potential cannot exceed zero. As the membrane potential decreases, the Sodium channel inactivation gate closes and the Potassium activation gate opens. Therefore, a rapid loss of intracellular positive ions occurs. This process in which the membrane potential reaches the resting potential is called the repolarization period. After the end of the action potential, i.e. after the membrane resting potential is reached, the potassium channel remains open for a few ms due to the slow closure of the activation gate and hyperpolarization of the membrane occurs. This hyperpolarization state is defined as "positive afterpotential" (Yerdelen, 2013). This formation is shown in Figure 1.

Figure 1.

Change in Na^+ K^+ ion permeability simultaneously with action potential (pittmedneuro.com)

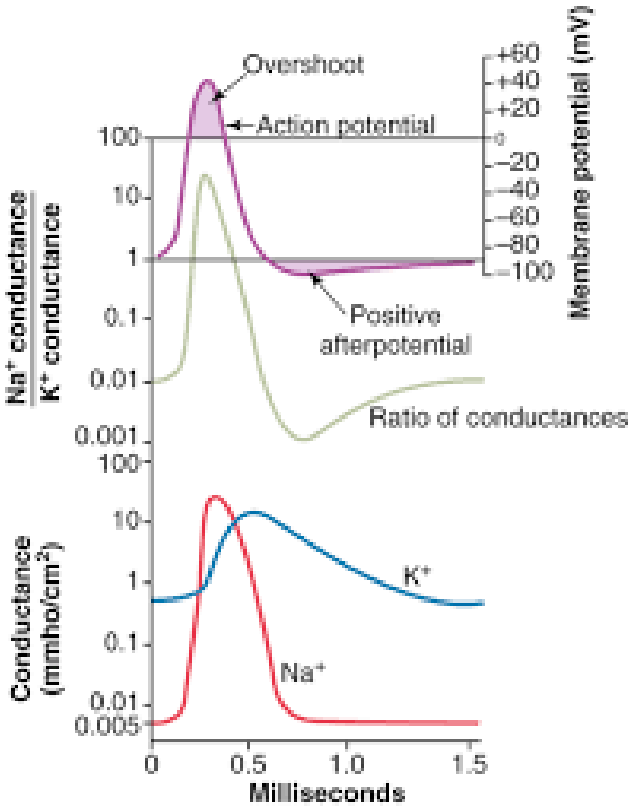

Electrical Transmission of Nerves

There is a potential difference between the inner and outer surface of the nerve due to the difference in the concentration of ions inside and outside the plasma membrane. In the resting state, the nerve is positively charged on the outside and negatively charged on the inside, making the plasma membrane impermeable to sodium ions. This is the polarized state of the membrane.

When the nerve is stimulated, the stimulus reduces the potential difference across the plasma membrane. This decrease, when it reaches a certain critical level, leads to a concentration in the permeability of the membrane to sodium ions. This results in a change in the ion concentration inside and outside and the decrease in the potential difference continues until a reverse charge occurs. In this state, the inside of the membrane is positively charged and the outside negatively charged (Figure 2). Immediately after this activity, sodium ions are pumped out and this part of the nerve returns to its resting state. The potential difference between the active and resting part of the nerve causes local electron flow between the active and adjacent parts of the nerve (Foster, 1987;Naillioğlu, 2002).

Current flows through the nerve fiber in the opposite direction to the potential difference across the membrane. The nerve fiber shows a resistance to the current. The passage of current reduces the potential difference. The membrane thus becomes permeable to sodium ions.These changes are then transmitted along the nerve fiber. This change in polarized state ensures the passage of an impulse along the nerve (Figure 2).

Figure 2.

Passage of a nerve impulse (Johnson, 2015)

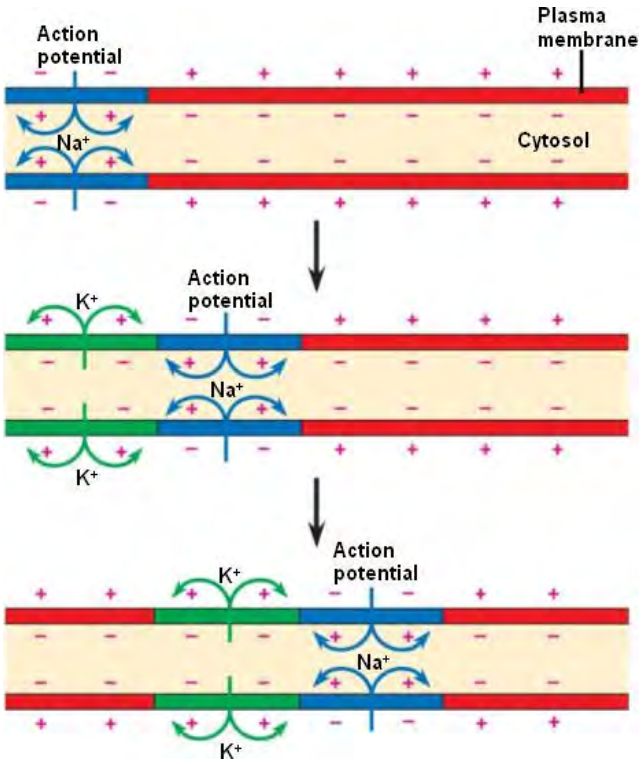

Threshold, accommodation and the law of all-nothing

For the onset of the action potential, there must be a sudden decrease of 15-30 mV in the membrane resting potential. The membrane potential at which the action potential starts is called the threshold potential. For example; the threshold value in motor neurons is -45 mV. When the threshold is reached, the activation gates of sodium channels suddenly open and there is a rapid Na^+ entry into the cell. Thus, the action potential starts (Konrad, 1989).

The time taken to reach the threshold value decreases as the intensity of the electrical stimulus increases. In other words, the time to reach the threshold value is long with weak stimuli and short with strong stimuli. This relationship is shown in the analytical plane by a graph called the intensity-duration curve. When current is applied for 1000 ms, the minimum current intensity that triggers the generation of an action potential is defined as rheobase, and the minimum time required for a current of two rheobase intensities to generate an action potential is defined as chronaxia. In motor nerve, rheobase is 6.25 mA, chronaxis is 0.250 ms, and in muscle fiber, 8 mA and 5 ms, respectively (Figure 3).

Figure 3.

Severity - duration curve *(wikipedia.org/wiki/Rheobase)*

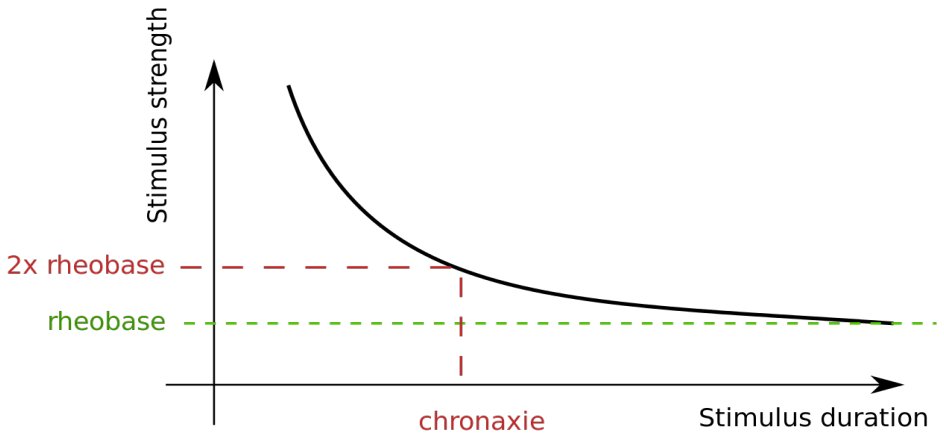

Action potential generation occurs when the activation gates of voltage-gated Na+ channels open abruptly when the threshold potential is reached at the membrane. If a weak electrical stimulus is applied, the activation gates of sodium channels open while the inactivation gates begin to close and rapid Na+ entry into the cell cannot be achieved. In other words, the threshold value (e.g. from -45 mV to -30 mV) that can stimulate Na+ channels starts to rise. The rise in the threshold value that allows the Na+ channel activation gate to open in response to the electrical stimulus is called accommodation. Meanwhile, the voltage-gated Potassium channels start to open slowly and K+ begins to leak out of the cell. The outflow of K+ out of the cell increases through the leakage channels. Thus, the hypopolarization of the membrane caused by the electric current is eliminated (Fleshman, 1981).

The process of raising the threshold and allowing the membrane potential to stabilize takes place at a certain speed. In human motor neurons, accommodation occurs in 50 ms. When the membrane potential is almost at the threshold potential, the quiescent potential is reached in about 300 µs by compensatory K^+ ion movements when electrical stimulation is terminated.

Therefore, for an electrical stimulus to generate an action potential, it must be able to change the membrane potential much faster than this compensation mechanism (usually in less than 200 µs). This situation is shown in Figure 4.

Figure 4.

Accommodation and action potential generation by electrical stimulation (Hodgkin, A 1949)

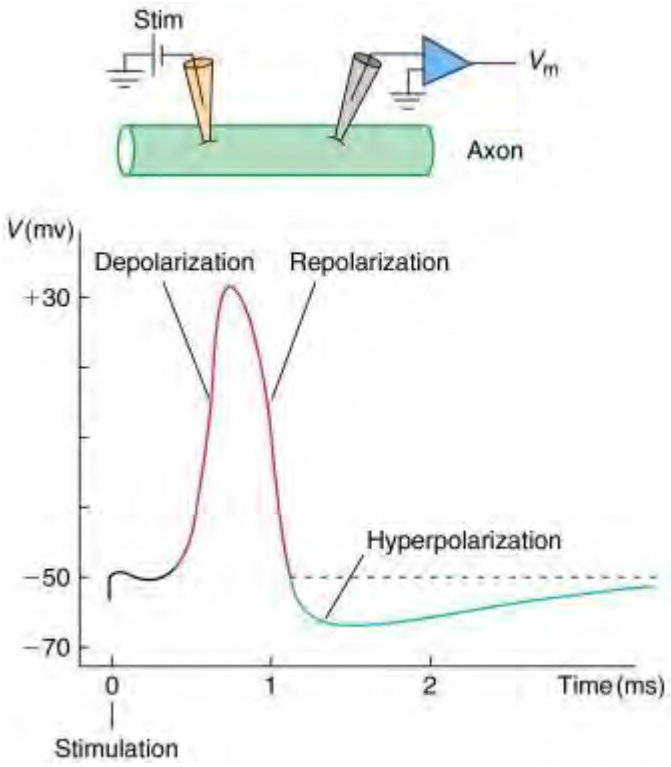

In a cell with a membrane resting potential of -90 mV and a threshold value of -45 mV, an action potential is generated by a short-term strong stimulus that provides a membrane potential change faster than the rate of development of accommodation (Hodgkin, 1949).

Physıology in Electrotherapy

Pain Modulation

One of the aims of electrical devices used in physical therapy is to reduce the patient's pain. The cause of pain is often pain. Therefore, it is important to know how pain is felt, transmitted and perceived by the brain. The basic concepts that need to be known for pain relief are tried to be explained below (Al-Neami, 2023; Kocer, 2000).

For the patient, pain is often considered pathology in itself. Therefore, even if the underlying causes are not eliminated, pain reduction is perceived as a treatment in itself. The perception of pain is a chain of events in which peripheral receptors are stimulated by an undesirable physical or chemical effect, the stimulus is transmitted to the spinal cord via peripheral nerves, transmitted along the cord to the brain stem and from there to the cerebral cortex and determined at the level of consciousness. Figure 5 shows this chain of events.

Figure 5.

The path followed by the chain of events in the perception of pain (Johnson, 2015)

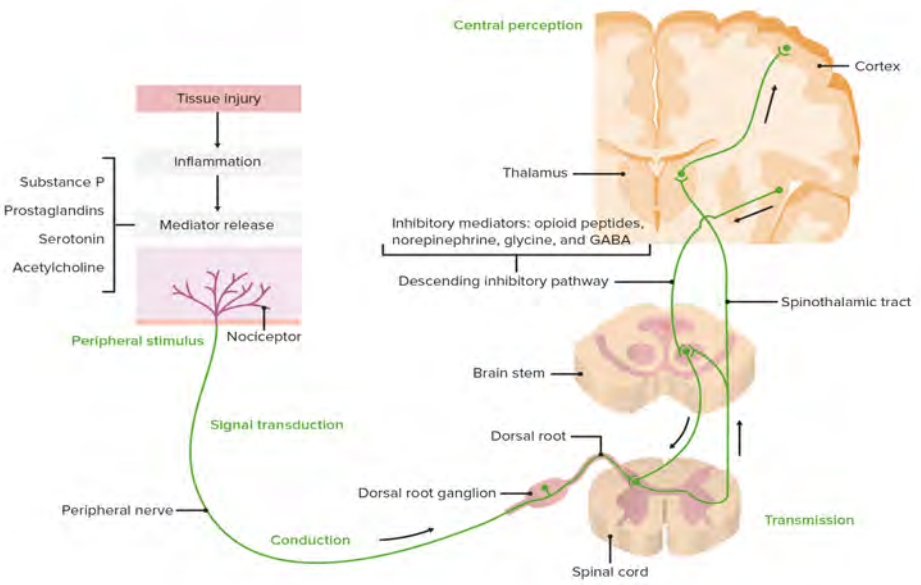

Summation of Contraction

The process of contraction and relaxation resulting from an action potential is called muscle contraction. If several muscle jerks occur simultaneously or at very short time intervals, their effects overlap. This is called summation of contraction. As the definition suggests, there are two ways of summation: Frequency summation when the same muscle fiber contracts one after the other and multifiber summation when different muscle fibers contract together (Vance, 2014; Johnson, 2014).

Frequency Summation

The contractile force generated by a single muscle fiber increases with the frequency of the impulse sent to this fiber for contraction. However, after a certain frequency, no increase in muscle force is observed, and the muscle fiber is in a continuously contracted state. This state is defined as tetanization.

General Indications for Electrotherapy

Increasing muscle strength

Electrical stimulation increases muscle strength in normal muscle. However, conflicting results have been reported in comparative studies with isometric exercise. Every method used to increase muscle strength is based on loading the contractile elements of the muscle. Muscle loading can be achieved by repetitive or prolonged contractions. Increased loading has been shown to increase protein synthesis, decrease protein breakdown and increase sarcomere number in muscle.

As the current intensity increases, the strength of the contraction increases. By increasing the frequency of the current, these strong contractions, at first intermittent, can be made continuous. Eventually, the frequency of a full tetanic contraction is reached, where the muscle contracts continuously and with maximum force without ever relaxing. This frequency is between 30-2500 pps.

Reciprocal inhibition

Antagonists can be stimulated to produce reciprocal inhibition in the muscle. It can be applied in two different ways: Intermittent tetanic current (pulse duration 200 μs, frequency 33 pps, 7 s stimulation, 10 s rest). The current intensity is adjusted between 1-100 mA according to the patient's tolerance. Three sessions a day, seven days a week (half an hour each session) this is the most commonly used method.

Low-intensity current (current delivered at an intensity below motor threshold) can be applied in combination with voluntary contraction. Low-intensity current favors voluntary contraction.

Skin Ulcers

Human skin is more electronegative than deeper tissue layers. Therefore, injured skin develops a natural bioelectric current from the deeper layers to the wound site, which is supplied by ionic body fluids. When electrical stimulation is applied to the wound site, changes occur in the biological events involved in the wound healing process that can lead to accelerated healing. Electric current increases the number and activity of fibroblasts, collagen, protein and DNA synthesis. Fibroblasts and epithelial cells migrate to the cathode along the voltage gradient (galvanotaxic effect). Electrical stimulation suppresses mast cells, reduces fibrotic scar formation and improves cosmetic wound healing. Stimulation also increases local blood flow. Thus, tissue damage due to free oxygen radicals is prevented. Electric current has also been shown to have bacteriostatic and bactericidal effects. This effect occurs at the cathode. This antimicrobial effect becomes more pronounced as the duration and voltage of the applied current increases (Kumar, 2018).

Electrical stimulation accelerates healing of ischemic pressure ulcers and success rates ranging between 88-100% have been reported in different studies. The most effective form of stimulation is pulsed electrical stimulation. Because it allows stimulation with high intensity current without causing irritation or burns in the tissue. The treatment is applied for 1-24 hours a day for 2-3 months on average.

Fracture Healing

Bone has piezoelectric properties. Under mechanical stress, electrical charge changes on the bone surface. During the fracture healing process, if there is angulation between

the axes of the fracture fragments, negative electrical charge accumulation occurs on the concave side of the fracture and callus tissue is first formed in this region. On the convex side of the fracture, positive electrical charge accumulation and osteolysis occurs. The remodeling process stimulated in this way ensures that the angulation between the axes is eliminated (Jones, 2007).

With or without axis abnormality, fracture healing can be accelerated by utilizing the osteogenic properties of negative electric charge. Low or medium frequency currents are used for this purpose. If there is more than 1 cm separation between the dead bone and the fracture ends, electrical stimulation is contraindicated (counterproductive).

Properties of TENS Electric Current

The frequency, intensity and voltage of the current play an important role in the magnitude of skin resistance (Gökhan, 2023).

Current Type (Frequency)

As the electric current passes through the tissues, it causes the accumulation of an opposite electric charge at the interfaces and cell membranes separating the different tissues below the electrode. This electric charge creates a potential difference in the opposite direction to the electric current, preventing the passage of the electric current through the tissues.

This opposing electrical potential, which occurs reactively in tissues, is called reactance or capacitive resistance. Reactance is actually the resistance of the current itself to the passage of electric current through the tissue. Therefore, the magnitude of the resistance varies depending on the type of current. The skin resistance to direct current is greater than the resistance to alternating current. The resistance to alternating current decreases as the frequency of the current increases. Skin resistance to direct current can be as high as 100,000 Ohms. In alternating current with a frequency of 50 Hz, the resistance is 3,000 Ohms and in alternating current with a frequency of 4,000 Hz, the resistance is 40 Ohms.

Current voltage

Another way to overcome skin resistance is to apply a high voltage current, such as 100 volts. This causes the skin resistance to drop abruptly and the drop continues at a slower rate.

Current Intensity

The greater the current intensity, defined as the amount of current flowing through one square centimeter of cross-sectional surface in one second, the greater the amount of electric charge passing through one centimeter of surface.

This causes an increase in the resistance to current passing through the skin, similar to the difficulty of passing through the same door when the number of people passing through it at the same time increases. If the electrode surface or skin-electrode contact surface through which the current passes is reduced, the skin resistance will likewise increase. The widely accepted clinical approach is that the current intensity used in electrotherapy should be the lowest current intensity that can produce the desired physiologic response (Koçer, 2000).

Signals Generated from the Device, Their Forms and Functions

Standard TENS devices are distinguished by their output characteristics. They usually deliver biphasic pulsed currents in a repetitive manner with a pulse duration between 50 µs and 1000 µs and pulse frequencies between 1 and 250 pulses per second (pps). The purpose of TENS is to activate selectively different populations of nerve fibres in order to produce particular physiological outcomes (Jones, 2009; Goncu Berk, 2018). Pulses are usually delivered in a continuous pattern, although most modern-day devices have other patterns available such as burst and modulation. (Figure 6)

Figure 6.

Signals that the device can generate (www.musculoskeletalkey.com)

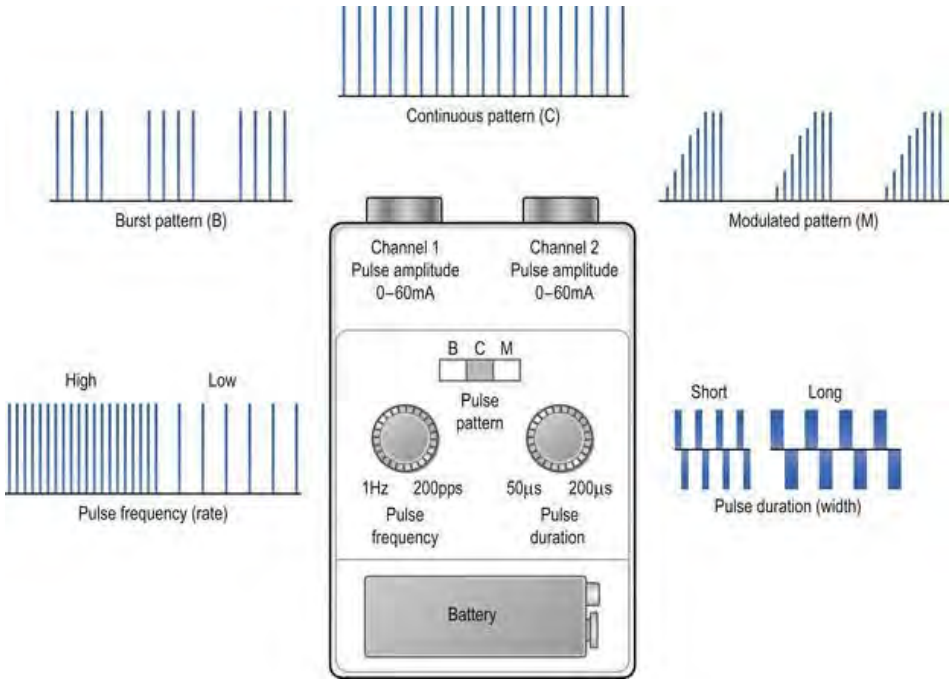

A.Continuous currents

1. Galvanic Current

B. Discontinuous currents

1. Sawtooth wave
2. Spike wave (high voltage pulse current)

3. TENS

a) Bunch (Burst), rectangular

b) Alternative biphase

4. PWM

5. Initiative

Continuous currents

Galvanic current

a) Muscle contraction

Continuous galvanic current application increases the stimulation threshold in motor nerve and muscle fibers. It increases the chronaxia value. Contraction can only be achieved with intermittent galvanic current. Only superficial nerve fibers can be stimulated. In denervated muscle stimulation, denervated muscle fibers are directly stimulated by intermittent galvanic current. The fact that the effect of this stimulation is superficial, inevitably produces only a twitch-like contraction response and is painful limits its clinical efficacy (Kocer, 2020).

b) Impact on sensory nerves

Although it is effective on pain, it should not be the first choice in pain management due to its unpleasant effects (Figure 7). It can be used as a last resort, especially in painful conditions arising from superficial anatomical structures (Kumar., 2018; Jones, 2007; Gökhan, 2023).

A few examples of treatments with continuous currents:

- In a knee arthritis to release a nerve paralyzed by pressure in a bone fracture
- In the treatment of a shoulder joint
- Treatment of the hip joint
- In the treatment of an entercostal neuralgia
- In the treatment of a sciatic neuralgia
- Treatment of deafness
- In the treatment of facial paralysis.

Figure 7.

Examination of galvanic current waveform on oscilloscope (Volt/div=0.2 Volt with x100 probe)

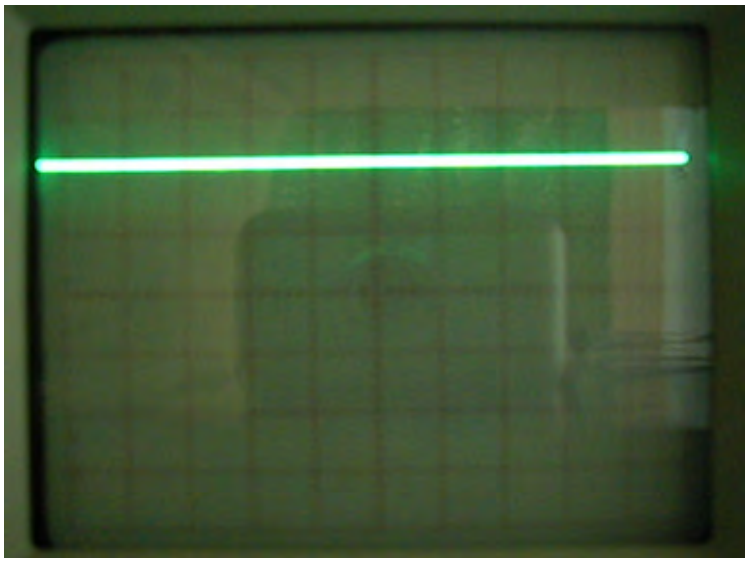

Discontinuous currents

Sawtooth wave

This waveform is very suitable for muscle strengthening. f= 4-100 Hz, Duty duration: 5-40ms (Figure 8).

Figure 8.

Examination of the sawtooth waveform on an oscilloscope (Time/div=20 ms Volt/div=0.2 Volt with x100 probe)

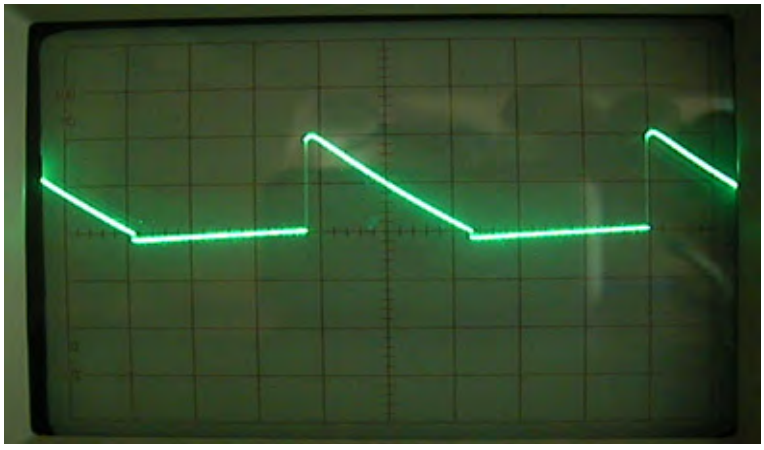

Needle wave (high voltage pulsed current)

This waveform, which is one of the Faraday currents, is the best example of treatment utilizing its trophic and pain relieving properties in the treatment of small joint sprains. As seen in Figure 9, it is a monophasic current consisting of pulse packets containing

twin-peaks. The applied voltage is more than 100 volts. The phase duration is 5-20 µs. Pulse duration is 100 (maximum 200) µs, pulse frequency is 1-25 pps, total current is 1.2-1.5 mA because the phase duration is very short (Figure 9).

High voltage current is reported to be effective in the treatment of muscle spasm by causing pain, joint effusion, edema, tetanic contraction, wound healing and muscle training. Since the pulse duration is very short, it is not effective enough in denervated muscle stimulation (f:5-40Hz).

Figure 9.

Examination of the needle waveform on an oscilloscope (Time/div=20 ms Volt/div=0.2 Volt with x100 probe)

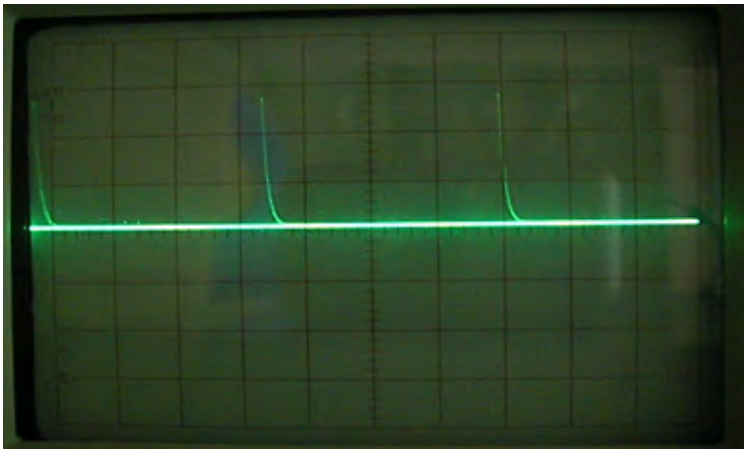

Transcutaneous electrical nerve stimulation (TENS)

TENS is the most common and most important method of electroanalgesia. It was developed shortly after the introduction of the gate control theory. According to the gate control theory, it was suggested that if the neurons that function as gates are stimulated with painless stimuli, the transmission of pain sensation to the higher centers can be inhibited. TENS was developed in researches to inhibit pain transmission by creating painless sensory stimulation with electrical stimulation. Its widespread use has been adopted with successful results (Kocer & Dundar, 2022)

Monophasic or biphasic pulsed (intermittent) current is used to stimulate thick myelinated A beta fibers. In TENS, intermittent asymmetric biphasic currents are generally preferred. This prevents the electrolytic and iontophoretic effects seen in monophasic currents and the unpleasant sensory stimuli observed in symmetrical waveforms. Intermittent current is preferred to prevent stimulation of unmyelinated C fibers that are sensitive to continuous currents. The frequency of TENS current can be varied between 1-200 Hz, impulse duration between 10-400 µs, and current intensity between 1-100 mA (51). Accordingly, there are six different types of TENS applications (Table 1).

Conventional TENS

It is the most widely researched type of TENS. It is high frequency and low amplitude current. Optimal analgesic current frequency is 60 pps. In A-beta fibers, although the chronaxis is 200 µ, the pulse duration is kept between 50-100 µs. In this case, A beta fibers are specifically stimulated by temporal summation. Pulses of 50-100 µs stimulate the nerves 60 times per second in succession. This summation only stimulates the A beta fiber. A current intensity is used that does not cause muscle contraction and produces numbness and tingling sensation. During the session, the current intensity can be increased periodically as accommodation often develops. The duration of treatment is 30 minutes to several hours. The analgesic effect starts in 10-15 minutes and lasts for 10-15 minutes (Jones, 2009; Goncu Berk, 2018).

Table 1.

Most Commonly Used TENS Types (www.musculoskeletalkey.com)

	Physiological intention	TENS parameters	Patient experience	Electrode location	Analgesic profile	Regimen
Conventional TENS	To stimulate large diameter non-noxious afferents (Aβ) to produce segmental analgesia	Low intensity (amplitude), high frequency (10–200 pps)	Strong, non-painful TENS paraesthesia with minimal muscle activity	Dermatomes Site of pain	Usually rapid onset and offset	Use TENS whenever in pain
AL-TENS	To stimulate small diameter cutaneous and motor afferents (Aδ) to produce extrasegmental analgesia	High intensity (amplitude), low frequency (1–5 bursts of 100 pps)	Strong comfortable muscle twitching	Myotomes Site of pain Muscles Motor nerves Acupuncture points	May be delayed onset and offset	Use TENS for 20–30 minutes at a time
Intense TENS	To stimulate small diameter cutaneous afferents (Aδ) to produce counterirritation	High amplitude (uncomfortable/ noxious), high frequency (50–200 pps)	Uncomfortable (painful) electrical paraesthesia	Dermatomes Site of pain Nerves proximal to pain	Rapid onset and delayed offset	Short periods only 5–15 minutes at a time

TENS similar to acupuncture

Low frequency is applied with high voltage. Current frequency is selected between 1-10 pps, but generally 1-4 pps is used. Treatment duration is 30-60 minutes. A current voltage is used that provides rhythmic muscle contraction as intense as the patient can tolerate. The effect starts within a few hours and can last between 2-6 hours. It is more effective in chronic pain than conventional TENS. More resistant to the development of accommodation.

Burst type TENS

Two currents with a frequency of 60-100 and 0. 5-4 pps are alternated. The duration of treatment is 30-60 minutes. It can be considered as a mixture of conventional and acupuncture-like TENS.

Brief-Intense TENS (Hyperstimulation)

High frequency and high voltage current is applied. Treatment time is 15-30 minutes.

Both sensory and motor fibers are stimulated. Current is applied at an intensity to produce irregular tetanic muscle contractions.

Indications

The most common indication for TENS application is acute and chronic pain. Apart from pain, it is indicated in the treatment of spasticity, tinnitus and chronic skin ulcers. TENS is more effective in peripheral pain rather than central pain. TENS has been used with varying degrees of success for chronic low back pain, chronic neck pain, headache, ischemic pain, peripheral nerve injury, phantom pain, postphlebitic syndrome, tooth extraction and in the first stage of labor.

Success in pain treatment varies between 25-95% depending on stimulation parameters, electrode placement, and whether or not previous treatment has been applied. TENS reduces the use of simple analgesics and narcotic analgesics. TENS means stimulation of the peripheral nerves through the skin. The purpose of using it for treatment is to relieve or eliminate pain (Figure 10).

Figure 10.

Examination of burst waveform on oscilloscope

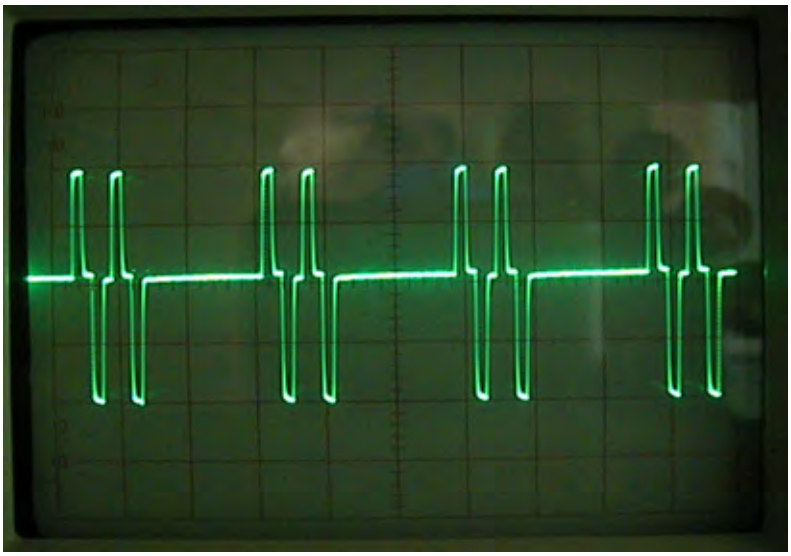

Time/div=5 ms Volt/div=0.2 Volt (x100 probe)

(a)

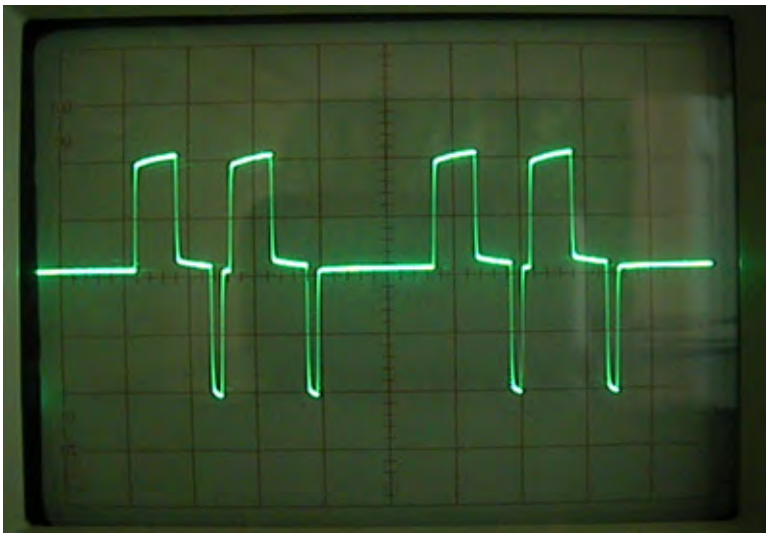

Time/div=5 ms Volt/div=0.2 Volt (x100 probe)

(b)

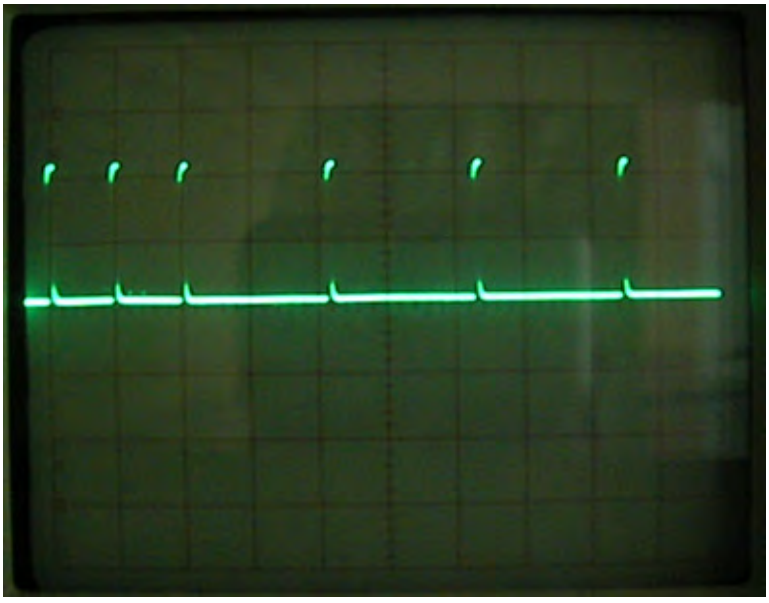

Time/div=2 ms Volt/div=0.2 Volt (with x100 probe)

Automatic PWM (Pulse Width Modulation)

In this modulation, the frequency of the pulsed current automatically increases and then decreases for a fixed duty cycle (Figure 11). The purpose of pulse modulation is to delay accommodation.

Figure 11.

Examination of automatic PWM waveform on oscilloscope (Time/div=20 ms Volt/ div=0.2 Volt with x100 probe)

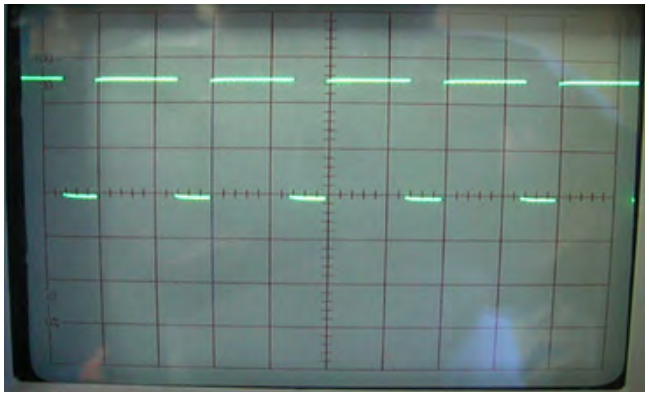

Interference current (Amplitude Modulated Signal)

Electrophysiologic effects

Interference current is voltage modulated alternating current. Since the frequency of the sinusoidal currents that generate this current is around 4000 Hz, the skin resistance is lower than that of low frequency currents. In the subcutaneous tissue where interference occurs, as a result of amplitude modulation and summation, the voltage of the interference current can exceed the threshold value and stimulate the nerves. The frequency of this stimulation is equal to the pulse frequency of the interference current. Another important effect of amplitude modulation is the prevention of accommodation of nerve fibers in the subcutaneous tissues where the interference occurs, due to the continuous change in voltage.

Stimulation of motor units

Tetanic contraction by electric current occurs at a frequency of 30-2500 pps and all motor units are stimulated simultaneously and muscle fibers contract simultaneously. Because the frequency of tetanic stimulation is higher than the physiological stimulation frequency and muscle fibers contract synchronously, maximal contraction by electric current is more fatiguing than voluntary maximal contraction. However, as the frequency of the current producing tetanic contraction increases, less fatigue occurs. This is explained as follows. Since the voltages of the sinusoidal waves in the interference current stimulus packets are not equal, not every sinusoidal wave can generate an action potential. On the other hand, since the absolute refractory period in motor nerve fibers is approximately 1/2500 ms, when a sinusoidal current with a frequency of around 4,000 Hz is applied, some sinusoidal waves will coincide with the absolute refractory period and will not generate an action potential. The carrier of the signal generated by the device is a 4 KHz rectangular signal and the modulating signal is a user-adjustable sinusoidal signal between 2-100 (Figure 12).

Figure 12.

Examination of the interference waveform on an oscilloscope (Time/div=5 ms Volt/ div=0.2 Volt with x100 probe)

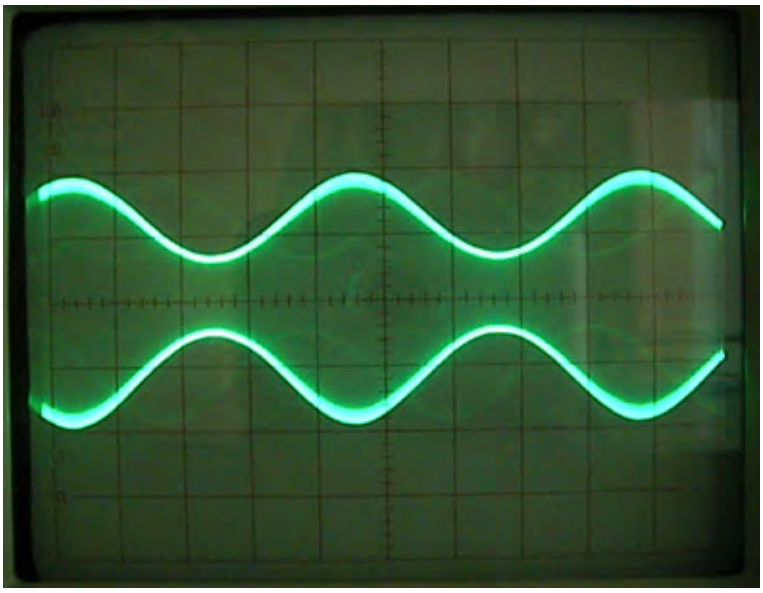

Realized Electrotherapy Devices

Electrotherapy devices used in both slimming and physical therapy centers in Turkey are not manufactured in Turkey. There are various realized TENS devices. However, the electrotherapy devices used are imported from abroad. This device is one of the most advanced electrotherapy devices manufactured in the U.S.A. under the brand name "INTELECT" with ISO 13485 standard. The front panel of the device is equipped with a graphic display in special dimensions. In order to prevent the user from making mistakes, the placement of the electrodes according to the signals is shown on the human body. There are also two channels in the device. Another feature is that it contains an ultrasonic pen. In order to keep track of which signals are applied to the patient at which times, they are recorded using a memory card. In this thesis, the catalog of this device was used to select the signals and features to be applied.

General Structure and Operation of the Device

General Block Diagram of the Device

Figure 13.

Block diagram of the device

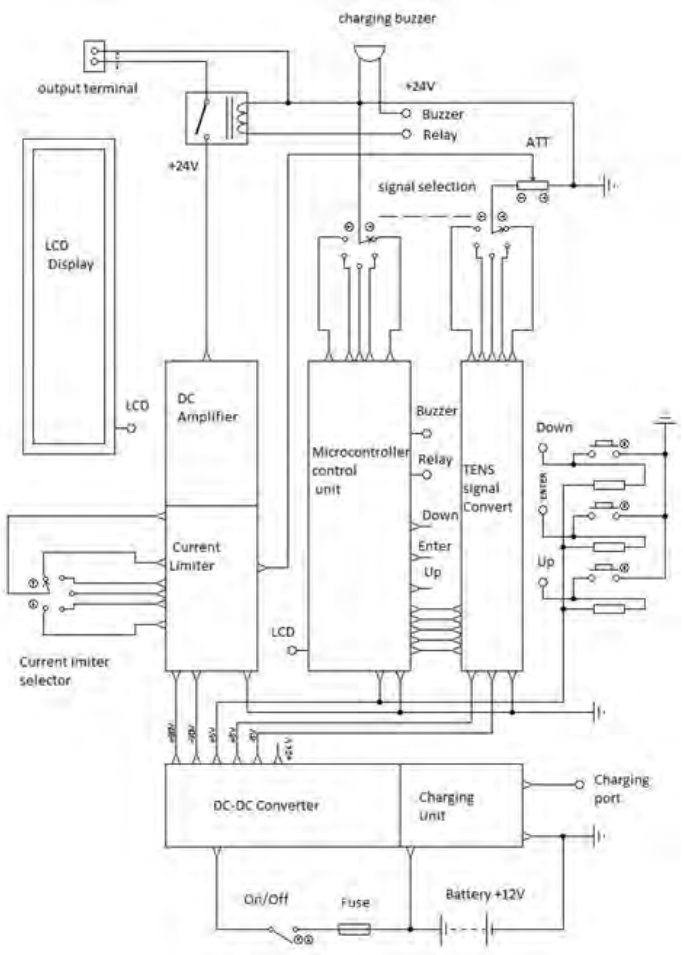

General Working Principle of the Device

A portable electrotherapy signal generator with a 12 V / 7 Ah battery is designed. The voltage from the battery is connected in series to the on/off switch with a 3 A fuse just in case.

The DC to DC converter circuit is a step-up switching power supply. The power supply is designed to generate various voltages from its output by stepping up the 12 volt voltage at its input with a switching process. The output voltages are +90 V, -90 V, +8 V, -8 V, +5 V and +24 V. These voltages constitute the feeds of other circuits as shown in the block diagram.

A charging circuit is designed to charge the battery when it runs out of charge and is added to the printed circuit board of the converter unit. In addition, voltage is applied to the charging input with a box containing a transformer (Figure13).

Microchip's PIC 16F877 integration is used as the control and signal generating element of the system (Kocer, 2022). The microcontroller transmits the variables belonging to the properties of the signal selected with the help of the commutator to the user with the LCD screen and waits for the user to enter information with the "up", "enter", "down" keys. According to this information, it starts to generate signals at the desired frequency at the desired duty cycle. These signals are converted into the desired signals by the signal shaper unit. The obtained signal is attenuated with an attenuator and connected to the input of the dc amplifier unit. The calibrated output voltage level is displayed on the LCD screen with the help of a potentiometer connected to the same shaft as the internatuar. After specifying the features with the keys, the last "enter" key is pressed, the output relay is connected and the signals reach the electrode. In addition, the microcontroller continuously measures the battery voltage and when the battery voltage drops below the set 10.88V, the device turns off and the charging buzzer notifies the user by beeping intermittently. In the meantime, the LCD screen displays a message to turn off and charge the device. The device is turned off and charged. The end of the charging process is recognized when the "Charging Indicator" LED on the front panel starts blinking (Kocer & Butuner, 2021; Dundar & Koyuncu, 2023)

If charging continues, charging is automatically stopped. Continuous charging of the device is not harmful for the battery. The device can also be used for therapy while charging. Current limiting devices are connected in series to the output behind the DC amplifier circuit. The desired signals from the output are applied to the electrode and then to the patient's skin so as not to exceed the current selected with the commutator. In overcurrent draws, when the desired limit is exceeded, it controls the output current until the limit level. In case of short circuit of the electrodes, the system limits itself in the same way.

This device provides 11 hours of service when fully charged. Proteus simulation program and Eagle printed circuit drawing program were used to design the system.

Conclusion

As a result of the researches, based on the documents, information and materials on the market, a portable electrotherapy function generator that can serve 11 hours with a 12 Volt mini battery; working time, time, frequency, duty time can be adjusted; galvanic current, sawtooth signal, high voltage pulse currents, TENS signals (burst, alternating biphase), automatic PWM and interference signals; 2-100 mA stepped current limit, manual output voltage control, ± 0-90 V DC voltage, peak-to-peak 180 V AC voltage can produce, 5. 5 kg weight microcontroller prototype electrotherapy function generator has been designed and manufactured. All signals can be applied to the patient with currents of 2, 10, 30, 50, 100 mA with dwell and duty times from 0 to 500 ms depending on user-adjustable values between + 90 V - 0 V, 0 V- (-90 V), + 90 V- (- 90 V).

One of the shortcomings of the circuit is the absence of the ultrasonic pen found in electrotherapy devices. The other is that not all combinations of electrotherapy signals can be generated. This is because the memory of the microcontroller is not enough. The most favorable aspect of the system can be improved by changing only the signal shaping unit without changing the shape of the case.

In future studies, the structure of the system will be adjusted digitally to provide more precise current adjustments; a graphic LCD will be used to show which signals are applied and where they should be applied on the human body, the LCD screen will also be used as an oscilloscope screen, and DSPIC with a digital signal processing unit will be used to implement all of these. If necessary, an ultrasonic pen unit will also be created.

References

Al-Neami, A. Q., Mohammed, H. M., & Hammoodi, Q. A. (2023), Transcutaneous Electrical Nerve Stimulation Unit for Therapeutic Purposes.

Benarroch, J. M., & Asally, M. (2020). The microbiologist's guide to membrane potential dynamics. Trends in microbiology, 28(4), 304-314.

Chrysafides, S. M., Bordes, S. J., & Sharma, S. (2019). Physiology, resting potential.

Dündar, Ö. & Koyuncu, B. (2023). Kabin İçi 4G (LTE) ve WiFi Kablosuz Haberleşme Sistemlerinde Kullanılmak Üzere Mikroşerit Anten Tasarımı. Aerospace Research Letters (ASREL) Dergisi, 2(1), 19-26.

Fleshman, J. W., Munson, J. B., Sypert, G. W., & Friedman, W. A. (1981). Rheobase, input resistance, and motor-unit type in medial gastrocnemius motoneurons in the cat. *Journal of Neurophysiology*, *46*(6), 1326-1338.

Foster, A., "Clayton'un Elektroterapi Kitabı", İzmir Güven Yayınevi, İzmir (1987)

Gidon, A., Zolnik, T. A., Fidzinski, P., Bolduan, F., Papoutsi, A., Poirazi, P., ... & Larkum, M. E. (2020). Dendritic action potentials and computation in human layer 2/3 cortical neurons. *Science*, *367*(6473), 83-87.

Goncu Berk, G. (2018). Design of a wearable pain management system with embroidered TENS electrodes. *International Journal of Clothing Science and Technology*, *30*(1), 38-48.

Gökhan, N. U. R., Barış, B. N., Levent, B., Sazaklıoğlu, B. S., & Elvan, A. K. (2023). BUSER Transcutaneous Electric Nerve Stimulator Device Design. *Natural and Engineering Sciences*, *8*(1), 18-30.

Harrison, J. E., Weber, S., Jakob, R., & Chute, C. G. (2021). ICD-11: an international classification of diseases for the twenty-first century. *BMC medical informatics and decision making*, *21*(6), 1-10.

Hodgkin, A. L., & Katz, B. (1949). The effect of sodium ions on the electrical activity of the giant axon of the squid. *The Journal of physiology*, *108*(1), 37.

Johnson, M. I. (2014). *Transcutaneous electrical nerve stimulation (TENS): research to support clinical practice*. Oxford University Press, USA.

Johnson, M. I., Paley, C. A., Howe, T. E., & Sluka, K. A. (2015). Transcutaneous electrical nerve stimulation for acute pain. *Cochrane Database of Systematic Reviews*, (6).

Jones, I., & Johnson, M. I. (2009). Transcutaneous electrical nerve stimulation. *Continuing Education in Anaesthesia, Critical Care & Pain*, *9*(4), 130-135.

Jones, K. R., Vojir, C. P., Hutt, E., & Fink, R. (2007). Determining mild, moderate, and severe pain equivalency across pain-intensity tools in nursing home residents. *Journal of rehabilitation research and development*, *44*(2), 305.

Karacan, İ., Koyuncu, H., "Fiziksel Tıp ve Rehabilitasyonda Elektroterapi" *Güneş Kitabevi Ltd. Şti.,* Ankara, (2003)

Kocer S., Ocal H., & Dundar H. B., (2022). Use of IoT and Wearable Technology Design Fundamentals in Healthcare Industry, In S. Kocer, O. Dundar (Eds .), Current Studies in Basic Sciences Engineering and Technology (pp. 168–182). ISRES Publishing.

Kocer, S. & Butuner, R. (2021). Pic Microcontroller. In S. Kocer, O. Dundar & R. Butuner (Eds .), Programmable Smart Microcontroller Cards (pp. 126 –148). ISRES Publishing.

Koçer, S., Canal, M. R., & Güler, İ. (2000). Design of low-cost general purpose microcontroller based neuromuscular stimulator. Journal of medical systems, 24, 91-101.

Konrad, P. E., Geddes, L. A., Tacker Jr, W. A., Reuter, D., Schooler, D., & Dull, S. (1989). Existence of a strength-duration curve for spinal cord motor evoked potentials in cats. *Electroencephalography and Clinical Neurophysiology/Evoked Potentials Section*, *74*(6), 463-468.

Kumar, V., Pandey, S., Raj, R., & Jadhav, M. S. (2018). Design and Development of Electrical Simulation Unit for Pain Control. *International Journal of Pure and Applied Mathematics*, *118*, 24.

Naillioğlu, M., "Deri Üzerinden Elektrikli Kas Sinir Uyarıcı Tasarımı ve Uygulaması", Tezsiz Yüksek Lisans Tezi, Gazi Üniversitesi Fen Bilimleri Enstitüsü, Ankara, (2002)

Pitt Medical Neuroscience | Action Potentials (pittmedneuro.com)

Raghavan, M., Fee, D., & Barkhaus, P. E. (2019). Generation and propagation of the action potential. *Handbook of clinical neurology*, *160*, 3-22.

Rheobase - Wikipedia (en.wikipedia.org/wiki/Rheobase)

Rueda, A. J., Martínez-Cruz, C., Díaz-Fernández, Á., & Osuna-Pérez, M. C. (2023). Flexible evaluation of electrotherapy treatments for learning purposes. *Expert Systems with Applications*, *219*, 119621.

Sonkaya, A. R., & Karaoğlan, M. (2019). Investigation of concordance between referral diagnosis and electroneuromyographic diagnosis. *Journal of Surgery and Medicine*, *3*(3), 250-253.

Trayanova, N. A., Popescu, D. M., & Shade, J. K. (2021). Machine learning in arrhythmia and electrophysiology. *Circulation research*, *128*(4), 544-566.

Types of TENS, www.musculoskeletalkey.com/transcutaneous-electrical-nerve-stimulators-for-pain-management/

Vance, C. G., Dailey, D. L., Rakel, B. A., & Sluka, K. A. (2014). Using TENS for pain control: the state of the evidence. *Pain management*, *4*(3), 197-209.

Yerdelen, D., & Koc, F. (2013). Peripheral Nerve Axonal Excitability in Epileptic Patients. *Journal of Neurological Sciences*, *30*(1).

About The Authors

Sabri KOCER, PhD, He graduated from the Electrical Engineering Department of Selcuk University. He completed his graduate and his doctorate in Gazi University. Currently, Necmettin Erbakan University, Faculty of Engineering, Computer Engineering is working. Electronics, Computer, Telecommunication, Signal Processing and Biomedical studies in the area.

Email: skocer@erbakan.edu.tr , ORCID: 0000-0002-4849-747X

Ozgur DUNDAR, PhD, works at Necmettin Erbakan University, Department of Astronautical Engineering. He graduated from the Electrical and Electronics Engineering Department of Selcuk University. He worked as an Automation Engineer for a while. His master's and doctorate degrees are from Selçuk University, Institute of Science and Technology, Department of Electrical and Electronics Engineering. Special fields of study are Automation, Robotic, Communication, Electromagnetic and Micro Strip Patch Antenna designs.

Email: ozdundar@erbakan.edu.tr , ORCID: 0000-0002-4142-4446

Similarity Index

The similarity index obtained from the plagiarism software for this book chapter is 9%.

CHAPTER 9

Implementation of Artificial Intelligence Techniques for Boosting Performance on Skın Cancer Classification

Muhammed KARAALTUN
KTO Karatay University, Türkiye

Omer OZCAN
Selcuk University , Türkiye

To Cite This Chapter:
Karaaltun, M. & Ozcan, O. (2023). Implementation of Artificial Intelligence Techniques for Boosting Performance on Skın Cancer Classification.In S. Kocer. & O. Dundar (Eds.), *Artificial Intelligence Applications in Intelligent Systems* (pp. 145–168). ISRES Publishing.

Introduction

Thanks to recent advances in computer science, artificial intelligence (AI) is quickly becoming an integral part of modern healthcare. AI algorithms are used to support medical professionals in clinical settings and ongoing research. Convolutional neural network (CNN) which is a subset of AI is widely used in predicting diseases, handwriting recognition, computer vision, and image classification (Kayumov et al., 2020; D. Li et al., 2019; Luongo et al., 2021; Šprogar et al., 2021). Although classification studies conducted with CNN on the ImageNet dataset have yielded successful results recently regrettably the classification performance decreases in imbalanced datasets (Reshma Prakash & Nath Singh, 2020; Russakovsky et al., 2015; Shorten & Khoshgoftaar, 2019). To solve this problem, imbalanced image datasets are balanced using image data augmentation techniques, which are known as an oversampling process. Because of the importance of image data augmentation, many image augmentation techniques are proposed including kernel filters, color space transformations, random erasing, geometric transformations, and mixing of images. Furthermore, deep learning-based augmentation techniques have also been proposed for imbalanced datasets such as adversarial training, neural style transfer, and general adversarial networks (W. Li et al., 2022; Shorten & Khoshgoftaar, 2019). In general, image augmentation techniques boost the performance of the classification algorithms (Abdelhalim et al., 2021).

However, the classification performance may be low when the augmentation technique generates synthetic image samples similar to the original image data, and problems may occur during the training phase such as overfitting (Abdelhalim et al., 2021).

In addition to image augmentation techniques, transfer learning techniques are also used to solve classification problems caused by imbalanced image datasets (Ali et al., 2022). In transfer learning, networks that have been pre-trained with the ImageNet dataset are used to classify imbalanced image datasets (Ali et al., 2022). Furthermore, transfer learning techniques such as ResNet, VGG, DenseNet, and EfficientNet have also given appealing results on imbalanced datasets (Ali et al., 2022; Bansal et al., 2022; Barata et al., 2019; Hosny et al., 2019; Hossain et al., 2022; Muhammad Attique Khan et al., 2021). The imbalanced image dataset problem comes across frequently in medical datasets and this problem causes a decline in the classification performance of classification algorithms. Therefore, in this study, a very important disease, skin cancer, has been considered, and the proposed edge detection-based image augmentation technique has been applied to minority classes. According to the World Health Organization, 30% of people in the world have been diagnosed with skin cancer (Ali et al., 2022). Malignant melanoma, which has been more common recently, is one of the deadly types of skin cancer (Muhammad Attique Khan et al., 2020). The type of melanoma can spread from the skin to other organs such as the lungs and brain (Nordmann et al., 2017). A total of 3 million skin cancers are diagnosed worldwide each year, along with more than 132,000 melanomas and other types of skin cancer (Siegel et al., 2016). Being diagnosed in the early stages of the disease in deadly types of skin cancer such as melanoma increases the chances of survival (Tsao et al., 2015). One of the methods used to diagnose skin cancer types is dermoscopy. The method of Dermoscopy, which gives a better result than an examination with the naked eye, is the examination of the skin under a magnifying glass and strong light or the examination of a detailed picture of the skin (Binder et al., 1995; Silveira et al., 2009). The success rate of a dermatologist's diagnosis of suspected cancer by examining the skin through dermoscopic images or manually examining it under a magnifying glass varies depending on the expertise and experience of the dermatologist. Thus, this may lead to a wide range of success rates (Binder et al., 1995). In this context, computer-assisted diagnostic systems attract attention in terms of bringing a new perspective to the dermoscopy method (Binder et al., 1995). Especially the success of deep learning-based approaches in image classification has been an important topic in the classification of dermoscopic images with these methods (Chaves et al., 2021; M. Attique Khan et al., 2020; Nahata & Singh, 2020; Pande et al., 2022). However, limited dermoscopic image data on skin cancer types constitutes one of the main problems in diagnosing cancer with deep learning algorithms (Tschandl et al., 2018). Datasets consisting of a limited amount of data constitute imbalanced datasets, which reduces the classification accuracy and increases the rate of misdiagnosis (Abdelhalim et al., 2021).

In this study, an image augmentation technique named edge detection-based technique

(EDBT) has been proposed to balance imbalanced image datasets. CNN models have been used to evaluate the performance of the proposed EDBT on the imbalanced skin image dataset. The experimental results have demonstrated the effectiveness of the proposed EDBT on an imbalanced skin cancer image dataset in terms of classification evaluation metrics.

This study is organized as follows: The related works of image augmentation techniques are given in section 2. The image augmentation techniques are discussed in detail in section 3. Section 4 gives the details of the proposed image augmentation technique. The evaluation and experimental results of the proposed technique are explained in section 5. Finally, the results and future works are discussed in section 6.

Related Work

In classification problems with CNN, data preprocessing provides significant benefits in terms of classification performance. Oversampling and undersampling are data preprocessing methods that are applied to imbalanced datasets to increase the performance of the classification algorithms (Tarekegn et al., 2021). In imbalanced datasets, oversampling is used to increase the sample size of the minority class(es), while undersampling is used to reduce the sample size of the majority class(es). Due to increasing the number of imbalanced datasets in various areas, many balancing techniques have been proposed in the literature recently. One of the simplest techniques for increasing the sample number of minority class(es) in imbalanced datasets is duplicating minority class(es) samples randomly (Ogundimu, 2019). However, this random increase may cause an overfitting problem which is one of the classification problems (Frid-Adar et al., 2018). Although a classification model with the overfitting problem can provide better results in the training phase, the accuracy of this model does not promising results in the test phase (Mutasa et al., 2020). Therefore, many solutions have been proposed to overcome the overfitting problems in oversampling techniques. One of the solutions developed against the overfitting problem is the Generative Adversarial Network (GAN) based techniques. Guan et al. proposed a GAN-based technique to increase the sample size of minority class(es) in the skin lesion dataset(s) (Guan et al., 2022). In addition to techniques using deep learning approaches such as GAN, techniques using basic image processing operations have also been proposed. To increase the number of minority class(es) samples, Cubuk et al. proposed a technique that automatically selects the one that gives the best accuracy rate from image conversion, image rotation, and random erasing techniques (Cubuk et al., 2018). In addition to basic image processing operations, transfer learning methods are also used. In their study on skin lesions, Calderon et al. used ResNet50 and VGG16 transfer learning methods along with rotation, width shift, height shift, zoom, horizontal flip, and vertical flip basic image processing operations (Calderón et al., 2021). Since transfer learning methods have pre-trained weights, they

allow better results in classification problems caused by imbalanced datasets. Fuzzy logic-based approaches have also been exploited in the imbalanced dataset problem. Liu et al. proposed a fuzzy rule-based oversampling technique (FRO) for the class imbalance problem (G. Liu et al., 2018). Liu et al. proposed the fuzzy logic-based information decomposition method (FID) for class imbalance and missing values problems (S. Liu et al., 2017). Ren et al. proposed a fuzzy representative difference-based oversampling technique for the class imbalance problem (Ren et al., 2020). Moreover, clustering operations are used in oversampling approaches. Gong et al. proposed a cluster-based oversampling technique to tackle with the class imbalance problem (Gong et al., 2019). Khan et al. proposed a membership-based oversampling technique and synthetically re-sampled the image data based on the membership score for each minority class (F. U. Khan & Aziz, 2019). Additionally, Radial-based oversampling (RBO) (Koziarski et al., 2019), sequential regression-based oversampling (SMOR) (Zhu et al., 2019), vector quantization-based oversampling (LVQ-SMOTE) (Nakamura et al., 2013) and geometric mean-based oversampling (Kim et al., 2015) techniques have been proposed by researchers as solutions to the imbalanced dataset problem.

In this study, the widely used patch-based mixing image technique was used with a modified canny edge detector (Lewy & Mańdziuk, 2022). The patch images obtained by edge detection were added to the original images by mixing images technique for oversampling.

Augmentation Techniques

When trying to obtain a dataset consisting of real-world data, it is a difficult problem to obtain enough examples from each class (Allken et al., 2021; Chaitanya et al., 2021; Jaipuria et al., 2020). For this reason, different numbers of samples are usually collected from each class and as a result, imbalanced datasets occur. To balance imbalanced datasets, flipping, color space transformations, cropping, rotation, translation, noise injection, kernel filters, mixing images, random erasing, feature space augmentation, and GAN-based approaches are suggested as solutions (Shorten & Khoshgoftaar, 2019).

The Flipping Technique is the process of flipping images horizontally or vertically relative to an axis, and in Equation 1, the flipping technique is performed relative to the x-axis.

$$\{(x,y)\rightarrow(width-x-1,y)\} \tag{1}$$

In this commonly used technique, classification performance may be low or decrease classification performance in cases where the flipped version of the image is very similar to it (Srivastava et al., 2014; Wang et al., 2022). In addition, the flipped version of images such as handwriting may cause classification errors in cases where it looks like another character (Shorten & Khoshgoftaar, 2019).

Digital images are usually encoded in a structure consisting of dimensions and color

channels (width x height x Color Channels). In the color space transformation technique, the image augmentation process is quite easy with the changes made to the color channels (Wan et al., 2017)

$$\text{Gray} = \frac{R+G+B}{3} \tag{2}$$

An example of image augmentation with color channels can be given as the gray level conversion given in Equation 2.

In the cropping image augmentation technique, a region is taken from the middle of the image, a desired part, or a random region, and used as a new image sample. While obtaining synthetic images with this technique, cutting out the blank areas in the original image or cutting the same areas multiple times can cause overfitting problems because they cause similar images(Takahashi et al., 2020). In the rotation technique, new images obtained by rotating the image between 1° and 359° to the right or left are used in image augmentation. In this technique, if the rotated image is like it, it may negatively affect the classification performance(Tajbakhsh et al., 2015). Equation 3 shows the rotation technique.

$$\begin{Bmatrix} (x,y) \rightarrow (X,Y) \\ X = \cos(angle) * x - \sin(angle) * y \\ Y = \sin(angle) * x + \cos(angle) * y \\ angle = \{1° - 359°\} \end{Bmatrix} \tag{3}$$

In the translation technique, shifting images to the right, left, down, and up operations are very useful for image augmentation. This process gives good results for image augmentation, especially when the dataset consists of centered images (Gupta et al., 2019). Equation 4 shows the image translation technique.

$$\{(x,y) \rightarrow (X,Y)\ X = x + dx\ Y = y + dy\} \tag{4}$$

The noise injection technique is the process of adding noise to images with random values or filters such as a Gaussian Filter given in Equation 5.

$$G(x,y) = \frac{1}{2\pi\sigma^2} e^{-\frac{x^2+y^2}{2\sigma^2}} \tag{5}$$

Image augmentation by adding noise to images increases the performance of deep learning algorithms. However, in cases where excessive noise is added or the original image loses its distinctive features when noise is added, it negatively affects the classification performance (Moreno-Barea et al., 2019)

Kernel filters are one of the popular image-processing operations used to sharpen or blur images. The image is blurred or sharpened by sliding various filters on the images in the form of N x N matrices. Additionally, sharpening images can bring out details when

used in image augmentation techniques. Significant effects of kernel filters have been observed in these studies (Kang et al., 2017). However, since kernel filters are in CNN layers, they can negatively affect the performance of the network(Shorten & Khoshgoftaar, 2019)

Mixing images is an unreasonable process in terms of image augmentation techniques, but mixing images with some developed methods turns into an efficient technique (Inoue, 2018). The proposed technique includes the technique of mixing images, and the mixing of images with the developed technique has yielded successful results.

In the random erasing technique, the N x M patch determined on the image is masked with pixel values between 0- 255, average pixel values , or random pixel values. In these studies, it has been seen that the random erasing technique increases the accuracy rate and reduces the error rate (Zhong et al., 2020).

In the feature space augmentation technique, images are converted to n x 1 vectors. By converting images to vectors, many vector operations can be performed on these images (DeVries & Taylor, 2017). One of the vector operations performed is to add noise on the vector as in Equation 6.

$$C_i' = C_i + \lambda X \tag{6}$$

In the GAN technique, which consists of two neural networks in conflict with each other, one of the networks creates synthetic images, while the other network tries to distinguish whether these images are real or not (Dewi et al., 2021). The image augmentation techniques performed using the images produced by the generative network in this architecture provide successful results (Bowles et al., 2018; Maaten & Hinton, 2008). However, in some cases, overfitting can occur as a result of the network producing very similar images (Dewi et al., 2021).

Proposed Augmentation Technique

There are many techniques for image data augmentation, unfortunately, some of these techniques may not tackle the overfitting and underfitting problems which affect the performance of the classification models adversely (Nanni et al., 2022). To address this issue in this study, an edge detection-based image data augmentation technique is proposed to enhance the performance of the CNN models by increasing the sample number of the minority class(es). In the proposed EDBT, the synthetic image data generated consistent with the minority class original samples are obtained from the minority class original samples. This consistency is provided by taking advantage of the modified canny edge detector algorithm. Utilizing the modified canny edge detector algorithm, the similarity relationship between the minority class samples is done very well and as a result, obtains a synthetic image with distinctive features. Unlike the proposed EDBT, commonly used

augmentation techniques use basic geometric operations such as rotating, flipping, and shifting to the existing image; this may lead to losing a critical feature map. As a comparison, the proposed EDBT uses an effective image-processing operation for the augmentation process.

To increase the number of minority class(es) samples, it is aimed to obtain synthetic images by obtaining the most distinctive parts of minority class(es) samples and adding them as watermarks on the original samples. A modified Canny Edge Detector algorithm was used to obtain watermark images consisting of the most distinctive features of the original images. The Canny Edge Detector Algorithm is one of the common algorithms used in the literature to detect edges in images (Canny, 1986). In this study, this algorithm has been modified using a new method for calculating the threshold values required by the Canny edge detector algorithm. Additionally, the edge detector-based image augmentation technique proposed in this study contains innovations since an edge detector-based image augmentation technique has not previously been proposed in the literature (Barata et al., 2019; Piccialli et al., 2021; Shorten & Khoshgoftaar, 2019; Tarekegn et al., 2021). The proposed EDBT based on edge detection and mixing images differs from techniques using basic geometric operations with its ability to obtain new synthetic samples without losing class properties (Shorten & Khoshgoftaar, 2019). In basic geometric operations-based image augmentation techniques, a completely new image is not produced, synthetic samples are obtained by applying various basic geometric operations such as rotating, flipping, and shifting to the existing image. By using Color Space Transformations, Noise Injection, and Kernel Filter techniques, synthetic samples are obtained by changing the color values of the pixels of the image or by changing the number of color channels. However, in these techniques, the patterns or objects contained in the image remain the same, although their color is different. Therefore, it has a disadvantage over the proposed technique that produces new images, both in terms of color and content. Another technique used for image augmentation is the Feature Space Transformation technique. In this technique, because the images are converted to one-dimensional vectors, the operations on these vectors are difficult compared to two-dimensional images (Nanni et al., 2022). These vectors can be converted to two-dimensional images, but this will cost additional computation time. In the GAN technique, new examples can be produced without losing class information like the proposed technique (Frid-Adar et al., 2018). However, overfitting problems may occur as a result of producing new samples that are very similar to each other in various situations. The development steps of the proposed EDBT are as follows.

Step 1. Determination of the number of synthetic samples

In this step, the majority class and the minority class(es) are specified, and according to the gained information as to minority class(es), the number of synthetic samples (NSS) for minority class(es) is determined by Equation 7.

$$NSS = \frac{SP * NSM}{100} \tag{7}$$

Where SP is the value of the Oversampling Percentage Value which can be set by the user, it can be set according to Equation 8. also NSM represents the number of samples in the minority class(es) (Ibrahim, 2021).

$$SP = \left(\left(\frac{Number\ of\ Samples\ in\ Majority\ Class}{Number\ of\ Samples\ in\ Minority\ Class} \right) - 1 \right) x100 \tag{8}$$

To obtain synthetic images for minority class(es), Step 2 and the next steps are applied to each of the original images in the minority class(es) respectively.

Step 2. Noise reduction

Blurring image is a technique for averaging a group of pixels to reduce noise and sharpness at the edges. A way to reduce noise in images is to apply Gaussian Blur to the images (Cao et al., 2014). The Gaussian Blur filter applied to the images is given in Equation 9.

$$S[i,j] = G[i,j,\sigma] x I[i,j] \tag{9}$$

In Equation 9, $I[i,j]$ the original image, $G[i,j,\sigma]$ the Gaussian blurring filter, and σ the standard deviation of the Gaussian filter. The resulting $S[i,j]$ represents the convolution of the original $I[i,j]$ image and the $G[i,j,\sigma]$ filter.

Step 3. Gradient calculation

At this stage, the density and direction of the edges in the image are determined. Image gradients are compelling cues for detecting edges within an image. This is because pixels belonging to one object are likely to have similar pixel intensities, resulting in low gradient magnitudes among those pixels. For this, the derivatives of the horizontal and vertical axis of the image obtained according to Equation 9 are obtained according to Equations 10 and 11.

$$P[i,j] = \left(S[i,j+1] - S[i,j] + S[i+1,j+1] - S[i+1,j] \right) / 2 \tag{10}$$

$$Q[i,j] = (S[i,j] - S[i+1,j] + S[i,j+1] - S[i+1,j+1])/2 \tag{11}$$

In Equations 10 and 11, $P[i,j]$ and $Q[i,j]$ represent the derivative on the horizontal axis and the derivative on the vertical axis, respectively.

Accordingly, the intensity of the gradient is calculated according to Equation 12, and the direction is calculated according to Equation (13).

$$M[i,j] = \sqrt{(P[i,j]^2 + Q[i,j]^2)} \quad (12)$$

$$Q[i,j] = arctan(Q[i,j], P[i,j]) \quad (13)$$

In Equation 12, $M[i,j]$ represents the density of the gradient and in Equation 13, $Q[i,j]$ is the direction of the gradient.

Step 4. Non-maximum suppression

It is expected that the edge lines of the algorithm in the resulting image will be as thin as possible. For this, some pixels in the image edges obtained in the Noise Reduction step are eliminated according to Equation 14. In Equation 14, if the gradient density of each pixel in the image obtained in the Noise Reduction step is greater than the gradient density of the neighboring pixel, the neighboring pixel is eliminated, otherwise, the neighboring pixel is preserved.

$$N[i,j] = NMS(M[i,j], S[i,j]) \quad (14)$$

In Equation 14, $N[i,j]$ is the image obtained as a result of the Non-Maximum Suppression process and NMS is the Non-Maximum Suppression process.

Step 5. Double threshold

It is possible that incorrect edges may occur due to noise in the images obtained as a result of Non-Maximum Suppression. Two-level thresholding is used to solve this problem. These thresholds are called High Threshold and Low Threshold. Pixels stronger than High Threshold values are called Strong, pixels weaker than a Low Threshold value are suppressed, and Pixels between these two threshold values are called weak pixels.

In this step of the proposed technique, a new method is proposed to determine the threshold values required for the two-level thresholding step of the Canny Edge Detector algorithm.

$$Avg = Average(N) \quad (15)$$

Problems such as the increase in the number of incorrectly detected edges or the destruction of the necessary edges may be encountered due to the incorrect determination of the Threshold values. To obtain the correct threshold values, first, the average of the pixels of the image obtained as a result of Non-Maximum Suppression was calculated according to Equation 15.

Figure 1 shows the distribution of pixels between [0-255] of a sample image from the dataset used and also shows the average of all pixels.

Figure 1.

Average of image pixels

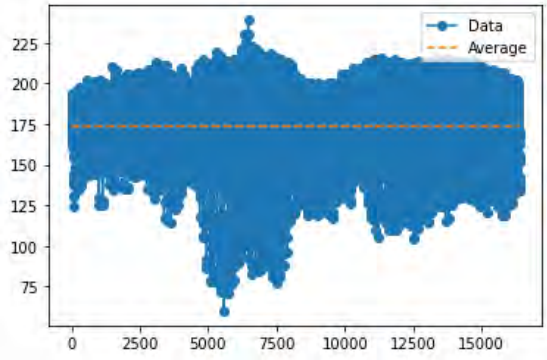

After this step, the pixels of the image are divided into 2 separate parts, the pixels that are below average relative to the average are low pixels and the pixels that are above average are high pixels. Then, the low pixel and high pixel values were also averaged within themselves. Figure 2 shows these values.

Figure 2.

Low pixels and high pixels averages

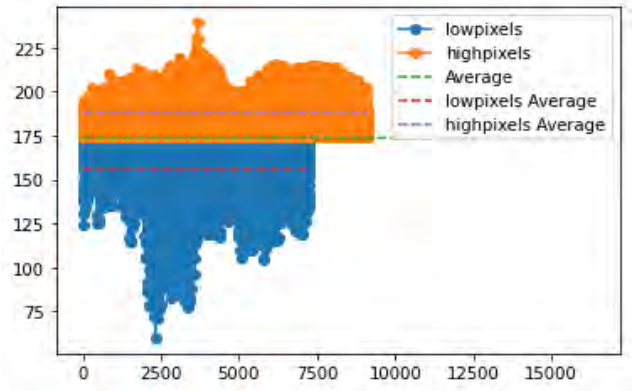

After obtaining low pixels and high pixels values, the standard deviation of low pixel and high pixel values are calculated separately according to Equation 16. The standard deviation was calculated to determine to what extent the pixel values vary compared to the arithmetic mean. Xi; Value of the i'th element in the pixel array, X; The mean value of the pixel array, n; The number of elements of the pixel array.

$$Standart\ Deviation = \sqrt{\frac{\sum_{i=1}^{n}\left(Xi - \underline{X}\right)}{n-1}} \tag{16}$$

After calculating the standard deviation for high pixels and lowpixels, the Low Threshold and High Threshold values are calculated according to Eqs. 17 and 18.

$$LowThreshold = Average\left(Lowpixels\right) - Standart\ Deviation_{Lowpixels} \tag{17}$$

$$High\,Threshold = Average\left(Highpixels\right) - Standart\ Deviation_{Highpixels} \quad (18)$$

The Canny Algorithm uses the Low Threshold and High Threshold values to determine which pixels to highlight and which pixels to suppress when detecting edges (Canny, 1986).

Step 6. Edge tracking by hysteresis

It is the process of replacing weak pixels with strong ones in pixel neighborhoods to obtain the final image of the edge as a result of the Threshold operation. Figure 3 shows this process.

Figure 3.

Edge tracking by hysteresis

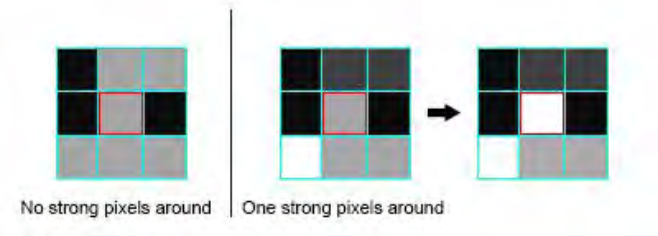

As a result of this step, the edge detection process ends. The edge image obtained after this step is added to the original images, and the final versions of the synthetic images are obtained.

Step 7. Mixing Edges and Original Images

To obtain more different synthetic samples from the original image after the detection of the edges, the pixel values of the resulting edges are changed according to Equation 19. RN = A random number between 0 and Average (EdgePixels).

$$Watermark = EdgePixels - RN \quad (19)$$

Since the input images are 128 x 128, the dimensions of the resulting edge images are also 128 x 128. In the proposed technique, edge images are added as watermarks on the input images. However, to obtain more synthetic images than an input image, the edge image was reduced to 32 x 32 dimensions and randomly placed position above the input image. Additionally, the blank sections in the resulting watermark images were made transparent, allowing the original image to appear below the watermark.

Watermark images reduced to 32 x 32 dimensions are placed in a random position on the original image for each synthetic sample. Additionally, when adding a watermark image to each synthetic sample, the pixel values of the watermark image were changed according to Equation 19.

Examples of synthetic images obtained in step 7 are shown in Figure 4.

Figure 4.
Synthetic images

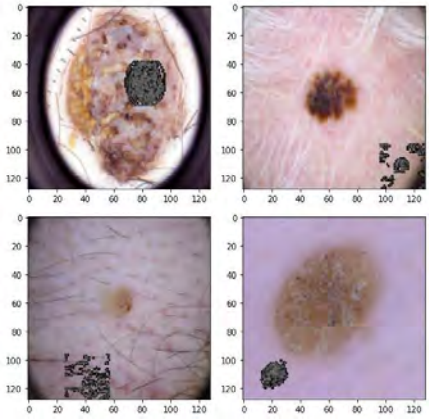

The watermark images generated in the proposed EDBT were obtained from the image samples taken from each class itself, thus preserving the distinctive differences between the classes. The pseudo-code of the proposed EDBT is given below.

INPUT: Imbalanced image dataset
OUTPUT: Balanced image dataset
Determine the majority class and minority class(es)
For each majority and minority class(es)
  Resize the image to 128 x 128
For each minority class
  generatedSamples= (0)
  Determine the number of synthetic samples (NSS)
  While Length of generatedSamples < NSS
    For each image in the minority class
      if Length of generatedSamples < NSS
        reduction of the noise of the image according to Equation 9.
        calculation of the gradient of the image according to Equation 10.11.12.13.
        calculation Non-Maximum Suppression of the image according to Equation 14.
        calculation average of the image pixels according to Equation 15.
        split image pixels into arrayLow and arrayHigh according to the obtained average
        calculate averages of arrayLow and arrayHigh
        calculate standard deviations of arrayLow and arrayHigh according to Equation 16.
        calculate lowthreshold and highthreshold according to Equation 17.18.
        apply Double Threshold to the image
        apply Edge Tracking by Hysteresis to the image
        calculate the averagePixels of Edge pixels
        calculate Watermark according to Equation 19.
        resize Watermark to 32 x 32
        place Watermark image to random (x,y) position on image
        append image to generatedSamples
      end if
    end for
  end while

append generatedSamples to the minority class

end for

Experimental Results

In this part of the study, the imbalanced dataset used, the algorithm used for classification, evaluation metrics, classification results, and comparisons are included.

Dataset

Therefore, to obtain a successful model, we should prepare appropriate and consistent input data for CNN. Unfortunately, each field's dataset has different problems, for example, medical datasets miss balancing. In this study, the HAM10000 dataset was used to test the effect of the proposed image augmentation technique on classification performance (Tschandl et al., 2018). This dataset consists of 10015 dermoscopic images and includes 7 classes. These classes are actinic keratosis and intraepithelial carcinoma (akiec), basal cell carcinoma (bcc), benign keratosis (bkl), dermatofibroma (df), melanoma (mel), melanocytic nevi (nv), and vascular skin legions (vasc) (Tschandl et al., 2018). As can be seen from Table 1, it creates an imbalanced dataset because the sample numbers of the classes are not the same. The number of samples included in the dataset, their proportional distribution in the dataset, and the number of oversampling to be made according to Equation 7 are shown in Table 1. The oversampling numbers for minority classes in the dataset seen in Table 1 were determined according to Equation 7 and 8. The nv class constitutes the majority class and accounts for 66.95% of the dataset with 6705 samples.

Table 1.

The Dataset

Class Name	Number of Samples	Percent	Number of Oversampling
mel	1113	11.11%	5592
df	115	1.15%	6590
akiec	327	3.27%	6378
bkl	1099	10.97%	5606
vasc	142	1.42%	6563
bcc	514	5.13%	6191

Performance Evaluation

In this study, CNN models using transfer learning methods that provide successful results in the classification of imbalanced datasets were used (Reshma Prakash & Nath Singh, 2020; Russakovsky et al., 2015). CNN is a kind of neural network that simulates the human visual cortex using evolutionary mathematical operations and extracts features from input images, passes these features through successive layers, and produces the

final output (LeCun et al., 1998). Although neural network architectures such as CNN provides good results in balanced datasets, their performance decreases in imbalanced datasets. One of the techniques used to solve this problem is the transfer learning method. In transfer learning methods, the CNN is used after being previously trained with large datasets such as ImageNet. It has been observed that pre-trained networks improve classification performance (Hossain et al., 2022). All experiments were performed on Windows 10 OS with a computer with an Intel Core i7@2.9 GHz processor and 32GB memory. In this study, the ResNet50 architecture, which is one of the transfer learning methods, was used. The ResNet50 architecture is a network of 50 layers trained with the ImageNet dataset (de Leeuw den Bouter et al., 2022). The ResNet architecture has three alternative layer structures: 34, 50, and 101. The details of the ResNet architecture are displayed in Table 2.

Table 2.

ResNet Architecture

Layer	34-layer	50-layer	101-layer
Conv1	7 x 7, 64, stride 2		
	3 x 3 max pool, stride 2		
Conv2_x	$\begin{bmatrix} 3x3,64 \\ 3x3,64 \end{bmatrix}$ x3	$[1x1,64\ 3x3,64\ 1x1,256]$ x3	$[1x1,64\ 3x3,64\ 1x1,256]$ x3
Conv3_x	$\begin{bmatrix} 3x3,128 \\ 3x3,128 \end{bmatrix}$ X4	$[1x1,128\ 3x3,128\ 1x1,512]$ x4	$[1x1,128\ 3x3,128\ 1x1,512]$ x4
Conv4_x	$\begin{bmatrix} 3x3,256 \\ 3x3,256 \end{bmatrix}$ X6	$[1x1,256\ 3x3,256\ 1x1,1024]$ x6	$[1x1,256\ 3x3,256\ 1x1,1024]$ x23
Conv5-x	$\begin{bmatrix} 3x3,512 \\ 3x3,512 \end{bmatrix}$ X3	$[1x1,512\ 3x3,512\ 1x1,2048]$ x3	$[1x1,512\ 3x3,512\ 1x1,2048]$ x3

Evaluation Metrics

Accuracy (AC), precision (PRE), recall (REC) and F1-score (F1-S), false positive rate (FPR), and false negative rate (FNR) metrics were used to evaluate the classification results. The AC value given in Equation 20 shows the ratio of correctly estimated samples to all samples. The PRE value given in Equation 21 is the ratio of the correct positive estimates to all positive estimates. The REC value given in Equation 22 is the ratio of the correct positive estimates to all the true positives. The F1-S value given in Equation 23 is the harmonic mean of the precision and recall values. The FPR value given in Equation 24 is the ratio of false positive estimates to all negatives. The FNR value given in Equation 25 is the ratio of false negative predictions to all positives.

$$AC = \frac{TP + TN}{TP + TN + FP + FN} \tag{20}$$

$$PRE = \frac{TP}{TP + FP} \tag{21}$$

$$REC = \frac{TP}{TP + FN} \tag{22}$$

$$F1 - S = 2x\frac{precision\,x\,recall}{precision + recall} \tag{23}$$

$$FPR = \frac{FP}{FP + TN} \tag{24}$$

$$FNR = \frac{FN}{FN + TP} \tag{25}$$

Results and Discussion

The images in the Ham10000 dataset have a resolution of 600 x 450, but the input images have been reduced to 128 x 128 dimensions. In many studies, input images for deep learning algorithms have been preferred in 128 x 128 dimensions both in terms of algorithm performance and in terms of computational time (de Leeuw den Bouter et al., 2022; Gangopadhyay et al., 2020; Pain et al., 2022; Sabottke & Spieler, 2020). The learning rate for the Adaptive Moment Estimation (ADAM) optimizer in the ResNet50 architecture used for classification was chosen as 0.001 (Kingma & Ba, 2014). The parameters of transfer learning have been adjusted to continue learning with our dataset. With the proposed image augmentation technique, the dataset was balanced, and as a result of the classification, a significant improvement was achieved according to the imbalanced state of the dataset.

Table 3 shows the classification results of the original and balanced versions of the imbalanced dataset. When the classification results of the imbalanced dataset are examined, extreme differences are observed between the results. For example, while the FPR value of the nv class is 0.712 and the FNR value is 0.02, the FPR value of the df class is 0 and the FNR value is 1.0. These values show that the imbalanced dataset increases the rate of incorrect predictions and negatively affects the classification results. When the results of the balanced dataset are examined, it is seen that the classification results are more evenly distributed among the classes. When the FPR and FNR metrics in the classification results of the balanced dataset are examined, it is seen that the rate

of incorrect predictions decreases compared to the imbalanced dataset.

Table 3.

Classification reports for balanced and imbalanced datasets

	Imbalanced dataset classification report					**Balanced dataset classification report**				
Class	Precision	Recall	f1-score	FPR	FNR	**Precision**	**Recall**	**f1-score**	**FPR**	**FNR**
nv	0.730	0.980	0.830	0.712	0.020	**0.950**	**0.930**	**0.940**	**0.008**	**0.072**
mel	0.550	0.130	0.210	0.014	0.860	**0.960**	**0.960**	**0.960**	**0.006**	**0.035**
bkl	0.330	0.000	0.010	0.001	0.990	**0.960**	**0.980**	**0.970**	**0.007**	**0.017**
bcc	0.370	0.580	0.450	0.054	0.410	**1.000**	**0.980**	**0.990**	**0.000**	**0.016**
akiec	0.000	0.000	0.000	0.000	1.000	**0.990**	**0.990**	**0.990**	**0.001**	**0.005**
vasc	0.750	0.120	0.210	0.000	0.880	**1.000**	**1.000**	**1.000**	**0.000**	**0.000**
df	0.000	0.000	0.000	0.000	1.000	**1.000**	**1.000**	**1.000**	**0.000**	**0.001**
	Classification Accuracy			0.690		**Classification Accuracy**			**0.980**	

In this study, balanced datasets were obtained by performing image augmentation on the dataset used in this study with flipping, rotation, and random erasing techniques, which are other image augmentation techniques. The obtained balanced datasets and the original version of the dataset were tested with the same deep learning architecture under the same conditions, and the results in Table 4 were obtained.

Table 4.

Comparison of the classification results of the proposed technique with other image augmentation techniques under the same conditions

Class Name	Evaluation Metric	Imbalanced Dataset	Balanced Dataset			
			Flipping	Rotation	Random Erasing	Proposed Technique
	Accuracy	0.690	0.880	0.570	0.610	**0.980**
nv	FPR	0.712	0.039	0.031	0.065	**0.008**
	FNR	0.020	0.221	0.114	0.209	**0.072**
Mel	FPR	0.014	0.033	0.029	0.038	**0.006**
	FNR	0.860	0.164	0.731	0.368	**0.035**
bkl	FPR	0.001	0.038	0.286	0.040	**0.007**
	FNR	0.990	0.181	0.173	0.409	**0.017**
bcc	FPR	0.054	0.004	0.108	0.189	**0.000**
	FNR	0.410	0.150	0.342	0.292	**0.016**
akiec	FPR	0.000	0.013	0.042	0.006	**0.001**
	FNR	1.000	0.064	0.635	0.562	**0.005**
vasc	FPR	0.000	0.002	0.002	0.101	**0.000**
	FNR	0.880	0.010	0.283	0.439	**0.000**
df	FPR	0.000	0.006	0.005	0.009	**0.000**
	FNR	1.000	0.043	0.760	0.421	**0.001**

When the results in Table 4 are evaluated, it is seen that balancing the dataset does not always give better results. Although the flipping technique gave better results than the rotation and random erasing techniques, the proposed technique gave better results than the flipping technique. Figure 5 shows the accuracy and loss rates during the training of the ResNet50 CNN architecture. When the accuracy and loss rates are evaluated, the performance of the proposed technique is seen.

Figure 5.

Accuracy and loss rates

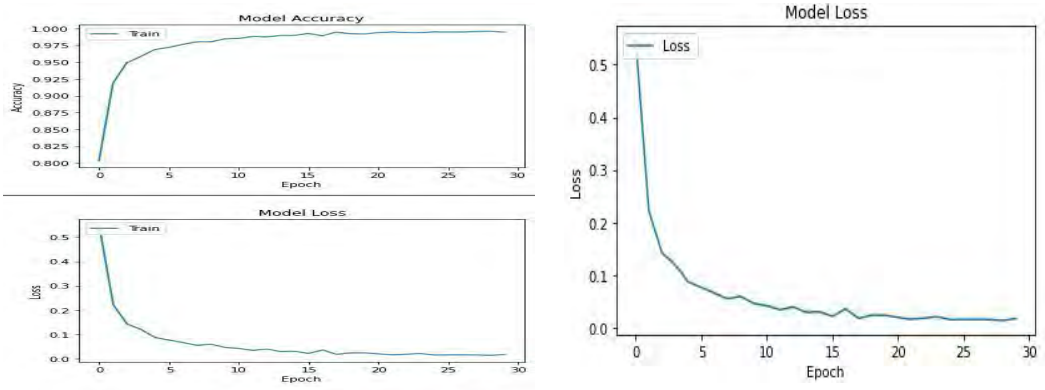

There are multi-class classification studies conducted on the HAM10000 dataset in the literature. In this study, it was seen that the proposed technique gave successful results compared to the studies in the literature. In Table 5, the results obtained in this study are compared with the results obtained in other studies using the same dataset.

Table 5.

Comparison of the proposed technique with other techniques using the HAM10000 dataset

Technique	CNN models	Augmentation technique	Accuracy	Precision	f1-score
(Shahin et al., 2019)	ResNet and Inception V3	Flipping, Rotation, Cropping	89.90%	86.20%	82.70%
(Sevli, 2021)	CNN Model	Flipping, Rotation, Cropping, Reflecting	91.51%	90.00%	90.00%
(Carcagnì et al., 2019)	DenseNet	Flipping, Rotation	90.00%	88.00%	82.00%
(Bansal et al., 2022)	Integrated HG and EfficientNet	Color Space Transformation, Noise Injection, Flipping, Rotation	94.90%	92.60%	94.80%
The proposed EDBT	ResNet50	Edge Detection, Mixing Images	**98.00**%	**97.88**%	**97.87**%

Table 5 shows other studies using the dataset used in this study and their classification results. Shahin et al. balanced the dataset with geometric image augmentation techniques and achieved an accuracy rate of 89.9% with CNN and the ResNet architecture also used in this study. Sevli balanced the dataset with geometric image augmentation techniques and achieved an accuracy rate of 91.51% with CNN. Carcagni et al. have balanced the dataset with geometric image augmentation techniques and achieved an

accuracy rate of 90% with CNN and DenseNet architecture. Bansal et al. balanced the dataset with Color Space Transformation, Flipping, Rotation, and Noise Injection-based image augmentation techniques and achieved an accuracy rate of 94.9% with CNN and EfficientNet architecture. In the proposed technique in this study, the dataset was balanced using edge detection and mixing images-based technique, and 98% accuracy was achieved with CNN and the ResNet50 architecture. Bansal et al. achieved a 94.9% accuracy rate by using multiple image augmentation techniques and hair removal techniques. In the proposed technique, the feature map obtained by feature extraction with edge detection was combined with the mixing images image augmentation technique, and a 98% accuracy rate was achieved.

Conclusion

The augmentation techniques used to balance imbalanced datasets have a significant influence on the performance of the classification algorithms. The tests of this study have proved this negative effect. Thus, this study has focused on image augmentation techniques and has proposed a novel augmentation technique named EDBT for solving classification problems caused by imbalanced datasets. As a result of insufficient sample numbers of some classes in the data sets, overfitting is observed. As a result of overfitting, the model memorizes the training data and gives unsuccessful classification results for the test data. As a solution to this problem, the sample number of minority classes is increased by using image augmentation techniques. In this study, the sample numbers of minority classes of the Ham10000 dataset were increased by the proposed EDBT. With the proposed EDBT. With the proposed EDBT, the edges of the minority class samples were detected with a modified Canny edge detector. The detected edge images were added to the minority class samples as watermarks. With these synthetic samples with watermarks, the sample numbers of the minority classes and the majority classes were equalized. The dataset consisting of 10015 skin cancer images was balanced and tested on a CNN model in the ResNet50 architecture. The proposed EDBT has been shown to give successful results in the comparative tests performed. Further, to test the effectiveness of the proposed method, it can be tested on more data sets and tested with other pre-trained CNN models.

References

Abdelhalim, I. S. A., Mohamed, M. F. & Mahdy, Y. B. (2021). Data augmentation for skin lesion using self-attention based progressive generative adversarial network. *Expert Systems with Applications, 165*. https://doi.org/10.1016/J.ESWA.2020.113922

Ali, K., Shaikh, Z. A., Khan, A. A. & Laghari, A. A. (2022). Multiclass skin cancer classification using EfficientNets – a first step towards preventing skin cancer. *Neuroscience Informatics, 2*(4), 100034. https://doi.org/10.1016/J.NEURI.2021.100034

Allken, V., Rosen, S., Handegard, N. O. & Malde, K. (2021). A real-world dataset and data simulation algorithm for automated fish species identification. *Geoscience*

Data Journal, *8*(2), 199–209. https://doi.org/10.1002/GDJ3.114

Bansal, P., Garg, R. & Soni, P. (2022). Detection of melanoma in dermoscopic images by integrating features extracted using handcrafted and deep learning models. *Computers and Industrial Engineering*, *168*. https://doi.org/10.1016/J.CIE.2022.108060

Barata, C., Celebi, M. E. & Marques, J. S. (2019). A Survey of Feature Extraction in Dermoscopy Image Analysis of Skin Cancer. *IEEE Journal of Biomedical and Health Informatics*, *23*(3), 1096–1109. https://doi.org/10.1109/JBHI.2018.2845939

Binder, M., Schwarz, M., Winkler, A., Steiner, A., Kaider, A., Wolff, K. & Pehamberger, H. (1995). Epiluminescence Microscopy: A Useful Tool for the Diagnosis of Pigmented Skin Lesions for Formally Trained Dermatologists. *Archives of Dermatology*, *131*(3), 286–291. https://doi.org/10.1001/ARCHDERM.1995.01690150050011

Bowles, C., Chen, L., Guerrero, R., Bentley, P., Gunn, R., Hammers, A., Dickie, D. A., Hernández, M. V., Wardlaw, J. & Rueckert, D. (2018). *GAN Augmentation: Augmenting Training Data using Generative Adversarial Networks*. https://doi.org/10.48550/arxiv.1810.10863

Calderón, C., Sanchez, K., Castillo, S. & Arguello, H. (2021). BILSK: A bilinear convolutional neural network approach for skin lesion classification. *Computer Methods and Programs in Biomedicine Update*, *1*, 100036. https://doi.org/10.1016/J.CMPBUP.2021.100036

Canny, J. (1986). A Computational Approach to Edge Detection. *IEEE Transactions on Pattern Analysis and Machine Intelligence*, *PAMI-8*(6), 679–698. https://doi.org/10.1109/TPAMI.1986.4767851

Cao, Z., Wei, Z. & Zhang, G. (2014). A no-reference sharpness metric based on the notion of relative blur for Gaussian blurred image. *Journal of Visual Communication and Image Representation*, *25*(7), 1763–1773. https://doi.org/10.1016/J.JVCIR.2014.06.010

Carcagnì, P., Leo, M., Cuna, A., Mazzeo, P. L., Spagnolo, P., Celeste, G. & Distante, C. (2019). Classification of skin lesions by combining multilevel learnings in a DenseNet architecture. *Lecture Notes in Computer Science (Including Subseries Lecture Notes in Artificial Intelligence and Lecture Notes in Bioinformatics)*, *11751 LNCS*, 335–344. https://doi.org/10.1007/978-3-030-30642-7_30/COVER

Chaitanya, K., Karani, N., Baumgartner, C. F., Erdil, E., Becker, A., Donati, O. & Konukoglu, E. (2021). Semi-supervised task-driven data augmentation for medical image segmentation. *Medical Image Analysis*, *68*, 101934. https://doi.org/10.1016/J.MEDIA.2020.101934

Chaves, H., Dorr, F., Costa, M. E., Serra, M. M., Slezak, D. F., Farez, M. F., Sevlever, G., Yañez, P. & Cejas, C. (2021). Brain volumes quantification from MRI in healthy controls: Assessing correlation, agreement and robustness of a convolutional neural network-based software against FreeSurfer, CAT12 and FSL. *Journal of Neuroradiology*, *48*(3), 147–156. https://doi.org/10.1016/J.NEURAD.2020.10.001

Cubuk, E. D., Zoph, B., Mane, D., Vasudevan, V. & Le, Q. v. (2018). AutoAugment: Learning Augmentation Policies from Data. *Cvpr 2019*, *Section 3*, 113–123. https://doi.org/10.48550/arxiv.1805.09501

de Leeuw den Bouter, M. L., Ippolito, G., O'Reilly, T. P. A., Remis, R. F., van Gijzen, M. B. & Webb, A. G. (2022). Deep learning-based single image super-resolution for low-field MR brain images. *Scientific Reports*, *12*(1). https://doi.org/10.1038/S41598-022-10298-6

DeVries, T. & Taylor, G. W. (2017). Dataset Augmentation in Feature Space. *5th International Conference on Learning Representations, ICLR 2017 - Workshop Track Proceedings*. https://doi.org/10.48550/arxiv.1702.05538

Dewi, C., Chen, R. C., Liu, Y. T. & Yu, H. (2021). Various generative adversarial networks model for synthetic prohibitory sign image generation. *Applied Sciences (Switzerland), 11*(7). https://doi.org/10.3390/APP11072913

Frid-Adar, M., Diamant, I., Klang, E., Amitai, M., Goldberger, J. & Greenspan, H. (2018). GAN-based synthetic medical image augmentation for increased CNN performance in liver lesion classification. *Neurocomputing*, *321*, 321–331. https://doi.org/10.1016/J.NEUCOM.2018.09.013

Gangopadhyay, T., Locurto, A., Michael, J. B. & Sarkar, S. (2020). Deep Learning Algorithms for Detecting Combustion Instabilities. *Energy, Environment, and Sustainability*, 283–300. https://doi.org/10.1007/978-981-15-0536-2_13/COVER

Gong, L., Jiang, S. & Jiang, L. (2019). Tackling Class Imbalance Problem in Software Defect Prediction through Cluster-Based Over-Sampling with Filtering. *IEEE Access, 7*, 145725–145737. https://doi.org/10.1109/ACCESS.2019.2945858

Guan, Q., Chen, Y., Wei, Z., Heidari, A. A., Hu, H., Yang, X. H., Zheng, J., Zhou, Q., Chen, H. & Chen, F. (2022). Medical image augmentation for lesion detection using a texture-constrained multichannel progressive GAN. *Computers in Biology and Medicine, 145*, 105444. https://doi.org/10.1016/J.COMPBIOMED.2022.105444

Gupta, A., Venkatesh, S., Chopra, S. & Ledig, C. (2019). *Generative Image Translation for Data Augmentation of Bone Lesion Pathology*. https://doi.org/10.48550/arxiv.1902.02248

Hosny, K. M., Kassem, M. A. & Foaud, M. M. (2019). Classification of skin lesions using transfer learning and augmentation with Alex-net. *PLoS ONE, 14*(5). https://doi.org/10.1371/JOURNAL.PONE.0217293

Hossain, S. I., de Goër de Herve, J., Hassan, M. S., Martineau, D., Petrosyan, E., Corbin, V., Beytout, J., Lebert, I., Durand, J., Carravieri, I., Brun-Jacob, A., Frey-Klett, P., Baux, E., Cazorla, C., Eldin, C., Hansmann, Y., Patrat-Delon, S., Prazuck, T., Raffetin, A., … Nguifo, E. M. (2022). Exploring convolutional neural networks with transfer learning for diagnosing Lyme disease from skin lesion images. *Computer Methods and Programs in Biomedicine, 215*. https://doi.org/10.1016/J.CMPB.2022.106624

Ibrahim, M. H. (2021). ODBOT: Outlier detection-based oversampling technique for imbalanced datasets learning. *Neural Computing and Applications*, *33*(22), 15781–15806. https://doi.org/10.1007/S00521-021-06198-X

Inoue, H. (2018). *Data Augmentation by Pairing Samples for Images Classification*. https://arxiv.org/abs/1801.02929v2

Jaipuria, N., Zhang, X., Bhasin, R., Arafa, M., Chakravarty, P., Shrivastava, S., Manglani, S. & Murali, V. N. (2020). Deflating dataset bias using synthetic data augmentation. *IEEE Computer Society Conference on Computer Vision and Pattern Recognition Workshops, 2020-June*, 3344–3353. https://doi.org/10.1109/CVPRW50498.2020.00394

Kang, G., Dong, X., Zheng, L. & Yang, Y. (2017). *PatchShuffle Regularization*. https://doi.org/10.48550/arxiv.1707.07103

Kayumov, Z., Tumakov, D. & Mosin, S. (2020). Hierarchical Convolutional Neural Network for Handwritten Digits Recognition. *Procedia Computer Science, 171,*

1927–1934. https://doi.org/10.1016/J.PROCS.2020.04.206

Khan, F. U. & Aziz, I. B. A. (2019). Reducing high variability in medical image collection by a novel cluster based synthetic oversampling technique. *2019 IEEE Conference on Big Data and Analytics, ICBDA 2019*, 45–50. https://doi.org/10.1109/ICBDA47563.2019.8987171

Khan, M. Attique, Akram, T., Sharif, M., Javed, K., Rashid, M. & Bukhari, S. A. C. (2020). An integrated framework of skin lesion detection and recognition through saliency method and optimal deep neural network features selection. *Neural Computing and Applications*, *32*(20), 15929–15948. https://doi.org/10.1007/S00521-019-04514-0

Khan, Muhammad Attique, Sharif, M., Akram, T., Bukhari, S. A. C. & Nayak, R. S. (2020). Developed Newton-Raphson based deep features selection framework for skin lesion recognition. *Pattern Recognition Letters*, *129*, 293–303. https://doi.org/10.1016/J.PATREC.2019.11.034

Khan, Muhammad Attique, Zhang, Y. D., Sharif, M. & Akram, T. (2021). Pixels to Classes: Intelligent Learning Framework for Multiclass Skin Lesion Localization and Classification. *Computers and Electrical Engineering*, *90*. https://doi.org/10.1016/J.COMPELECENG.2020.106956

Kim, M. J., Kang, D. K. & Kim, H. B. (2015). Geometric mean based boosting algorithm with over-sampling to resolve data imbalance problem for bankruptcy prediction. *Expert Systems with Applications*, *42*(3), 1074–1082. https://doi.org/10.1016/J.ESWA.2014.08.025

Kingma, D. P. & Ba, J. L. (2014). Adam: A Method for Stochastic Optimization. *3rd International Conference on Learning Representations, ICLR 2015 - Conference Track Proceedings*. https://doi.org/10.48550/arxiv.1412.6980

Koziarski, M., Krawczyk, B. & Woźniak, M. (2019). Radial-Based oversampling for noisy imbalanced data classification. *Neurocomputing*, *343*, 19–33. https://doi.org/10.1016/J.NEUCOM.2018.04.089

LeCun, Y., Bottou, L., Bengio, Y. & Haffner, P. (1998). Gradient-based learning applied to document recognition. *Proceedings of the IEEE*, *86*(11), 2278–2323. https://doi.org/10.1109/5.726791

Lewy, D. & Mańdziuk, J. (2022). An overview of mixing augmentation methods and augmentation strategies. *Artificial Intelligence Review*, 1–59. https://doi.org/10.1007/S10462-022-10227-Z/FIGURES/28

Li, D., Haritunians, T., Mengesha, E., Targan, S. R. & McGovern, D. (2019). 151 – Using Deeplearning and Genetic Bigdata to Predict Crohn's Disease. *Gastroenterology*, *156*(6), S-35. https://doi.org/10.1016/S0016-5085(19)36864-7

Li, W., Li, J., Polson, J., Wang, Z., Speier, W. & Arnold, C. (2022). High resolution histopathology image generation and segmentation through adversarial training. *Medical Image Analysis*, *75*, 102251. https://doi.org/10.1016/J.MEDIA.2021.102251

Liu, G., Yang, Y. & Li, B. (2018). Fuzzy rule-based oversampling technique for imbalanced and incomplete data learning. *Knowledge-Based Systems*, *158*, 154–174. https://doi.org/10.1016/J.KNOSYS.2018.05.044

Liu, S., Zhang, J., Xiang, Y. & Zhou, W. (2017). Fuzzy-Based Information Decomposition for Incomplete and Imbalanced Data Learning. *IEEE Transactions on Fuzzy Systems*, *25*(6), 1476–1490. https://doi.org/10.1109/TFUZZ.2017.2754998

Luongo, F., Hakim, R., Nguyen, J. H., Anandkumar, A. & Hung, A. J. (2021). Deep learning-based computer vision to recognize and classify suturing gestures in robot-assisted surgery. *Surgery (United States)*, *169*(5), 1240–1244. https://doi.org/10.1016/J.SURG.2020.08.016

Maaten, L. van der & Hinton, G. (2008). Visualizing Data using t-SNE. *Journal of Machine Learning Research*, *9*(86), 2579–2605. http://jmlr.org/papers/v9/vandermaaten08a.html

Moreno-Barea, F. J., Strazzera, F., Jerez, J. M., Urda, D. & Franco, L. (2019). Forward Noise Adjustment Scheme for Data Augmentation. *Proceedings of the 2018 IEEE Symposium Series on Computational Intelligence, SSCI 2018*, 728–734. https://doi.org/10.1109/SSCI.2018.8628917

Mutasa, S., Sun, S. & Ha, R. (2020). Understanding artificial intelligence based radiology studies: What is overfitting? *Clinical Imaging*, *65*, 96–99. https://doi.org/10.1016/J.CLINIMAG.2020.04.025

Nahata, H. & Singh, S. P. (2020). *Deep Learning Solutions for Skin Cancer Detection and Diagnosis*. 159–182. https://doi.org/10.1007/978-3-030-40850-3_8

Nakamura, M., Kajiwara, Y., Otsuka, A. & Kimura, H. (2013). LVQ-SMOTE - Learning Vector Quantization based Synthetic Minority Over-sampling Technique for biomedical data. *BioData Mining*, *6*(1). https://doi.org/10.1186/1756-0381-6-16

Nanni, L., Paci, M., Brahnam, S. & Lumini, A. (2022). Feature transforms for image data augmentation. *Neural Computing and Applications*, *34*(24), 22345–22356. https://doi.org/10.1007/S00521-022-07645-Z

Nordmann, N., Hubbard, M., Nordmann, T., Sperduto, P. W., Clark, H. B. & Hunt, M. A. (2017). Effect of Gamma Knife Radiosurgery and Programmed Cell Death 1 Receptor Antagonists on Metastatic Melanoma. *Cureus*. https://doi.org/10.7759/CUREUS.1943

Ogundimu, E. O. (2019). Prediction of default probability by using statistical models for rare events. *Journal of the Royal Statistical Society: Series A (Statistics in Society)*, *182*(4), 1143–1162. https://doi.org/10.1111/RSSA.12467

Pain, C. D., Egan, G. F. & Chen, Z. (2022). Deep learning-based image reconstruction and post-processing methods in positron emission tomography for low-dose imaging and resolution enhancement. *European Journal of Nuclear Medicine and Molecular Imaging*, *49*(9), 3098–3118. https://doi.org/10.1007/S00259-022-05746-4

Pande, S. D., Jadhav, P. P., Joshi, R., Sawant, A. D., Muddebihalkar, V., Rathod, S., Gurav, M. N. & Das, S. (2022). Digitization of handwritten Devanagari text using CNN transfer learning – A better customer service support. *Neuroscience Informatics*, *2*(3), 100016. https://doi.org/10.1016/J.NEURI.2021.100016

Piccialli, F., Somma, V. di, Giampaolo, F., Cuomo, S. & Fortino, G. (2021). A survey on deep learning in medicine: Why, how and when? *Information Fusion*, *66*, 111–137. https://doi.org/10.1016/J.INFFUS.2020.09.006

Ren, R., Yang, Y. & Sun, L. (2020). Oversampling technique based on fuzzy representativeness difference for classifying imbalanced data. *Applied Intelligence*, *50*(8), 2465–2487. https://doi.org/10.1007/S10489-020-01644-0

Reshma Prakash, S. & Nath Singh, P. (2020). Object detection through region proposal based techniques. *Materials Today: Proceedings*, *46*, 3997–4002. https://doi.org/10.1016/J.MATPR.2021.02.533

Russakovsky, O., Deng, J., Su, H., Krause, J., Satheesh, S., Ma, S., Huang, Z., Karpathy, A., Khosla, A., Bernstein, M., Berg, A. C. & Fei-Fei, L. (2015). ImageNet Large Scale Visual Recognition Challenge. *International Journal of Computer Vision, 115*(3), 211–252. https://doi.org/10.1007/S11263-015-0816-Y

Sabottke, C. F. & Spieler, B. M. (2020). The effect of image resolution on deep learning in radiography. *Radiology: Artificial Intelligence, 2*(1). https://doi.org/10.1148/RYAI.2019190015

Sevli, O. (2021). A deep convolutional neural network-based pigmented skin lesion classification application and experts evaluation. *Neural Computing and Applications, 33*(18), 12039–12050. https://doi.org/10.1007/S00521-021-05929-4

Shahin, A. H., Kamal, A. & Elattar, M. A. (2019). Deep Ensemble Learning for Skin Lesion Classification from Dermoscopic Images. *2018 9th Cairo International Biomedical Engineering Conference, CIBEC 2018 - Proceedings*, 150–153. https://doi.org/10.1109/CIBEC.2018.8641815

Shorten, C. & Khoshgoftaar, T. M. (2019). A survey on Image Data Augmentation for Deep Learning. *Journal of Big Data, 6*(1). https://doi.org/10.1186/S40537-019-0197-0

Siegel, R. L., Miller, K. D. & Jemal, A. (2016). Cancer statistics, 2016. *CA: A Cancer Journal for Clinicians, 66*(1), 7–30. https://doi.org/10.3322/CAAC.21332

Silveira, M., Nascimento, J. C., Marques, J. S., Marçal, A. R. S., Mendonça, T., Yamauchi, S., Maeda, J. & Rozeira, J. (2009). Comparison of segmentation methods for melanoma diagnosis in dermoscopy images. *IEEE Journal on Selected Topics in Signal Processing, 3*(1), 35–45. https://doi.org/10.1109/JSTSP.2008.2011119

Šprogar, M., Colnaric, M. & Verber, D. (2021). On data windows for fault detection with neural networks. *IFAC-PapersOnLine, 54*(4), 38–43. https://doi.org/10.1016/J.IFACOL.2021.10.007

Srivastava, N., Hinton, G., Krizhevsky, A., Sutskever, I. & Salakhutdinov, R. (2014). Dropout: A Simple Way to Prevent Neural Networks from Overfitting. *Journal of Machine Learning Research, 15*(56), 1929–1958. http://jmlr.org/papers/v15/srivastava14a.html

Tajbakhsh, N., Gotway, M. B. & Liang, J. (2015). Computer-aided pulmonary embolism detection using a novel vessel-aligned multi-planar image representation and convolutional neural networks. *Lecture Notes in Computer Science (Including Subseries Lecture Notes in Artificial Intelligence and Lecture Notes in Bioinformatics), 9350*, 62–69. https://doi.org/10.1007/978-3-319-24571-3_8/COVER

Takahashi, R., Matsubara, T. & Uehara, K. (2020). Data Augmentation Using Random Image Cropping and Patching for Deep CNNs. *IEEE Transactions on Circuits and Systems for Video Technology, 30*(9), 2917–2931. https://doi.org/10.1109/TCSVT.2019.2935128

Tarekegn, A. N., Giacobini, M. & Michalak, K. (2021). A review of methods for imbalanced multi-label classification. *Pattern Recognition, 118*. https://doi.org/10.1016/J.PATCOG.2021.107965

Tsao, H., Olazagasti, J. M., Cordoro, K. M., Brewer, J. D., Taylor, S. C., Bordeaux, J. S., Chren, M. M., Sober, A. J., Tegeler, C., Bhushan, R. & Begolka, W. S. (2015). Early detection of melanoma: Reviewing the ABCDEs American Academy of Dermatology Ad Hoc Task Force for the ABCDEs of Melanoma. *Journal of the American Academy of Dermatology, 72*(4), 717–723. https://doi.org/10.1016/J.

JAAD.2015.01.025

Tschandl, P., Rosendahl, C. & Kittler, H. (2018). The HAM10000 dataset, a large collection of multi-source dermatoscopic images of common pigmented skin lesions. *Scientific Data, 5*. https://doi.org/10.1038/SDATA.2018.161

Wan, M., Gu, G., Qian, W., Ren, K. & Chen, Q. (2017). Hue preservation based color space transformation for brightness-robust tracking. *Optik, 144*, 26–33. https://doi.org/10.1016/j.ijleo.2017.06.073

Wang, H., Zhou, Y., Zhang, J., Lei, J., Sun, D., Xu, F. & Xu, X. (2022). Anomaly segmentation in retinal images with poisson-blending data augmentation. *Medical Image Analysis, 81*, 102534. https://doi.org/10.1016/J.MEDIA.2022.102534

Zhong, Z., Zheng, L., Kang, G., Li, S. & Yang, Y. (2020). Random erasing data augmentation. *AAAI 2020 - 34th AAAI Conference on Artificial Intelligence,* 13001–13008. https://doi.org/10.1609/AAAI.V34I07.7000

Zhu, T., Lin, Y., Liu, Y., Zhang, W. & Zhang, J. (2019). Minority oversampling for imbalanced ordinal regression. *Knowledge-Based Systems, 166*, 140–155. https://doi.org/10.1016/J.KNOSYS.2018.12.021

About the Authors

Muhammed KARAALTUN received a B.S. degree in Software Engineering from Northern Technique University, Kirkuk, Iraq. He received M.S. and Ph.D. degrees in Computer Engineering from Selcuk University, Konya, Turkey. His research aims to develop and apply methods for data mining and machine learning and aims to use these methods in embedded systems and control. He has published more than 18 research papers in reputed international journals indexed in SCI, SCOPUS, and Web of Science.

E-mail: muhammed.karaaltun@karatay.edu.tr, ORCID: 0000-0002-6093-6105

Omer OZCAN graduated from Selcuk University Computer Engineering in 2007 and completed his master's degree in 2011. He has been giving programming and 3D modeling courses at Selcuk University since 2007. He is interested in deep learning, image processing, ransomware, random numbers, and embedded systems.

E-mail: oozcan@selcuk.edu.tr, ORCID: 0000-0003-4122-4329

Similarity Index
The similarity index obtained from the plagiarism software for this book chapter is 23%.

CHAPTER 10

Building Intelligent Systems Using JETSON TX2:A Robot Design Example

Mehmet Tugrul KAYA
City Technologies Center - Konya Metropolitan Municipality, Türkiye

Burak YILMAZ
Konya Technical University - Software Engineering Department, Türkiye

To Cite This Chapter:
Dursun M., Unler T., (2023). Building Intelligent Systems Using JETSON TX2:A Robot Design Example.In S. Kocer. & O. Dundar (Eds.), *Artıfıcıal Intelligence Applications in Intteligent System* (pp. 169–182). ISRES Publishing.

Introduction

As a result of the digitalization process, the capabilities we acquired through our past experiences are now acquired through data processed through digital platforms. These platforms save and process data instantaneously and then activate a decision support system. Jetson TX2, a card used to obtain data with digital platforms, takes its place among artificial intelligence development and application cards.

The development of intelligent systems for autonomous driving using the Jetson TX2 platform has great potential to revolutionize transportation and make roads safer. Leveraging advanced computing capabilities and state-of-the-art algorithms, Jetson TX2 enables real-time data processing and analysis, enabling vehicles to perceive their environment with high precision and make informed decisions in various driving scenarios (Özsoy, 2020). Figure 1 shows the physical structure of the Jetson TX2 development board.

Figure 1.
Jetson TX2 development board

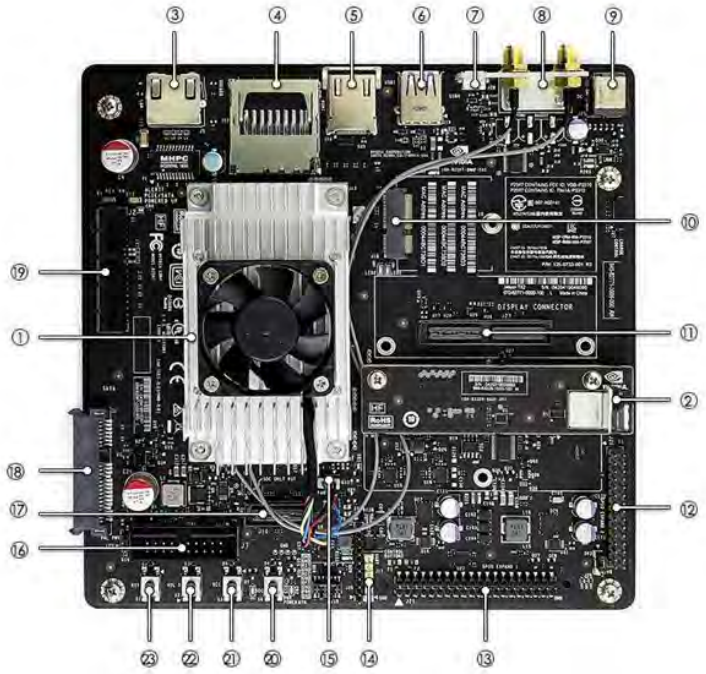

The description of the components shown in the physical structure of the Jetson TX2 board is as shown in Table 1.

Table 1.
Jetson TX2 Specifications

1.	Jetson TX2: Jetson TX2 core module with cooling fan	13.	40PIN GPIO expansion header: Compatible with Raspberry Pi GPIO header
2.	Camera	14.	UART interface
3.	Gigabit Ethernet port: 10/100/1000BASE-	15.	Fan connector
4.	SD card slot	16.	JTAG connector
5.	HDMI (Type-A)	17.	Debug interface
6.	USB3.0 port	18.	SATA connector
7.	Micro USB port	19.	PCIE connector
8.	Antenna connector	20.	Power button
9.	Power jack	21.	Recovery button
10.	M.2 key A interface	22.	Volume button
11.	Screen interface	23.	Reset button
12.	30PIN GPIO expansion slot		

The Role and Importance of Jetson TX2 in Intelligent Systems

Jetson TX2 plays an important role in the mainstreaming of AI applications in intelligent systems. Thanks to its powerful performance and energy efficiency, Jetson TX2 is able to deliver real-time performance in AI applications such as image processing,

voice recognition, natural language processing and machine translation. Due to these capabilities, Jetson TX2 is used in smart systems in the following areas (Carvalho, Anderson 2019):

- Autonomous vehicles
- Smart buildings
- Smart cities
- Smart production
- Smart health
- Smart security

Studies on the usage potential of Jetson TX2 in smart systems show that this platform can be used effectively in many areas. In this context, we can discuss the details of different application areas of Jetson TX2 below:

1. General Use and Potential in Smart Systems:

- Jetson TX2 enables intelligent systems to be more efficient, safe and comfortable. This is particularly emphasized by (Carvalho, Anderson 2019). This platform is preferred in many embedded systems thanks to its high computational capacity and energy efficiency.

2. Autonomous Navigation and Vehicle Localization:

- Jetson TX2 was used in vehicle localization for autonomous navigation. This shows the versatility and effectiveness of this platform in improving overall system performance (Kaya, 2021).
- In autonomous driving systems, the integration of deep learning and vision applications with

Jetson TX2 makes it possible for vehicles to move more safely and effectively in traffic. (Kaya, 2021)

3. Deep Learning and Vision Applications:

-Convolutional Neural Networks have been successfully applied on Jetson TX2 platforms in tasks such as traffic sign identification, autonomous image enhancement, single camera real time depth reconstruction and image captioning. In road object detection, researchers have developed modular fused feature map detectors using Jetson TX2. These detectors enable autonomous vehicles to navigate safely (Kaya, 2021).

4. Object Detection and Warning Systems:

-Another important application of Jetson TX2 in autonomous driving is object detection and warning systems. In particular, a UAV warning system based on YOLOv2 and a connection and cable detection method have been successfully implemented with the Jetson TX2.

-In a study by Liu et al. (2020), Jetson TX2 was found to be effective in real-time 3D object detection from distant 3D point clouds.

5. Unmanned Aerial Vehicles (UAV) Applications:

-The computational capabilities of Jetson TX2 have also been utilized in the field of unmanned aerial vehicles. In this context, the researchers developed a YOLOv2-based UAV warning system to prevent potential collisions in the airspace.

Designing an Intelligent System Based on Jetson TX2

Considering the mentioned features and usage areas of Jetson TX2, it is seen that its use in smart system design is the right choice. An example of these designs is given below as a summary of the steps to be followed while creating a Jetson TX2-based smart system. In the example, the Roomba robot platform was transformed into a robot platform used for mapping algorithm applications with Jetson TX2. Figure 2 shows this design.

Figure 2.

Appearance of the prepared smart system (a) Jetson Nano Based System (b) Jetson TX2 Based System

(a)

(b)

The navigation capabilities of autonomous mobile robots, especially in unstructured environments, have attracted the interest of many researchers in recent years. A study by (Ciocirlan et al., 2023) shows how object recognition accuracy can be improved by combining HQ stereo cameras and RP LIDAR sensors. This is a critical step for robots to be able to detect obstacles more accurately.

A wide field of view of the cameras is especially important for robots moving in narrow corridors. In this context, there is a study (Zhang & Zhang, 2019) on vanishing point detection in corridors using monocular low-resolution fisheye cameras. This allows robots to move more accurately.

Research on how RGB-D cameras can be used for obstacle detection in agricultural applications (Skoczen et al., 2021) shows that such cameras can improve obstacle mapping accuracy through their ability to provide depth data.

One of the most important features of robots that work in this way is the combination of many electronic devices. The software needed for multiple electronic devices to work with each other is an operating system. The operating ROS (Robot Operating System) software is required to enable the devices to communicate with each other. This software enables multiple electronic devices to open the communication mechanism called nodes and communicate.

The combined use of ROS (Robot Operating System) and Jetson TX2 is critical for robots to move autonomously. In particular, there is a study (Fares, 2021) for a robot based on a fourwheeled omnidirectional platform to move in an unknown semi-structured indoor environment. In this work, the robot is able to autonomously perform tasks such as Simultaneous Localization and Mapping (SLAM), navigation, obstacle detection and object recognition using Hokuyo 2D Lidar and Realsense D435i camera.

Finally, a study on combining an Orbbec Astra camera and Lidar for a robot to map an unknown indoor environment (Reddy & Kumar, 2021) shows that by combining data from these two sensors, the robot can create clearer and more detailed maps.

Robot Components and Electronic Equipment Roomba Platform

It is a stand-alone vacuum cleaner sold by iRobot. It is designed to navigate a living space and avoid common obstacles such as furniture when sweeping the floor. This platform is preferred because it is easier and less costly than other commercial platforms. Figure 3 shows the Roomba e782 platform in its simplest form.

Figure 3.

Roomba e782 Platform

Onboard PC

To handle the ROS client and user interface, Ubuntu and ROS program must be installed on the PC. The computer must be in local connection on the same LAN as the Jetson TX2 on the robot.It can be connected to the robot via SSH. Figure 4 shows the on-board PC used in the system.

Figure 4.

Resident PC

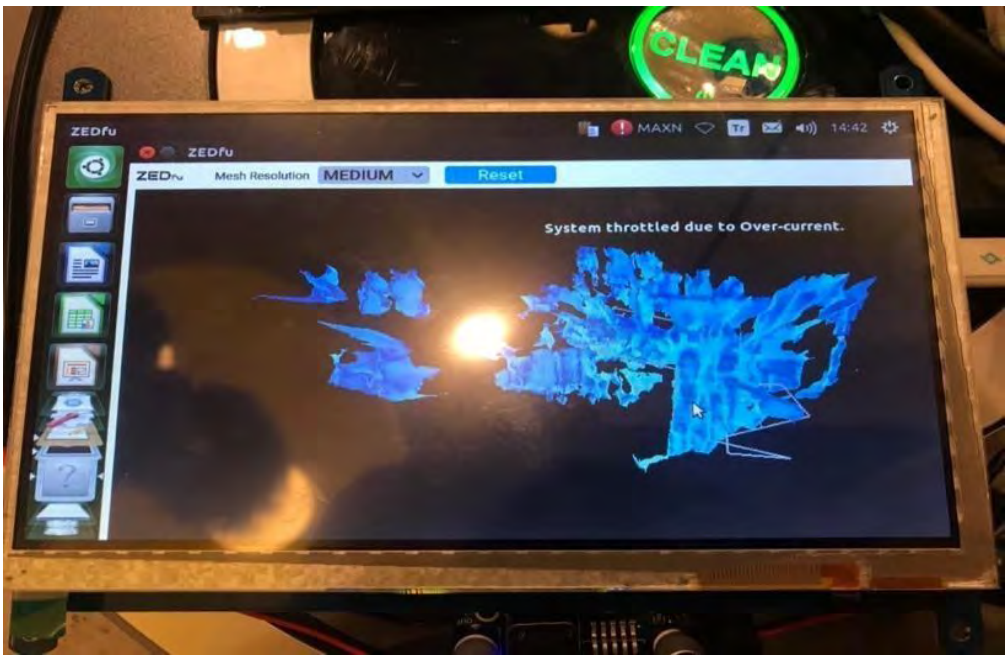

Joy Pad

A ROS-based game controller for controlling the robot. It contains a joy_node, a node that connects the game controller to the ROS. This node allows the game controller to perform a gesture involving the current state of each of its buttons and axes. The game controller used is shown in Figure 5.

Figure 5.

Game Controller

USB Serial Cable Components

In order to control the Roomba robot platform, it needs to be in constant communication with the Jetson TX2 platform. In order to ensure communication, a converter design is needed to provide voltage level and communication protocol conversion between the USB ports of the Jetson TX2 and the UART port of the Roomba platform. This converter consists of the following components:

FTDI: TTL-232R-5V: USB to Serial converter card is a converter card that contains FT232RL integration on it. By creating a virtual serial port on the connected computer, it allows communication between the computer and UART port external devices.

7 DIN Pin: The robot platform used is the e782 series of Roomba robot. Serial port sockets of 700 series robots are 7 pin embedded system.

Figure 6.

USB to UART Cable Conversion Jetson TX2

Exploration vehicles need accurate localization to perform tasks such as autonomous navigation. Images captured from stereo cameras allow to estimate both the motion of the robot and the structure of the environment. With this work, some of the solutions for SLAM compatible with the ROS (Robot Operating System) middleware have been implemented with the Jetson TX2. The main contributions of this work to the existing literature are twofold: first, we evaluate the algorithm performances with respect to an NVIDIA Jetson TX2 card respectively, instead of a common workstation-class computer. (Kaya, 2021) Figure 7 shows the Jetson TX2 AI Development Board before it was integrated into the Roomba Platform.

Figure 7.

Jetson TX2 Artificial Intelligence Development Board

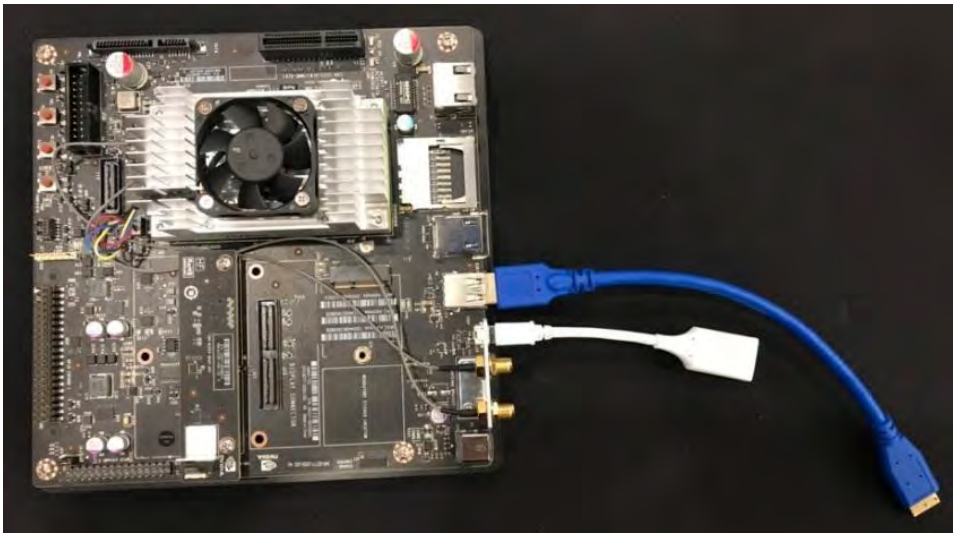

Kinect XBOX 360

For the mobile robot developed using the Roomba platform, the ROS (robot operating system) control scheme was developed, which allows controlling the robot using velocity vector references. A Kinect sensor was included in the system and a controller was also added that monitors processes in other situations and communicates with the remote control.

The system is flexible enough to be replicated in other Roomba robots in the future. With this scheme, it is possible to control the motion of the robot using velocity vector parameters generated from spatial references extracted from the environment using the Kinect sensor.

Figure 8.

Kinect Sens e.g. , Power Supply and Feeds

A 6000Mah 5S LiPo battery was used for the power supply of the robot. From the LiPo battery, 19V outputs were taken for the Jetson TX2 on the robot, 12V for the Kinect 360 camera and 12V for the USB multiplexer. A voltage regulator was used to reduce these outputs to the desired voltage value.

Figure 9.

Battery system for Kinect 360 camera (a) Demonstration of Kinect supply with converter. (b) Inserting switch into power supply. (c) Connecting lipo batteries

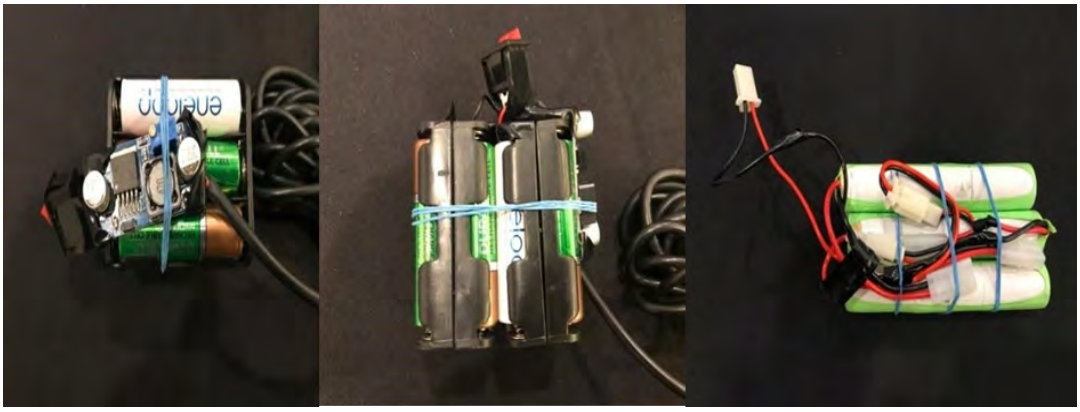

(a) (b) (c)

A Review on the Advantages and Disadvantages of Using Jetson TX2 in Smart Systems

NVIDIA's Jetson TX2 platform is a highly suitable option for unmanned aerial vehicles (UAVs) and autonomous driving systems. This platform features a portable GPU powered by the NVIDIA Pascal architecture. Having such a powerful GPU in embedded systems is a huge advantage for performing complex operations such as real-time image processing, sensor fusion and deep learning. Energy efficiency is a critical factor for long-term operations. For UAVs and UCAVs, this means longer navigation times.

In addition to its advantages, Jetson TX2 also has some disadvantages. Firstly, it has a higher price tag than other embedded platforms in terms of cost, which can be an obstacle for projects with limited budgets. Secondly, the fact that the Jetson TX2 is a relatively new product on the market means that there may not yet be extensive community support or customized solutions. This may complicate the process of finding solutions to problems that users may encounter. Finally, the heterogeneous CPU-GPU architecture of the Jetson TX2 may be complex for some developers. Especially for developers who are inexperienced in CUDA programming or parallel computing, this may create a curve that complicates the learning process (Comparing Computing Platforms for Deep Learning on a Humanoid Robot, 2018).

Conclusion and Discussion

This study detailed the use of Jetson TX2 and related technologies for autonomous robot locomotion in unstructured environments. The effectiveness of Jetson TX2 is evaluated in realtime 3D object detection and processing of data from various sensors. Data from sensors such as LIDAR, cameras and encoders are processed by the algorithms and the results are compared with the ground truth.

The gmapping algorithm was able to accurately map the walls of the laboratory, but also revealed certain limitations. This shows potential areas for improvement of Jetson TX2 and the other technologies used. This study also revealed that the Hector SLAM algorithm shows more promise in small areas, suggesting that the Jetson TX2 and related technologies are suitable for such applications.

etson TX2's performance was evaluated in terms of map generation speed and accuracy and satisfactory results were obtained. This shows that Jetson TX2 is an effective solution for autonomous robot locomotion. However, further research is needed in areas such as map resolution and the performance of other algorithms.

In conclusion, Jetson TX2 and related technologies offer effective and efficient solutions for autonomous robot locomotion. The use of these technologies can significantly improve the environmental perception and locomotion capabilities of autonomous robots. In the future, further development and optimization of these technologies can further enhance the performance and functionality of autonomous robots. This study emphasizes the need for further research and development in this area. With the developed Jetson TX2 based robot, mapping algorithms were used to enable the robot to map its environment. Examples of maps obtained with these algorithms are shown in Figures 10 - 15. Figure 10 and Figure 11 show the results of the Gmapping algorithm, Figure 12 and Figure 13 show the results of the Hector Slam algorithm (Laksono & Kusuma, 2022), Figure 14 and Figure 15 show the results of the Cartographer algorithm (Wang et al., 2016).

Figure 10.

Gmapping Map Sample

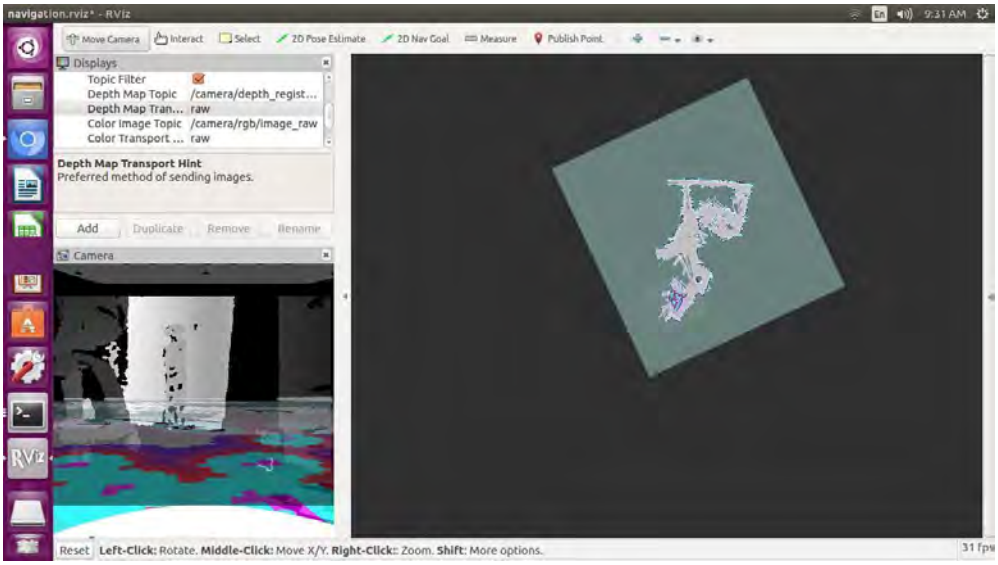

Figure 11.

Gmapping Map Sample 2

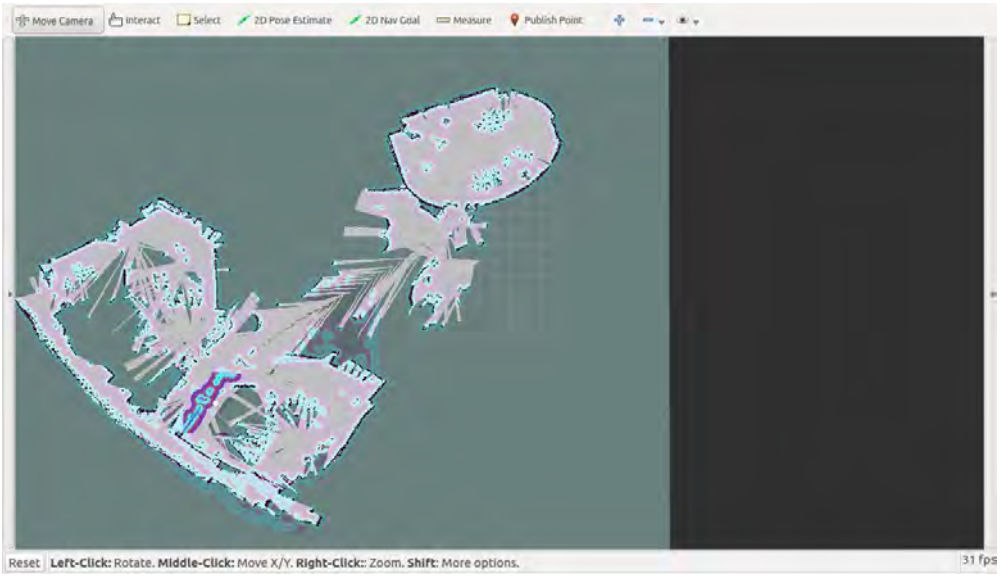

Figure 12.

Hector Slam Sample 1

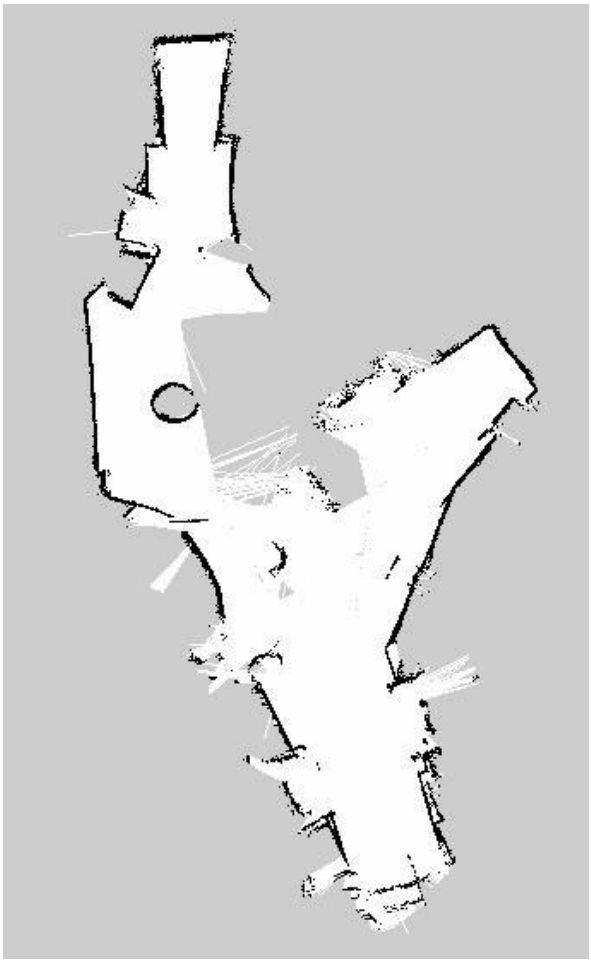

Figure 13.

Hector Slam Sample 2

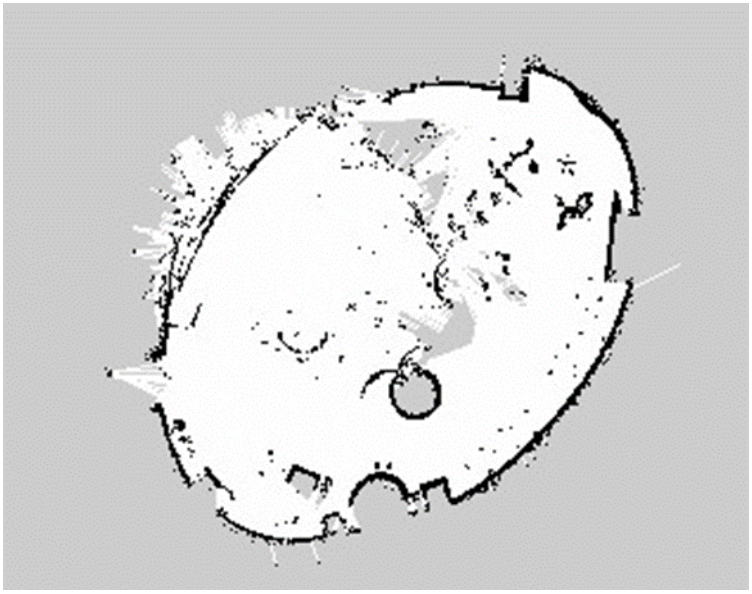

Figure 14.

Cartographer Sample 1

Figure 15.

Cartographer Sample 2

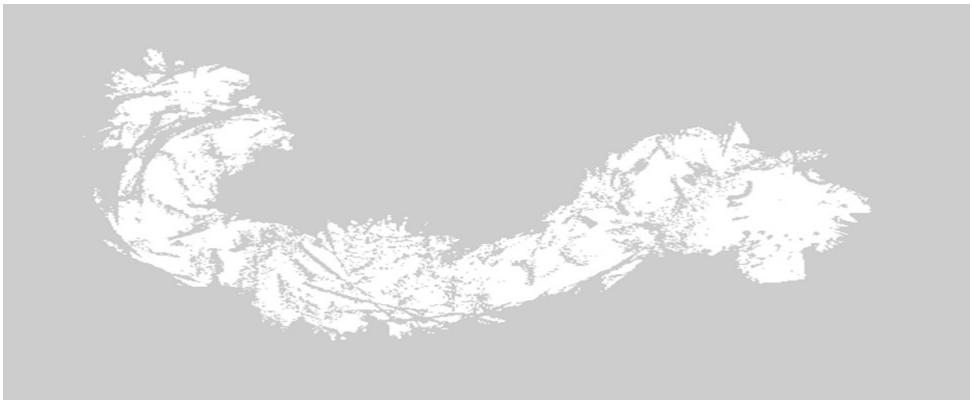

As seen in the results, it is possible to use Jetson TX2 in smart systems and to apply it to various platforms to turn them into smart systems. The unique features offered by the Jetson TX2 show that it has the potential for application in many areas, from autonomous vehicles to smart security systems. The integration of various sensors such as Kinect and other components allows robots to move more accurately and effectively.

In this context, further research into the use of the Jetson TX2 in smart systems could unlock the full potential of this platform. Furthermore, increasing community support and reducing cost could encourage wider adoption of the Jetson TX2 by a wider user base.

References

Biddulph, A., Houliston, T., Mendes, A., & Chalup, S. (2018). Comparing computing platforms for deep learning on a humanoid robot.

Carvalho, A., O' Mahony, N., Krpalkova, L., Campbell, S., Walsh, J., & Doody, P. (2019). At the edge of Industry 4.0. *Procedia Computer Science, 155*, 276-281.

https://doi.org/10.1016/j.procs.2019.08.039

Ciocirlan, C., Popa, V., Radu, S., Stoica, P., & Voicu, R. (2023). Autonomous mobile navigation robots in unknown environments using the HQ stereo cameras and the RPLIDAR sensors to increase the recognition accuracy. Retrieved from https://dblp.org/rec/conf/cscs/CiocirlanPVRSPV23

Fares, B., Souifi, H., Ghribi, M., & Bouslimani, Y. (2021). Omnidirectional platform for autonomous mobile industrial robot. In *2021 IEEE 3rd Eurasia Conference on IOT, Communication and Engineering (ECICE)* (pp. 633-638). Yunlin, Taiwan. https://doi.org/10.1109/ECICE52819.2021.9645621

Kaya, M. T. (2020). SLAM usage for autonomous robot movements in unstructured environments (Master's thesis). Konya Food and Agriculture University, Konya.

Laksono, & Kusuma. (2022). Performance analysis of HECTOR SLAM and GMAPPING for navigation for mobile robot navigation. *Jurnal Ilmiah Teknologi dan Rekayasa, 27*(2). https://doi.org/10.35760/en.2022.v27i2.6063

Liu, Y., Zhu, H., Zhang, B., & Su, Y. (2020). Real-time segmentation of sparse 3d point clouds on a tx2. *DEStech Transactions on Computer Science and Engineering, (cisnr)*. Retrieved from https://doi.org/10.12783/dtcse/cisnr2020/35171

Ozsoy, A. (2020). Comprehensive performance comparison of dedicated and embedded GPU systems. Retrieved from https://scite.ai/reports/10.24012/dumf.742732

Reddy, B. R., & Kumar, R. (2021). ROS based 3D mapping of an indoor environment using fusion of Orbbec Astra camera and Lidar on Turtlebot mobile robot. Retrieved from https://doi.org/10.1109/ICEECCOT52851.2021.9708058

Skoczen, A., Osinski, K., Nowakowski, K., Przybyl, A., & Przybyl, K. (2021). Obstacle detection system for agricultural mobile robot application using RGB-D cameras. Retrieved from https://dblp.org/rec/journals/sensors/SkoczenOSNKPP21

Wang et al. (2016). A loop closure improvement method of Gmapping for low cost and resolution laser scanner. *IFAC-PapersOnLine*. https://doi.org/10.1016/j.ifacol.2016.07.569

Zhang, Y., & Zhang, L. (2019). Vanishing point detection in corridor for autonomous mobile robots using monocular low-resolution fisheye vision.

About the Authors

Mehmet Tugrul KAYA has been working as the coordinator of the City Technologies Center established within Konya Metropolitan Municipality since 2015.

E-mail: mehmettugrulkaya@gmail.com, ORCID: 0009-0005-8713-3539

Burak YILMAZ is an Assistant Professor at Konya Technical University, Department of Software Engineering.

E-mail: byilmaz@ktun.edu.tr ,ORCID: 0000-0001-5549-8385

Similarity Index

The similarity index obtained from the plagiarism software for this book chapter is 18%.

CHAPTER 11

Sleep Staging and Automatic Sleep Staging Systems

Mehmet DURSUN
Necmettin Erbakan University, Türkiye

Tarık UNLER
Necmettin Erbakan University, Türkiye

To Cite This Chapter:
Dursun, M, Unler, T. (2023). Sleep Staging and Automatic Sleep Staging Systems..In S. Kocer. & O. Dundar (Eds.), *Artificial Intelligence Applications in Intelligent Systems* (pp. 183–193). ISRES Publishing.

Introduction

Sleep is an indispensable part of the vital cycle of human beings, which constitutes a very important place. Approximately one third of our life is spent in sleep. For this reason, sleep has been a very popular field of study for researchers. Important studies have been carried out for centuries to unravel the secret of sleep. Despite this, sleep still has mysteries waiting to be discovered.

Just like eating, drinking and breathing, we need sleep to continue our lives. When we do not get a quality sleep or do not sleep at all, unwanted effects begin to appear in our body. These changes can sometimes cause temporary effects such as drowsiness during the day, lack of attention and concentration, stress, irritable attitude, anxiety, and if it becomes chronic, it can cause weakening of the immune system, high blood pressure, heart attack, depression, obesity risk and loss of labour force (Ağargün et. al.1995). In fact, contrary to popular belief, sleep is far from the definition of a completely inactive, uncommunicative state of almost death.

From the moment we close our eyes and start to fall asleep, brain waves begin to slow down, this process brings along the secretion of a hormone called melatonin, which is secreted throughout the night and controls our sleep patterns. In addition, growth hormone is also secreted during sleep during the deep sleep period. In summary, sleep is actually a phenomenon with different processes within itself.

With an adequate and quality sleep, we can provide maximum efficiency during the day. We can focus on the work we have done and have a more peaceful and comfortable day. Otherwise, we may face a process that negatively affects our daily life. Although this situation is sometimes experienced temporarily, it can sometimes become chronic. Here is where our sleep patterns need to be clinically investigated.

Sleep disorders are based on the principle that the patient usually stays overnight in sleep laboratories, where physiological signals are taken and recorded from the body with the help of a number of electrodes and transducers during sleep. The recording is then evaluated by a sleep specialist. This evaluation process is called scoring. Scoring is done by scoring both physiological signals and respiratory data.

Investigating Sleep

Polysomnography is the most basic and accepted method in the study of sleep (Spriggs, 2014). Polysomnography is defined as simultaneous real-time recording of neurophysiological, cardiorespiratory and physiological parameters during sleep (Köktürk,1999).

Standard polysomnography parameters are given in Table 1 below. Sleep is analysed by dividing the recordings of these parameters into 30-second segments. Sometimes only one of these parameters provides the necessary information for the estimation of a stage, while sometimes several parameters should support each other.

Table 1.

Standard Polysomnography Parameters

Standard Polysomnography Parameters
1. Electroencephalography (EEG)
2. Electrooculography (EOG)
3. Electromyography (EMG-submentalis)
4. Oronasal airflow
5. Thoracoabdominal movements
6. Oxygen saturation
7. Electrocardiography (ECG)
8. Electromyography (EMG-tibialis.)
9. Body position

A research team including Rechtschaffen and Kales (R&K) first published the terminology and technical scoring manual of sleep stages in 1968. According to this scoring manual, sleep is divided into two main sections as Rapid eye movement sleep (REM) and Non Rapid eye movement sleep (NREM). NREM sleep is divided into four subcategories

as NREM Stage I, NREM Stage II, NREM Stage III and NREM Stage IV (Kales & Rechtschaffen, 1968).

In a more comprehensive study prepared in 2007 by a team headed by Dr Iber Conrad of the American Academy of Sleep Medicine (AASM), new rules for scoring sleep were developed and published as a manual (İber et. al., 2007). In the following period, the second version of the previously prepared manual was published in 2012 by a working group under the chairmanship of Dr Richard B. Berry, who was also appointed by the AASM. Today, sleep is scored within these guidelines. As the most striking innovations of this report, NREM Stage III and NREM Stage IV sleep sections were combined and defined as NREM Stage III and NREM Stage IV was removed from sleep terminology (Berry et. al.,2012).

Sleep Stages

Stage W (wakefulness phase)

Wake (W) stage (Figure 1) is defined as the period between the drowsiness period when people are about to fall asleep from the fully active state. In this stage, low amplitude beta activity is usually observed in the EEG when the eyes are open and alpha activity is observed when the eyes are closed. High frequency muscle artefacts can be seen on EEG. Rapid eye movements and vertical blinking movements in the range of 0.5 - 2 Hz are observed, these movements decrease with falling asleep and slow eye movements begin to be seen. If the eyes are open during this period, reading eye movements can also be seen. Jaw EMG is variable compared to other stages of sleep and generally has high amplitude. If the alpha rhythm taken from the occipital region is present in more than 50% of the epoch, the relevant epoch is scored as W stage (Köktürk, 2013) Figure 1 shows an epoch scored as W stage.

Figure 1

Wake Stage (Software SS, 2018)

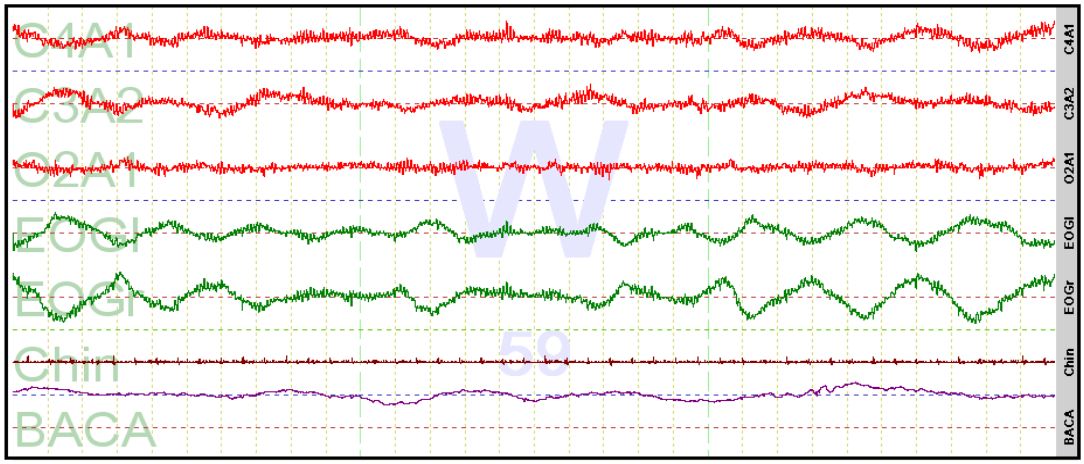

NREM Stage I

NREM Stage I (Figure 2), which is the process in which sleep starts first, corresponds to 2% to 5% of the total sleep time. When a person is stimulated and awakened by a stimulus at this time of sleep, he/she will generally not accept that he/she is asleep, although he/she is not aware of the events around him/her.

In order for a stage to be scored as NREM Stage I, if there is an alpha rhythm in the epoch, it is checked for the presence of a low amplitude and mixed frequency activity instead of this rhythm in more than 50% of the epoch. If there is no alpha rhythm, there should be slow eye movements defined as conjugated, regular sinusoidal eye movements that start with a deviation of at least 0.5 s, in which the basal frequency slows down in the range of 4-7 Hz, waves known as vertebral sharp waves with a maximum sharp tip of 0.5 s are seen. NREM Stage I scoring ends with the appearance of the elements that determine the next stage (Köktürk, 2013). Figure 2 shows an epoch scored as NREM I Stage.

Figure 2

NREM Stage I (Software SS, 2018)

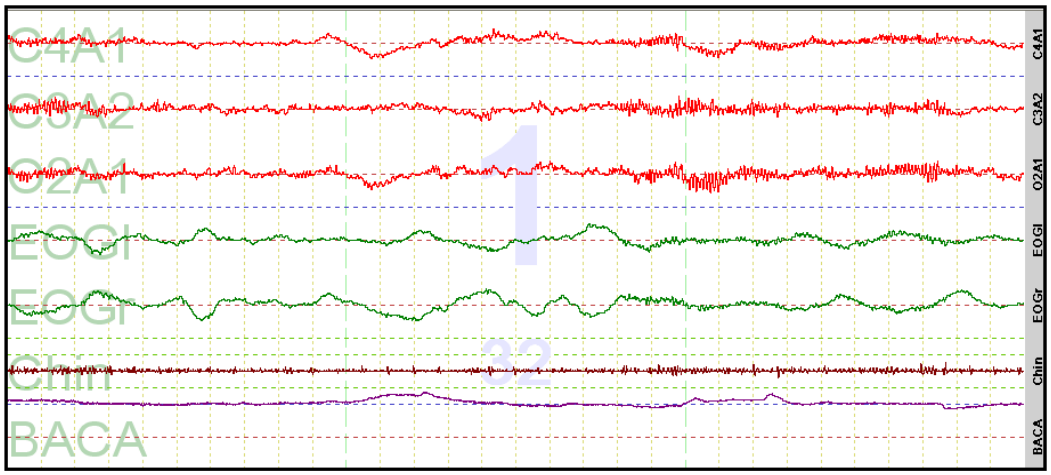

NREM Stage II

Approximately 45-55% of the total duration of sleep is covered by NREM Stage II (Figure 3). A person in this stage of sleep remembers that he/she is asleep when awakened. In order for a stage to be scored as NREM Stage II, there must be a K complex or sleep spindles without partial wakefulness either in the first half of the epoch analysed or in the second half of the previous epoch. The K complex is a prominent negative wave longer than 0.5 s followed by a positive signal pattern. If there is a K complex accompanied by partial wakefulness for approximately one second, the epoch continues to be scored as NREM Stage I. Sleep spindle is defined as 12-14 Hz high frequency activity lasting longer than 0.5 s. In this stage, eye movements are absent in EOG. Although the amplitude of EMG may vary, it is generally lower than the amplitude in the W stage (Köktürk, 2013).

Figure 3.

NREM Stage II (Software SS, 2018)

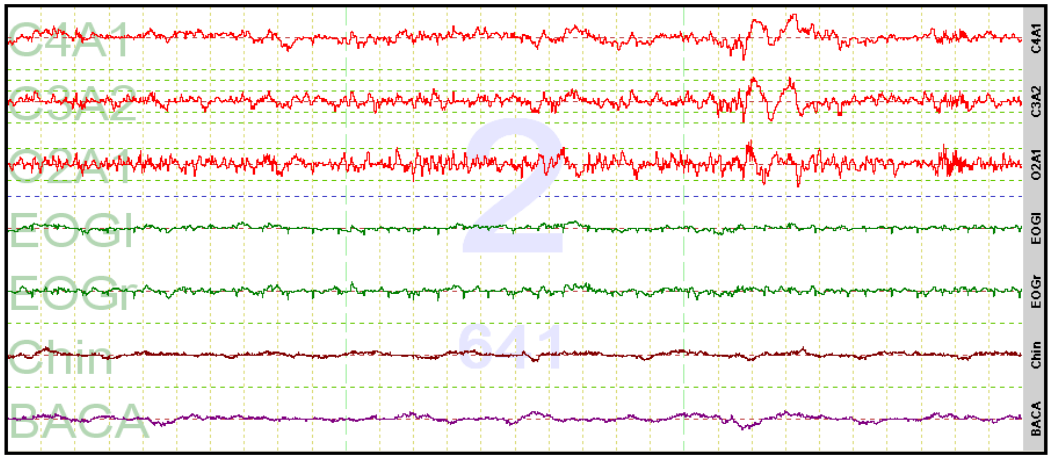

NREM Stage III

Slow wave EEG signals are observed in NREM Stage III. The frequency range is between 0.3 and 0.5 Hz and these signals are called Delta waves. The amplitudes of Delta signals from the frontal region are greater than 75 µV. NREM Phase III, which is known as the deepest part of sleep, is the period that has a restful and healing feature for the whole body. It includes 20 to 25 per cent of all night sleep and growth hormone is secreted especially during this period in children.

If more than 20% of an episode has slow wave activity, i.e. delta signals, that stage is directly scored as NREM Stage III. In this stage, sleep spindles can be seen, there is no typical eye movement and EMG amplitude varies (Köktürk, 2013). Figure 4 shows an epoch scored as NREM III stage.

Figure 4

NREM Stage III (Software SS, 2018)

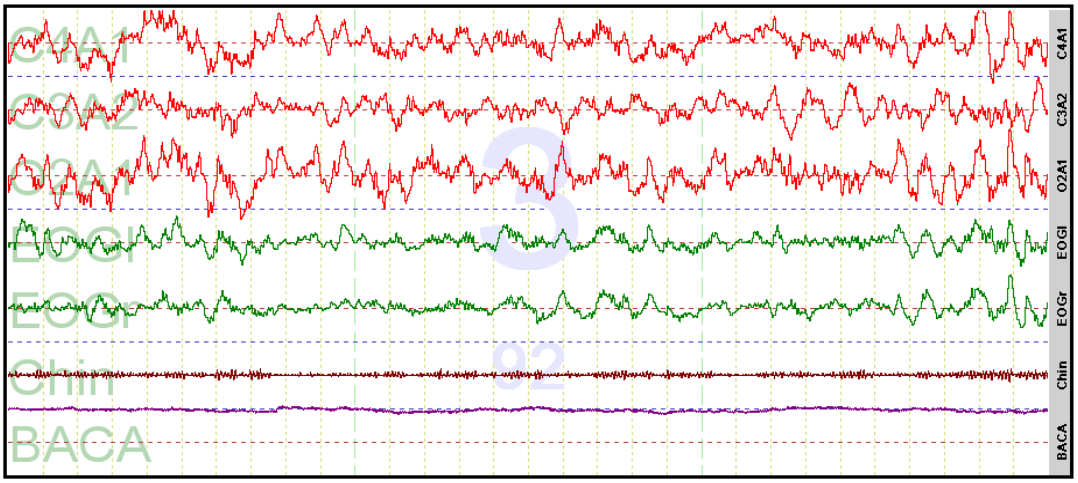

REM Stage

The REM Stage covers %20 to %25 per cent of all night sleep. A fast activity with low amplitude is observed in EEG. It is known that 80% of the dreams that appear during the night are in this part and that the dreams seen can be remembered after sleep because of the permanent memory record. The REM Stage is a stage that occurs in periods of 5 to 30 minutes in periods of 90 minutes on average. It is a stage interspersed in sleep. Studies on the measurement of blood flow in the brain during this stage indicate that blood flow and the amount of oxygenation of the brain increase similar to wakefulness. However, heartbeat and respiration become irregular in this phase. Irregular muscle movements occur, especially in the eyes. In general, there is a decrease in muscle tone in the body. The REM period is the closest period of sleep to wakefulness. Against all kinds of stimuli in the environment, even sadness and fear in a dream seen during this period can cause us to wake up.

While scoring this stage, the presence of EEG signals, also known as sawtooth waves, which are wavy and sharp-edged triangular waves with a frequency range of 2 to 6 Hz, received over the central region is the most important criterion for scoring the stage as REM. In Figure 5, sawtooth waves are clearly seen in C4A1 and C3A2 channels. In addition, the jaw EMG tone is low in this stage and the presence of eye movements that form reciprocal and sharp peaks manifested by a 0.5 s deflection is decisive in scoring this stage (Köktürk, 2013).

Figure 5.

REM Stage (Software SS, 2018)

The development of Wake, NREM Stage I, NREM Stage II, NREM Stage III and REM periods during an average of 9 hours of sleep is shown in Figure 6.

Figure 6.

Sleep processes of an adult individual throughout the night (Berry et. al. 2017)

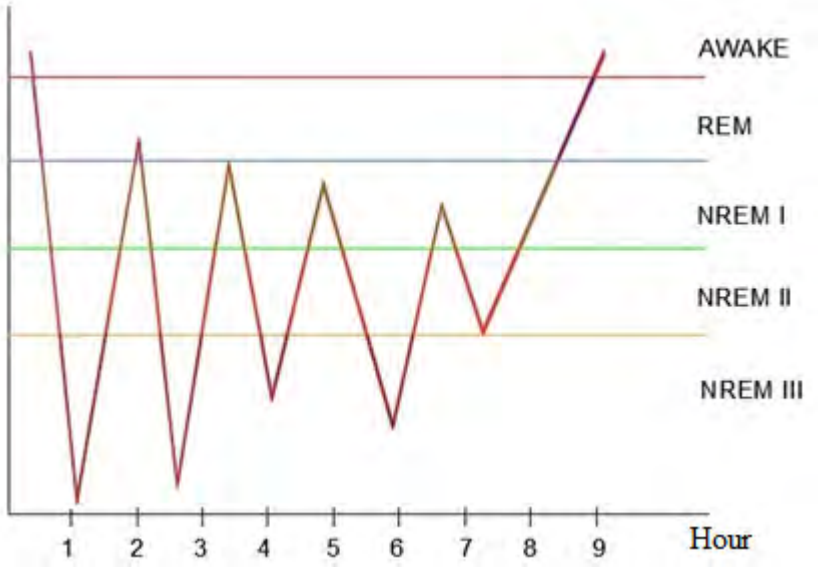

This process, which first starts with wakefulness, takes a fast path towards deepening of sleep. Considering a sleep period of one hour in general, deepening takes place in a very short time. After falling asleep, the deepest sleep process, NREM Stage III, is observed in an average of 50-70 minutes. After this first sleep depth is seen, the sleep depth decreases and the first REM period is reached. The first REM period is a short period of 5-15 minutes and if there is no awakening afterwards, sleep starts to deepen again. This cycle is repeated 4-6 times in periods of 80-100 minutes during sleep. These processes may vary according to age (Berry et. al. 2017).

The parameters of the data obtained from the patient who stayed in the hospital overnight are given in Table 1. The data recorded in the following process are analysed by specialist physicians. However, this analysis, called scoring, is both a time-consuming and laborious process. In addition, if the same data are scored by different specialists, different evaluations may ocur (Danker-Hopfe et. al.,2004). These can be counted among the disadvantages of manual scoring procedures. With the technological developments, researchers have started to carry out studies on the feasibility of performing the procedures performed by specialist physicians in the field of health by computers. These studies aim to diagnose the patient with the support of artificial intelligence by using signal processing and image processing algorithms of physiological signals and images, and to plan treatment accordingly.

Automatic Sleep Staging Systems

Automatic sleep staging systems have started to be developed in order to provide faster and safer sleep staging procedures. When these studies are analysed in detail, it is seen that sleep EEG signals are generally used as a data set. EEG signals are very sensitive

signals in terms of frequency and amplitude. These signals can be easily exposed to interference from the body surface or external disturbances. Even the movement of the patient's eyes while receiving data from the patient can cause distortion of these signals. Considering this situation, EEG signals have been purified from artefacts by using some digital filters. Even special algorithms have been developed for these processes (Dursun et. al 2017;Dursun et.al,2019). Feature extraction is then performed from the clean signals obtained. Commonly, time domain features, frequency domain features, spectral features and nonlinear features are extracted.

The artificial intelligence trained with these extracted features is used in the classification of sleep EEG data, that is, in the scoring of sleep. It is very important that the system produces accurate results in order to be an auxiliary tool in the clinic for scoring work or a system used directly for scoring. For this reason, some unnecessary features are removed or other features are added to improve the classification accuracy.

Various classification methods such as Artificial Neural Network (ANN), Support Vector Machine (SVM), K-Means Clustering, Ensemble Classification and Bootstrap Aggregating are preferred in automatic sleep staging systems, which have a role in assisting sleep specialists in diagnosis. However, the findings of the studies show that standard machine learning techniques are weak in classifying with high precision and accuracy when processing high-dimensional data such as polysomnography (Faust et. al. 2019).

Deep learning models are more successful in working with high dimensional data. For example, one of the most important advantages is that they allow the training of polysomnography records without feature reduction. Deep learning techniques have the ability to learn features that are useful in feature selection and neglect features that are not useful. Systems designed with deep learning techniques utilise all available information, automatically extract features from the signals themselves and provide training to interpret the data on their own (Faust et. al. 2018).

Studies show that deep learning techniques give better results than traditional machine learning techniques when working with high-dimensional signals such as polysomnography. Therefore, we can say that deep learning techniques are the most advanced methods that can provide high classification accuracy for automatic sleep staging systems.

The most widely used deep learning techniques are Convolutional Neural Network (CNN), Recurrent Neural Network (RNN) and Long Short-Term Memory (LSTM), Autoencoders (AEs) and Hybrid Models. (Yıldırım, 2022) Among these, the recently popular and widely used technique for automatic sleep staging systems is CNN. CCNs are very successful in feature extraction (Ucar & Kocer, 2022). Figure 7 shows a block

diagram of an automatic sleep staging system developed using deep learning techniques. Here, polysomnography signals are subjected to a data preprocessing and then divided into two parts: training and testing. The training part is used to train the system, the validation part is used to fine-tune the model and the test part is used to measure the system performance. As a result, the system classifies sleep stages into five stages as Wake, NREM Stage I, NREM Stage II, NREM Stage III and REM (Loh et. al. 2020).

Figure 7.

Automated sleep stage classification block diagram (Loh et. al. 2020)

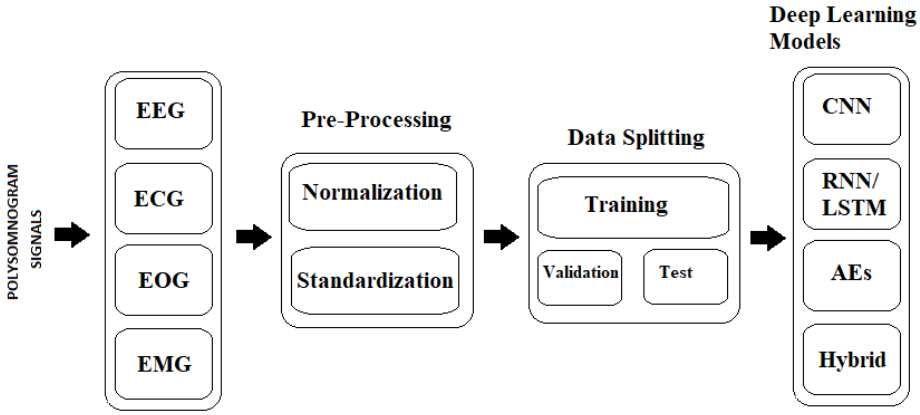

Deficiencies of Developed Automatic Sleep Staging Systems

Different signal groups have been used in automatic sleep staging systems. While many studies have used only EEG data, some have used EOG, ECG and EMG data together with EEG data for training purposes. Some studies use only ECG, EOG-EMG, EMG data as test data without using EEG and perform automatic sleep staging with these data. However, all polysomnography signals are used in an integrated manner by sleep specialists during sleep staging. Sometimes a single channel may be sufficient for scoring a sleep stage, while sometimes two, three or even four channels of physiological data can be evaluated simultaneously to score the episode correctly. Sometimes the stage of an episode can be scored with the support of different channels.

In addition, the criteria, patterns and features sought in the signals for the detection of sleep stages may sometimes not be found in the epoch being evaluated. In this case, the expert returns to the previous epoch or the next epoch and evaluates the relevant epoch. For example, this situation has not been brought up before in the proposed automatic sleep staging systems. Since the deficiencies listed here have the effect of decreasing the classification accuracy of automatic sleep staging systems, they cannot be used in the clinic.

References

Berry RB, Brooks R, Gamaldo CE, Harding SM, Marcus CL and Vaughn BV, (2012), For the American Academy of Sleep Medicine. The AASM Manual for the Scoring of Sleep and Associated Events: Rules, Terminology and Technical Specifications, Version 2.0. www.aasmnet.org, Darien, Illinois: American Academy of Sleep Medicine.

Berry RB, Brooks R, Gamaldo CE, Harding SM, Lloyd RM, Quan SF, Troester MM, Vaughn BV, (2017), The AASM Manual for the Scoring of Sleep and Associated Events Rules, Terminology and Technical Specifications VERSION 2.4. Medicine AAoS. Darien USA.

Dursun M., Özşen S., Yücelbaş C., et al. (2017), A new approach to eliminating EOG artifacts from the sleep EEG signals for the automatic sleep stage classification. Neural Comput & Applic 28, 3095-3112. https://doi.org/10.1007/s00521-016-2578-z.

Dursun M., Özşen S., Güneş S., Akdemir B., Yosunkaya Ş., (2019), Automated elimination of EOG artifacts in sleep EEG using regression method, Turkish Journal of Electrical Engineering and Computer Sciences: Vol. 27: No. 2, Article 31. https://doi.org/10.3906/elk-1809-180.

Faust, O.; Razaghi, H.; Barika, R.; Ciaccio, E.J.; Acharya, U.R., (2019), A review of automated sleep stage scoring based on physiological signals for the new millennia. Comput. Methods Programmes Biomed. 2019, 176, 81-91.

Faust, O.; Hagiwara, Y.; Hong, T.J.; Lih, O.S.; Acharya, U.R., (2018), Deep learning for healthcare applications based on physiological signals: A review. Comput. Methods Programmes Biomed., 161, 1-13.

H. Danker-Hopfe, D. Kunz, G. Gruber, G. Klösch, J.L. Lorenzo, S.-L. Himanen, B. Kemp, T. Penzel, J. Röschke, H. (2004), Dorn Interrater reliability between scorers from eight european sleep laboratories in subjects with different sleep disorders J. Sleep Res., 13 (1), pp. 63-69.

Iber C, Ancoli-Israel S, Chesson A, Quan SF, (2007), The AASM Manual for the Scoring of Sleep and associated Events. Rules Terminology and Technical Specifications. 1st Ed. Westchester, Illinois: American Academy of Sleep Medicine.

Kales A., Rechtschaffen A., (1968), A manual of standardised terminology, techniques and scoring system for sleep stages of human subjects. 204, United States, Bethesda, Md., U. S. National Institute of Neurological Diseases and Blindness, Neurological Information Network.

Köktürk O., (1999), Uykunun izlenmesi (1). Normal uyku. Tüberküloz ve Toraks, 47: 372-80.

Köktürk O., (2013), Uyku Kayıtlarının Skorlanması, Türkiye Solunum Araştırmaları Derneği (TÜSAD), 14-29).

Loh, H.W.; Ooi, C.P.; Vicnesh, J.; Oh, S.L.; Faust, O.; Gertych, A.; Acharya, U.R., (2020) Automated Detection of Sleep Stages Using Deep Learning Techniques: A Systematic Review of the Last Decade (2010-2020). Appl. Sci. 2020, 10, 8963. https://doi.org/10.3390/app10248963.

Software SS, (2018). Somno-Star Polisomnografi Cihazi Arayüzü.

Spriggs, W.H., (2014) Essentials of Polysomnography; Jones & Bartlett Learning: Burlington, MA, USA.

Ucar K, Kocer H. E. (2022). Robotic Vision with Deep Learning. In S. Kocer & O. Dundar (Eds .), Current Studies in Basic Sciences Engineering and Technology (pp. 1–11). ISRES Publishing

Yıldırım S. (2022). Natural Language Processing Applications in Engineering. In S. Kocer & O. Dundar (Eds .), Current Studies in Basic Sciences Engineering and Technology (pp. 12–30). ISRES Publishing.

Yücel A., Ekrem A., Hayrettin K., Kürşad T., (1995), Necmettin Erbakan Üniversitesi Tıp Dergisi, cilt 11 sayı 2-3-4 sayfa 193-197.

About the Authors

Mehmet DURSUN, PhD, is an Assistant Professor of Aviation Electrical and Electronic at Necmettin Erbakan University in Konya, Türkiye. He holds a PhD in Electric-Electronic Engineering from Selçuk University. His main areas of interest are signal processing, image processing, electronics and fiber optics communication systems.

E-mail: mehmet.dursun@erbakan.edu.tr, ORCID: 0000-0002-0558-6309

Tarik UNLER, PhD, is an Assistant Professor of Aviation Electrical and Electronic at Necmettin Erbakan University in Konya, Türkiye. He holds a PhD in Electric-Electronic Engineering from Konya Technical University. His main areas of interest are embedded systems, autonomous systems, RADAR and aviation applications.

E-mail: tunler@erbakan.edu.tr, ORCID: 0000-0002-2658-1902

Similarity Index
The similarity index obtained from the plagiarism software for this book chapter is 16%.

CHAPTER 12

Deep Learning for Cloud Detection and Segmentation in Remote Sensing Images

Sabri KOCER
Necmettin Erbakan University, Türkiye

Yasin ER
Necmettin Erbakan University, Türkiye

To Cite This Chapter:
Dursun, M, Unler, T. (2023). Deep Learning for Cloud Detection and Segmentation in Remote Sensing Images..In S. Kocer. & O. Dundar (Eds.), *Artificial Intelligence Applications in Intelligent Systems* (pp. 194–210). ISRES Publishing.

Introduction

Numerous techniques for detecting clouds have been presented in recent years. The threshold-based and classification-based approaches can be used to generally categorize these techniques. The purpose of threshold-based techniques is to establish appropriate brightness temperature or spectral reflectance thresholds using certain channels so that various sensors can distinguish between cloud patches. The advances in pattern recognition, machine learning, and computer vision have led to several noteworthy breakthroughs in the field of picture classification (Tracewski et al., 2017). In recent years, there has been a constant advancement in classification-based cloud detection approaches to enhance the training process for more accurate cloud recognition. This is achieved by utilizing geometric, texture, or color information of the tagged pictures (R. Zhang et al., 2013) - (Q. Zhang & Xiao, 2014). To produce combination pictures with ten bands, the Landsat 8 sensor's visible, near-infrared (NIR), shortwave infrared (SWIR), and thermal infrared (TIR) bands are used. the multiscale features-convolution neural network (MF-CNN) is built by using each pixel of combination photos as the fundamental research unit.Convolutional neural networks, or CNNs (Sutskever et al., 2017), are excellent choices for segmentation, object identification, and picture classification.CNNs identify the most crucial characteristics on their own without the need for domain experts to explicitly generate or choose them.

All current cloud classification techniques, notwithstanding their benefits, employ the same methodology of treating each pixel separately during model training and then using the learned model. It is classified that a complete picture holistically by using a unique CNN architecture for image segmentation. Because repeated actions on neighbouring pixels are avoided, this fully utilizes the spatial information during model construction and for the effective assessment of the trained model. Multispectral geostationary satellite data covering the continuous nature of clouds in the environment is obtained using CNN architecture. This is a difficult process since multispectral data are made up of several channels, each with unique features that might vary across scenes due to the sun's daily cycle, temperature changes in the atmosphere, and other factors.

Applications of the different spectral bands of satellite sensors have been the main focus of remote sensing of cloud characteristics (Choi et al., n.d.). When compared to a clear sky, clouds are often cooler and more reflective in remote sensing applications. This results in a substantial reflection of solar radiation at the top of the atmosphere (TOA) (Ahmad & Quegan, 2012). Determining the significance of clouds in the climate system and retrieving surface and aerosol features need precise information about the physical and radiative properties of clouds, including cloud coverage (Bley & Deneke, 2013).

In August 2002, the Meteosat Second Generation (MSG) satellite was launched. When compared to the previous Meteosat radiometer, MSG's Spinning Enhanced Visible and Infrared Imager (SEVIRI)'s visible and infrared bands mark a major advancement (Schmetz et al., 2002). Compared to the Meteosat radiometer, which provides half-hourly sampling, MSG offers a greater temporal sample (quarterly). Besides its 3.9 μm channel, MSG's twelve spectral bands enable precise cloud cover analysis. Additionally, it can compute several products in cloud-free locations, including integrated water vapor content of the atmosphere, snow cover, and sea and land surface temperatures (Schmetz et al., 2002) - (Roebeling & van Meijgaard, 2009).

For the detection and classification of clouds using visible/infrared (VIS/IR) imaging, several different approaches have been put forth, and the majority of them rely on a combination of threshold tests applied to various spectral channels (Feijt et al., 2000; Reynolds & Haar, 1977), such as multispectral thresholding models (Derrien et al., 1993; Saunders & Kriebel, 1988) or simple intensity threshold analysis and IHS threshold technique (Roy et al., 2001; Sullivan et al., 1992) applied to individual pixels. The other models include dynamic cloud clustering based on histogram analysis (Desbois et al., 1982; Seze & Desbois, 1987) or spatial coherence approaches (Coakley Jr & Bretherton, 1982).

Scene classification with remote sensing, which has received a lot of interest, attempts to automatically classify visual scenes into appropriate groupings such as residential areas, agricultural land, woods, etc.(Li et al., 2021). In an effort to attain maximum accuracy,

deep learning (DL) application for the classification is a current growing trend.

As shown on Figure 1, the classification applications progress pixel to object level. The pixel size corresponding to the item of interest was caused by the comparatively poor spatial resolution of early remote sensing photographs (Janssen & Middelkoop, 1992). Consequently, pixel-level categorization was the basis for work on remote sensing classification (Janssen & Middelkoop, 1992; Tuia et al., 2009). Following this, the increase in spatial resolution refocused the study on object-level remote sensing classification, yielding better classification results than per-pixel analysis (Mukherjee & Acton, 2002). For decades, this method dominated the field of remote sensing classification (Blaschke, 2010). But the constant expansion of remote sensing pictures makes it easier to capture different classes of objects, thus conventional pixel-level and object-level approaches are insufficient for precise classification of images. Scene-level classification becomes essential in this situation in order to utilize the global contents of remote sensing products (Cheng et al., 2020).

Figure 1.

The classification applications progress pixel to object level

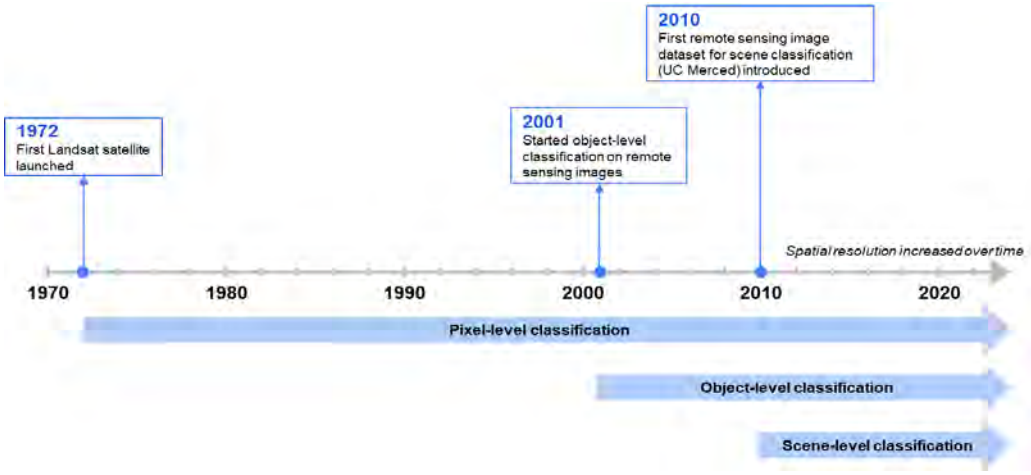

The weakness in low-level and mid-level approaches stated earlier have been addressed by DL models in recent years. To train discriminative features for efficient feature extraction, DL architectures employ a variety of methods, such as Generative Adversarial Networks (GANs), Vision Transformers (ViT), and Convolutional Neural Networks (CNNs) (Jogin et al., 2018; Scarpa et al., 2018). CNN architectures for remote sensing scene classification, such as Residual Network (ResNet) (M. Wang et al., 2019), AlexNet (Hu et al., 2015), GoogleNet (Q. Wang et al., 2022), etc., are often utilized.

Materials and Methods

Multiscale Features-Convolutional Neural Network (MF-CNN)

It is required to separate the 107 areas from several Landsat 8 satellite photos into a test set (63 pictures) and a training set (44 images). They have both cloud and noncloud areas in the majority of their photos. Small, medium, and big clouds compose cloud regions; the surface environment beneath them is made up of vegetation, water, snow, and urban and agricultural structures.

The training set's 63 band-combination photos are split up into 128x128 picture blocks. Using Landsat 8 imagery, 1236 training and 806 test sets are generated. The usefulness of the suggested technique is demonstrated by comparing two data sets that contain clear pixels that are readily confused with clouds, such as snow-covered surfaces and light buildings, with thin and thick clouds with varying cloud contents.

Figure 2.

Model structure of MF-CNN

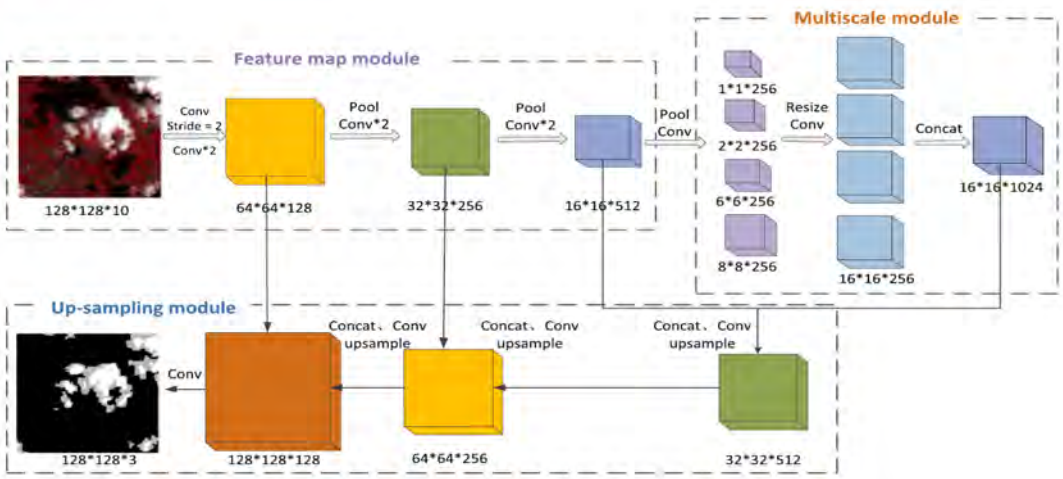

The combined picture block with a size of 128 128 10 is the initial layer in the feature map module and is treated as the input data. Two convolutional layers are indicated by the Conv*2

The Relu7 (16 x 16 × 512) output features are considered the input layer in the multiscale module. Varied widths of average pooling filter to acquire the multiscale global characteristics typical of thick and thin clouds in combination photos are used. In order to create four parallel feature maps that have the same height and width as Relu7, bilinear interpolation (represented by Bl#) and convolutional layers are used after each average pooling layer.

The up-sampling module jointly applies high-level semantic and low-level spatial

information to obtain improved identification accuracy of thick and thin clouds than the model using only high-level information. The multiscale module's Concat# layer is linked to the Relu7 feature layer (16 × 16 × 512). The up-sampling feature map (designated by Upsampling#) will grow by two times as a result of the bilinear interpolation.

Remote Sensing Image Scene Classification

Several methods have been investigated to enhance the feature extraction procedure for precise CNN-based remote sensing scene classification. They are separated into two groups: CNNs that were taught from scratch and CNNs that were pretrained.

Large-scale pre-trained datasets are commonly used to train pretrained CNNs, however these datasets are not easily customized to the unique features of the target dataset. Pretrained CNNs are complicated and need a lot of compatibility, making their modification difficult.

Figure 3.

The aerial picture dataset's features were extracted using a pre-trained CNN. The new CNN uses the weight parameters that were pretrained on the ImageNet dataset.

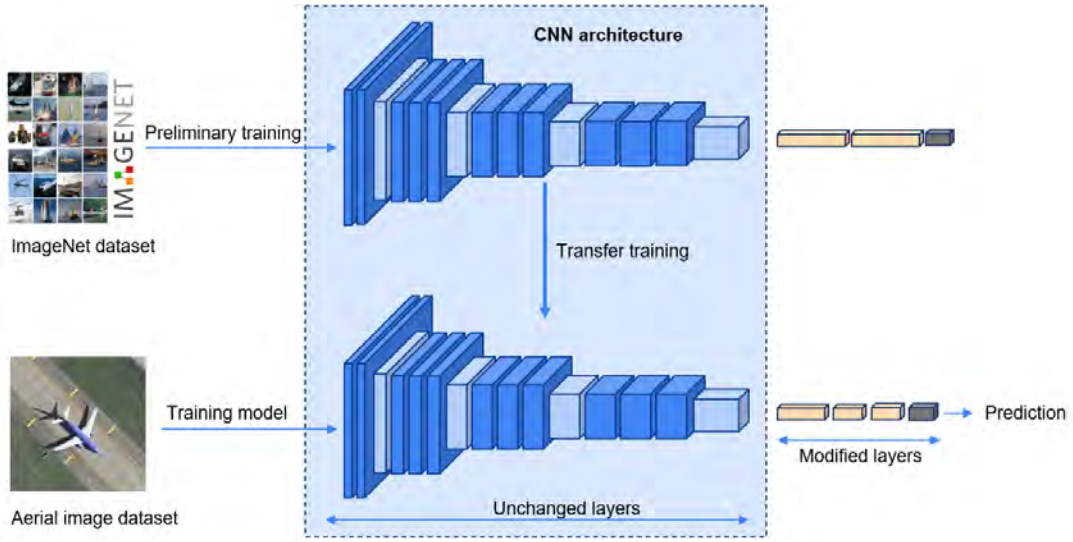

Vision Transformer-Based Scene Classification Methods (ViT) (Figure 4) divide an input picture into fixed-size patches, and then uses a technique called linear embedding to convert each patch into a continuous vector.

Remote sensing scene classification is efficiently accomplished by supervised learning techniques. Unlabelled data can be used by GAN (Mirza & Osindero, 2014) to extract relevant information. Figure 5 depicts the generator and discriminator models, which are the two main components of GAN. The generator tricks the discriminator by producing fake data that seems real. The discriminator is also trained the real data.

Figure 4.

A ViT Architecture

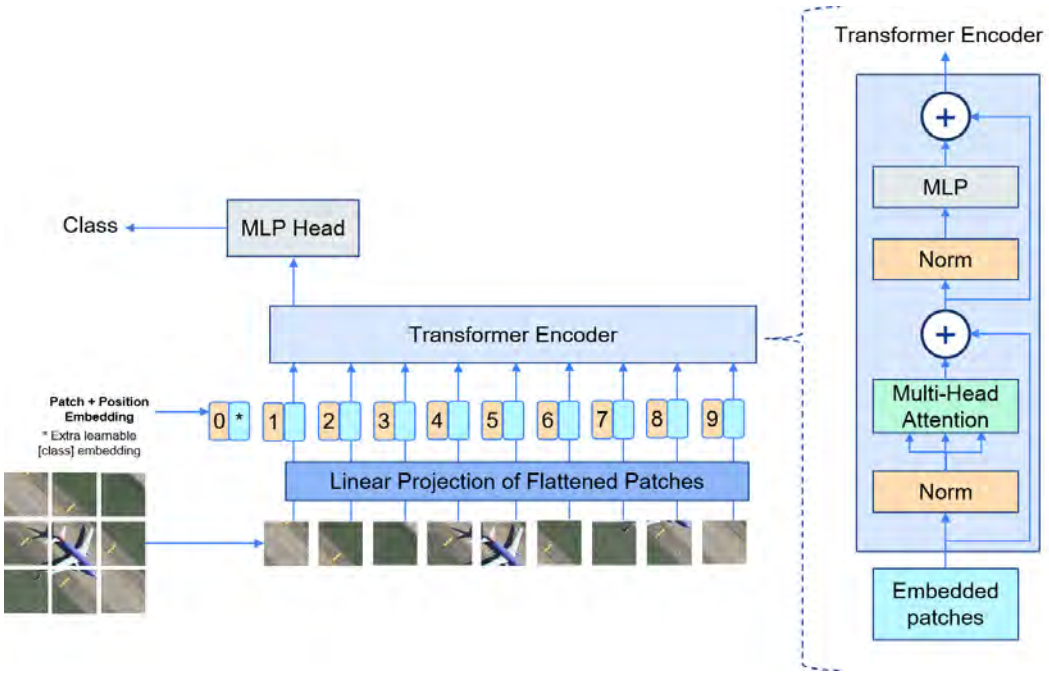

Figure 5.

A GAN Architecture

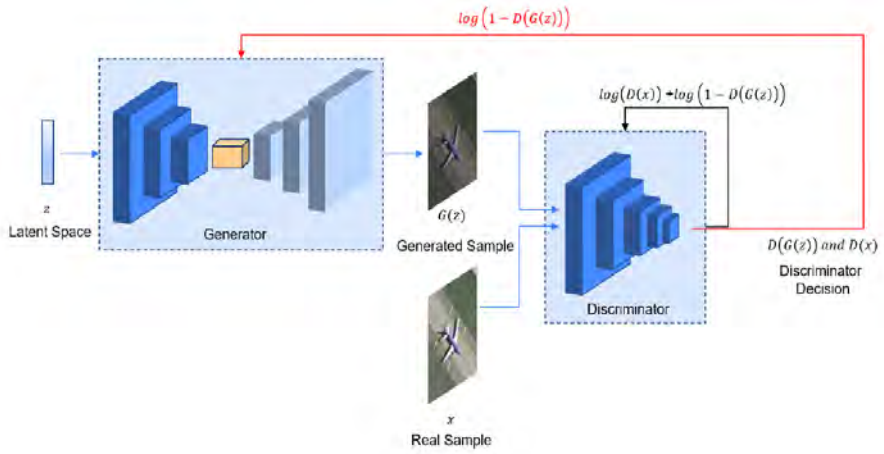

Cloud Segmentation Convolutional Neural Network (CS-CNN)

High-quality spatial classifications can be produced from multispectral remote sensing data using CS-CNN. Furthermore, in order to add spatial information, the CS-CNN simply uses the original data and does not require created features. The goal of CS-CNN is to extract cloud masks from multispectral remote sensing information. The architecture must consume multispectral satellite pictures and produce a segmentation in which each input scene pixel is categorised into a certain cloud class. CS-CNN doesn't require a pre-built architecture or trained model available for this task.

Table 1.

MSG SEVIRI Channels

Table 1. MSG SEVIRI channels.

Number	Channel *	Spectral Domain	Central Wavelength	Solar (Reflectance)	Remarks
1	VIS0.6	VIS	0.6 µm	yes	visualized as Blue
2	VIS0.8	VIS	0.8 µm	yes	visualized as Green
3	NIR1.6	SWIR	1.6 µm	yes	visualized as Red
4	IR3.9	MIR	3.9 µm	daytime	
5	WV6.2	MIR	6.2 µm	no	Water vapor absorption
6	WV7.3	MIR	7.3 µm	no	Water vapor absorption
7	IR8.7	TIR	8.7 µm	no	
8	IR9.7	TIR	9.7 µm	no	Ozone absorption
9	IR10.8	TIR	10.8 µm	no	
10	IR12.0	TIR	12.0 µm	no	
11	IR13.4	TIR	13.4 µm	no	

* Official channel/band names for SEVIRI given by EUMETSAT.

The MSG program's satellites offer full-disc views of a hemisphere that includes the Atlantic, Europe, and Africa. At the sub-satellite point (SSP) at 0~N, 0~E, each scan yields a raster image with a size of 3712 ~ 3712 pixels and a resolution of 3km ~ 3km. Its temporal resolution is 15 minutes, which is how long a complete scan with all necessary onboard processing takes. According to Table 1, the eleven primary SEVIRI channels are centred at wavelengths.

At night, the channels are dark and don't offer any information. During the day, water surfaces may reflect sunlight, creating the appearance of glare or sunglint. The parameters of Channel 4 vary in response to sun radiation. During the day, the solar irradiation reflection is more prominent than the infrared signal. Classification techniques frequently need an input raster containing the sun zenith angle for each pixel in order to address these effects (Figure 6).

Figure 6.

An overview over all SEVIRI channels

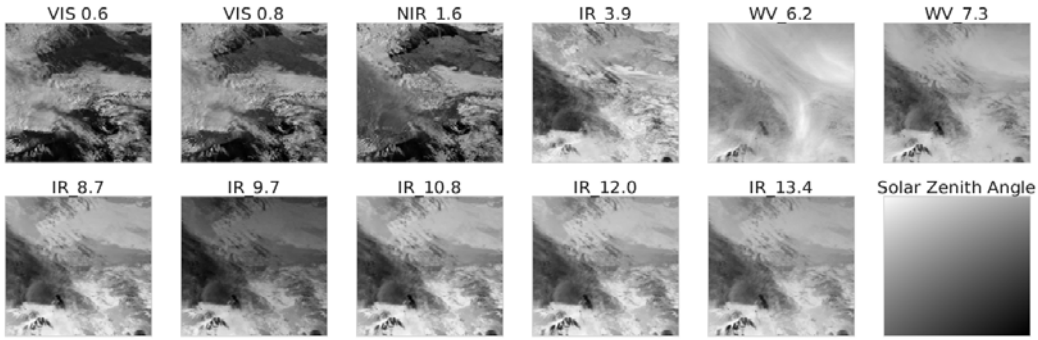

Its nearly symmetrical layout, which consists of a series of down-sampling layers followed by a second sequence of up-sampling layers, is similar to numerous previous CNN architectures for image segmentation (Noh et al., 2015).

Figure 7.

CS-CNN architecture

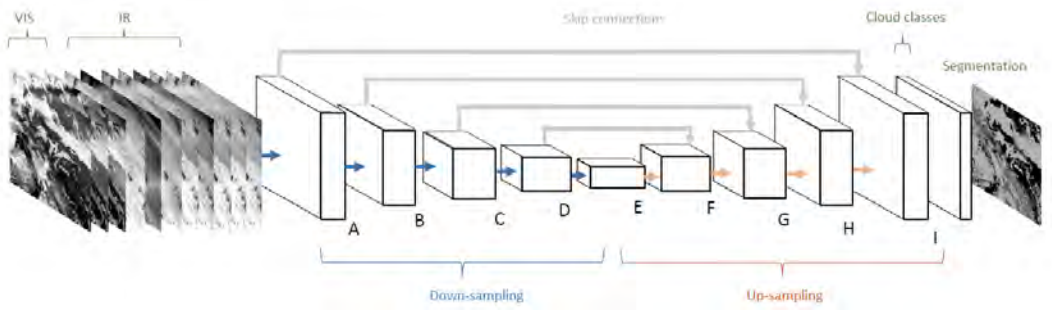

The input for the network is displayed on the left side of Figure 7. The size of the chosen study area is matched by the 508x508 pixel spatial coverage. The number of selected channels in each scene determines the input's depth. Next to the input layer is a series of learning blocks made up of several convolution layers. The labels (A–I) on each block in Table 2, which contains information on the convolution layer blocks and how they are connected. Figure 7's right side shows the computed cloud classes that return probabilities for each class for each pixel.

Table 2.

Architecture For Cloud Segmentation

Block	Layer Type	Output Size	Skip Connection
input	input	$\{7, 8, 11\} \times 508 \times 508$	
A	3×3 conv, relu	$32 \times 506 \times 506$	
A	3×3 conv, relu	$32 \times 504 \times 504$	I
A	3×3 conv, stride 2	$32 \times 252 \times 252$	
B	3×3 conv, relu	$64 \times 250 \times 250$	
B	3×3 conv, relu	$64 \times 248 \times 248$	H
B	3×3 conv, stride 2	$64 \times 124 \times 124$	
C	3×3 conv, relu	$128 \times 122 \times 122$	
C	3×3 conv, relu	$128 \times 120 \times 120$	G
C	3×3 conv, stride 2	$128 \times 60 \times 60$	
D	3×3 conv, relu	$256 \times 58 \times 58$	
D	3×3 conv, relu, dropout	$256 \times 56 \times 56$	F
D	3×3 conv, stride 2	$256 \times 28 \times 28$	
E	3×3 conv, relu	$512 \times 26 \times 26$	
E	3×3 conv, relu, dropout	$512 \times 24 \times 24$	
E	3×3 deconv, relu	$256 \times 48 \times 48$	
F	3×3 conv, relu	$256 \times 46 \times 46$	
F	3×3 conv, relu	$256 \times 44 \times 44$	
F	3×3 deconv, relu	$128 \times 88 \times 88$	
G	3×3 conv, relu	$128 \times 86 \times 86$	
G	3×3 conv, relu	$128 \times 84 \times 84$	
G	3×3 deconv, relu	$64 \times 168 \times 168$	
H	3×3 conv, relu	$64 \times 166 \times 166$	
H	3×3 conv, relu	$64 \times 164 \times 164$	
H	3×3 deconv, relu	$32 \times 328 \times 328$	
I	3×3 conv, relu	$32 \times 326 \times 326$	
I	3×3 conv, relu	$32 \times 324 \times 324$	
output	3×3 deconv, relu	$5 \times 324 \times 324$	

In CS-CNN, each block is composed of two layers that execute convolutions of 3x3 pixels using rectified linear units (ReLUs) as activation functions. Dropout avoids over-fitting in Blocks D and E. In Blocks A–D, downsampling is the final procedure. Auxiliary data including terrain elevation, the satellite viewing angle, and manually created geo-statistical texture features are frequently used in RF approaches (Egli et al., 2018). These comprise both geo-statistical texture features and integrated channels (differences). The geographic structure of the SEVIRI data is shown by these geo-statistical features.

The cloud masks for CS-CNN (left) and RF (right) are displayed in Figure 8. The four classes-snow/ice, cloud-filled, cloud-contaminated, and cloud-free are shown graphically. A new coloration is applied to pixels where the model's class is.

Figure 8.

CS-CNN and Random Forest Classification

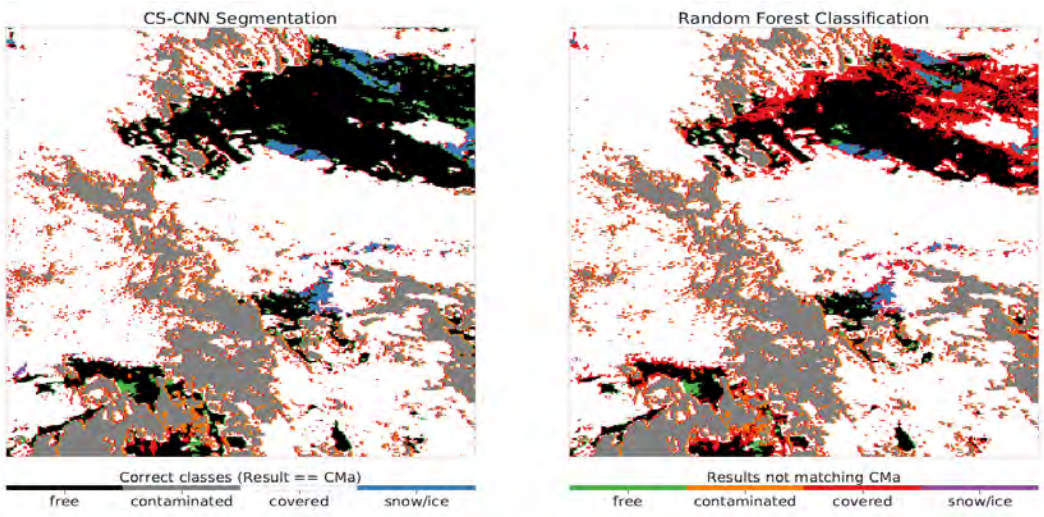

Table 3 a, b shows that the RF archives a skill of 0.885 and the CS-CNN's total skill is 0.905.

Table 3.

Statistics For The Scene

(a) CS-CNN Scenario

Class	Accuracy	HSS	POD	FAR	POFD	Bias
Combined	0.942	0.905				
1: cloud-free	0.961	0.920	0.957	0.047	0.036	1.004
2: cloud-cont.	0.973	0.885	0.886	0.082	0.013	0.968
3: cloud-fill	0.950	0.898	0.946	0.060	0.047	1.006
4: snow/ice	0.999	0.824	0.788	0.124	0.0002	0.913

(b) RF Scenario

Class	Accuracy	HSS	POD	FAR	POFD	Bias
Combined	0.931	0.885				
1: cloud-free	0.937	0.865	0.928	0.083	0.062	1.012
2: cloud-cont.	0.984	0.934	0.928	0.039	0.006	0.967
3: cloud-fill	0.942	0.882	0.934	0.064	0.052	0.998
4: snow/ice	0.999	0.668	0.631	0.256	0.0004	0.888

Cloud classification and multispectral remote sensing data processing are two areas. When it comes to expert knowledge and effort, CS-CNN takes substantially less than a random forest technique, which is a commonly utilized method. The outputs of CS-CNN are far more robust, produced faster, and exhibit superior accuracy when compared to the random forest technique.

Multiscale Features-Convolutional Neural Network (MF-CNN)

By combining high-level semantic information with low-level spatial information, the MF-CNN model has been able to learn the multiscale global properties of different types of clouds, both thick and thin. In the test step, the combination photos are classified as thin, thick, or no-cloud regions using the trained model. Low-level spatial information with multiple scales is abandoned and the multiscale module is swapped out for a traditional convolutional layer in order to assess the efficacy of the MF-CNN model. The MF-CNN-based structure is known as a self-contrast model since it lacks multiscale feature information. Additionally, the FCNN model described in (Zhan et al., 2017) acquires image features by means of several convolutional and pooling layers. Subsequently, distinct feature layers are directly up-sampled to the same size as the original input image, and the concatenated features are ultimately applied to differentiate between snow and clouds using a softmax classifier.

Figure 9.

Original combination image with NIR, red, green band and Cloud detection result of MF-CNN method.

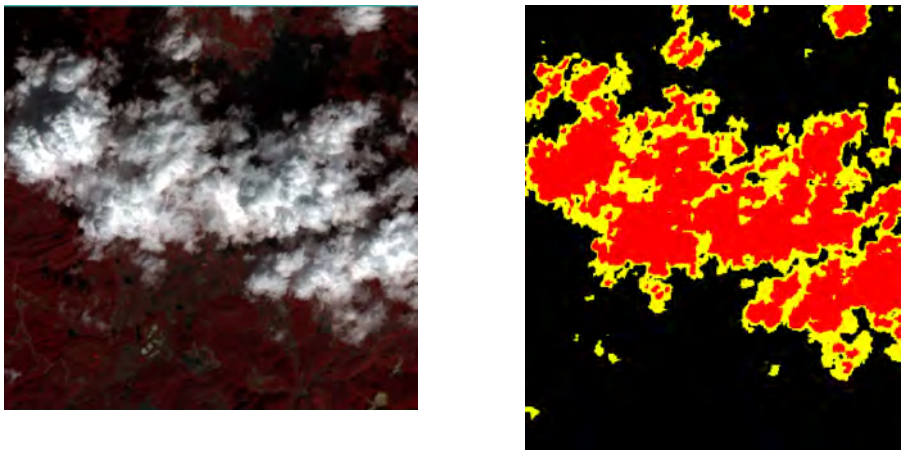

Figure 10.

Distribution of cloud detection accuracy in test data set Comparison of MF-CNN method with self-contrast model.

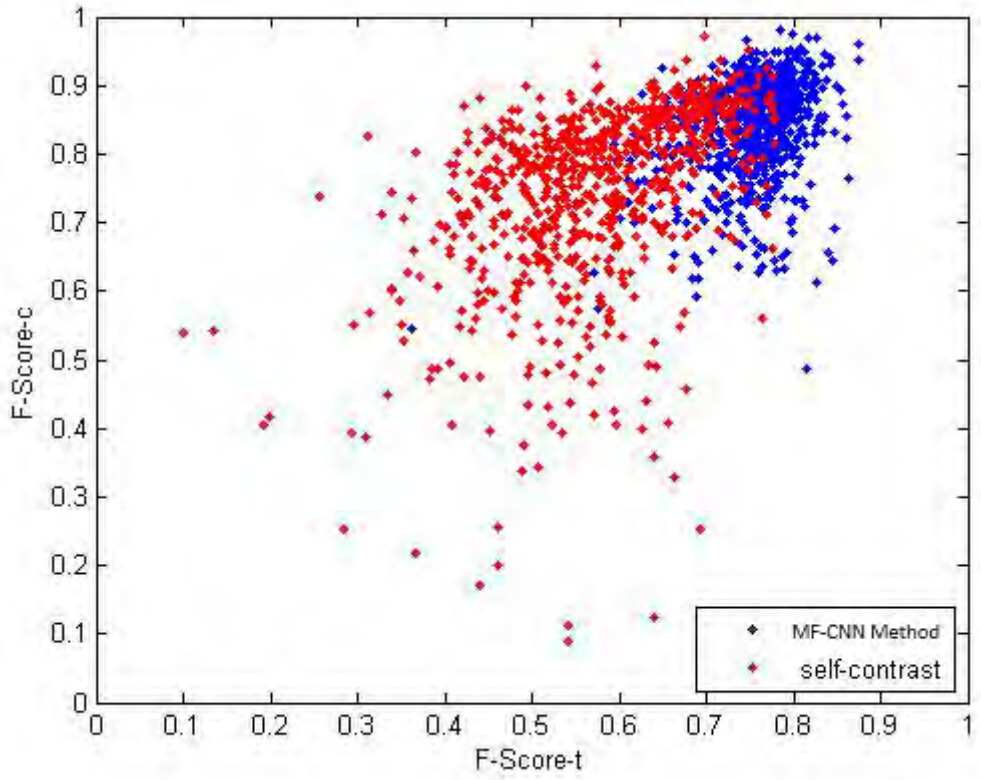

Table 4.

Detection Performance Of MF-CNN Method For Entire Clouds

RR	ER	FAR	RER
0.9340	0.0385	0.0693	24.22

Table 5.

Detection Performance of MF-CNN Method For Thick And Thin Clouds. Columns precision_c, recall_c, and f_score_c Describe Thick Clouds, While precision_t, recall_t, and f_score_t Describe Thin Clouds

precision_c	recall_c	F_Score_c	precision_t	recall_t	F_Score_t
0.9074	0.8946	0.8920	0.7813	0.7693	0.7753

The MF-CNN model achieves high accuracy thick cloud recognition and significantly improves pixel-level thin cloud detection for Landsat 8 satellite pictures. Regarding the whole work of cloud detection, the MF-CNN method guarantees high RR while managing the ER and stays clear of the over-detection issue.

Multilayer Perceptron (MLP) Neural Networks Model

The optimal structure for pixel-level classifications has been determined to be the Multilayer Perceptron (MLP) (Christopher M. Bishop, 1995). The MLP model is a classifier that uses feed-forward artificial neural networks. In an MLP, all perceptrons are connected in a forward manner, with the exception of the output layer, which provides the result directly. Each perceptron in the following layer is connected to all other perceptrons (Dündar, Ö, 2022).

For daylight cloud identification, additional information has been found in visible bands at 0.6 and 0.8 µm, near-infrared at 1.6 µm, infrared 3.9 µm, water vapor channels at 6.2 µm, and infrared 10.8 µm (Derrien & le Gléau, 2010). In addition to being crucial for detecting low clouds in conjunction with the IR 3.9 µm channel, visible channels are also necessary for Rayleigh and aerosol scattering (haze, smoke, dust, pollen, etc.) throughout the day (Bennouna et al., 2010; Derrien & Le Gléau, 2005). Clouds in the two visible channels (0.6 and 0.8 µm) are comparable, although land surfaces seem brighter at 0.8 µm while the sea surface has a stronger reflection at 0.6 µm (Bennouna et al., 2010). Therefore, to provide a strong contrast between cloud and surface targets, the two visible channels, 0.6 and 0.8 µm, have been chosen.

NIR channel (1.6 µm) has been utilized to differentiate between snow, ice, and water cloud. The temperature of thin clouds has been measured using the water vapor channel (6.2 µm) (Bennouna et al., 2010). The 10.8 µm infrared channel is crucial for determining the surface and cloud-top temperatures of the sea and land, as well as for identifying clouds of volcanic ash and cirrus clouds (Prata, 1989).

Upon visual examination when compared to the EUMETSAT cloud mask (CLM) findings, the machine learning classifier produces respectable detection results across a range of circumstances (Figure 11). With a standard deviation of 1.68%, 3.88%, and 11.04% for commission (the samples committed to the incorrect class) and omission (the samples omitted from the correct class) errors average, respectively, the accuracy of the entire test dataset categorized by MLP NNs is 88.96%. With a standard deviation of 2.47%, 7.27%, and 13.90% for commission and omission errors average, respectively, the average accuracy calculated for the MPEF CLM is 86.10%.

Figure 11.

RGB Combination of Meteosat Second Generation SEVIRI Images, MLP NN, EUMETSAT Cloud Map

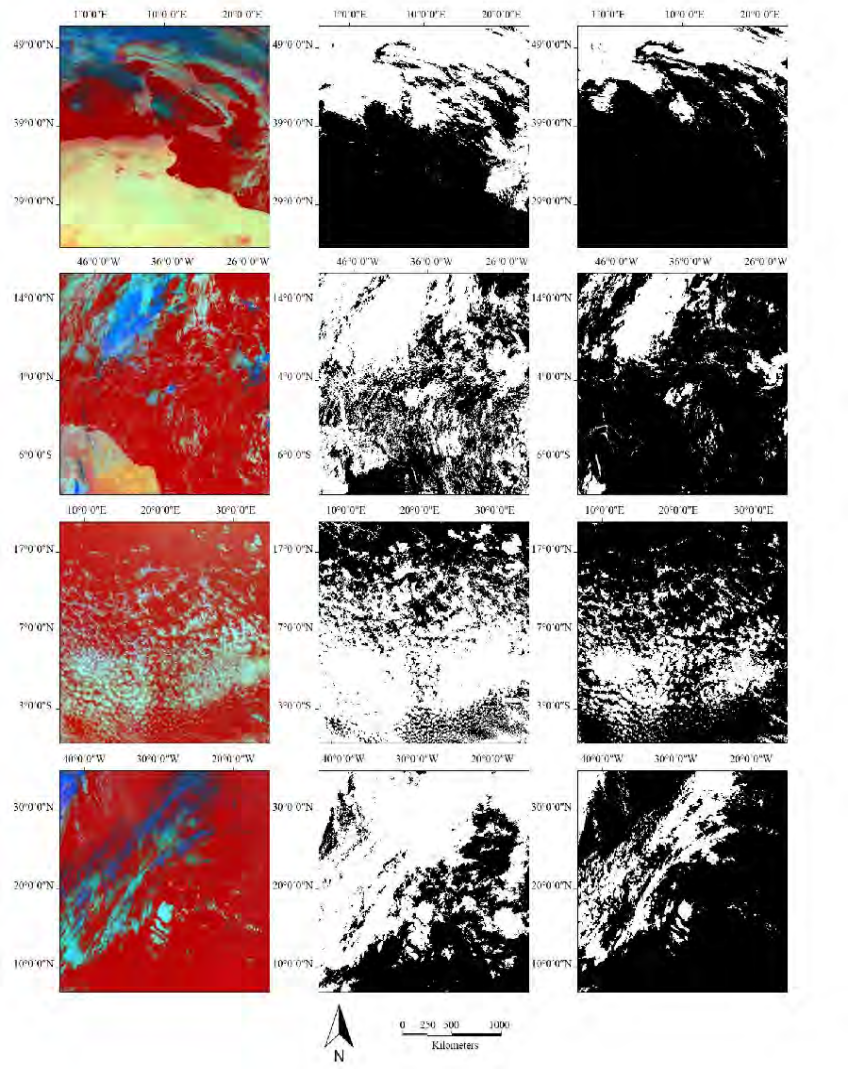

Table 6.

Minimum, maximum and average values of the accuracies for different models (in %).

Model	Mean	Min	Max	St.Dev	MeanComm	MeanOmm
MLP NN	88.96	85	91.8	1.68	3.88	11.04
MPEF CLM	86.10	82	89.2	2.47	7.27	13.90

Conclusion

The application of deep learning techniques for classifying scenes in satellite photos, addressing the drawbacks of conventional methods and emphasizing the development of deep learning architectures. It gives researchers in the field important insights and points

up areas for further study and development in remote sensing scene categorization.

The MF-CNN approach is presented as a possible remedy for the shortcomings of the existing techniques. The work contributes to the field of cloud identification by outlining a strategy to improve the precision and dependability of cloud recognition in remote sensing photographs.

Cloud detection, especially in areas covered with snow, the cloud mask algorithm, which is based on a neural network classifier powered by radiative transfer simulations, offers a threshold-free solution that performs better than conventional techniques. Because of its adaptability, it may be used with a variety of sensors, which makes it an important tool for satellite remote sensing. A potential method for classifying clouds that accurately and effectively classifies multispectral satellite data is the CS-CNN approach.

For SEVIRI MSG pictures, the machine learning methodology provides an automatic, robust, rapid, and accurate classification method without the need for auxiliary data. When it comes to cloud recognition in big datasets, the model performs better than the MPEF cloud mask and offers a viable substitute. The authors propose that evaluating alternative artificial neural network topologies and training techniques, as well as expanding the breadth and variety of the training and testing sets, can provide even greater benefits. In general, the study shows how machine learning techniques may be used to identify clouds in MSG SEVIRI images, emphasizing their value when supplementary data is scarce.

References

Ahmad, A., & Quegan, S. (2012). Cloud Masking for Remotely Sensed Data Using Spectral and Principal Components Analysis. In *Engineering, Technology & Applied Science Research* (Vol. 2, Issue 3, pp. 221–225). D. G. Pylarinos.

Bennouna, Y. S., Curier, L., Piazzola, J., de Leeuw, G., Roebeling, R., & de Valk, P. (2010). An automated day-time cloud detection technique applied to MSG-SEVIRI data over Western Europe. *International Journal of Remote Sensing, 31*(23), 6073–6093.

Blaschke, T. (2010). Object based image analysis for remote sensing. *ISPRS Journal of Photogrammetry and Remote Sensing, 65*(1), 2–16.

Bley, S., & Deneke, H. (2013). A threshold-based cloud mask for the high-resolution visible channel of Meteosat Second Generation SEVIRI. In *Atmospheric Measurement Techniques* (Vol. 6, Issue 10, pp. 2713–2723). Copernicus Publications.

Cheng, G., Xie, X., Han, J., Guo, L., & Xia, G. (2020). Remote Sensing Image Scene Classification Meets Deep Learning: Challenges, Methods, Benchmarks, and Opportunities. In *IEEE Journal of Selected Topics in Applied Earth Observations and Remote Sensing, Selected Topics in Applied Earth Observations and Remote Sensing, IEEE Journal of, IEEE J. Sel. Top. Appl. Earth Observations Remote Sensing* (Vol. 13, pp. 3735–3756). IEEE.

Choi, Y.-S., Ho, C.-H., Ahn, M.-H., & Kim, Y.-M. (n.d.). *Remote Sensing of Cloud*

Properties from the Communication, Ocean and Meteorological Satellite (COMS) Imagery.

Christopher M. Bishop. (1995). Neural Networks for Pattern Recognition. *Clarendon Press*.

Coakley Jr, J. A., & Bretherton, F. P. (1982). *Cloud cover from high-resolution scanner data - Detecting and allowing for partially filled fields of view*. NASA Center for Aerospace Information (CASI).

Derrien, M., Farki, B., Harang, L., LeGléau, H., Noyalet, A., Pochic, D., & Sairouni, A. (1993). Automatic cloud detection applied to NOAA-11 /AVHRR imagery. *Remote Sensing of Environment*, *46*(3), 246–267.

Derrien, M., & Le Gléau, H. (2005). MSG/SEVIRI cloud mask and type from SAFNWC. *International Journal of Remote Sensing*, *26*(21), 4707–4732. 8

Derrien, M., & le Gléau, H. (2010). Improvement of cloud detection near sunrise and sunset by temporal-differencing and region-growing techniques with real-time SEVIRI. *International Journal of Remote Sensing*, *31*(7), 1765–1780.

Desbois, M., Seze, G., & Szejwach, G. (1982). Automatic Classification of Clouds on METEOSAT Imagery: Application to High-Level Clouds. In *Journal of Applied Meteorology (1962-1982)* (Vol. 21, Issue 3, pp. 401–412).

Egli, S., Thies, B., & Bendix, J. (2018). A hybrid approach for fog retrieval based on a combination of satellite and ground truth data. *Remote Sensing*, *10*(4).

Feijt, A., de Valk, P., & van der Veen, S. (2000). Cloud Detection Using Meteosat Imagery and Numerical Weather Prediction Model Data. In *Journal of Applied Meteorology (1988-2005)* (Vol. 39, Issue 7, pp. 1017–1030).

Hu, F., Xia, G.-S., Hu, J., & Zhang, L. (2015). Transferring Deep Convolutional Neural Networks for the Scene Classification of High-Resolution Remote Sensing Imagery. In *Remote Sensing* (Vol. 7, Issue 11, pp. 14680–14707). MDPI AG.

Janssen, L. L. F., & Middelkoop, H. (1992). Knowledge-based crop classification of a Landsat Thematic Mapper image. In *International Journal of Remote Sensing* (Vol. 13, pp. 2827–2837). Informa UK Limited.

Jogin, M., Mohana, Madhulika, M. S., Divya, G. D., Meghana, R. K., & Apoorva, S. (2018). Feature Extraction using Convolution Neural Networks (CNN) and Deep Learning. In *2018 3rd IEEE International Conference on Recent Trends in Electronics, Information & Communication Technology (RTEICT), Recent Trends in Electronics, Information & Communication Technology (RTEICT), 2018 3rd IEEE International Conference on* (pp. 2319–2323).

Koçer, S., Jama, B. S. A., Er, Y. & Dündar, Ö. (2022). A Comparative Study for Evaluating the Performance of Various Classification Techniques on Brain Tumour, Five Zero, 2(1), 1-12

Li, Y., Zhu, Z., Yu, J., & Zhang, Y. (2021). Learning Deep Cross-Modal Embedding Networks for Zero-Shot Remote Sensing Image Scene Classification. In *IEEE Transactions on Geoscience and Remote Sensing, Geoscience and Remote Sensing, IEEE Transactions on, IEEE Trans. Geosci. Remote Sensing* (Vol. 59, Issue 12, pp. 10590–10603). IEEE.

Mirza, M., & Osindero, S. (2014). *Conditional Generative Adversarial Nets*.

Mukherjee, D. P., & Acton, S. T. (2002). Cloud Tracking by Scale Space Classification. In *IEEE TRANSACTIONS ON GEOSCIENCE AND REMOTE SENSING* (Vol. 40,

Issue 2).

Noh, H., Hong, S., & Han, B. (2015). *Learning Deconvolution Network for Semantic Segmentation*.

Prata, A. J. (1989). Observations of volcanic ash clouds in the 10-12 μm window using AVHRR/2 data. In *International Journal of Remote Sensing* (Vol. 10, pp. 751–761). Informa UK Limited. 8

Reynolds, D. W., & Haar, T. H. V. (1977). A Bispectral Method for Cloud Parameter Determination. In *Monthly Weather Review* (Vol. 105, pp. 446–457). American Meteorological Society.

Roebeling, R. A., & van Meijgaard, E. (2009). Evaluation of the Daylight Cycle of Model-Predicted Cloud Amount and Condensed Water Path over Europe with Observations from MSG SEVIRI. In *Journal of Climate* (Vol. 22, Issue 7, pp. 1749–1766).

Roy, G., Hayman, S., & Julian, W. (2001). Sky analysis from CCD images: cloud cover. *Lighting Research & Technology*, *33*(4), 211–222.

Saunders, R. W., & Kriebel, K. T. (1988). An improved method for detecting clear sky and cloudy radiances from AVHRR data. *International Journal of Remote Sensing*, *9*(1), 123–150.

Scarpa, G., Gargiulo, M., Mazza, A., & Gaetano, R. (2018). A CNN-based fusion method for feature extraction from sentinel data. *Remote Sensing*, *10*(2).

Schmetz, J., Pili, P., Tjemkes, S., Just, D., Kerkmann, J., Rota, S., & Ratier, A. (2002). AN INTRODUCTION TO METEOSAT SECOND GENERATION (MSG). In *Bulletin of the American Meteorological Society* (Vol. 83, Issue 7, pp. 977–992).

Seze, G., & Desbois, M. (1987). Cloud Cover Analysis from Satellite Imagery Using Spatial and Temporal Characteristics of the Data. In *Journal of Climate and Applied Meteorology* (Vol. 26, Issue 2, pp. 287–303).

Sullivan, G. D., Griggs, D. J., & Davis, G. B. (1992). Automatic Estimation of Cloud Amount Using Computer Vision. In *Journal of Atmospheric and Oceanic Technology* (Vol. 9, pp. 81–85). American Meteorological Society.

Sutskever, I., Krizhevsky, A., & Hinton, G. E. (2017). ImageNet classification with deep convolutional neural networks. In *Communications of the ACM* (Vol. 60, pp. 84–90). Association for Computing Machinery (ACM).

Tracewski, L., Bastin, L., & Fonte, C. C. (2017). Repurposing a deep learning network to filter and classify volunteered photographs for land cover and land use characterization. In *Geo-spatial Information Science* (Vol. 20, Issue 3, pp. 252–268). Taylor & Francis Group.

Tuia, D., Ratle, F., Pacifici, F., Kanevski, M. F., & Emery, W. J. (2009). Active Learning Methods for Remote Sensing Image Classification. In *IEEE Transactions on Geoscience and Remote Sensing, Geoscience and Remote Sensing, IEEE Transactions on, IEEE Trans. Geosci. Remote Sensing* (Vol. 47, Issue 7, pp. 2218–2232). IEEE.

Wang, M., Zhang, X., Niu, X., Wang, F., & Zhang, X. (2019). Scene Classification of High-Resolution Remotely Sensed Image Based on ResNet. *Journal of Geovisualization and Spatial Analysis*, *3*(2).

Wang, Q., Huang, W., Xiong, Z., & Li, X. (2022). Looking Closer at the Scene: Multiscale Representation Learning for Remote Sensing Image Scene Classification. In *IEEE Transactions on Neural Networks and Learning Systems, Neural Networks and*

Learning Systems, IEEE Transactions on, IEEE Trans. Neural Netw. Learning Syst. (Vol. 33, Issue 4, pp. 1414–1428). IEEE.

Zhan, Y., Wang, J., Shi, J., Cheng, G., Yao, L., & Sun, W. (2017). Distinguishing Cloud and Snow in Satellite Images via Deep Convolutional Network. In *IEEE Geoscience and Remote Sensing Letters, Geoscience and Remote Sensing Letters, IEEE, IEEE Geosci. Remote Sensing Lett.* (Vol. 14, Issue 10, pp. 1785–1789). IEEE.

Zhang, Q., & Xiao, C. (2014). Cloud Detection of RGB Color Aerial Photographs by Progressive Refinement Scheme. In *IEEE Transactions on Geoscience and Remote Sensing, Geoscience and Remote Sensing, IEEE Transactions on, IEEE Trans. Geosci. Remote Sensing* (Vol. 52, Issue 11, pp. 7264–7275). IEEE.

Zhang, R., Sun, D., Li, S., & Yu, Y. (2013). A stepwise cloud shadow detection approach combining geometry determination and SVM classification for MODIS data. *International Journal of Remote Sensing*, *34*(1), 211–226.

About the Authors

Sabri KOCER, He is a professor and senior researcher in the Department of Computer Engineering at Konya Necmettin Erbakan University. He completed his doctorate at the Department of Electronic Computer Education at Gazi University. He has held academic positions at different Universities in Turkey and has made great contributions to the ongoing technological academic development in the region. His main research interests are biomedical engineering, artificial intelligence, optimization, and machine learning and microcontroller applications. In addition, he has many academic works such as books, articles, essays, posters published in many national and international journals.

E-mail: skocer@erbakan.edu.tr, **ORCID:** 0000-0002-4849-747X

Yasin ER, he works as a computer engineer at the Turkish State Meteorological Service. He has a master's degree from Hoca Ahmet Yesevi University. His studies are meteorological communication, enterprise-specific software development, and Windows/Linux-based system management. He is a member of various expert groups and working groups at the World Meteorological Organization, currently, He is studying for a doctorate at the Institute of Pure and Applied Science of Necmettin Erbakan University.

E-mail: yasineryasiner@gmail.com, **ORCID:** 0000-0001-6729-5278

Similarity Index

The similarity index obtained from the plagiarism software for this book chapter is 16%.

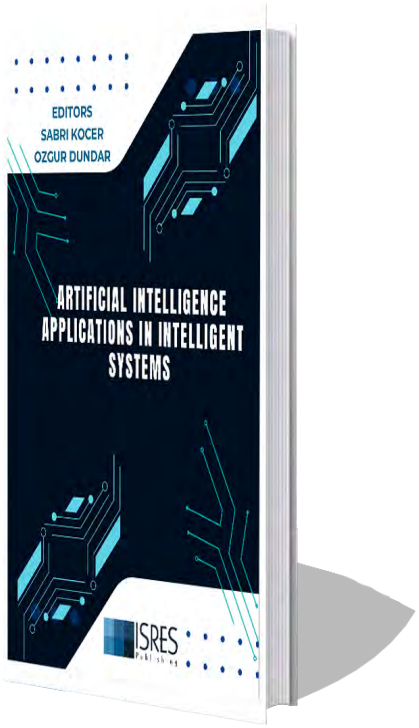

Artificial Intelligence Applications in Intelligent System is published from the selected papers invited by the editors.

This edition includes 12 sections from the engineering and technology etc of used in today's technology. All submissions are reviewed by at least two international reviewers.

The purpose of the book is to provide the readers with the opportunity of a scholarly refereed publication in the field of in Electronics, Communications, Mechatronics, Software, Artificial Intelligence, Aviation and Biomedical Engineering and Technology.

Artificial Intelligence Applications in Intelligent System is published by ISRES Publishing.

ISRES Publishing